COMPREHENSIVE CHEMICAL KINETICS

EDITED BY

N.J.B. GREEN

VOLUME 42

MODELING OF CHEMICAL REACTIONS

R.W. CARR

VOLUME EDITOR

COMPREHENSIVE CHEMICAL KINETICS

COMPREHENSIVE

Section 1. THE PRACTICE AND THEORY OF KINETICS (3 volumes)

Section 2. HOMOGENEOUS DECOMPOSITION AND ISOMERISATION REACTIONS (2 volumes)

Section 3. INORGANIC REACTIONS (2 volumes)

Section 4. ORGANIC REACTIONS (5 volumes)

Section 5. POLYMERISATION REACTIONS (3 volumes)

Section 6. OXIDATION AND COMBUSTION REACTIONS (2 volumes)

Section 7. SELECTED ELEMENTARY REACTIONS (1 volume)

Section 8. HETEROGENEOUS REACTIONS (4 volumes)

Section 9. KINETICS AND CHEMICAL TECHNOLOGY (1 volume)

Section 10. MODERN METHODS, THEORY AND DATA

CHEMICAL KINETICS

EDITED BY

N.J.B. GREEN
King's College London
London, England

VOLUME 42

MODELING OF CHEMICAL REACTIONS

ROBERT W. CARR
Professor Emeritus,
University of Minnesota, USA

ELSEVIER

AMSTERDAM - BOSTON - HEIDELBERG - LONDON - NEW YORK - OXFORD - PARIS
SAN DIEGO - SAN FRANCISCO - SINGAPORE - SYDNEY - TOKYO

Elsevier
Radarweg 29, PO Box 211, 1000 AE Amsterdam, The Netherlands
Linacre House, Jordan Hill, Oxford OX2 8DP, UK

First edition 2007

Library of Congress Cataloging-in-Publication Data
A catalog record for this book is available from the Library of Congress

British Library Cataloguing in Publication Data
A catalogue record for this book is available from the British Library

ISBN: 978-0-444-51366-3
ISSN: 0069-8040 (Series)

Printed and bound in Italy

07 08 09 10 11 10 9 8 7 6 5 4 3 2 1

COMPREHENSIVE CHEMICAL KINETICS

ADVISORY BOARD

Volumes in the Series

Section 1. THE PRACTICE AND THEORY OF KINETICS (3 volumes)

Volume 1 The Practice of Kinetics
Volume 2 The Theory of Kinetics
Volume 3 The Formation and Decay of Excited Species

Section 2. HOMOGENEOUS DECOMPOSITION AND ISOMERISATION REACTIONS (2 volumes)

Volume 3 Decomposition of Inorganic and Organometallic Compounds
Volume 5 Decomposition and Isomerisation of Organic Compounds

Section 3. INORGANIC REACTIONS (2 volumes)

Volume 6 Reactions of Non-metallic Inorganic Compounds
Volume 7 Reactions of Metallic Salts and Complexes and Organometallic Compounds

Section 4. ORGANIC REACTIONS (5 volumes)

Volume 8 Proton Transfer
Volume 9 Addition and Elimination Reactions of Aliphatic Compounds
Volume 10 Ester Formation and Hydrolysis and Related Reactions
Volume 12 Electrophilic Substitution at a Saturated Carbon Atom
Volume 13 Reactions of Aromatic Compounds

Section 5. POLYMERISATION REACTIONS (3 volumes)

Volume 14 Degradation of Polymers
Volume 14A Free-radical Polymerisation
Volume 15 Non-radical Polymerisation

Section 6. OXIDATION AND COMBUSTION REACTIONS (2 volumes)

Volume 16 Liquid-phase Oxidation
Volume 17 Gas phase Combustion

Section 7. SELECTED ELEMENTARY REACTIONS (1 volume)

Volume 18 Selected Elementary Reactions

Section 8. HETEROGENEOUS REACTIONS (4 volumes)

Volume 19 Simple Processes at the Gas-Solid Interface
Volume 20 Complex Catalytic Processes
Volume 21 Reactions of Solids with Gases
Volume 22 Reactions in the Solid State

This page intentionally left blank

Contents

List of Contributors

Robert W. Carr
Department of Chemical Engineering and Materials Science, Minneapolis, MN 55455, USA

Hans-Heinrich Carstensen
Chemical Engineering Department, Colorado School of Mines, Golden, CO 80401, USA

Anthony M. Dean
Chemical Engineering Department, Colorado School of Mines, Golden, CO 80401, USA

Ryan Feeley
Department of Mechanical Engineering, University of California at Berkeley, Berkeley, CA 94720-1740, USA

Michael Frenklach
Department of Mechanical Engineering, University of California at Berkeley, Berkeley, CA 94720-1740, USA

Karl K. Irikura
Physical and Chemical Properties Division, National Institute of Standards and Technology, Gaithersburg, MD 20899-8380, USA

Andrew Packard
Department of Mechanical Engineering, University of California at Berkeley, Berkeley, CA 94720-1740, USA

Mark T. Swihart
Department of Chemical and Biological Engineering, The University at Buffalo (SUNY), Buffalo, NY 14260-4200, USA

This page intentionally left blank

Preface

The overall chemical transformations that occur in nature and in many processes designed by chemists and engineers can be very complex. They frequently consist of hundreds, or even thousands, of different kinds of molecular reactions through which the overall chemical transformation occurs. These are called elementary chemical reactions, and they are the fundamental quantities governing the molecular pathways by which chemical compounds are converted during overall chemical transformations. Elementary chemical reactions are the basis for a detailed understanding of how complex chemical reactions occur, and at what rate they occur.

The historical development of chemical kinetics, which is the study of the rates of chemical reactions, started with empirical observations of the overall rates at which chemical compounds are converted into final reaction products, because knowledge of the underlying elementary chemical reactions was very meager. Consequently, the chemical process industries developed empirical models to describe process chemistry, a practice which still comprises a significant part of chemical engineering. Generations of chemical engineers have learned and developed these methods, frequently to a high degree of sophistication. Textbooks of chemical reaction engineering amply describe this branch of applied chemical kinetics. The empirical models, however, have limitations. They are limited to the range of experimental variables over which they were developed, and should not be used outside that range. They do not have predictive ability. And they do not incorporate detailed chemistry, making it very difficult to see how process improvements can be made.

The twentieth century saw an enormous amount of experimental and theoretical research on elementary chemical reactions, an effort which continues today. The fruits of this work are extensive kinetics databases, and molecular theories from which to make estimates when experimental data are not available. Equally important are parallel developments in thermochemistry. All of this information makes possible the development of detailed chemical kinetics models of overall chemical reactions. Models have been constructed and applied to such diverse topics as atmospheric chemistry, combustion, low temperature oxidation, chemical vapor deposition, and reactions in traditional chemical process industries. The rate of each elementary reaction in a model is expressed as

an ordinary differential equation, so the models are dynamical systems. Furthermore, the rates vary by many orders of magnitude, and the models are very stiff. Advances in the speed and memory of digital computers, along with the development of methods for handling stiffness, are the final piece of the puzzle, making facile numerical computations possible.

This book covers several topics that are essential for the construction of detailed chemical kinetics models. I hope that it will be useful to chemists and chemical engineers who are just starting to delve into this subject, and to others whose technical training lies outside kinetics, even outside chemistry, and who wish to undertake the construction of a detailed chemical kinetics model for their own purposes. Complex chemical reactions are not solely the purview of chemists any more. The subject of chemical kinetics has been important to chemical engineers since the inception of the discipline over 100 years ago. Mechanical engineers have for a long time been interested in combustion, the chemical aspects of microelectronics processing has involved electrical engineers, and civil engineers are becoming ever more involved with environmental chemistry. Researchers in all of these disciplines, and perhaps in others as well, may come up against chemical reactions that need to be modeled for understanding.

The coverage is restricted to gas phase chemical reactions because this is the most highly developed area, and the one permitting the most accurate and predictive models at the present time. Reactions in the liquid phase and at solid interfaces present difficulties, although progress is being made. Reactions in solids are the most undeveloped currently. Chapter 1 is a brief introduction to the subject. One of the most important advances in recent years is the improvement in quantum chemistry methods for the computation of molecular structure and energetics. Methods capable of computing energies to "chemical accuracy" (a few kilojoules per mole) are now available, although some judgment is needed to assess the results. Chapter 2 discusses these methods and shows how to use the results to obtain thermochemical quantities for stable molecules. Part of Chapter 5 shows how to extend these methods to transition states. Chapter 3 is titled "Elements of Chemical Kinetics." It is a summary of some basic principles of kinetics, and of theories of bimolecular reactions. Its usefulness will be primarily for those who have very little background in kinetics. Chapter 4 treats pressure dependent reactions. These are unimolecular reactions and certain bimolecular reactions. Many detailed chemical kinetics models in the past have not included the pressure dependence of these reactions, although they are not rare, and should be included in models when appropriate. Chapter 4

provides the theoretical basis for the pressure dependence, and presents practical methods for estimating rate parameters. One of the most time consuming and laborious tasks in detailed modeling is putting together the list of elementary reactions, called the reaction mechanism. It is also one of the most crucial tasks. Chapter 5 deals with this subject, and goes beyond the ordinary to show how to proceed when there are few experimental data on which to rely. Chapter 6 addresses the very important issue of building predictive reaction models. The data used in constructing a reaction model have uncertainty, whether they are obtained from experiment, quantum chemistry, or estimation methods, and the individual errors are propagated in the model. This chapter examines mathematical approaches to incorporate the uncertainty into the model, and thus provide information on the predictive reliability of the model.

Robert Carr
Minneapolis
December, 2006

This page intentionally left blank

Chapter 1

Introduction

Robert W. Carr

Chemical reactions abound in nature. They are essential for life, in both living organisms and systems that support life. Chemical reactions occur in all states of matter—gas, liquid, and solid. For example, gas phase reactions occur in interplanetary space, planetary atmospheres (those in Earth's atmosphere are of particular interest to us), flames and combustion, microelectronics processing, and many industrial processes. In the case of Earth's atmosphere, the chemical details of urban air pollution and stratospheric ozone depletion must be described by large numbers of gas phase chemical reactions involving man-made pollutants. These reactions account for the formation of harmful substances, and in the case of the stratosphere account for depletion of Earth's protective ozone shield by man-made chlorofluorocarbons. Understanding the chemical details is essential for undertaking policies to mitigate the effects of pollution. Liquid phase reactions include biological reactions, such as enzyme catalysis and cellular processes, and a large number of industrial applications from the manufacture of polymers to organic and inorganic chemicals. Examples of solid state reactions may be found in Earth's crust, cooking, and detonation of explosives. Many more examples of reactions in all three states of matter could be cited. Chemical reactions are also of great commercial importance. In the majority of chemical processes the chemical industry depends on chemical reactions to convert raw materials or other feedstocks into higher value substances. For example, ethylene, the largest volume industrial organic substance produced in the world today, is produced by the gas phase thermal decomposition of ethane.

Describing the rates at which chemical reactions occur is the subject of chemical kinetics. It is the study of the rates at which chemical compounds interact with one another to produce new chemical species, and the insight into factors governing chemical reactivity that derives therefrom. The rates of chemical change span an enormous range of time

Comprehensive Chemical Kinetics, Volume 42, 1–6

ISSN: 0069-8040/doi:10.1016/S0069-8040(07)42001-5

scales, from the slowness of geologic change (perhaps millennia) to the speed of detonations and explosions (fractions of a second). At the molecular level, events such as bond dissociations and molecular rearrangements may occur in times that are on the order of one vibrational period, $\sim 10^{-12}$ to 10^{-13} sec. Modern developments in pulsed laser technology make it possible to record the motions of atomic nuclei with a time resolution as short as 10^{-15} sec, which is the lower limit of times that are of chemical interest. Researchers are now armed with weapons for studying chemical reactivity over the entire range of relevant time scales.

The beginnings of the study of chemical kinetics as we know it today were in the nineteenth century, and consisted primarily of empirical measurements of rates of chemical change, the rates at which reactants are transformed into reaction products. The transformation of a reactant into a final product is known as an overall reaction, or stoichiometric reaction. Research on the kinetics of overall reactions has served to characterize chemical reactions important to broad areas of science, and to lay down the basic principles of the field.

The empirical approach tells one very little about the underlying chemistry of the reaction and nothing about the (sometimes very many) kinds of reactions between the individual chemical species that are present during the overall reaction. Most chemical reactions occur via the intermediacy of highly reactive chemical species such as atoms, free radicals, and ions, which are not detected by classical analytical methods, and go unnoticed unless special efforts are made. The individual molecular interactions among the intermediates and observed reactants and reaction products are called elementary reactions. There is an old aphorism that says that there is nothing as rare as a simple chemical reaction. By simple reaction is meant the transformation of a reactant into a product by a single molecular reactive event. There are, of course, a good number of these known, but they are a minority among chemical reactions. The drive to better understand how overall chemical reactions occur was led by the development of experimental techniques for direct detection and identification of reactive intermediates, and by the development of reaction rate theories based on statistical and quantum mechanics. This was accompanied by the oftentimes slow and patient experimental work of uncovering the elementary reactions that comprise a particular overall reaction. The experimental methods burgeoned in the last half of the twentieth century, leading to an enormous increase in the number of known elementary reactions and the parameters that govern their rates. This work, which has gone on for decades now, has produced large and growing databases of elementary reactions, and has provided remarkable insight into chemical reactivity.

In the last half of the twentieth century, the development of highly sensitive spectroscopies, molecular beam technology, and rapid response electronics led to experimental methods for probing translational, vibrational, rotational, and electronic energy states during elementary chemical reactions. This third approach permits the roles that these forms of molecular energy play in governing rates and reactivity to be investigated. This research area is known as chemical dynamics, and it is adding a wealth of microscopic detail to our knowledge of chemical reactivity.

We can see that there are three levels at which work in kinetics is done: the empirical description of overall reactions, investigations of elementary reactions, and studies of chemical dynamics. These form a trinity of chemical kinetics, each member of which has an indispensable place today. Empirical studies of overall reactions are the beginning point for investigation of any newly discovered reaction, and they still play a significant role in modeling industrial chemistry. Elementary reactions describe the fundamental chemistry underlying any overall reaction, and chemical dynamics provides insight into the details of how an elementary reaction occurs. Chapters 3 and 4 contain, in part, material on the relationship of chemical dynamics to elementary reactions, and show when chemical dynamics data play a role in modeling reactions.

Elementary reactions are the fundamental building blocks for modeling overall chemical reactions. The rate coefficient for an elementary reaction (see Chapter 3) is a fundamental physical quantity that is an attribute of that particular reaction. It is a measurable quantity that has a firm grounding in theory. The rate coefficient is transferable, in the sense that when its value is determined, it can be used in any overall reaction in which that reaction occurs. This statement is rigorously true of gas phase reactions, and may be true of reactions in solution unless solvent effects are important.

An important topic in kinetics, and the central activity in creating a reaction model, is the development of chemical kinetic mechanisms. A mechanism is the list of elementary reactions that occur during the course of an overall reaction. It need not be an exhaustively complete list because some elementary reactions will play a negligible role, and can be omitted without appreciable errors being made. At the same time, it must be complete enough to describe the features of the overall reaction that are of interest. Sensitivity analysis, covered in Chapters 5 and 6, addresses this issue. It is important to recognize that as the overall reaction proceeds the elementary reactions may change in relative importance, because their contributions to the overall reaction rate depend on composition, which is always changing. Constructing a reaction

mechanism can be a painstaking and time consuming process, but it is essential to the success of a reaction model and needs to be done carefully. Chapter 5 is devoted to methods for the development of mechanisms.

The rate of an overall reaction is a composite of the rates of the elementary reactions in the mechanism, which form a set of ordinary differential equations coupled through the concentrations of chemical species, and can be expressed as the following initial value problem:

$$\frac{\mathrm{d}\mathbf{c}}{\mathrm{d}t} = \mathbf{f}(\mathbf{c}, \mathbf{k}), \quad \mathbf{c}(0) = \mathbf{c}_0 \tag{1}$$

For a system of S chemical species and R reactions $\mathbf{c}$ is the S vector of concentrations, $\mathbf{k}$ the R vector of time independent parameters (rate coefficients), and $\mathbf{f}$ the vector of the R rate expression functions. If the overall reaction is isothermal and takes place in a well-mixed vessel, equation (1) comprises a detailed chemical kinetic model (DCKM) of the reaction. The integration of the model equations can present difficulties because the rate coefficients may vary from one another by many orders of magnitude, and the differential equations are stiff. Numerical methods for the solution of stiff equations are discussed by Kee *et al.* [1]. Efficient solvers for stiff sets of equations have been developed and are available in various software packages. Some of these are described in Chapter 5. Additional information can be found in Refs. [2,3].

If the reaction is not isothermal the energy balance must also be considered. In a closed system the energy balance is given by equation (2),

$$C_p \frac{\mathrm{d}T}{\mathrm{d}t} = \sum_{j=1}^{R} -\Delta H_j(T) r_j - \frac{Q}{V} \tag{2}$$

where r_j is the rate expression for the jth elementary reaction, C_p the average heat capacity of the mixture, ΔH_j the enthalpy of reaction for the jth reaction, T the temperature, V the reactor volume, and Q the rate of heat removal. Equations (1) and (2) comprise a model for a well-mixed, non-isothermal batch reactor, and their simultaneous solution gives the dynamical concentration and temperature behavior of the reaction system. DCKMs for other well-mixed reactors, such as continuous stirred tanks and plug flow tubular reactors, both isothermal and non-isothermal, are obtained by inserting the rate expression for each step in the mechanism into the well-known material and energy balances for these reactor types [4]. In many reactive flows the composition and temperature are non-uniform. These are sometimes called distributed parameter systems, and modeling them involves incorporation of

convection, diffusion, and heat transfer rates. The model equations for distributed parameter systems are partial differential equations [5–7].

The development of DCKMs has been facilitated by the coming together of many things, but the effort would not be successful without the steady accumulation of data on elementary reactions that has occurred over the last few decades through the efforts of many researchers around the world. The databases for elementary reactions are of immense utility as extensive repositories of information for the construction of fundamentally based models for a wide variety of disparate chemical reactions. The models have played a significant role in advancing our understanding of important complex reactions such as those in air pollution and other aspects of atmospheric chemistry, planetary atmospheres, and combustion. They are also playing an increasing role in industrial practice, where they can replace the traditional empirical methods [8].

The goal is to construct models that can reproduce not just experimental data, but that in addition are predictive. Predictive models are a key for improving chemical technology, mitigating the effects of pollution, and understanding how complex reactions affect anything of which they are a part.

The subject matter in this book is confined to gas phase reactions. In the gas phase, collisions between chemical species take place in isolation, unperturbed by the surrounding molecules, which at most pressures of interest are far enough away that medium effects are negligible. And collisions are the events through which chemical change happens. It is the isolation of gas phase collisions that simplifies the problem, for it makes the rate parameters of the elementary reaction transferable. In the gas phase, the parameters that govern the rate of an elementary reaction in a certain overall reaction are the same as the parameters that govern it in a different overall reaction with a different chemical environment. Special experiments are usually devised to determine the kinetics of an elementary reaction in isolation, that is, where it is uninfluenced, or at least minimally influenced, by any other reaction. The data so obtained can then be used in entirely different chemical environments. A database with a finite (albeit large) number of elementary reactions can be used to model the much larger number (infinite?) of possible overall reactions.

Reactions at solid surfaces are not included here, although they occur at reactor walls and other surfaces that may be present, and they can be an important influence on the observed chemistry and overall reaction rate. Surface reactions are frequently included in mechanisms, but in general the rate parameters are not transferable because they depend on the nature of the surface and the environment to which it is exposed. A previous volume in this series is devoted to heterogeneous reactions [9],

and a monograph by Tovbin [10] covers many physical phenomena at the gas–solid interface. Additionally, Kondrat'ev [11] gives a kinetic treatment of heterogeneous removal of free radicals and atoms that is very convenient for gas phase reactions. The kinetics of reactions in the solid state are not as highly developed as gas and liquid phase kinetics, and the DCKM approach is unlikely to be appropriate in any case. Volume 22 of *Comprehensive Chemical Kinetics* provides coverage of solid state reactions [12].

There is a large body of literature on the mechanisms of liquid phase reactions, but theory is not as highly developed as it is for gas phase reactions. The rates of liquid phase reactions are influenced by bulk properties of the medium, in contrast with the gas phase. The theory of solvent effects is an active research topic at the present time. In addition, fast liquid phase reactions are rate limited by reactant diffusion rates. Various aspects of liquid phase reactions have been covered in several previous volumes in this series.

REFERENCES

[1] R.J. Kee, M.E. Coltrin, P. Glarborg, *Chemically Reacting Flow. Theory and Practice*. Wiley, Hoboken, NJ, 2003, Chapter 15.
[2] M.J. Pilling, ed., Low-Temperature Combustion and Autoignition, in: R.G. Compton, G. Hancock (eds.), *Comprehensive Chemical Kinetics*, Volume 35. Elsevier, Amsterdam, 1997, pp. 313, 314.
[3] W.C. Gardiner, Jr., ed. *Gas Phase Combustion Chemistry*. Springer-Verlag, New York, 2000, p. 17.
[4] R. Aris, *Elementary Chemical Reactor Analysis*. Prentice-Hall, Englewood Cliffs, NJ, 1969.
[5] R.J. Kee, M.C. Coltrin, P. Glarborg, *Chemically Reacting Flow, Theory and Practice*. Wiley, Hoboken, NJ, 2003.
[6] D.E. Rosner, *Transport Processes in Chemically Reacting Flow Systems*. Butterworths, Stoneham, MA, 1986.
[7] G.F. Froment, K.B. Bischoff, *Chemical Reactor Analysis and Design*, 2nd ed., Wiley, New York, 1990.
[8] S.M. Senkan, *Adv. Chem. Eng.*, **18** (1992) 95.
[9] C.H. Bamford, C.F.H. Tipper, R.G. Compton, eds., Simple Processes at the Gas–Solid Interface, *Comprehensive Chemical Kinetics*, Volume 19. Elsevier, Amsterdam, 1984.
[10] Yu.K. Tovbin, *Theory of Physical Chemistry Processes at a Gas–Solid Interface*. CRC Press, Boca Raton, 1991.
[11] V.N. Kondrat'ev, *Chemical Kinetics of Gas Reactions*. Addison-Wesley, Reading, 1964, pp. 588–590.
[12] C.H. Bamford, C.F.H. Tipper, eds., Reactions in the Solid State, *Comprehensive Chemical Kinetics*, Volume 22. Elsevier, Amsterdam, 1980.

Chapter 2

Obtaining Molecular Thermochemistry from Calculations

Karl K. Irikura

1 INTRODUCTION AND OVERVIEW

The thermochemistry of a chemical reaction dictates the position of equilibrium, which is independent of any rate constant. However, since the equilibrium constant is the ratio of the forward and the reverse rates, it is a helpful piece of information when evaluating the consistency of kinetics data (e.g., equations (1) and (2)). Furthermore, if the reverse rate constant (k_r) is unknown, it may be computed from the forward rate constant (k_f) and the equilibrium constant (K).

$$\mathrm{A} + \mathrm{B} \underset{k_r}{\overset{k_f}{\rightleftharpoons}} \mathrm{C} + \mathrm{D} \tag{1}$$

$$K = \left(\frac{[\mathrm{C}][\mathrm{D}]}{[\mathrm{A}][\mathrm{B}]}\right)_{\text{equilibrium}} = \frac{k_f}{k_r} \tag{2}$$

If the equilibrium constant for a reaction is unknown, it can be computed from the corresponding thermochemistry according to equation (3). Unfortunately, the exponential

$$K = \exp\left(\frac{-\Delta G}{RT}\right) \tag{3}$$

relationship amplifies the uncertainties, especially at lower temperatures. For example, if $\Delta G = 50\,\mathrm{kJ\,mol^{-1}}$, an uncertainty of $1\,\mathrm{kJ\,mol^{-1}}$ in ΔG corresponds to a 40% uncertainty in K at room temperature. This is particularly important to bear in mind when thermochemistry is obtained by using approximate computational methods.

This chapter is restricted to gas-phase thermochemistry. In condensed phases (solutions, surfaces, etc.) medium effects may be small, so that the gas-phase values are often useful in condensed-phase work, at least as a

Comprehensive Chemical Kinetics, Volume 42, 7–42

ISSN: 0069-8040/doi:10.1016/S0069-8040(07)42002-7

first approximation. This chapter is further restricted to popular computational methods for obtaining thermochemistry. Many experimental methods have been reviewed recently [1–4].

Empirical methods are systematic procedures for using existing experimental data to predict the properties of similar compounds. As suggested by the name, empirical methods depend on compilations of experimental data for determining the values of adjustable parameters. Empirical methods are computationally inexpensive and are generally quite reliable when dealing with "typical" compounds for which copious experimental data exist. For thermochemical properties, the most popular empirical methods are group additivity (GA) and molecular mechanics (MM). The predominant GA method is that developed by Benson and coworkers [5,6]; a user-friendly implementation is available on-line as part of the *NIST Chemistry WebBook* [7]. However, other related methods exist, such as that by Pedley [8], also for organic compounds, and that by Drago and co-workers [9,10], which is applicable to inorganic and organometallic molecules as well. In MM, a molecule is modeled as a mechanical system of masses (atoms) and springs (bonds), with additional forces for describing hydrogen bonding, van der Waals interactions, etc. [11]. MM is the predominant theoretical approach for biomolecular modeling, as used extensively in the pharmaceutical industry [12]. In the field of molecular thermochemistry, the MM3 and MM4 methods, continually under development by Allinger and coworkers, are most popular [13,14]. Where MM methods are applicable, they are often quite precise, with uncertainties of $5\,\mathrm{kJ\,mol^{-1}}$ or so.

When empirical methods are not applicable, the next appeal is often semiempirical molecular orbital theory (SEMOT). This is a quantum-mechanical theory that treats electrons and nuclei explicitly. However, many of the integrals are ignored or replaced by adjustable parameters, reducing the cost of the calculations by one or more orders of magnitude. The parameter values are determined by fitting to tables of experimental data, including thermochemistry. Although new parameterizations continue to be developed, the most popular are known as AM1 [15], PM3 [16], and MNDO/d [17]. Since SEMOT is based on quantum mechanics, it is more general (i.e., more broadly applicable) than MM. However, since experimental data are required for obtaining the values of parameters, SEMOT is still restricted to molecules of types that have been fairly well characterized. Where applicable, SEMOT methods often have modest precision, with uncertainties of $\sim 30\,\mathrm{kJ\,mol^{-1}}$ ($\sim 55\,\mathrm{kJ\,mol^{-1}}$ for hypervalent molecules) [18].

If semiempirical theory is either inapplicable or insufficiently precise, the next recourse is generally *ab initio* molecular orbital theory (MOT)

or density functional theory (DFT). Although people quarrel about the definition, the term *ab initio* will be used in this chapter to refer to both MOT and DFT. *Ab initio* calculations are more computationally intensive than SEMOT and frequently require more effort and expertise to execute properly. There is a wide range of such methods, varying in both computational cost and reliability. Ordinarily one begins with the least expensive methods. Since MOT and DFT procedures have only a few (or even zero) adjustable parameters, they are broadly general and can be used confidently even where experimental data are scant. Nonetheless, they are also subject to uncertainties and can have substantial errors.

Table 1 provides a qualitative comparison of the reliability and cost of the various categories of computational approach. When using MOT and DFT approaches, one may take advantage of experimental data on related compounds to improve the reliability of the results, as will be explained later in this chapter. To illustrate this, two entries are given for each such method in Table 1, the first using a simple, mechanical procedure and the second using a more thoughtful strategy. A good strategy often yields a dramatically improved result.

In Table 1, the reported computational times are for a laptop computer (800 MHz Pentium III). The GA calculations were done using the *NIST Chemistry WebBook* [7]. The MM3 calculations were done using a commercial software package [19,20]. The SEMOT and MOT calculations were also done using commercial software [20,21].

2 MOLECULAR MECHANICS

In MM, a molecule is modeled as a collection of masses (atoms) and springs (bonds), with additional forces added to describe other interactions such as hydrogen bonding, electrostatics, and dispersion forces. Although such simulations have been done using carefully constructed mechanical models [22], MM has been most successfully implemented computationally. The present discussion will focus on the MM3 method [13], since it is popular and is implemented in a number of software packages. Beware that not all implementations of MM3 provide thermochemical information.

Different methods of MM are distinguished by the mathematical form chosen for the energy expression and by the choice of parameter values used in that energy expression. The combination of energy expression and parameter values is termed the *force field*. For this reason, MM methods are sometimes called ''force field'' methods. The energy of a molecule is determined completely by the force field and the molecular geometry, i.e., the bond lengths, bond angles, and torsional angles.

TABLE 1
Sample results and approximate computational times for various computations of gas-phase thermochemistry

Method	Category	Acetaldehyde				9,10-Anthraquinone			
		$\Delta_f H^0_{298}$ (kJ mol^{-1})		Time (sec)		$\Delta_f H^0_{298}$		Time (sec)	
GA	GA	−164		<1		Failed		<1	
MM3	MM	−168		<1		−69		1	
PM3	SEMOT	−185		8		−58		35	
		Atomization[a]	Reaction[b]	Atomization[a]	Reaction[b]	Atomization[a]	Reaction[b]	Atomization[a]	Reaction[b]
HF/6-31G(d)	MOT	627	−148	140	240	3450	−71	2.1×10^4	2.3×10^4
B3LYP/6-31G(d)	DFT	−157	−163	390	520	1	−78	1.8×10^4	2.3×10^4
MP2/6-31G(d)[c]	MOT	22	−174	520	780	329	−104	6.8×10^5	7.2×10^5
MP2//HF/6-31G(d)[d]	MOT	27	−173	160	300	364	−104	2.3×10^4	2.5×10^4
MP2/cc-pVTZ//HF/6-31G(d)[e]	MOT	−141	−166	910	1100	−185	−100	9.8×10^4	1.2×10^5
G3(MP2)	MOT	−164	−168	1100	1300	−85	−89	2.5×10^5	2.8×10^5
[Experiment][f]		−170.7 ± 1.5				−75.7 ± 2.9			

Enthalpy changes are in kJ mol^{-1}.
[a]Based upon atomization reaction.
[b]Based upon the reactions $CH_3CHO + H_2 = CH_4 + H_2CO$ and 9,10-anthraquinone + $2C_2H_4 = 2C_6H_6 + p$-benzoquinone.
[c]The MP2/6-31G(d) calculation produces one imaginary-valued vibrational frequency for 9,10-anthraquinone, indicating that the molecule is non-planar within this computational model.
[d]Energy from MP2/6-31G(d), geometry and vibrational frequencies from HF/6-31G(d).
[e]Energy from MP2/cc-pVTZ, geometry and vibrational frequencies from HF/6-31G(d).
[f]Experimental data from Refs. [114,116].

The principal step in a MM calculation is to optimize the molecular geometry. This is an automated procedure in which the geometry is adjusted to minimize the total energy of the molecule. A stable conformation of the molecule results. However, it is typically guaranteed only to be a geometry for which the forces (i.e., gradient of the energy) are very small. In careful work, one must verify that the final structure is an energy minimum. This is usually tested by computing the vibrational frequencies. If any frequencies are imaginary-valued (often printed as negative-valued real numbers in computer outputs), then the structure is not a minimum, but a saddle point requiring further energy minimization. Ideally, one would like to find the most stable conformation, i.e., the global minimum of energy, but this cannot always be achieved. (Note that geometries from MM3 should not be compared directly with geometries from MOT or DFT, since MM3 has been parameterized for thermally averaged structures, not for equilibrium structures [23].) Once the geometry has been optimized, the resulting energy is converted to an enthalpy of formation at 298.15 K using additional parameters that describe bond increments, group increments, enthalpy contributions from torsional vibrations, from other accessible conformations, etc. Since these thermochemical parameters were developed using ideal-gas enthalpies of formation at 298.15 K, the enthalpies of formation in the computer output are also for the ideal gas at 298.15 K, frequently in units of kcal mol^{-1} (1 kcal $\approx$ 4.184 kJ).

The MM3 force field includes hundreds of parameters, which describe bond stretching, angle bending, thermochemistry, etc., for each combination of atoms. Correspondingly large amounts of reference data were required for parameter development. Lack of the requisite experimental data is a serious problem, as it is for other empirical procedures such as GA. However, as molecular orbital and density functional calculations have become less expensive, they have been used more heavily as surrogates for experimental measurements, permitting further parameter development in MM3 and other methods. Thermochemical MM3 parameters have been published for many types of organic compounds: aliphatic [24] and aromatic [25] hydrocarbons, olefins [26], alkynes [27], alkyl radicals [28], alcohols and ethers [29], aldehydes and ketones [30], quinones [31], conjugated ketones [32], carboxylic acids and esters [33], furans and vinyl ethers [34], alkyl peroxides [35], saturated [36] and conjugated amines [37], aromatic N-heterocycles [38] and S-heterocycles [39], imines and diazenes [38], nitriles [27], hydrazines [40], amides and polypeptides [41], aliphatic and aromatic nitro compounds [42], azoxy compounds [43], sulfides [44], disulfides [45], alkyl iodides [46], silanes [47], and organogermanes [48]. Thermochemical predictions from MM3 are most reliable for functional groups that were parameterized using large sets of high-quality data, i.e.,

for the most common functional groups. In some cases the software automatically "guesses" values for missing parameters; the resulting predictions will be more approximate than usual. One should also be cautious about commingling results obtained using different software packages. The parameters are under continual development, so different software may use slightly different parameter values, yielding somewhat different results.

Traditionally, MM has been used for modeling stable molecules, predicting thermochemistry but not kinetics. The past few years have seen the emergence of force fields that are designed to accommodate bond breaking and bond formation [49–52]. These "reactive force fields" are still in the developmental stage, but it is hoped that they will prove useful for predicting reactivity, modeling transition states, and eventually predicting rate constants with reasonable reliability.

3 SEMIEMPIRICAL MOLECULAR ORBITAL THEORY

As in all molecular orbital theories, the fundamental computation in SEMOT is to determine the electronic wavefunction for the molecule of interest. Semiempirical approximations were developed of necessity, when computers were too slow for *ab initio* calculations to be chemically useful [53]. Although many of the approximations are severe, the use of empirical parameters was successful in restoring accuracy. In many cases, the resulting accuracy even exceeds that of simple *ab initio* calculations, since higher order effects are incorporated into the parameterization. Thus, semiempirical methods remain popular today despite the widespread availability of inexpensive, powerful computers.

The choice of fundamental approximation, combined with the choice of parameter values, defines a particular SEMOT method, analogous to a force field in MM. Several established and novel SEMOT methods have been reviewed and compared elsewhere [54]. Among the three popular SEMOT methods mentioned earlier, MNDO/d is least widely available in commercial software packages. The other two methods, AM1 and PM3, differ only in their parameterization. Since the PM3 method was parameterized more recently and more carefully, it is expected to be more reliable and will be the focus of discussion here. However, performance varies, so it should be compared with that of the experiment for related systems before putting faith in the predictions. Note that AM1 and PM3 predictions are included in the Computational Chemistry Comparison and Benchmark Database (CCCBDB), which is a convenient, on-line resource for comparing theoretical predictions with experimental data [55].

As in a MM calculation, the principal step is geometry optimization. Vibrational frequencies should be computed to verify that the final structure is an energy minimum and not a saddle point, i.e., all frequencies are real-valued. In most software packages, the final, minimized energy constitutes the predicted enthalpy of formation at 298.15 K. However, the units are typically kcal mol^{-1} (1 kcal $\approx$ 4.184 kJ) or even hartree (1 hartree $\approx$ 2625.5 kJ mol^{-1}).

As in any parameterized method, best performance is expected where there are ample experimental data available for developing robust parameter values. For exotic species not represented in the parameterization sets, predictions should be viewed with skepticism. In particular, results for transition states of chemical reactions are likely to be only qualitatively correct. In Fig. 1, the thermochemical errors of PM3 and AM1, as compared with experimental benchmarks, are plotted for ~200 compounds composed of the common "organic" elements C, H, N, and O. For this data set, the root-mean-square (rms) errors are 24 and 36 kJ mol^{-1} for PM3 and AM1, respectively. For comparison, the rms error is 10 kJ mol^{-1} for Benson's GA method. The data for Fig. 1 were taken from the CCCBDB [55].

PM3 requires 18 parameters per element (except only 11 parameters for hydrogen). The values of the parameters were generated by fitting a large set of experimental data for enthalpy of formation (or atomization),

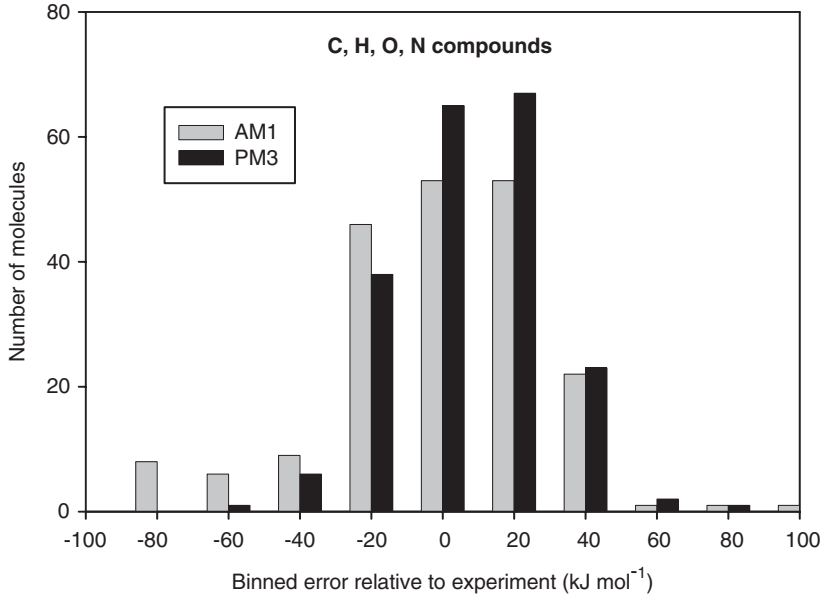

Fig. 1. Errors in SEMOT enthalpies of formation, $\Delta_f H_{298}$.

ionization energy, electric dipole moment, and molecular geometry. Thus, there are fewer adjustable parameters than for purely empirical methods, but still hundreds. Parameters are available for the elements H, C, O, N, S, F, Cl, Br, I, Al, Si, and P [18], for Be, Mg, Zn, Ga, Ge, As, Se, Cd, In, Sn, Sb, Te, Hg, Tl, Pb, and Bi [56], for Li [57], and for Na [58]. Note that the existence of parameters does not mean that the corresponding predictions will be reliable, since some are based on scanty or questionable data.

There are newer SEMOT methods that include d-orbitals as well as s- and p-orbitals, notably MNDO/d [17,59]. The d-type basis functions allow significant improvements for hypervalent compounds and compounds containing heavier elements [17,54]. Beware that not all SEMOT methods are intended for thermochemical predictions. For example, the PM3(tm) method is intended only for structural predictions [60].

4 MOLECULAR ORBITAL THEORY

In MOT the goal is compute the electronic wavefunction by solving the Schrödinger equation (i.e., non-relativistic quantum mechanics). Many textbooks are available on the topic. The classic text by Hehre *et al.* [61] emphasizes understanding and planning actual calculations. This is complemented by the theoretical approach taken by Szabo and Ostlund [62]. Unlike SEMOT, no empirical parameters are used. However, approximations are necessary to make the problem computationally tractable. The approximations can be classified as either physical or numerical. The most serious physical approximations involve the treatment of the electrostatic repulsion among the electrons. The principal numerical approximation is the choice of mathematical functions for describing the molecular orbitals. Popular approximations are described in this section.

4.1 Physical approximations

Nearly all calculations ignore relativistic effects, as mentioned earlier, and accept the Born–Oppenheimer approximation, which is that the nuclei are so much heavier than the electrons that they may be regarded as infinitely more massive. This separates the problems of determining the electronic and nuclear wavefunctions. For the electronic problem, the simplest physical approximation is embodied in Hartree–Fock (HF) theory. This is a mean-field approximation, in which each electron moves independently of the other electrons. Electrons influence each other only

through their average electric fields. Although this may sound crude, HF theory is powerfully predictive for many properties, including molecular structure and vibrational spectra. When applied cleverly, results are fairly good even for thermochemistry (Table 1). However, one of the best known weaknesses of HF theory is its failure to describe bond dissociation correctly. This is illustrated in Fig. 2, in the dotted curve labeled "RHF" (for "spin-restricted" HF). The experimentally derived bond energy is indicated by the horizontal dotted line, and is clearly exceeded by the RHF dissociation curve. This problem occurs because standard HF theory requires electrons to remain paired ("spin-restricted"), which tends to dissociate bonds heterolytically instead of homolytically. Although this is not usually important for thermochemical applications, it causes difficulty in calculations of transition states, which often contain stretched bonds.

One solution to this problem is to use "spin-unrestricted" (UHF) theory, in which electrons are no longer paired within orbitals. Each electron has its own spatial orbital, leading to a better description of bond dissociation (Fig. 2, dash-double-dotted curve labeled "UHF"). The UHF approach is sufficiently popular that it is the default for open-shell molecules (e.g., free radicals) in many software packages. However,

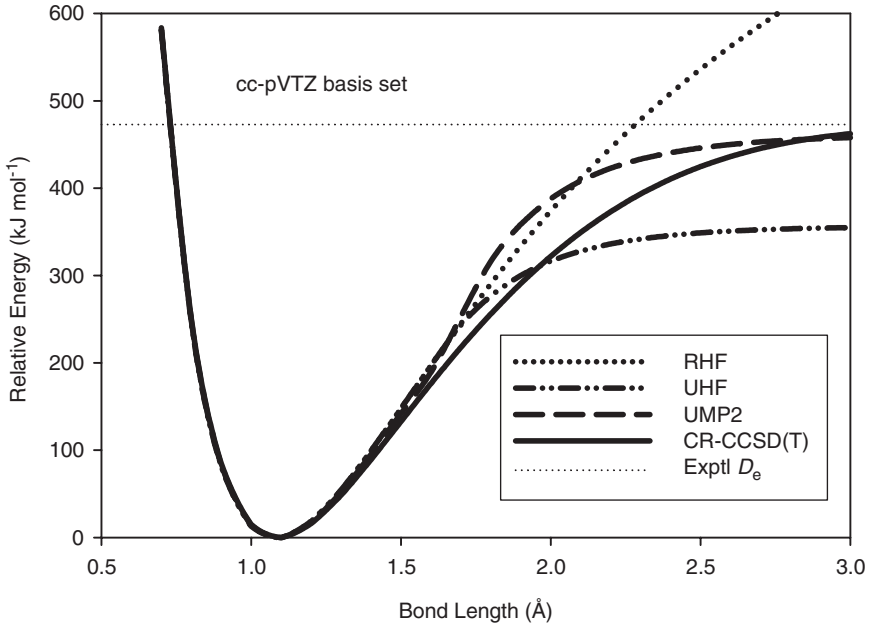

Fig. 2. Dissociation curve for CH_3–H.

it has drawbacks. Most importantly, UHF wavefunctions are subject to *spin contamination*, in which there are contributions from electronic states that have different numbers of unpaired electrons. Molecular properties may be distorted by these unwanted contributions. Spin contamination is identified by examining the expectation value of the spin operator $\hat{S}^2$, which is reported by most quantum chemistry software. For a wavefunction with well-defined spin, the value of this quantity is $\langle \hat{S}^2 \rangle = S(S+1)$, where S is the total electron spin on the molecule. For example, a radical with one unpaired electron should have $\langle \hat{S}^2 \rangle = (1/2)(3/2) = 3/4$. Poor values of $\langle \hat{S}^2 \rangle$ are a warning that the results may be less reliable than usual. As a rough guide, values that are wrong by more than 10%, or by more than 0.1, are often described as contaminated. In the example of Fig. 2, the total spin is $S = 0$, but $\langle \hat{S}^2 \rangle$ ranges from 0 (uncontaminated) at small bond length, to 0.14 (somewhat contaminated) where the UHF and RHF curves diverge, to 0.99 (badly contaminated) where the bond is stretched to 3.0 Å. Procedures for removing the effects of spin contamination are well established [63], but they are used surprisingly seldom.

Although the HF approximation is successful in many applications, it is usually inadequate for quantitative thermochemistry. Since it is a mean-field theory, it neglects the instantaneous repulsion between electrons, known as the *electron correlation*. Electron correlation is important in electron pairing and weak intermolecular forces. Thus, HF theory is inappropriate when electron pairs (such as bonding pairs) are broken apart, or when van der Waals interactions are important. More sophisticated theories include electron correlation in some manner. Most of these "correlated" theories are based on HF theory, so they are sometimes called "post-HF" theories. There are many. Only those most popular for thermochemical applications are described here.

The first step taken beyond the HF approximation is usually *perturbation theory*. In this approach, electron–electron repulsion is treated as a minor correction to the HF theory. However, it is often not minor at all, and perturbation theory may show poor convergence behavior [64,65]. Nonetheless, second-order perturbation theory ("MBPT2" or "MP2" theory, short for second-order "many-body perturbation theory" or "Møller–Plesset" theory) is the most economical post-HF method, often gives good results, and is popular. For example, the curve in Fig. 2 labeled "UMP2," indicating MP2 theory starting from a UHF reference, approaches the experimental dissociation energy more closely than the UHF curve does. The corresponding RMP2 curve, not shown in the figure, inherits excessive heterolytic character from its RHF reference and likewise increases unrealistically as the atoms are separated. Higher orders of

perturbation theory (e.g., MP4) are also available in many software packages, but are declining in popularity.

A popular alternative to perturbation theory is *coupled-cluster* theory. It has better convergence behavior and is more resistant to problems such as spin contamination. The lowest order theory that is popular is coupled-cluster with single and double excitations (CCSD). It is computationally expensive, comparable to MP4, and much greater than MP2. The quadratic configuration interaction with single and double excitations (QCISD) method was developed as a modification of configuration interaction theory (see below) but may also be considered a good approximation to CCSD. For the most accurate calculations typical of today, the energy is corrected in an approximate way for the triple excitations, yielding the CCSD(T) and QCISD(T) theories [66,67]. The most popular high-accuracy methods are based on QCISD(T) theory [68]. However, the most careful predictions of molecular thermochemistry generally employ CCSD(T) [69]. The excellent performance of CCSD(T) theory is illustrated by the solid curve in Fig. 2. The theory used here is a closed-shell variation, termed "completely renormalized," that was designed to avoid the dissociation problems of RHF and RMP2 [70].

An older method, now seldom used, is *configuration interaction*. Starting from the HF electron configuration, a large set of additional configurations is generated using a simple rule. The entire set of configurations is then used as a many-electron basis set to solve the many-electron equation (as opposed to the one-electron HF equations). The most common choice is configuration interaction with single and double excitations (CISD). CISD is seldom used because it is computationally expensive and not especially accurate. It also lacks size-consistency. This means, for example, that the energy for a doubled system is not equal to twice the energy for the single system. For example, the CISD/cc-pVTZ energy for He atom is -2.900232 hartree and the corresponding energy for two He atoms separated by 100 Å is -5.799862 hartree. Thus, the energy of the double system is 1.6 kJ mol^{-1} higher than twice the single system. For comparison, the discrepancies for HF, MP2, and CCSD are all zero to the precision of the calculations ($\sim 10^{-7}$ kJ mol^{-1}), since they are size-consistent. Since special care is required when using a model that is not size-consistent, such models are not popular for thermochemical applications.

A special CI calculation, called *full configuration interaction* (FCI), is the most accurate, and most expensive, for a given basis set. All possible electron configurations are included. This is equivalent to complete-order coupled-cluster theory. For an N-electron molecule, the FCI result is attained when Nth excitations are included in the CI or CC calculation. Unlike truncated CI, such as CISD, FCI is size-consistent. Continuing the

example above, the FCI/cc-pVTZ energies for He and He$\cdots$He (100 Å) are −2.900232 and −5.800464 hartree, respectively, which is size-consistent. The FCI and CISD energies for He are identical because CISD is the same as FCI for a two-electron system.

In post-HF calculations, the core electrons (e.g., $1s^2$ for C, $1s^22s^22p^6$ for Si) are usually left at the HF level, i.e., they are not correlated. This is called the *frozen-core* approximation. When desired, the contribution from core correlation is generally computed directly, although core-polarization potentials are effective [71,72] and parameterized estimation schemes are available [73].

Relativistic effects are sometimes important [74]. In thermochemistry, they appear most frequently as the spin–orbit splitting in atoms (or linear open-shell molecules), which is relevant for computations of atomization energies. For example, the chlorine atom has the valence electron configuration $3s^23p^5$, corresponding to the term symbol ^{2}P. In the absence of spin–orbit coupling, as in conventional MOT, this is sixfold degenerate. Spin–orbit coupling, however, splits this into $^2P_{3/2}$ (degeneracy = 4) and $^2P_{1/2}$ (degeneracy = 2) levels, whose energies differ by 10.6 kJ mol^{-1} [75]. The degeneracy-weighted average energy of the ^{2}P state is therefore $[4(0) + 2(10.6)]/6 = 3.52$ kJ mol^{-1} above the actual ground level ($^2P_{3/2}$). This averaged energy corresponds to that from the non-relativistic MOT calculation, which must therefore be corrected downward by 3.52 kJ mol^{-1}. Since this correction makes the atom more stable, the corresponding atomization energy or bond dissociation energy becomes smaller. Atomic energy levels are available in the classic compilation by Moore [75] and in the NIST Atomic Spectra Database (http://www.physics.nist.gov/cgi-bin/AtData/levels_form). The values of many such corrections have been tabulated in section II.C.2 of the CCCBDB [55] (section II.C.2).

Other, ''scalar'' relativistic effects are usually minor. Among them, the most important is the contraction of s-orbitals caused by the increase in electron mass due to high velocity near the nucleus. Except in the most careful work, such effects are modeled using relativistic effective core potentials (ECPs), also called core pseudopotentials [76]. When an ECP is used, the corresponding valence basis set should be used for the remaining electrons. A ''small-core'' ECP, in which fewer electrons are replaced by the effective potential, is a weaker approximation and therefore more reliable than the corresponding ''large-core'' ECP. The selection of basis sets to accompany ECPs is more restricted than the selection of all-electron basis sets, but appropriate correlation-consistent basis sets are available for heavy p-block elements [77–80].

A distinction is sometimes made between ''dynamical'' electron correlation, discussed above, and ''static'' or ''non-dynamical'' electron

correlation. The qualitative electronic structure of some molecules cannot be described well by HF theory, but requires a mixture of electron configurations. This mixture is intended to capture the non-dynamical correlation of the electrons. The most common examples are singlet diradicals, such as carbenes, which have two interesting electrons inhabiting two orbitals. One could draw a Lewis structure with both electrons in either orbital or put one electron in each orbital, but the most accurate picture is a mixture of these. Computationally, this is handled using a *multiconfiguration* (MCSCF) calculation instead of HF. Analogous to post-HF calculations are *multireference* (i.e., post-MCSCF) calculations, which also recover some of the dynamical correlation. The most economical multireference techniques are based on second-order perturbation theory, i.e., analogs of MP2 theory. Multireference configuration interaction (MRCI) is also used, but is far more expensive. Multireference techniques are not popular for thermochemical applications because they require substantial experience to apply reliably [81]. The easiest of such techniques is generalized valence-bond theory (GVB), which describes non-dynamical correlation within electron pairs [82]. Followed by localized perturbation theory (GVB-LMP2), it shows promise for precise thermochemistry at modest cost [83].

4.2 Numerical approximations

A theoretical model corresponds to a choice of physical approximations. Performing an actual calculation also requires numerical approximations. In particular, a *basis set* must be selected. This is the set of functions used to describe the molecular orbitals. A large basis set contains many *basis functions* and describes orbital shapes better than a small basis set. However, the improved accuracy of a larger basis set is counterbalanced by greater computational cost. The nomenclature and notation for basis functions may appear mysterious, but do have logical structure; some are described below.

A typical basis function is a fixed linear combination of simpler, *primitive* functions. Such a composite function is termed a *contracted* basis function. Each primitive basis function is centered at an atomic nucleus and has a Gaussian dependence on distance from that nucleus. Except for s-functions, it also has a Cartesian factor to describe its angular dependence. For example, a p_x primitive function looks like $x\exp(-\zeta r^2)$, where ζ (zeta) is the *exponent* of the Gaussian function. A p_x contracted function is a fixed linear combination of two or more primitive functions with different exponents.

The most popular of the older basis sets are those by Pople and coworkers. For example, the 6-31G(d) basis set, formerly labeled 6-31G*, is probably the most popular basis set in use [84]. It was originally developed for first-row atoms such as carbon. To understand the notation, notice that there is only one digit, "6," before the hyphen. This indicates that only one contracted function is used to describe the core (1s) orbital of the atom. The value of that digit (6) indicates that the contracted 1s-function is formed from six primitive functions. After the hyphen there are two digits, indicating that two basis functions describe each valence orbital (i.e., the 2s- and 2p-orbitals). Each of the inner (tighter) four functions (s, p_x, p_y, p_z) is composed of three primitive functions. Each of the outer four functions is only a single primitive, i.e., uncontracted. The vestigial "G" simply indicates that Gaussian functions are used. The trailing "(d)" or asterisk indicates that a single, primitive set of d-functions is added. The purpose of these *polarization* functions is to allow finer angular adjustments to the orbitals. For calculations on negatively charged ions, *diffuse* functions, with small exponents, are also added. If this is a set of primitive s- and p-functions, the result is denoted 6-31 + G(d). Larger basis sets have similar notation. For example, in the 6-311G(2df,p) basis, the valence orbitals are described by three functions (two of them uncontracted), there are two sets of d-functions and one set of f-functions added for polarization of first-row ("heavy") atoms, and there is one set of p-functions added for polarization of hydrogen atoms.

Although the language suggests otherwise, there is no restriction about which functions describe core orbitals and which describe valence orbitals. All functions are available to all orbitals. The language, as above, merely explains why certain numbers of functions were chosen.

For post-HF calculations, newer series of basis sets, by Dunning and coworkers [85], are increasingly popular. They are arranged in sequences that can be extrapolated to the large-basis limit, a valuable property in careful work. The smallest such basis set is denoted cc-pVDZ. The prefix "cc" stands for "correlation-consistent," indicating that the basis was designed for post-HF calculations (i.e., including electron correlation). The small "p" indicates that polarization functions are included. "VDZ" stands for "valence double-zeta," which means that each valence orbital is described using two basis functions. The term "zeta" refers to the Greek letter traditionally used to represent the Gaussian exponent (see above). The next basis set in the series is cc-pVTZ, for "valence triple-zeta," followed by quadruple (cc-pVQZ) and larger (cc-pV5Z, etc.). A number of specialized, parallel series have also been published. The most

important of these is the "augmented" series, aug-cc-pV*n*Z (*n* = D, T, Q, 5, …), which includes diffuse functions and is therefore appropriate for negative ions and weakly bound complexes. In precise work, the property of interest may be computed using a series of correlation-consistent basis sets and then extrapolated to the "complete basis" limit for the series [85]. Note that the basis sets for the 3p elements (Al–Ar) have been revised to include a set of tight d polarization functions; the new sets have labels like cc-pV(*n* + d)Z [86].

The ideal basis set is infinitely large, or mathematically "complete." The error introduced by using a finite basis is often termed "basis set truncation error." It is more serious for post-HF methods than for self-consistent methods such as HF and DFT (see below). This is because post-HF theories rely on good descriptions of unoccupied orbitals as well as occupied orbitals, and more functions are needed to describe the larger number of orbitals. Truncating the basis set raises the energy in a calculation, since it prevents orbitals from attaining their ideal shapes. One subtle consequence is known as *basis set superposition error* (BSSE), which is important to consider for weakly bound molecular complexes. BSSE is an artificial lowering of the energy that occurs when two molecules are brought together in a calculation. Since the basis set for each molecule is incomplete, its energy is lowered by the availability of the other molecule's basis functions. *Counterpoise* calculations, which can be done with all the common software packages, are used to correct for BSSE [87]. For typical thermochemical and kinetics calculations, BSSE is traditionally ignored. This tradition may be rationalized by observing that BSSE artificially lowers the energy, thus canceling part of the primary error from basis set truncation and improving the result [88,89].

A *minimal basis set* includes only one basis function per orbital. For example, a minimal basis for carbon has two s-functions (for the 1s- and 2s-orbitals) and one set of p-functions (for the 2p-orbitals). Computations with minimal basis sets are fast, but are not useful for quantitative work. However, they may be useful for obtaining a qualitative understanding of the electronic structure of a challenging molecule. In particular, unoccupied orbitals most closely resemble textbook diagrams when a minimal basis is used. The most popular minimal basis sets are labeled STO-3G and MINI.

Most of the basis sets in use can be downloaded, in formats tailored to popular software packages, from the website http://www.emsl.pnl.gov/forms/basisform.html. This valuable resource is maintained at the Environmental Molecular Sciences Laboratory (part of Pacific Northwest National Laboratory).

5 DENSITY FUNCTIONAL THEORY

HF and post-HF theories are concerned with computing the electronic wavefunction. In contrast, DFT focuses on the electron density [90]. The fundamental theorem of DFT states that the exact energy of the system can be expressed as a functional (i.e., a function of a function) of the electron density. Unfortunately, the functional itself remains unknown; much research is devoted to the development of improved functionals. For thermochemical applications, it is necessary to use "GGA" or "non-local" functionals, which depend explicitly on the gradient of the density ($\nabla\rho$) in addition to the density (ρ). "B3LYP" [91] is the most popular functional for thermochemistry. In this label, "B3" refers to a three-parameter exchange functional by Becke; the values of the parameters were determined by fitting to experimental thermochemical data [92]. "LYP" refers to a correlation functional by Lee, Yang, and Parr [93]. The terms "exchange" and "correlation" here refer to electron–electron repulsion between electrons of same and different spins, respectively. B3LYP is called a "hybrid" functional because it contains a contribution from HF exchange energy ("exact exchange").

Although the theorem of DFT is in terms of the total electron density, in practical calculations the density is described in terms of orbitals, which are solved self-consistently as in HF theory. The wild popularity of DFT is due to its low computational expense (comparable to HF) and generally good accuracy, even for "difficult" systems such as radicals that contain transition metal atoms. For high precision, however, DFT is inappropriate, since convergent series are unavailable. Current functionals do not include the dispersion interaction, which is necessary for describing weakly bound molecular complexes [94]. Thus, DFT methods should be avoided wherever van der Waals interactions are important.

Most molecular DFT software employs basis sets, as in MOT software. However, additional numerical integration is required, which is typically done on a spatial grid. The use of a grid is an additional numerical approximation. As expected, a finer grid produces a more precise result but increases the computational cost.

Many choices of functional are available and their number is increasing. Some are intended to excel for both thermochemistry and reaction barrier heights [95,96]. In applied work, it may be acceptable to test the performance of several functionals on a related, benchmark system, and then adopting the most successful functional for the prediction of interest. However, the "best" functional may be different for a different project.

6 THEORY AND BASIS SET: EXAMPLES

The combination of theory with basis set is often called a quantum chemistry *model* [61]. The standard notation for an energy calculation done using theory T1 and basis set B1 is "T1/B1." If the geometry was obtained from a T2/B2 calculation, the combination is denoted "T1/B1//T2/B2." This section includes examples intended to illustrate the sensitivity of different problems to the choice of *ab initio* method and basis set. In these examples, the core is frozen in all post-HF calculations. The software packages used were ACES II [97] for the larger coupled-cluster calculations, GAMESS [98] for the multireference calculations, and Gaussian [99] for the remaining calculations [20].

6.1 *Electron affinity of fluorine*

The electron affinity of the fluorine atom, EA(F), is the minimum energy required to achieve reaction (4). Although EAs are usually reported in units of electron volts ($1\,\mathrm{eV} \approx 96.485\,\mathrm{kJ\,mol^{-1}}$), $\mathrm{kJ\,mol^{-1}}$ is used here for consistency with later examples. The results from several *ab initio* computations are compiled in Table 2, after correcting for the spin–orbit splitting in the F atom ($1.611\,\mathrm{kJ\,mol^{-1}}$). The F^- ion is closed-shell and has no spin–orbit splitting. The theories are ordered by their expected accuracy [HF < MP2 ≈ B3LYP < CCSD < CCSD(T)]. The basis sets are ordered from smallest to largest, although this is not necessarily worst to best. However, the "worst" (i.e., most approximate) calculation is in the upper left corner, HF/6-31G(d); it predicts that the F atom will not bind an additional electron at all! Conversely, the "best" (i.e., least approximate) calculation is in the lower right corner, CCSD(T)/aug-cc-pVQZ (frozen-core); it is $3.8\,\mathrm{kJ\,mol^{-1}}$ below the experimental value.

$$F^- \rightarrow F + e^- \tag{4}$$

TABLE 2
Electron affinity of atomic fluorine (in $\mathrm{kJ\,mol^{-1}}$; $1\,\mathrm{eV} \approx 96.5\,\mathrm{kJ\,mol^{-1}}$) computed using a variety of theories and basis sets (including spin–orbit correction)

Basis set	HF	MP2	B3LYP	CCSD	CCSD(T)
6-31G(d)	−39.6	101.7	99.6	81.9	81.7
6-31 + G(d)	121.6	326.6	337.3	289.5	295.7
cc-pVTZ	47.7	229.5	227.6	198.1	203.2
aug-cc-pVTZ	113.7	349.6	338.9	302.6	317.9
aug-cc-pVQZ	112.3	356.6	338.6	307.8	324.4

The experimental value is $328.16493 \pm 0.00024\,\mathrm{kJ\,mol^{-1}}$ [127].

There is dramatic improvement from the 6-31G(d) to the 6-31 + G(d) basis set. The diffuse functions (" + ") provide the extra room needed by the additional electron in the negative ion. There is a similar improvement from cc-pVTZ to aug-cc-pVTZ for the same reason. Moving to aug-cc-pVQZ has a smaller effect because the additional functions are mostly in the tighter "valence" region.

There is also dramatic improvement when correlation is included (i.e., everything in Table 2 besides HF). Correlation is important whenever the number of electron pairs changes, as here. As discussed above, the HF and B3LYP results are less sensitive to the basis set than the post-HF methods (compare the aug-cc-pVTZ and aug-cc-pVQZ results). The strong dependence on both basis set and electron correlation makes EA(F) a "difficult" quantity to calculate. The most rigorously calculated value yet published is 328.32 kJ mol^{-1} [100], only 0.16 kJ mol^{-1} above the experimental benchmark.

6.2 *Bond dissociation energy in methane*

The bond dissociation energy in methane, $D_0(CH_3–H)$, is the minimum energy to achieve reaction (5). The results from several *ab initio* computations are compiled in Table 3. Vibrational zero-point energies (see Section 7) are included, and were computed using unscaled B3LYP/6-31G(d) frequencies. Geometries were also computed at the B3LYP/6-31G(d) level.

$$CH_4 \rightarrow CH_3 + H \tag{5}$$

There is weaker dependence on basis set than in the previous example because the spatial extent of the orbitals does not change as much in reaction (5) as in reaction (4). Including electron correlation is important because the number of electron pairs changes. The "best" calculation in

TABLE 3
Bond dissociation energy in methane, $D_0(CH_3–H)$ (in kJ mol^{-1}), computed using a variety of theories and basis sets [geometries and ZPEs from B3LYP/6-31G(d)]

Basis set	HF	MP2	B3LYP	CCSD	CCSD(T)
6-31G(d)	321.6	394.2	431.6	394.9	397.0
6-31 + G(d)	317.4	388.6	426.0	389.6	391.6
cc-pVTZ	316.6	422.0	425.2	420.8	425.0
aug-cc-pVTZ	315.9	422.4	423.5	421.2	425.3
cc-pVQZ	316.3	425.9	424.6	423.7	428.1

The experimental value is 432.4 ± 0.6 kJ mol^{-1} [113].

Table 3 is CCSD(T)/cc-pVQZ//B3LYP/6-31G(d); the corresponding result is 4.3 kJ mol^{-1} below the experimental value. The most rigorous published calculations [using experimentally derived zero-point energies (ZPEs)] provide $D_0 = 432.6\,\text{kJ mol}^{-1}$ [101], which is indistinguishable from the experimental value.

6.3 *Proton affinity of ammonia*

The proton affinity of ammonia, PA(NH_3), is the enthalpy change for reaction (6) at the temperature 298.15 K. The results from several *ab initio* computations are compiled in Table 4. Geometries and vibrational frequencies were obtained at the B3LYP/6-31G(d) level and used to compute ZPEs and enthalpy content (see Section 7). The electronic energy of H^+ is zero.

$$NH_4^+ \rightarrow NH_3 + H^+ \tag{6}$$

There is only mild dependence on basis set, since the contracted electron distribution of the cation is adequately described using the usual basis sets. Including electron correlation also makes little difference, since the number of electron pairs is unchanged. Thus, this is an "easy" quantity to calculate. Even the "worst" calculation in the table is only 24 kJ mol^{-1} higher than the experimental value. The "best" calculation is indistinguishable from the experimental value. The most rigorous published calculation (including anharmonic calculations of ZPE) yielded PA(NH_3) = $853.1 \pm 1.3\,\text{kJ mol}^{-1}$ [102] and is considered more reliable than the experimental measurements [103].

6.4 *Excitation energy of singlet O_2*

The excitation energy for the lowest singlet state of O_2, $T_e(^1\Delta_g)$, is the vibrationless energy required to excite O_2 from its ground state ($^3\Sigma_g^-$).

TABLE 4
Proton affinity of ammonia, PA(NH_3) (in kJ mol^{-1}), computed using a variety of theories and basis sets [geometries, ZPEs, and thermal functions from B3LYP/6-31G(d)]

Basis set	HF	MP2	B3LYP	CCSD	CCSD(T)
6-31G(d)	875.2	874.7	874.2	878.9	878.5
6-31 + G(d)	863.5	854.0	852.9	859.9	858.5
cc-pVTZ	875.0	859.8	859.9	866.7	864.0
aug-cc-pVTZ	869.0	847.0	849.6	855.7	851.8
aug-cc-pVQZ	869.4	846.9	850.1	856.1	852.0

The experimental value is $851 \pm 3\,\text{kJ mol}^{-1}$ [128].

Although spectroscopic quantities are usually reported in units of wavenumbers ($83.59\,cm^{-1} \approx 1\,kJ\,mol^{-1}$), $kJ\,mol^{-1}$ is used here for consistency with earlier examples. The results from several *ab initio* computations are compiled in Table 5. Geometries were optimized for each calculation, except that cc-pVQZ energies were calculated at aug-cc-pVTZ geometries and Davidson-corrected energies were computed at the corresponding uncorrected (i.e., SOCI) geometries. The first five theories listed in Table 5 are familiar from the previous examples: HF, DFT, and post-HF. Comparing them reveals strong dependence on the correlation treatment but almost no dependence on basis set. However, even CCSD(T) is not enough for this problem; multireference approaches are required.

The last four rows in Table 5 are multireference theories. CASSCF is the most popular version of MCSCF, in which all configurations are included without any selection or filtering. The parenthetical modifier (8,6) indicates that eight electrons populate the "active space" of six orbitals. This particular choice corresponds to all the 2p electrons and orbitals. Including the non-dynamical correlation (comparing HF and CASSCF) is more important than including the dynamical correlation [comparing HF and CCSD(T)] for this problem. This is expected because the singlet state of O_2 is essentially a diradical. The computational cost of these CASSCF calculations is comparable to HF and DFT, and the results are good even without dynamical correlation.

Dynamical correlation can be added to the CASSCF reference as to single-reference HF. "MCQDPT2" is one variety of second-order perturbation theory, "SOCI" is analogous to CISD, and "SOCI + Q" includes the renormalized Davidson correction [104–106] for higher

TABLE 5
Excitation energy of dioxygen, $T_e(O_2\ ^1\Delta_g)$ (in $kJ\,mol^{-1}$; $1\,kJ\,mol^{-1} \approx 83.6\,cm^{-1}$), computed using a variety of theories and basis sets

Theory	6-31G(d)	6-31 + G(d)	cc-pVTZ	aug-cc-pVTZ	cc-pVQZ
HF	222.9	223.4	223.6	223.9	224.1
MP2	130.9	127.6	123.6	121.3	119.9
B3LYP	164.4	161.5	162.1	160.8	161.4
CCSD	141.1	140.6	137.9	137.5	136.6
CCSD(T)	128.6	128.2	125.1	124.5	123.8
CASSCF(8,6)	85.9	85.3	86.7	86.6	86.9
MCQDPT2(8,6)	102.0	102.0	98.9	98.2	97.5
SOCI(8,6)	97.8	97.2	93.7	93.2	92.2
SOCI(8,6) + Q	99.4	99.0	95.4	94.9	93.9

The experimental value is $94.722\,kJ\,mol^{-1}$ [129].

excitations and size-consistency. Comparing the post-CASSCF methods with CASSCF shows that dynamical correlation actually contributes little to the singlet excitation energy, contrary to the inference from the single-reference calculations.

Thus, this is an example of a problem that is "hard" only because non-dynamical correlation is important. The effects of basis set truncation and dynamical correlation are minor. (However, they are important if one is interested in bond lengths instead of excitation energies.) The most rigorous calculation yet published yielded $T_e = 93.6\,\mathrm{kJ\,mol^{-1}}$ [107], $\sim 1.1\,\mathrm{kJ\,mol^{-1}}$ below the experimental value.

7 THERMOCHEMISTRY FROM *AB INITIO* CALCULATIONS

Unlike MM or SEMOT software, *ab initio* software does not report enthalpies of formation. Instead, the user is responsible for choosing, performing, and combining appropriate computations. Assuming that the target quantity is the enthalpy of formation of molecule M, the following are the basic steps:

1. Write a balanced chemical reaction involving M, in which the enthalpies of formation of all other species are known reliably.
2. Optimize the geometries of all molecules in the reaction using an adequate model. B3LYP/6-31G(d) is a common choice for production work.
3. Compute the vibrational frequencies of all molecules using the same model as was used to obtain the geometries. Vibrational frequencies are frequently scaled by an empirical correction factor before use [108].
   a. Check for imaginary-valued (often printed as negative-valued) vibrational frequencies. For a stable molecule, there should be none. There should be exactly one for a transition structure.
   b. The ZPE equals one-half the sum of the vibrational frequencies (in the harmonic-oscillator approximation).
   c. Compute the thermodynamics functions $H(T)$ and possibly $S(T)$ for each molecule. The rigid-rotor/harmonic-oscillator (RRHO) approximation is usually used to compute partition functions. Include electronic degeneracies and low-lying excited states if needed.
   d. It is usually an error to compute vibrational frequencies at a geometry that is not a stationary point (e.g., energy minimum or transition structure) for the theoretical model being used.

4. Compute the electronic energies of all molecules at their optimized geometries. Choose a model that balances your requirements for accuracy and computational economy. B3LYP/6-31G(d) is a common choice for production work. CCSD(T)/aug-cc-pVTZ or CCSD(T)/cc-pVTZ is a good choice for more precise work.
   a. Add the ZPE for each species to its electronic energy to produce a zero-temperature energy.
   b. Add the ideal-gas enthalpy content (i.e., integrated heat capacity) to the energy of each species to produce an enthalpy. For example, for $T = 298.15\,\mathrm{K}$, add $\Delta_0^{298.15}H \equiv H(298.15) - H(0) = \int_0^{298.15} C_\mathrm{p}(T)\mathrm{d}T$.
5. Compute the enthalpy change for the reaction.
6. From the auxiliary data collected in step 1 and the reaction enthalpy from step 5, compute the enthalpy of formation of M at the selected temperature.

There are methods that automate some of these steps. They are called "composite" methods because they combine results from several calculations to estimate the result that would be obtained from a more expensive calculation. The most popular families of composite methods are represented by Gaussian-3 (G3) theory [68,109] and CBS-APNO theory [110,111], where CBS stands for "complete basis set." Both families of methods, which are considered reliable, include empirical parameters. The CBS theories incorporate an analytical basis set extrapolation based on perturbation theory, which is in contrast to the phenomenological extrapolation mentioned above. When the Gaussian software is used to perform these calculations, steps 2–4, above, are performed automatically, with the result labeled "G3 enthalpy" (or the like) in the output file [20,99]. The user must still choose a reaction (step 1) and manipulate the molecular enthalpies (steps 5 and 6). The most precise composite methods are the Weizmann-*n* methods, which however are very intensive computationally [112].

Many choices must be made during steps 1–6, above. The choice in step 1, often the most important, involves a balance among user convenience and time, computational cost, and accuracy. A good reaction will cause systematic errors in the calculations to cancel, but will require the user to find auxiliary thermochemical data and run calculations on additional molecules. In contrast, a convenient reaction will require only handy reference data and small auxiliary calculations. The most convenient choice of reaction is atomization. However, the most reliable results are usually obtained using a reaction that is both *isogyric*

(spin-conserving) and *isodesmic* (conserving of bond types such as C–C and C=C).

As an example, consider the gas-phase enthalpy of formation of cyclopentene oxide (C_5H_8O) at 298.15 K. The fastest calculations are the empirical methods. Unfortunately, the GA estimate is frustrated by missing ring-strain parameters. Molecular mechanics (MM3) yields $\Delta_f H^\circ_{298.15} = 2\ \text{kJ mol}^{-1}$. As a check, the PM3 prediction is $-71\ \text{kJ mol}^{-1}$. The PM3 result is probably more reliable, but the severe disagreement with the empirical estimate reduces confidence. Both these calculations were done using commercial software [19,20].

More confidence can be obtained from *ab initio* calculations. We will compare four choices of working reaction (step 1, above): atomization (reaction (7)), hydrogenation (reaction (8)), and two isodesmic reactions (reactions (9) and (10)). Reliable thermochemical data are required for all auxiliary species in each reaction, and are most conveniently obtained from data compilations [8,113–117]. Data for reactions (7)–(10) are collected in Table 6. The ideal reaction will effect a cancellation of errors in the various molecular calculations, leading to an accurate value for the enthalpy change. Good reactions often have small enthalpy changes.

$$C_5H_8O \rightarrow 5C + 8H + O \tag{7}$$

$$C_5H_8O + 7H_2 \rightarrow 5CH_4 + H_2O \tag{8}$$

(9)

(10)

For this example, we choose to compute geometries and vibrational frequencies (steps 2 and 3) at the B3LYP/6-31G(d) level. All vibrational frequencies of each molecule (ignoring the six translational and rotational "modes") are real-valued, confirming that the structures are properly optimized. The vibrational frequencies are scaled by 0.9806 for the computation of ZPEs, as recommended [108]. They are not scaled in the computation of the enthalpy function.

Calculations are needed for every species. For example, for H_2O the B3LYP/6-31G(d)-optimized structure has rotational constants of 787.96, 431.85, and 278.96 GHz ($1\ \text{GHz} \approx 0.033356\ \text{cm}^{-1}$) and an electronic energy of -76.408953 hartree. The structure also has an external symmetry number $\sigma = 2$, which affects the entropy. The computed vibrational frequencies are 1713.1, 3724.3, and 3846.6 cm^{-1} (unscaled), so the scaled ZPE is $4552.0\ \text{cm}^{-1} = 54.45\ \text{kJ mol}^{-1}$. The enthalpy function

TABLE 6
Auxiliary gas-phase enthalpies of formation (at 298.15 K) for reactions (7)–(10)

Species	$\Delta_f H^\circ_{298.15}$	Reference
C	716.68 ± 0.45	[114]
H	217.998 ± 0.006	[114]
O	249.18 ± 0.1	[114]
H_2	0	[113]
CH_4	−74.6 ± 0.3	[113]
H_2O	−241.83 ± 0.04	[114]
C_2H_6	−84.0 ± 0.4	[113]
Cyclopentane	−76.4 ± 0.7	[8]
Ethylene oxide	−52.6 ± 0.8	[8]
Cyclopropane	53.3 ± 0.5	[8]
Bicyclo[3.1.0]hexane	38.3 ± 0.6	[8]

Values are in kJ mol^{-1}. Error limits are believed to represent the standard uncertainties.

(or integrated heat capacity), assuming the RRHO model, is given by equation (11) for non-linear molecules without low-lying excited states, where the three terms are the contributions from translation, rotation, and vibrations, respectively. The reduced vibrational frequencies are $x_i \equiv h\nu_i/kT$. Such calculations may be done conveniently using the Perl script thermo.pl, which is included in the software supplement to this book and is available at the website http://www.nist.gov/compchem/. As input, this small program will accept either a Gaussian [20] output file or a keyword-driven input file. The rotational constants listed above, plus the molecular mass and the unscaled vibrational frequencies, lead to an ideal-gas enthalpy content $\Delta_0^{298.15}H = 9.92$ kJ mol^{-1}.

$$H(T) - H(0) = \left[\frac{5}{2}RT\right] + \left[\frac{3}{2}RT\right] + \left[RT\sum_i \frac{x_i\, e^{-x_i}}{1 - e^{-x_i}}\right] \qquad (11)$$

These calculations are repeated for all the species in reactions (7)–(10). For the atoms, experimental energy levels are used for computing the enthalpy functions [75,118] and the spin–orbit corrections [55]. The calculations are routine, except for the geometry optimization for cyclopentane, which is difficult because of the floppy ring. In the Gaussian program, the ''ultrafine'' DFT integration grid may be needed in such cases. For consistency with the other molecules, the default grid should be used for calculating the electronic energy. Also note that energies obtained using different software packages may not be interchangeable, especially for open-shell molecules or for DFT.

Some of the computed vibrational frequencies are significantly lower than kT ($\approx 207\,\mathrm{cm}^{-1}$ at 298.15 K); in precise work an anharmonic model would be required for such vibrations. The computed electronic energies, ZPEs, enthalpy contents, and spin–orbit corrections (which are subtracted from the electronic energies) are listed in Table 7 for all species in reactions (7)–(10).

Tables 6 and 7 are sufficient for computing the enthalpy of formation of cyclopentene oxide by using all four working reactions. This is done by requiring that the reaction enthalpy, as computed from enthalpies of formation, be equal to the reaction enthalpy obtained from the *ab initio* calculations. The predictions from reactions (7)–(10), along with intermediate results, are listed in Table 8. Each quantity in the table, except for the experimental uncertainty, is determined simply as the product values minus the reactant values. That is, the change in a quantity E is given by $\Delta E = \Sigma_i \chi_i E_i$, where E_i is the quantity for the ith species and χ_i the corresponding stoichiometric coefficient (positive for products, negative for reactants). For the experimental uncertainty, the aggregate uncertainty u is given by $u^2 = \Sigma_i (\chi_i u_i)^2$, where u_i is the experimental uncertainty for the ith species. This expression is strictly valid only when the uncertainties u_i are uncorrelated with each other. This does not include uncertainties in the theoretically calculated quantities, which are often large. Unfortunately, quantifying such theoretical bias is still a nascent research topic and beyond the scope of this chapter [119].

TABLE 7
Computed electronic energies, ZPEs (scaled by 0.9806), ideal-gas enthalpy content, and experimental spin–orbit corrections for the species in reactions (7)–(10)

Species	Energy (hartree)	ZPE ($\mathrm{kJ\,mol^{-1}}$)	$\Delta_0^{298.15}H$ ($\mathrm{kJ\,mol^{-1}}$)	Spin–orbit ($\mathrm{kJ\,mol^{-1}}$)
C	−37.846280	0.00	6.54	0.354
H	−0.500273	0.00	6.20	0
O	−75.060623	0.00	6.73	0.933
H_2	−1.175482	26.10	8.68	0
CH_4	−40.518389	116.40	10.00	0
H_2O	−76.408953	54.45	9.92	0
C_2H_6	−79.830417	193.70	11.58	0
Cyclopentane	−196.557086	364.07	16.11	0
Ethylene oxide	−153.786262	148.44	10.74	0
Cyclopropane	−117.895208	210.53	11.29	0
Bicycle[3.1.0]hexane	−234.630800	379.02	16.00	0
Cyclopentene oxide	−270.532342	316.49	15.47	0

B3LYP/6-31G(d) model. 1 hartree $\approx 2625.5\,\mathrm{kJ\,mol^{-1}}$.

TABLE 8
Ideal-gas values of $\Delta_f H^\circ_{298.18}$ for cyclopentene oxide, along with intermediate quantities from the calculations

Reaction	Experimental uncertainty	ΔE(electronic)	Δ(ZPE)	$\Delta(\Delta_0^{298.15} H)$	ΔE(spin–orbit)	$\Delta_f H^\circ_{298.18}$
(7)	2.3	5876.2	−316.5	73.6	−2.7	−54.0
(8)	1.5	−630.6	137.3	−16.3	0.0	−105.2
(9)	1.1	51.0	2.3	−0.2	0.0	−98.1
(10)	1.1	27.5	0.4	0.0	0.0	−95.6

B3LYP/6-31G(d) model. All quantities in kJ mol^{-1}.

Table 9 shows the results obtained using a variety of combinations of theory and basis set. In the table, B3LYP/6-31G(d) geometries and vibrational frequencies (scaled by 0.9806 for ZPEs [108]) were used for everything except HF, for which the corresponding HF/6-31G(d) results (frequencies scaled by 0.9135 for ZPEs and by 0.8905 for enthalpy [108]) were used. The bottom rows show the results obtained using a few composite methods [CBS-4M [111], CBS-Q [110], G3(MP2) [120], and G3 [68]]. These methods are relatively expensive computationally, but have been parameterized for improved accuracy. Most importantly, they are available as keywords in the Gaussian software and require little effort by the person doing the computations [20]. The final "enthalpy" printed at the end of the output file includes electronic energy, ZPE, and enthalpy content. Such "enthalpies" can be combined immediately to obtain reaction enthalpies at the specified temperature. This convenience often makes such a "canned" method a good choice.

The purpose of Table 9 is to illustrate how the conclusion depends on the choice of theory, basis set, and working reaction. For reference, the experimental enthalpy of formation is -97.1 ± 7.0 kJ mol^{-1} [114]. Across the range of models from HF/6-31G(d) to CCSD(T)/cc-pVTZ (the upper part of the table), values for the enthalpy of formation obtained by using atomization (reaction (7)) vary enormously, by 1595 kJ mol^{-1}. Atomization, which breaks most of the important electron pairs, is clearly a poor choice of working reaction, except with the better, parameterized, composite techniques [G3(MP2), CBS-Q, and G3]. The scatter among the values obtained by using hydrogenation (reaction (8)) is much smaller, at 216 kJ mol^{-1}, but even the parameterized methods give rather disappointing results. An undesirable feature common to reactions (7) and (8) is their large stoichiometric coefficients, which amplify errors associated with the atoms and small molecules.

Isodesmic reactions (9) and (10), in contrast, give results that depend only weakly on the choice of theory and basis set. Their ranges are only

TABLE 9
Ideal-gas values of $\Delta_f H^\circ_{298.18}$ for cyclopentene oxide, as computed using a variety of working reactions, theories, and basis sets

Theory	Basis	Reaction (7)	Reaction (8)	Reaction (9)	Reaction (10)
HF	6-31G(d)	1501	1	−94	−96
	6-31 + G(d)	1534	13	−93	−95
	6-311G(d,p)	1531	6	−95	−96
	cc-pVTZ	1501	4	−93	−95
B3LYP	6-31G(d)	−54	−105	−98	−96
	6-31 + G(d)	4	−67	−95	−94
	6-311G(d,p)	−10	−66	−97	−97
	cc-pVTZ	−31	−55	−94	−95
MP2	6-31G(d)	270	−198	−103	−93
	6-31 + G(d)	293	−182	−99	−93
	6-311G(d,p)	133	−134	−98	−91
	cc-pVTZ	−61	−113	−97	−90
CCSD	6-31G(d)	434	−168	−98	−94
	6-31 + G(d)	463	−151	−96	−94
	6-311G(d,p)	317	−95	−94	−92
	cc-pVTZ	151	−71	−94	−91
CCSD(T)	6-31G(d)	370	−203	−100	−94
	6-31 + G(d)	398	−187	−97	−94
	6-311G(d,p)	236	−123	−96	−92
	cc-pVTZ	56	−96	−95	−91
Range above		1595	216	10	7
CBS-4M composite		−124	−116	−94	−89
G3(MP2) composite		−90	−126	−96	−90
CBS-Q composite		−101	−138	−107	−98
G3 composite		−92	−102	−97	−91

All quantities are in $kJ\,mol^{-1}$.

10 and 7 $kJ\,mol^{-1}$, respectively, comparable with the uncertainty of the experimental value. For a rapid estimate, Table 9 suggests that a simple HF/6-31G(d) calculation, possibly checked with a B3LYP/6-31G(d) calculation, is adequate when using a well-balanced isodesmic reaction. The cost of these calculations is minimal. However, one must spend the time to find the auxiliary thermochemical data, compute the ZPEs, and compute the enthalpy content. These computations add to the burden on the user and provide opportunities for arithmetic errors. Fortunately, one can save time by a simple shortcut. Since reactions (9) and (10) are chemically well balanced, their reactants and products are expected to have similar ZPEs and enthalpy contents. Indeed, using our B3LYP

values, $\Delta\mathrm{ZPE} = 2.3$ and $0.4\,\mathrm{kJ\,mol^{-1}}$ for reactions (9) and (10), respectively, and $\Delta(\Delta_0^{298.15}H) = -0.2$ and $0.0\,\mathrm{kJ\,mol^{-1}}$. Thus, the shortcut is to ignore the ZPE and enthalpy content for well-balanced reactions, which means that vibrational frequencies are unneeded. In our example, if we used HF/6-31G(d) geometries and energies, neglecting ZPE and enthalpy content, we would infer $\Delta_\mathrm{f}H_{298.15} = -92$ and $-95\,\mathrm{kJ\,mol^{-1}}$ by using reactions (9) and (10), respectively. These results agree with the experimental value and with each other.

If a reaction is sufficiently well balanced, its enthalpy change will be close to zero. For reactions (7)–(10), the experimental enthalpies of formation imply gas-phase reaction enthalpies (298.15 K) of 5674 ± 7, -518 ± 7, 52 ± 7, and $30 \pm 7\,\mathrm{kJ\,mol^{-1}}$, respectively. All quantum calculations can be avoided by *assuming* the reaction enthalpy to be zero for a well-balanced reaction. This is the basis of empirical methods such as Benson's group-additivity scheme [5,6]. Where adequate auxiliary data are available, a group-balanced reaction is an excellent choice for quantum chemistry calculations [121].

7.1 Temperatures besides 298.15 K

Many compilations of standard, gas-phase enthalpies of formation provide values only at the temperature 298.15 K. Values are often needed at other temperatures. Quantum chemistry can be helpful by providing the enthalpy functions needed to make temperature corrections. The following thermodynamic cycle shows how these values are used. The corresponding expression is equation (12), where the symbol $\Delta^T_{298.15}$ denotes the change in a quantity associated with a temperature change from 298.15 K to T.

$$\Delta_\mathrm{r}H_T = \Delta_\mathrm{r}H_{298.15} + \Delta^T_{298.15}H(\mathrm{products}) - \Delta^T_{298.15}H(\mathrm{reactants}) \tag{12}$$

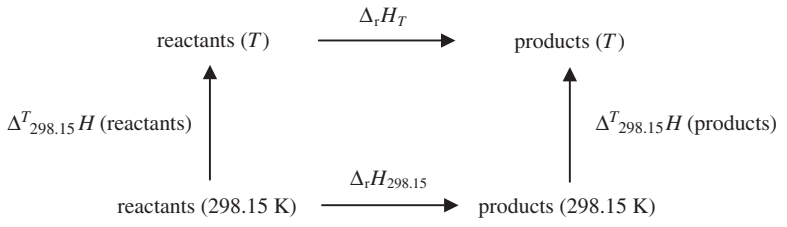

For example, consider the gas-phase enthalpy of formation of vinyl bromide (C_2H_3Br) at 900 K. The *NIST WebBook* provides a value only

at 298.15 K: $\Delta_f H_{298.15} = 79.2 \pm 1.9\,\mathrm{kJ\,mol^{-1}}$ [114]. This is the enthalpy change for the formation reaction, reaction (13).

$$2\mathrm{C(graphite)} + \frac{3}{2}\mathrm{H_2} + \frac{1}{2}\mathrm{Br_2} \rightarrow \mathrm{C_2H_3Br} \tag{13}$$

To apply equation (12), we require each species' change in enthalpy content, $\Delta^{900}_{298.15}H$. Values for the elements in their standard states can be obtained from reference books. For C(graphite), H_2, and Br_2, the values are $\Delta^{900}_{298.15}H = 9.672$, 17.676, and $53.286\,\mathrm{kJ\,mol^{-1}}$, respectively [115]. The large value for Br_2 reflects a phase change between 298.15 and 900 K. For C_2H_3Br, we can use the RRHO approximation with vibrational and structural parameters. Although experimental values of the vibrational frequencies and structure may be available, it is often more expedient to compute them. Here we choose inexpensive HF/6-31G(d) calculations. This yields $\Delta^{900}_{298.15}H = 45.88$ or $48.62\,\mathrm{kJ\,mol^{-1}}$ using unscaled or scaled (0.89) frequencies, respectively (computed using the script thermo.pl). Since scaling tends to help [108], we use the latter value. Substituting all values into equation (12) provides $\Delta_f H_{900}(\mathrm{C_2H_3Br}) = 55.3\,\mathrm{kJ\,mol^{-1}}$, with an uncertainty of a few $\mathrm{kJ\,mol^{-1}}$.

8 RECOGNIZING TROUBLE, *AB INITIO*

Despite following procedures correctly and avoiding overt mistakes, one may obtain incorrect results from *ab initio* calculations. Unfortunately, the mistake is often discovered only after it has caused some confusion, inefficiency, embarrassment, or other damage. There are tests that can expose problems earlier, thus avoiding trouble.

Prior experience is a good guide. A small database of known problems is available on-line, at http://srdata.nist.gov/sicklist/ [122]. It lists molecules for which particular *ab initio* models give poor results. In many cases, solutions to the problems are also listed.

For empirical (GA, MM) and SEMOT approaches, one must beware of missing or estimated parameter values, which can only yield crude results. Some software will estimate parameters without printing prominent warning messages. Some parameters values may be derived from limited or tentative reference data, but are not always identified by the software.

Molecules in which electronegative, 2p-block elements (N, O, F) are bonded to each other are often problematic for HF and post-HF methods, since dynamical correlation is unusually important. Fortunately, DFT methods are often successful in such cases. Transition metals often have substantial correlation (both dynamical and non-dynamical) and

spin–orbit effects. Coordinatively unsaturated transition metal compounds are probably the most challenging for computational modeling of any type. Although DFT is sometimes regarded as a safe way to treat such systems, there are many exceptions, and one must be cautious.

The RRHO model is popular for computing entropy, heat capacity, etc., because it is simple. When there are low vibrational frequencies, with $h\nu/kT < 1$, the RRHO approximation can become poor. An anharmonic vibrational model may be required, such as for hindered or free rotors (e.g., methyl groups). For a free rotor (barrier $\ll kT$), $\Delta_0^T H = (1/2)RT$. For a hindered rotor, one generally consults the tables by Pitzer and Gwinn [123,124]. Sometimes a working reaction can be contrived to balance anharmonic effects, minimizing their net effect and allowing them to be neglected.

For open-shell molecules, spin contamination can be a problem, as mentioned earlier. DFT and coupled-cluster theory are resistant to spin contamination and may be helpful. One may also choose spin-restricted open-shell HF (ROHF) as a starting point, instead of UHF, unless dissociation behavior is important. ROHF has no spin contamination.

Most users prefer to avoid multireference calculations, since they are more complex, require more judgment, and are more difficult to execute than single-reference calculations. However, as in the example of singlet O_2, above, some molecules have important non-dynamical correlation and require a multireference calculation. Fortunately, there are some simple ways to predict when such effects will be important.

First, draw a Lewis structure for the molecule of interest. If this is difficult or produces a strange-looking diagram, then non-dynamical correlation may be important. For example, a possible Lewis structure for ozone, a spin singlet, is shown here. To provide each atom with an octet of electrons requires a charge of $+1$ on the central atom. Since oxygen is electronegative, a positive charge is unusual in a neutral molecule. Thus, one might suspect non-dynamical correlation to be important. However, the Lewis structure for singlet O_2 is unremarkable.

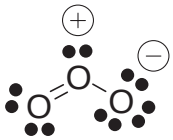

A more reliable test is to check for low-lying excited states. Sometimes this is known experimentally, but even simple calculations can provide the qualitative results needed here. Among SEMOT methods, the INDO/S (or ZINDO) method [125,126] is most popular for predicting valence

TABLE 10
Excitation energy of dioxygen, $T_e(O_2\ ^1\Delta_g)$ (in kJ mol^{-1}), computed using a variety of basis sets and spin-unrestricted theories

Theory	6-31G(d)	6-31 + G(d)	cc-pVTZ	aug-cc-pVTZ	cc-pVQZ
UHF	75.5	76.5	72.7	73.1	72.9
UMP2	48.8	48.3	45.7	45.3	123.8
UB3LYP	43.7	43.5	42.1	42.1	41.9
UCCSD	50.0	50.4	49.5	49.6	49.1
UCCSD(T)	42.5	42.6	42.7	41.0	42.6
$\langle S^2 \rangle_{UHF}$	*1.019*	*1.023*	*1.023*	*1.026*	*1.025*

The experimental value is 94.722 kJ mol^{-1} [129]. Expectation values $\langle S^2 \rangle$ are from the UHF calculations for the singlet, and would equal zero in the absence of spin contamination.

excitation energies. Among *ab initio* methods, the singles-only configuration interaction (CIS) method is least expensive. Time-dependent HF or DFT theory is increasingly popular. Using the B3LYP/6-31G(d) geometry, the lowest singlet excitation energy for ozone is computed to be 110, 210, and 200 kJ mol^{-1} using the ZINDO, CIS/6-31G(d), and TD-B3LYP/6-31G(d) models, respectively. Likewise, for singlet O_2, these calculations predict the next singlet state to lie at -40 kJ mol^{-1} (i.e., below the closed-shell singlet state), -50, and 0.1 kJ mol^{-1}, respectively. Although no threshold has been established for how high the excitation energy must be for single-reference theory to be reliable, values below 300 kJ mol^{-1} are low enough to dictate caution. Thus, both ozone and singlet O_2 are expected to require multireference calculations.

Finding an "excited" state at lower energy than the "ground" state, as for singlet O_2, above, should be disturbing. It frequently indicates that the HF calculation has produced an *unstable* wavefunction. Many software packages can check for a variety of HF instabilities. For singlet states, the most common is an RHF-to-UHF instability. For example, using a UHF wavefunction for singlet O_2, instead of RHF, results in a lower energy. Repeating the post-HF calculations of Table 5, but using unrestricted theory for the singlet, results in the values shown in Table 10. Whereas the spin-restricted calculations placed the singlet state too high, the spin-unrestricted calculations place it too low. As listed in the table for the HF calculations, spin contamination is severe; $\langle S^2 \rangle$ should equal zero for a singlet, but exceeds 1.0 in these calculations.

9 SUMMARY

There are several computational approaches for predicting gas-phase, molecular thermochemistry. For common organic compounds, empirical

methods are quick to compute and have been effectively parameterized. For uncommon compounds, the relative robustness of *ab initio* methods compensates their moderate or high computational cost. Intermediate situations may be addressed using SEMOT.

When using *ab initio* methods for predicting thermochemistry, a good choice of working reaction provides dramatically improved reliability. At the opposite extreme, atomization reactions are only compatible with high-level, composite, parameterized methods. Some simple guidelines are helpful for designing good working reactions and identifying molecules for which *ab initio* methods may perform poorly.

REFERENCES

[1] M.E. Minas da Piedade, ed. *Energetics of Stable Molecules and Reactive Intermediates*. Kluwer Academic, Dordrecht, 1999.
[2] K.M. Ervin, *Chem. Rev.*, **101** (2001) 391.
[3] K.M. Ervin, *Chem. Rev.*, **102** (2002) 855.
[4] S.J. Blanksby, G.B. Ellison, *Acc. Chem. Res.*, **36** (2003) 255.
[5] S.W. Benson, N. Cohen, Current status of group additivity, in: K.K. Irikura, D.J. Frurip (eds.), *Computational Thermochemistry: Prediction and Estimation of Molecular Thermodynamics, ACS Symposium Series 677*. American Chemical Society, Washington, DC, 1998, p. 20.
[6] N. Cohen, S.W. Benson, *Chem. Rev.*, **93** (1993) 2419.
[7] S.E. Stein, R.L. Brown, Structures and Properties Group Additivity Model, in: W.G. Mallard, P.J. Linstrom (eds.), *NIST Chemistry WebBook, NIST Standard Reference Database Number 69*. National Institute of Standards and Technology, Gaithersburg, MD, 2003.
[8] J.B. Pedley, *Thermochemical Data and Structures of Organic Compounds*, Volume 1. Thermodynamics Research Center, College Station, TX, 1994.
[9] R.S. Drago, N.M. Wong, *Inorg. Chem.*, **34** (1995) 4004.
[10] R.S. Drago, T.R. Cundari, Electrostatic-Covalent Model Parameters for Molecular Modeling, in: K.K. Irikura, D.J. Frurip (eds.), *Computational Thermochemistry: Prediction and Estimation of Molecular Thermodynamics, ACS Symposium Series 677*. American Chemical Society, Washington, DC, 1998.
[11] D.W. Rogers, Molecular Mechanics in Computational Thermochemistry, in: K.K. Irikura, D.J. Frurip (eds.), *Computational Thermochemistry: Prediction and Estimation of Molecular Thermodynamics, ACS Symposium Series 677*. American Chemical Society, Washington, DC, 1998.
[12] T. Lazaridis, M. Karplus, *Biophys. Chem.*, **100** (2003) 367.
[13] J.-H. Lii, N.L. Allinger, *J. Comput. Chem.*, **19** (1998) 1001.
[14] C.H. Langley, N.L. Allinger, *J. Phys. Chem. A*, **106** (2002) 5638.
[15] M.J.S. Dewar, E.G. Zoebisch, E.F. Healy, J.J.P. Stewart, *J. Am. Chem. Soc.*, **107** (1985) 3902.
[16] J.J.P. Stewart, *J. Comput. Chem.*, **10** (1989) 209.
[17] W. Thiel, A.A. Voityuk, *J. Phys. Chem.*, **100** (1996) 616.
[18] J.J.P. Stewart, *J. Comput. Chem.*, **10** (1989) 221.

[19] Alchemy2000, version 2.05, Tripos, Inc., St. Louis, 1998.
[20] Certain commercial materials and equipment are identified in this paper in order to specify procedures completely. In no case does such identification imply recommendation or endorsement by the National Institute of Standards and Technology, nor does it imply that the material or equipment identified is necessarily the best available for the purpose.
[21] M.J. Frisch, G.W. Trucks, H.B. Schlegel, G.E. Scuseria, M.A. Robb, J.R. Cheeseman, V.G. Zakrzewski, J.A. Montgomery Jr., R.E. Stratmann, J.C. Burant, S. Dapprich, J.M. Millam, A.D. Daniels, K.N. Kudin, M.C. Strain, O. Farkas, J. Tomasi, V. Barone, M. Cossi, R. Cammi, B. Mennucci, C. Pomelli, C. Adamo, S. Clifford, J. Ochterski, G.A. Petersson, P.Y. Ayala, Q. Cui, K. Morokuma, D.K. Malick, A.D. Rabuck, K. Raghavachari, J.B. Foresman, J. Cioslowski, J.V. Ortiz, B.B. Stefanov, G. Liu, A. Liashenko, P. Piskorz, I. Komaromi, R. Gomperts, R.L. Martin, D.J. Fox, T. Keith, M.A. Al-Laham, C.Y. Peng, A. Nanayakkara, C. Gonzalez, M. Challacombe, P.M.W. Gill, B. Johnson, W. Chen, M.W. Wong, J.L. Andres, C. Gonzalez, M. Head-Gordon, E.S. Replogle, J.A. Pople, *Gaussian 98, version A.7*. Gaussian, Inc., Pittsburgh, PA, 1998.
[22] C.F. Kettering, L.W. Shutts, D.H. Andrews, *Phys. Rev.*, **36** (1930) 531.
[23] B. Ma, J.-H. Lii, K. Chen, N.L. Allinger, *J. Am. Chem. Soc.*, **119** (1997) 2570.
[24] J.-H. Lii, N.L. Allinger, *J. Am. Chem. Soc.*, **111** (1989) 8566.
[25] N.L. Allinger, F. Li, L. Yan, J.C. Tai, *J. Comput. Chem.*, **11** (1990) 868.
[26] N.L. Allinger, F. Li, L. Yan, *J. Comput. Chem.*, **11** (1990) 848.
[27] E. Goldstein, B.Y. Ma, J.H. Lii, N.L. Allinger, *J. Phys. Org. Chem.*, **9** (1996) 191.
[28] R. Liu, N.L. Allinger, *J. Comput. Chem.*, **15** (1994) 283.
[29] N.L. Allinger, M. Rahman, J.-H. Lii, *J. Am. Chem. Soc.*, **112** (1990) 8293.
[30] N.L. Allinger, K. Chen, M. Rahman, A. Pathiaseril, *J. Am. Chem. Soc.*, **113** (1991) 4505.
[31] N.L. Allinger, Y. Fan, *J. Comput. Chem.*, **15** (1994) 251.
[32] N.L. Allinger, S. Rodriguez, K.S. Chen, *J. Mol. Struct. (Theochem)*, **92** (1992) 161.
[33] N.L. Allinger, Z.S. Zhu, K. Chen, *J. Am. Chem. Soc.*, **114** (1992) 6120.
[34] N.L. Allinger, L.Q. Yan, *J. Am. Chem. Soc.*, **115** (1993) 11918.
[35] K.S. Chen, N.L. Allinger, *J. Comput. Chem.*, **14** (1993) 755.
[36] L.R. Schmitz, N.L. Allinger, *J. Am. Chem. Soc.*, **112** (1990) 8307.
[37] N.L. Allinger, L.Q. Yan, K.H. Chen, *J. Comput. Chem.*, **15** (1994) 1321.
[38] J.C. Tai, L. Yang, N.L. Allinger, *J. Am. Chem. Soc.*, **115** (1993) 11906.
[39] L.R. Yang, N.L. Allinger, *J. Mol. Struct. (Theochem)*, **370** (1996) 71.
[40] B.Y. Ma, J.H. Lii, K.S. Chen, N.L. Allinger, *J. Phys. Chem.*, **100** (1996) 11297.
[41] J.H. Lii, N.L. Allinger, *J. Comput. Chem.*, **12** (1991) 186.
[42] N.L. Allinger, J. Kuang, H.D. Thomas, *J. Mol. Struct. (Theochem)*, **68** (1990) 125.
[43] Y. Fan, N.L. Allinger, *J. Comput. Chem.*, **15** (1994) 1446.
[44] N.L. Allinger, M. Quinn, M. Rahman, K.H. Chen, *J. Phys. Org. Chem.*, **4** (1991) 647.
[45] K.H. Chen, N.L. Allinger, *J. Phys. Org. Chem.*, **4** (1991) 659.
[46] X.F. Zhou, N.L. Allinger, *J. Phys. Org. Chem.*, **7** (1994) 420.
[47] K.S. Chen, N.L. Allinger, *J. Phys. Org. Chem.*, **10** (1997) 697.
[48] K.H. Chen, N.L. Allinger, *J. Phys. Org. Chem.*, **12** (1999) 528.
[49] M.R. Nyden, T.R. Coley, S. Mumby, *Polym. Eng. Sci.*, **37** (1997) 1496.
[50] S.J. Stuart, A.B. Tutein, J.A. Harrison, *J. Chem. Phys.*, **112** (2000) 6472.

[51] A.C.T. van Duin, A. Strachan, S. Stewman, Q.S. Zhang, X. Xu, W.A. Goddard III, *J. Phys. Chem. A*, **107** (2003) 3803.
[52] F. Jensen, P.-O. Norrby, *Theor. Chem. Acc.*, **109** (2003) 1.
[53] M.J.S. Dewar, *The Molecular Orbital Theory of Organic Chemistry*. McGraw-Hill, New York, 1969.
[54] W. Thiel, Thermochemistry from Semiempirical Molecular Orbital Theory, in: K.K. Irikura, D.J. Frurip (eds.), *Computational Thermochemistry: Prediction and Estimation of Molecular Thermodynamics, ACS Symposium Series 677*. American Chemical Society, Washington, DC, 1998, p. 142.
[55] R.D. Johnson, III, *Computational Chemistry Comparison and Benchmark DataBase*, http://srdata.nist.gov/cccbdb/.
[56] J.J.P. Stewart, *J. Comput. Chem.*, **12** (1991) 320.
[57] E. Anders, R. Koch, P. Freunscht, *J. Comput. Chem.*, **14** (1993) 1301.
[58] E.N. Brothers, K.M. Merz Jr., *J. Phys. Chem. B*, **106** (2002) 2779.
[59] W. Thiel, A.A. Voityuk, *Theor. Chim. Acta*, **81** (1992) 391.
[60] T.R. Cundari, J. Deng, W. Fu, *Int. J. Quantum Chem.*, **77** (2000) 421.
[61] W.J. Hehre, L. Radom, P.v.R. Schleyer, J.A. Pople, *Ab Initio Molecular Orbital Theory*. Wiley, New York, 1986.
[62] A. Szabo, N.S. Ostlund, *Modern Quantum Chemistry: Introduction to Advanced Electronic Structure Theory*, 1st (revised) ed. McGraw-Hill, New York, 1982.
[63] H.B. Schlegel, *J. Phys. Chem.*, **92** (1988) 3075.
[64] J. Olsen, O. Christiansen, H. Koch, P. Jørgensen, *J. Chem. Phys.*, **105** (1996) 5082.
[65] D. Cremer, Z. He, *J. Phys. Chem.*, **100** (1996) 6173.
[66] J.A. Pople, M. Head-Gordon, K. Raghavachari, *J. Chem. Phys.*, **87** (1987) 5968.
[67] K. Raghavachari, G.W. Trucks, J.A. Pople, M. Head-Gordon, *Chem. Phys. Lett.*, **157** (1989) 479.
[68] L.A. Curtiss, K. Raghavachari, P.C. Redfern, V. Rassolov, J.A. Pople, *J. Chem. Phys.*, **109** (1998) 7764.
[69] J.M.L. Martin, G. de Oliveira, *J. Chem. Phys.*, **111** (1999) 1843.
[70] K. Kowalski, P. Piecuch, *J. Chem. Phys.*, **113** (2000) 18.
[71] W. Müller, J. Flesch, W. Meyer, *J. Chem. Phys.*, **80** (1984) 3297.
[72] A. Nicklass, K.A. Peterson, *Theor. Chem. Acc.*, **100** (1998) 103.
[73] J.M.L. Martin, A. Sundermann, P.L. Fast, D.G. Truhlar, *J. Chem. Phys.*, **113** (2000) 1348.
[74] P. Pyykkö, *Chem. Rev.*, **88** (1988) 563.
[75] C.E. Moore, *Atomic Energy Levels*. U.S. Govt. Printing Office, Washington, DC, 1971.
[76] M. Krauss, W.J. Stevens, *Ann. Rev. Phys. Chem.*, **35** (1984) 357.
[77] C.W. Bauschlicher Jr., *Chem. Phys. Lett.*, **305** (1999) 446.
[78] J.M.L. Martin, A. Sundermann, *J. Chem. Phys.*, **114** (2001) 3408.
[79] K.A. Peterson, *J. Chem. Phys.*, **119** (2003) 11099.
[80] K.A. Peterson, D. Figgen, E. Goll, H. Stoll, M. Dolg, *J. Chem. Phys.*, **119** (2003) 11113.
[81] M.W. Schmidt, M.S. Gordon, *Annu. Rev. Phys. Chem.*, **49** (1998) 233.
[82] W.A. Goddard III, T.H. Dunning Jr., W.J. Hunt, P.J. Hay, *Acc. Chem. Res.*, **6** (1973) 368.
[83] B.D. Dunietz, R.B. Murphy, R.A. Friesner, *J. Chem. Phys.*, **110** (1999) 1921.
[84] V.A. Rassolov, M.A. Ratner, J.A. Pople, P.C. Redfern, L.A. Curtiss, *J. Comput. Chem.*, **22** (2001) 976.

[85] T.H. Dunning Jr., *J. Phys. Chem. A*, **104** (2000) 9062.
[86] T.H. Dunning Jr., K.A. Peterson, A.K. Wilson, *J. Chem. Phys.*, **114** (2001) 9244.
[87] F.B. van Duijneveldt, J.G.C.M. van Duijneveldt-van de Rijdt, J.H. van Lenthe, *Chem. Rev.*, **94** (1994) 1873.
[88] J.M.L. Martin, J.P. François, R. Gijbels, *Theor. Chim. Acta*, **76** (1989) 195.
[89] N. Oliphant, M.E. Rosenkrantz, D.D. Konowalow, *Chem. Phys. Lett.*, **223** (1994) 7.
[90] W. Kohn, A.D. Becke, R.G. Parr, *J. Phys. Chem.*, **100** (1996) 12974.
[91] P.J. Stephens, F.J. Devlin, C.F. Chabalowski, M.J. Frisch, *J. Phys. Chem.*, **98** (1994) 11623.
[92] A.D. Becke, *J. Chem. Phys.*, **98** (1993) 5648.
[93] C. Lee, W. Yang, R.G. Parr, *Phys. Rev. B*, **37** (1988) 785.
[94] T. van Mourik, R.J. Gdanitz, *J. Chem. Phys.*, **116** (2002) 9620.
[95] J.K. Kang, C.B. Musgrave, *J. Chem. Phys.*, **115** (2001) 11040.
[96] Y. Zhao, B.J. Lynch, D.G. Truhlar, *J. Phys. Chem. A*, **108** (2004) 2715.
[97] J.F. Stanton, J. Gauss, J.D. Watts, W.J. Lauderdale, R.J. Bartlett, *Int. J. Quantum Chem.*, **S26** (1992) 879.
[98] M.W. Schmidt, K.K. Baldridge, J.A. Boatz, S.T. Elbert, M.S. Gordon, J.H. Jensen, S. Koseki, N. Matsunaga, K.A. Nguyen, S.J. Su, T.L. Windus, M. Dupuis, J.A. Montgomery, *J. Comput. Chem.*, **14** (1993) 1347.
[99] M.J. Frisch, G.W. Trucks, H.B. Schlegel, G.E. Scuseria, M.A. Robb, J.R. Cheeseman, J.A. Montgomery Jr., T. Vreven, K.N. Kudin, J.C. Burant, J.M. Millam, S.S. Iyengar, J. Tomasi, V. Barone, B. Mennucci, M. Cossi, G. Scalmani, N. Rega, G.A. Petersson, H. Nakatsuji, M. Hada, M. Ehara, K. Toyota, R. Fukuda, J. Hasegawa, M. Ishida, T. Nakajima, Y. Honda, O. Kitao, H. Nakai, M. Klene, X. Li, J.E. Knox, H.P. Hratchian, J.B. Cross, C. Adamo, J. Jaramillo, R. Gomperts, R.E. Stratmann, O. Yazyev, A.J. Austin, R. Cammi, C. Pomelli, J.W. Ochterski, P.Y. Ayala, K. Morokuma, G.A. Voth, P. Salvador, J.J. Dannenberg, V.G. Zakrzewski, S. Dapprich, A.D. Daniels, M.C. Strain, O. Farkas, D.K. Malick, A.D. Rabuck, K. Raghavachari, J.B. Foresman, J.V. Ortiz, Q. Cui, A.G. Baboul, S. Clifford, J. Cioslowski, B.B. Stefanov, G. Liu, A. Liashenko, P. Piskorz, I. Komaromi, R.L. Martin, D.J. Fox, T. Keith, M.A. Al-Laham, C.Y. Peng, A. Nanayakkara, M. Challacombe, P.M.W. Gill, B. Johnson, W. Chen, W.W. Wong, C. Gonzalez, J.A. Pople, *Gaussian 03, version B.02*. Gaussian, Inc., Pittsburgh, PA, 2003.
[100] G. de Oliveira, J.M.L. Martin, F. de Proft, P. Geerlings, *Phys. Rev. A*, **60** (1999) 1034.
[101] H. Partridge, C.W. Bauschlicher Jr., *J. Chem. Phys.*, **103** (1995) 10589.
[102] J.M.L. Martin, T.J. Lee, *Chem. Phys. Lett.*, **258** (1996) 136.
[103] E.P.L. Hunter, S.G. Lias, *J. Phys. Chem. Ref. Data*, **27** (1998) 413.
[104] S.R. Langhoff, E.R. Davidson, *Int. J. Quantum Chem.*, **8** (1974) 61.
[105] P.E.M. Siegbahn, *Chem. Phys. Lett.*, **55** (1978) 386.
[106] P.J. Bruna, S.D. Peyerimhoff, R.J. Buenker, *Chem. Phys. Lett.*, **72** (1980) 278.
[107] T. Müller, M. Dallos, H. Lischka, Z. Dubrovay, P.G. Szalay, *Theor. Chem. Acc.*, **105** (2001) 227.
[108] A.P. Scott, L. Radom, *J. Phys. Chem.*, **100** (1996) 16502.
[109] L.A. Curtiss, K. Raghavachari, *Theor. Chem. Acc.*, **108** (2002) 61.
[110] J.W. Ochterski, G.A. Petersson, J.A. Montgomery, *J. Chem. Phys.*, **104** (1996) 2598.
[111] J.A. Montgomery Jr., M.J. Frisch, J.W. Ochterski, G.A. Petersson, *J. Chem. Phys.*, **112** (2000) 6532.

[112] A.D. Boese, M. Oren, O. Atasoylu, J.M.L. Martin, M. Kállay, J. Gauss, *J. Chem. Phys.*, **120** (2004) 4129.
[113] L.V. Gurvich, I.V. Veyts, C.B. Alcock, (eds.), *Thermodynamic Properties of Individual Substances*. Hemisphere, New York, 1989.
[114] H.Y. Afeefy, J.F. Liebman, S.E. Stein, (eds.), Neutral Thermochemical Data. in: *NIST Chemistry WebBook, National Institute of Standards and Technology*, Gaithersburg, MD, (2003). http://webbook.nist.gov/chemistry/
[115] M.W. Chase Jr., JANAF Thermochemical Tables, 4th ed., *J. Phys. Chem. Ref. Data Monograph*, **9** (1998).
[116] J.D. Cox, G. Pilcher, *Thermochemistry of Organic and Organometallic Compounds*. Academic Press, London, 1970.
[117] J.D. Cox, D.D. Wagman, V.A. Medvedev, *CODATA Key Values for Thermodynamics*. Hemisphere, New York, 1989.
[118] W.C. Martin, J.R. Fuhr, D.E. Kelleher, A. Musgrove, L. Podobedova, J. Reader, E.B. Saloman, C.J. Sansonetti, W.L. Wiese, P.J. Mohr, K. Olsen, *NIST Atomic Spectra Database (version 2.0)*, http://physics.nist.gov/asd
[119] K.K. Irikura, R.D. Johnson III, R.N. Kacker, *Metrologia*, **41** (2004) 369.
[120] L.A. Curtiss, P.C. Redfern, K. Raghavachari, V. Rassolov, J.A. Pople, *J. Chem. Phys.*, **110** (1999) 4703.
[121] T.H. Lay, J.W. Bozzelli, *J. Phys. Chem. A*, **101** (1997) 9505.
[122] R.D. Johnson III, *SickList Database*, http://srdata.nist.gov/sicklist/
[123] K.S. Pitzer, W.D. Gwinn, *J. Chem. Phys.*, **10** (1942) 428.
[124] K.S. Pitzer, *J. Chem. Phys.*, **14** (1946) 239.
[125] J. Ridley, M. Zerner, *Theor. Chim. Acta*, **32** (1973) 111.
[126] M.C. Zerner, Semiempirical Molecular Orbital Methods, in: K.B. Lipkowitz, D.B. Boyd (eds.), *Reviews in Computational Chemistry*, Volume 2. VCH, New York, 1991, p. 313.
[127] S.G. Lias, J.E. Bartmess, Gas-Phase Ion Thermochemistry, in: W.G. Mallard, P.J. Linstrom (eds.), *NIST Chemistry WebBook, NIST Standard Reference Database Number 69*. National Institute of Standards and Technology, Gaithersburg, Md, 1998.
[128] J.E. Szulejko, T.B. McMahon, *J. Am. Chem. Soc.*, **115** (1993) 7839.
[129] K.P. Huber, G. Herzberg (eds.), Constants of Diatomic Molecules (data prepared by J.W. Gallagher and R.D. Johnson III), in: *NIST Chemistry WebBook*. National Institute of Standards and Technology, Gaithersburg, MD, 2001, http://webbook.nist.gov

Chapter 3

Elements of Chemical Kinetics

Robert W. Carr

1 INTRODUCTION

This chapter is a primer on chemical kinetics. It should be useful to anyone who finds it desirable or necessary to get started on modeling a complex chemical reaction, and whose background does not include training in kinetics, or who wishes to brush up. Although the material in this chapter can be found in standard textbooks on kinetics, several of which are referenced below, it was thought that having a basic overview of the subject readily at hand would be a welcome convenience. Consulting other texts will be necessary to fill in many of the details. The chapter is divided into two parts. The first part is concerned with definitions and underlying principles of chemical kinetics; the second part provides an introduction to the theory of elementary reactions, with the exception of unimolecular reactions which are covered in Chapter 4.

2 ELEMENTARY CONCEPTS

2.1 Stoichiometry

Overall chemical reactions are described by stoichiometric relationships giving the relative number of moles of each reactant, which are those chemical compounds that are initially placed in contact, and the relative number of moles of each final chemical product that is formed from the reactants, as obtained from experiment. Overall reactions are frequently referred as stoichiometric reactions. The two terms are used interchangeably. An overall reaction may be quite complex, consisting of any number of molecular interactions between different chemical species, and there may be many intermediate species formed and consumed during the course of a reaction, but these do not appear in the stoichiometric relationship between reactants and products, which may be

Comprehensive Chemical Kinetics, Volume 42, 43–99

ISSN: 0069-8040/doi:10.1016/S0069-8040(07)42003-9

expressed as

$$aA + bB + \cdots \rightarrow mM + nN + \cdots \tag{1}$$

where the lower case letters are the stoichiometric coefficients and the upper case letters represent the chemical species. The stoichiometric coefficients prescribe the relative numbers of moles of each reactant producing the observed molar abundance of each of the products. For example, the stoichiometry for the complete combustion of methane is given by

$$CH_4 + 1.5O_2 \rightarrow CO_2 + 2H_2O \tag{2}$$

Note that in equation (2) atoms are conserved because the temperatures at which chemical reactions are normally carried out are insufficiently high to cause nuclear reactions to occur. The arrows in equations (1) and (2) denote that the chemical species on the left hand side are the reactants, and that they are being converted into the products given on the right hand side. It is conventional to place the reactants on the left hand side of the stoichiometric expression, and products on the right, and the reaction will proceed by depletion of reactants and formation of products, which is called the forward direction. If the products are mixed initially, in the absence of reactants, the reaction will proceed in the reverse direction. It will be shown below that all chemical reactions are reversible.

It is sometimes convenient to cast stoichiometry into the form of algebraic equations. Equation (1) can be rearranged to $-aA - bB - \cdots + mM + nN + \cdots = 0$, where the arrow is replaced by the equality. This equation can be thought of as a statement of the conservation of atoms. It can be rewritten in the compact notation for the S chemical species participating in the reaction as

$$\sum_{i=1}^{S} \nu_i A_i = 0 \tag{3}$$

In equation (3) ν_i is the stoichiometric coefficient of the ith chemical species, A_i. The stoichiometric coefficients are conventionally taken as being negative numbers for reactants and positive numbers for products. The summation runs over all S chemical species in the stoichiometric equation. The chemical species appearing in the stoichiometric equation must be determined experimentally.

2.2 The reaction rate

The rate at which reactants are converted to products is a key quantity for characterizing a chemical reaction. The rate of a stoichiometric reaction may be defined by dividing the observed rate of consumption of moles of each individual reactant and the rate of formation of moles of each individual product by their respective stoichiometric coefficients, where the rates are time derivatives. Division by the stoichiometric coefficients reduces the individual species rates to a common value, R, having the dimensions of moles per unit time. For the stoichiometric reaction of equation (1) the rate is defined by

$$R \equiv -a^{-1}\left(\frac{\mathrm{d}n_a}{\mathrm{d}t}\right) = -b^{-1}\left(\frac{\mathrm{d}n_b}{\mathrm{d}t}\right)\cdots = m^{-1}\left(\frac{\mathrm{d}n_m}{\mathrm{d}t}\right) = n^{-1}\left(\frac{\mathrm{d}n_n}{\mathrm{d}t}\right)\cdots \tag{4}$$

where n_a denotes number of moles of species A, and so on. The reaction rate may be expressed in terms of any of the i chemical species participating in the reaction as follows:

$$R = \frac{1}{v_i}\left(\frac{\mathrm{d}n_i}{\mathrm{d}t}\right) \tag{5}$$

where R is an extensive reaction rate, depending as it does on the number of moles of a chemical species present at any arbitrary time. It would be more convenient to work with rates that are independent of the quantity of material present, and an intensive reaction rate may be defined by dividing by the reaction system volume, $r \equiv R/V$. In non-constant volume systems r has two terms, the rate of change of concentration and the rate of change of the logarithm of the volume

$$r \equiv \frac{R}{V} = (v_i V)^{-1}\left\{\frac{\mathrm{d}}{\mathrm{d}t}(V[\mathrm{A}_i]\right\} = v_i^{-1}\left\{\frac{\partial[\mathrm{A}_i]}{\partial t} + [\mathrm{A}_i]\frac{\partial \ln V}{\partial t}\right\} \tag{6}$$

The species concentration, $[\mathrm{A}_i]$, is defined by $[\mathrm{A}_i] = n_i/V$. At constant volume equation (6) reduces to

$$r = \frac{1}{v_i}\frac{\mathrm{d}[\mathrm{A}_i]}{\mathrm{d}t} \tag{7}$$

This equation suffices to describe reaction rates in systems where the $[\mathrm{A}_i]$ are spatially uniform. If there are concentration non-uniformities an average rate may be obtained by integrating the rate over the reactor

volume. Kinetic investigations are normally done in systems designed to avoid concentration non-uniformities, but in practical chemical reactors concentration gradients may be unavoidable, and must be taken into account.

In open chemical reaction systems where matter is exchanged with the surroundings, concentration changes may also occur by forced flow, convection, and diffusion, and these must be taken into account in an equation of change. In most research on reaction rates experiments are designed to exclude transport effects on the rates of concentration change, since these may complicate, or even obscure, the principal objectives of the work. The interaction of transport and kinetics may be very important in practical chemical reaction systems. In cases where this is so reaction models become much more complex than otherwise.

2.3 The rate expression

The functional dependence of the rate on system parameters is called the rate expression. This is frequently referred to as the rate law, but the term "law" ought to be reserved for fundamental principles, and not used to describe an empirical equation. Important parameters are the concentrations of the reactants and (sometimes) the products, and the temperature. Other quantities may influence the reaction rate. In gas phase reactions total pressure may play a key role (see Chapter 4), while for reactions in solution bulk properties such as ionic strength and dielectric constant may influence the rate. Rate expressions for stoichiometric reactions must be empirically determined, taking any mathematical form that fits the data. The rate will be expressed as a function of temperature, concentrations of species present, and any other parameters that are found to influence the rate

$$r = f\{T, [\mathrm{A}_1], [\mathrm{A}_2], \ldots, \text{other quantities}\} \tag{8}$$

A form that is frequently found for reactions where the rate depends only on concentrations and temperature is

$$r = k(T) \prod_{i=1}^{S} [\mathrm{A}_i]^{\alpha_i} \tag{9}$$

where $k(T)$ is the rate coefficient or rate constant. The former is preferable because $k(T)$ is not a constant, but in a properly determined rate expression it is a function only of temperature. The α_i are called the order of the reaction with respect to each chemical species, A_i. While the orders may sometimes be numerically equal to the stoichiometric

coefficients, ν_i, in general the α_i are different from the ν_i. The α_i, which are empirically determined, are numbers that may be positive or negative, or zero for a reactant or product that does not influence the reaction rate. The α_i are normally not large numbers, and they may be fractional. For rate expressions of the form of equation (9) the overall order of a reaction is given by the sum of the orders with respect to each species:

$$\text{Overall order} = \sum_{i=1}^{S} \alpha_i \tag{10}$$

For other functional forms of the rate expression the overall order may not be defined. In addition, the rate expression may vary as the reaction proceeds. The rate expression found from experiments done at an early stage of the reaction, where the reactants are not appreciably converted to products, may be different from the rate expression found at later stages of the reaction.

Although the rate expressions for stoichiometric reactions are empirical, the mathematical form of the rate expression for the reaction proceeding in the reverse direction is constrained by thermodynamics and the rate expression in the forward direction for reactions of the form of equation (8). Denbigh [1] has shown that the reaction orders with respect to each component in the reaction mixture are related by the equation

$$\frac{\alpha_i' - \alpha_i}{\nu_i} = n \tag{11}$$

where α_i' is the order of the reaction with respect to species A_i in the reverse direction, α_i the order with respect to species A_i in the forward direction, ν_i the stoichiometric coefficient of A_i and n a number that can have any positive value, including fractions. All of the chemical species appearing in the stoichiometric equation obey this equation, and they all have the same value of n.

There is a large literature describing experimental methods for finding empirical rate expressions and analyzing rate data. Comprehensive treatments can be found in volume 8 of the Weissburger series [2] and in volume 1 of the *Comprehensive Chemical Kinetics* series [3]. In addition, almost every textbook on kinetics has material on this subject. See, for example, the texts by Espenson [4], Laidler [5], and Steinfeld *et al.* [6]. This book is devoted to detailed chemical kinetic modeling of chemical reactions, and is concerned primarily with elementary reactions.

A survey of methods for investigating the kinetics of stoichiometric reactions is outside the scope of the book.

2.4 Elementary reactions

The vast majority of stoichiometric reactions do not occur by transformation of the reactants to the products in a single step rearrangement of the constituent atoms. They occur via a series of reactive interactions at the atomic and molecular levels, and they involve reactive chemical species that are formed and then entirely consumed, so they do not appear in the stoichiometric equation. These molecular level interactions are called elementary chemical reactions. The reactants and products in an elementary reaction may be atoms, molecules, free radicals, ions, excited states, etc. An elementary chemical reaction is an isolated interaction between such species in which the transformation from reactants to products occurs by rearrangement of the constituent atoms. Elementary reactions are fundamental descriptions of how chemical transformations occur. The list of elementary reactions that take place during the course of a stoichiometric reaction is called the mechanism of the reaction. The mechanism thus embodies the detailed atomic and molecular level chemistry that accounts for the overall chemistry that is observed in a stoichiometric reaction.

The molecularity of an elementary reaction is defined as the number of molecules participating in the reaction. A unimolecular reaction describes the dissociation or rearrangement of a single reactant as in the reaction

$$\mathrm{A} \rightarrow \text{product(s)} \tag{12}$$

A bimolecular reaction describes the chemical transformation that occurs when two reactants undergo a collisional interaction resulting in chemical change

$$\mathrm{A} + \mathrm{B} \rightarrow \text{product(s)} \tag{13}$$

Similarly, a termolecular reaction describes the chemical transformation that occurs when three reactants undergo a simultaneous or near simultaneous isolated encounter leading to the formation of new product(s):

$$\mathrm{A} + \mathrm{B} + \mathrm{C} \rightarrow \text{product(s)} \tag{14}$$

Reactions of molecularity greater than 3 have never been observed because the probability of obtaining simultaneous or near simultaneous interaction between four or more species is very small.

In contrast with the rate expressions for stoichiometric reactions, which must be obtained empirically, the rate expressions for elementary reactions can be written down by inspection. The kinetic order of an elementary reaction is equal to its molecularity, and is thus limited to the positive integral values 1, 2, and 3. For example, the order of a bimolecular reaction is 2 because for the reaction to occur both reactants must interact via a collision. The maximum possible bimolecular reaction rate is the collision rate, which is proportional to the product of the concentration of each species, making the reaction first order with respect to each species, and second order overall. The rate of the elementary reaction between the hydroxyl radical and molecular hydrogen, to form water and atomic hydrogen,

$$OH + H_2 \rightarrow H_2O + H \tag{15}$$

is given by the following equation:

$$\frac{-d[OH]}{dt} = \frac{-d[H_2]}{dt} = k(T)[OH][H_2] \tag{16}$$

which is obtained by inspection of equation (15). This reaction plays an extremely important role in the combustion of hydrogen, and must occur in any overall reaction where both OH and H_2 are present.

Elementary reactions are fundamental descriptions of chemical change, in contrast with the empirical nature of overall reactions. Their rate coefficients can be described by molecular theories of rate processes as shown later in this chapter, and in Chapter 4. The rate coefficient of an elementary reaction is unique, and can be used with confidence in any overall reaction in which it occurs. This is particularly true of gas phase reactions, where the rate coefficient is not influenced by the chemical nature of the surroundings. Accordingly, much research effort has been expended in obtaining rate coefficients of elementary reactions, not only for use in the molecular description of overall reaction rates, but also for the insight into chemical reactivity provided.

2.5 State-to-state kinetics

In contrast with elementary reactions, where reactants and products have a distribution of energy states, state-to-state kinetics is the study of the rate at which a reactant(s) in a specific molecular energy state is (are) converted to a product(s), and what energy state is (are) populated in the product (s). Descriptions of reactions at this detailed level are also called microscopic kinetics or chemical dynamics. They yield insights into chemical reactivity that cannot be realized from studies of elementary

reactions or overall reactions, where observed reaction rates are averaged over the molecular energy distributions. The use of crossed molecular beams, where each reactant is formed into a unidirectional beam intersecting in a well defined volume where the product(s) is (are) formed and scattered in directions that can be experimentally determined, and the application of molecular spectroscopy, particularly with tunable lasers, have permitted great progress to be made in this area [7]. In principle, the rate coefficients of elementary reactions can be obtained from data on experiments where the reactants have been prepared in specific energy states. It is instructive to see, in a general way, how state-to-state kinetics are related to the kinetics of elementary reactions.

A state-to-state bimolecular reaction between state selected reactants A and B leading to C and D in a particular energy state may be represented as follows:

$$\begin{aligned} &\mathrm{A}(n_\mathrm{A}, v_\mathrm{A}, J_\mathrm{A}, u_\mathrm{A}) + \mathrm{B}(n_\mathrm{B}, v_\mathrm{B}, J_\mathrm{B}, u_\mathrm{B}) \\ &\rightarrow \mathrm{C}(n_\mathrm{C}, v_\mathrm{C}, J_\mathrm{C}, u_\mathrm{C}) + \mathrm{D}(n_\mathrm{D}, v_\mathrm{D}, J_\mathrm{D}, u_\mathrm{D}) \end{aligned} \tag{17}$$

The quantities n_i, v_i, and J_i represent the electronic, vibrational, and rotational energy levels of each species, and u_i represents translational energy. The connection between the rate of reaction (17) and the rate of an elementary reaction between A and B can be made if the rate of the state-to-state process can be written conventionally. If A_i is taken to represent the energy state of A in equation (17) and B_j the state of B, then the rate of the state-to-state reaction is

$$r_{ij} = k_{ij}[\mathrm{A}_i][\mathrm{B}_j] \tag{18}$$

where the square brackets denote concentration, as usual. In a situation where many states are populated, the total rate will be given by the sum over all of the energy states present

$$r = \sum_i \sum_j r_{ij} \tag{19}$$

Writing the relative population distribution as $f_i(\varepsilon) = [\mathrm{A}_i]/[\mathrm{A}]$ and $f_j(\varepsilon) = [\mathrm{B}_j]/[\mathrm{B}]$ the rate becomes

$$r = [\mathrm{A}][\mathrm{B}] \sum_i \sum_j k_{ij} f_i(\varepsilon) f_j(\varepsilon) \tag{20}$$

Since the rate of an elementary bimolecular reaction is written as $r = k(T)[\mathrm{A}][\mathrm{B}]$, it is evident that $k(T)$ is given by the double sum

$$k(T) = \sum_i \sum_j k_{ij} f_i(\varepsilon) f_j(\varepsilon) \tag{21}$$

In reactions where thermal equilibrium is maintained, the population distributions will be Boltzmann, $f(\varepsilon) = g \exp(-\varepsilon/kT)$, and the rate then is expressed as

$$r = [\mathrm{A}][\mathrm{B}] \sum_i \sum_j k_{ij} g_i g_j \exp\left[\frac{-(\varepsilon_i + \varepsilon_j)}{kT}\right] \tag{22}$$

In this case determination of $k(T)$ requires only that values of the k_{ij} be known. Reaction depletes energy levels of the reactants and thus perturbs the energy distribution function. In systems where the rate of reaction is slow compared with the rate of collisional redistribution of energy, the Boltzmann distribution will be an excellent approximation and equation (22) will be applicable. However, when the reaction rate is comparable with, or faster than, collisional energy redistribution, knowledge of $f(\varepsilon)$ becomes necessary. Theoretical methods for calculation of k_{ij} and for handling reactions with non-Boltzmann energy distributions are discussed elsewhere in this volume. Obtaining $k(T)$ from molecular properties is only feasible by application of molecular theories of kinetics because the enormous effort that would be required for experimental determination of all of the required k_{ij} (or equivalent quantities) precludes using this approach as a practical means of determining values for $k(T)$. In fact, there is not at present any reaction for which enough experimental k_{ij} data are available to permit evaluation of $k(T)$. Trajectory calculations, and the theory of unimolecular reactions and some bimolecular association reactions, utilize theoretical methods for the k_{ij}, from which thermal rate coefficients can be estimated.

2.6 The temperature dependence of the rate coefficient

The temperature dependence of many rate coefficients can be expressed by the following equation (the Arrhenius equation [8]):

$$k(T) = A \exp\left(\frac{-E_\mathrm{a}}{RT}\right) \tag{23}$$

The Arrhenius equation is an empirical expression in which the pre-exponential factor, A, and the activation energy, E_a, are temperature independent parameters, and R the gas constant. An interesting discussion of the search, undertaken in the second half of the nineteenth century, to find an appropriate functional form by which to express $k(T)$ has been given by Laidler [9]. Of several possible empirical forms, the Arrhenius equation emerged as the one most preferred. It predicts that a

plot of $\ln k(T)$ vs. T^{-1} (an Arrhenius plot) will be linear. In kinetic experiments over the years the linearity of such plots has been verified many times, although it should be noted that the temperature range over which most of these experiments were done was only a few tens of degrees over which the reaction rate was conveniently measurable. This is not a wide enough temperature range to discern the weak temperature dependence of E_a noted below, and any temperature dependence of A is overwhelmed by the strong temperature dependence of the exponential term. The Boltzmann-like appearance of the exponential factor in the Arrhenius equation suggests that an energy barrier must be surmounted for reaction to occur. The slope of the Arrhenius plot defines the activation energy according to the equation

$$E_a = -R\left\{\frac{d \ln k(T)}{d(1/T)}\right\} \tag{24}$$

In spite of its empiricism, the Arrhenius equation provides some insight into the role of energy in kinetics, and this is usually claimed to be a factor in its success over other empirical forms that were advanced at the time.

The shape of a plot of $k(T)$ vs. T for the Arrhenius equation is a sigmoid shaped curve with a high temperature asymptote $k(T \rightarrow \infty) = A$. Thus, the maximum value of $k(T)$ is the pre-exponential factor. However, at temperatures where many kinetic investigations are done the rate coefficients are much smaller than the pre-exponential factor, and are found in the low temperature region of the sigmoidal curve. This can be seen by considering the inflection point, which is given by $T_i = E_a/2R$. Activation energies range from a few $kJ\,mol^{-1}$ to chemical bond energies. For a very modest $E_a = 20\,kJ\,mol^{-1}$, $T_i = 1200\,K$, and for larger activation energies T_i is higher. Rate coefficients are commonly determined at temperatures well below the inflection point, in the region where $k(T)$ has a strong positive temperature dependence. In this region $k(T)$ has an approximately exponential dependence on T. If low activation energy reactions are carried out at high temperatures, however, $k(T)$ will have a much weaker than exponential temperature dependence.

Molecular theories of kinetics predict that rate coefficients can be expressed in terms of the product of a pre-exponential factor and an exponent, as does the Arrhenius equation, but in contrast to the Arrhenius equation, both the pre-exponential factor and the activation energy are usually predicted to be temperature dependent. Although theories do not predict a simple form for the temperature dependence of the pre-exponential factor, experimental data can seldom discern

the detailed predictions of theory and are frequently fitted to the equation

$$k(T) = BT^n \exp\left(\frac{-E_a}{RT}\right) \tag{25}$$

a modified Arrhenius equation where n is a fitting parameter, usually of order 1, that may be a positive or negative number. Equation (25) predicts that Arrhenius plots of $\log k(T)$ vs. T^{-1} will be curved, but Arrhenius plots frequently fail to show evidence of curvature because the temperature dependence of the exponent is much stronger than the temperature dependence of the pre-exponential factor. When experimental error is taken into account, curvature due to the pre-exponential factor is only observed when data are available over an extended temperature range. An example is given in Fig. 1 for the elementary reaction of the OH radical with CH_4.

The data are from a number of studies done by different groups of researchers, in different laboratories, and with different experimental

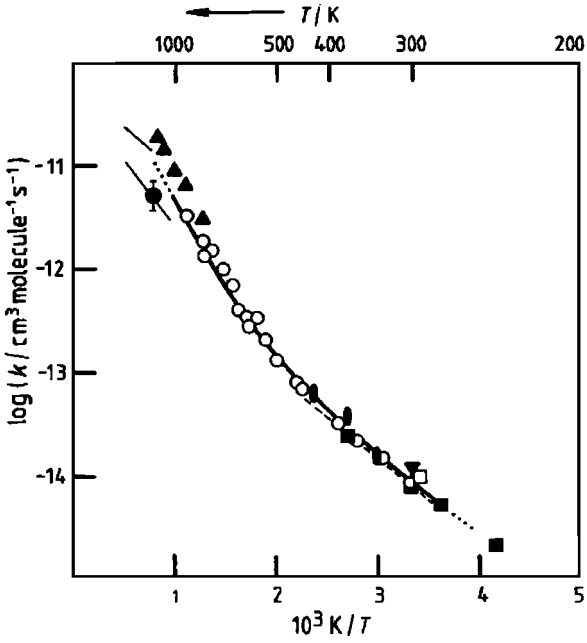

Fig. 1. Arrhenius plot of rate coefficients for the reaction of hydroxyl radical with methane. Symbols are experimentally determined rate coefficients from several different investigations. Solid line is a fit of equation (25) to the data, yielding the equation k (cm^3 molecule^{-1} sec^{-1}) $= 5.7 \times 10^{-21} T^{3.03} \exp[-2007(\text{cal})/RT]$. (Reproduced from Smith (1980) with permission of the author.)

methods. The reaction has a small activation energy, $\sim$1 kJ mol^{-1}, so the temperature dependence of the exponential factor is relatively weak. The rate data extend from 250 to $\sim$2000 K, and illustrate the range of temperature needed to discern curvature even in a favorable case for doing so. Over a temperature range of only 50–100 K, not uncommon in experimental studies, it is easy to see that curvature would go undetected, and the data over such a narrow range would be satisfactorily fit by the Arrhenius equation.

The activation energy is also temperature dependent, although the dependence is very weak and experimentally undetectable. A statistical mechanical argument attributed to R.C. Tolman, and derived in [10] gives the following equation for the activation energy

$$E_a = \langle E^* \rangle - \langle E \rangle \tag{26}$$

where $\langle E^* \rangle$ is the average energy of those reactant molecules that have enough energy to undergo reaction, and $\langle E \rangle$ is the average energy of all of the reactant molecules. The criterion for reaction is that a reactant molecule must have energy greater than the critical energy, a threshold energy below which it becomes unreactive. The weak temperature dependence of E_a is caused by the similar temperature dependencies of $\langle E^* \rangle$ and $\langle E \rangle$, which are largely compensated by taking the difference between them. An important aspect of equation (25) is the interpretation it gives to E_a. The activation energy is not to be loosely thought of as an energy barrier. Rather, it is precisely defined, and provides a framework for formulating barrier crossing problems, such as chemical reactions.

2.7 Kinetic data

The kinetics of a reaction is determined by measuring concentrations of the reactants and products as a function of time. It is desirable to make similar measurements of the products, and if possible, also of any reactive intermediate that one may be able to detect. Elementary reactions are studied by arranging experimental conditions so that the reaction being observed is the only kinetically important process, other reactions having negligible effect on the rate of the one being measured. Considerable effort is usually spent on experimental design to ensure this isolation of the elementary reaction, and accuracy of the rate coefficients. Physical methods for *in situ* determination of concentrations without perturbing system composition are most desirable. Optical spectroscopies and mass spectrometry are common methods, but other physical measurement techniques may be used. Chemical analysis and chromatographic methods are usually only suitable for analysis of the

final reaction mixture because they are slow and require removal of material. Reaction times that can be dealt with range from very long, days or more, to as short as femtoseconds with the use of femtosecond pulsed lasers. Modern optical and electronic technology has made investigations of highly reactive species in the microsecond to nanosecond time range almost routine. Fast reactions that require mixing of reagents are limited to milliseconds or perhaps slightly shorter times because of mixing rate limitations. Experimental methods are introduced in nearly all textbooks on kinetics. Many texts have bibliographies which can be used for entry into the extensive literature on experimental methods.

The National Institute of Standards and Technology (NIST) maintains a database for elementary reactions that is updated regularly [11]. The kinetic data in this database consist of experimental data on elementary reactions and come from laboratories all over the world. The data are carefully evaluated by a panel of experts, and recommended values of rate coefficients are given. This is a reliable source of kinetic data for use in modeling reactions. There are other sources of data, some of which can be found in Chapter 5.

2.8 Mechanism

It has already been stated that the list of all of the elementary reactions that occur during the course of an overall reaction is called the mechanism of the reaction. This is a set of simultaneous reactions, and we can readily extend the algebraic way of writing reactions to multiple reactions. If there are R simultaneous reactions between S species we can write

$$\sum_{i=1}^{S} \nu_{ij} A_i = 0, \quad j = 1, 2, \ldots, R \tag{27}$$

where ν_{ij} is the stoichiometric coefficient of A_i in the jth reaction. For the overall reaction equation (3), $\sum \nu_i A_i = 0$, also holds, and we see that from the stoichiometric relationships the concentrations of those species that are formed and then completely consumed (the intermediates) during the course of the stoichiometric reaction must cancel in doing the sums. This is simply a formal way of stating what we know must be true for species that appear during the reaction but do not survive to become part of the final product mix. The satisfaction of these algebraic relationships is an important first test of a proposed mechanism, for if they are not satisfied, the mechanism cannot be correct. For example, the gas phase decomposition of dinitrogen pentoxide, for which the

stoichiometric equation is $2N_2O_5 = 4NO_2 + O_2$, has been suggested to have the following mechanism [12]:

$$N_2O_5 \rightarrow NO_2 + NO_3$$
$$NO_2 + NO_3 \rightarrow N_2O_5$$
$$NO_2 + NO_3 \rightarrow NO + O_2 + NO_3$$
$$NO + NO_3 \rightarrow 2NO_2$$

Multiplying the first reaction by 3, and then summing, leads to cancellation of the intermediates NO and NO_3, and yields the stoichiometric equation. If the mechanism is long (some mechanisms consist of hundreds of reactions) the summation would be extremely laborious if done by hand, but still must yield the stoichiometric equation if the mechanism is accurate.

It may be necessary to include energy transfer processes in the mechanism. Energy transfer refers to unreactive bimolecular collisions in which translational, rotational, vibrational, and electronic energy are redistributed between collision partners. The energy transferred may be translational, rotational, vibrational, or electronic, and may consist of any combination of these forms of energy. All collisions involve energy transfer all of the time, and fortunately only certain ones of them become important for the correct description of a reacting system. These have to do with non-thermal equilibrium energy distributions which are created by chemical reactions. Non-thermal energy distributions result when reactions deplete the population of certain energy states of a reacting species faster than they can be repopulated by collisions, and as a result, thermal equilibrium energy distributions cannot be maintained. Non-thermal energy distributions also result when the products of exothermic reactions are initially formed with non-equilibrium energy distributions faster than the non-equilibrium distributions can be thermalized. These effects can substantially affect the rate of an overall reaction, and when they do so the failure to include them in the mechanism can seriously compromise reaction models. It is only relatively recently that researchers have begun to include energy transfer in reaction models, and many models in the literature do not take energy transfer into account at all. Energy transfer steps can sometimes simply be written as elementary bimolecular processes in the list of elementary chemical reactions. Approaches to modeling the rate at which energy transfer proceeds are dealt with in Chapter 4.

Writing the rate equation for each elementary reaction in the mechanism gives a set of coupled differential equations, and the problem to be

solved is to find the solution to this set of equations. The equations are coupled through the chemical species, which usually occur in more than one elementary reaction. In homogeneous systems with uniform composition, it is a set of ordinary differential equations. If spatial variations of concentration exist, then a set of partial differential equations must be solved. If the set of equations can be reduced to a single differential rate equation, it must agree with the empirical rate expression, and is an important test of a mechanism. Reduction to a single differential equation is frequently possible when the mechanism is limited to only a few reactions. In some cases, analytical solutions exist. See, for example, the text by Szabo [13]. See also Chapter 2 of Ref. [6], which, in addition, gives methods for solving sets of linear differential equations. For longer mechanisms with non-linear equations numerical simulation is necessary. Chapter 2 of Ref. [6] provides a good introduction to numerical methods. The simulation must give time dependent concentrations of reactants and products that agree with experimentally determined concentration profiles, and the predicted concentrations must agree with the concentration dependence of the overall rate expression.

More than one mechanism can usually be found to satisfy the stoichiometric and rate criteria. Distinguishing between mechanistic possibilities requires careful experimental diagnostics, and deep insight into the chemistry of the system. The nature of the experimentation is to attempt to disprove the involvement of certain postulated elementary reactions in the mechanism. Modern experimental methods are quite sensitive and fast, and frequently allow direct detection of intermediates and their time dependence. Experiments such as these are extremely valuable for discriminating between mechanistic possibilities, but they are costly and time consuming. Proving that a particular elementary reaction occurs can be very difficult, and gives rise to the caveat that a mechanism can never be proved, only disproved. When mechanistic predictions disagree with experimental data, the mechanism can unequivocably be stated to be deficient, but when the predictions of a particular mechanism agree with experiment it is always possible that an alternate mechanism could be found that would also agree with the experiments. Considerable time, effort, and care must be devoted to the development and validation of a reaction mechanism. Fortunately, there is an enormous chemical literature of experimental and theoretical work that has been accumulated, and can be brought to bear on this problem. Chapter 5 is devoted to the construction of reaction mechanisms, and Chapter 6 to methods of analysis aimed at judging accuracy and reliability of reaction models.

2.9 The steady state approximation

An important method that has been much used in the past to aid in the analysis of reaction mechanisms and that can be effectively used to reduce the computational effort required for numerical solution of a set of simultaneous differential rate equations is the steady state approximation. In this method, the net rates of formation of highly reactive intermediates, X, are set equal to zero, $d[X]/dt = 0$, thereby transforming some of the differential equations into algebraic equations, and the problem to be solved becomes a set of differential/algebraic equations. It is instructive to examine the steady state approximation more closely to better understand the conditions for which it is a good approximation. To this end the sequence of irreversible elementary reactions $A \rightarrow B \rightarrow C$, with rate coefficients k_1 and k_2, provides a good example. The rate expressions are: $-d[A]/dt = k_1[A]$; $d[B]/dt = k_1[A] - k_2[B]$; $d[C]/dt = k_2[B]$. With the initial conditions $[A] = [A_0],\ t = 0;\ [B_0] = [C_0] = 0,\ t = 0$, and setting $x = [A]/[A_0]$, $y = [B]/[A_0]$, $z = [C]/[A_0]$, there is an analytical solution, given below:

$$x = \exp(-k_1 t) \tag{28}$$

$$y = \left[\frac{k_1}{k_2 - k_1}\right][\exp(-k_1 t) - \exp(-k_2 t)] \tag{29}$$

$$z = 1 - \left[\frac{k_2}{k_2 - k_1}\right] \exp(-k_1 t) + \left[\frac{k_1}{k_2 - k_1}\right] \exp(-k_2 t) \tag{30}$$

Figure 2 shows $x(t)$, $y(t)$, and $z(t)$ for $k_1/k_2 = 10$ and 0.1. It is clear that as k_1/k_2 decreases, the concentration of the intermediate, B, decreases, and the time at which [B] is maximum shifts to shorter times. It can be shown that

$$y_{\max} = \left[\frac{k_1}{k_2}\right]^{k_2/(k_2 - k_1)} \tag{31}$$

$$t_{\max} = \frac{\ln(k_2/k_1)}{k_2 - k_1} \tag{32}$$

If $k_2 \gg k_1$, then $t_{\max} \rightarrow 1/k_2$. As $k_1/k_2 \rightarrow 0$, the time dependence of x, y, and z becomes

$$x = \exp(-k_1 t) \tag{33}$$

$$y \rightarrow \left(\frac{k_1}{k_2}\right) \exp(-k_1 t) \tag{34}$$

$$z \rightarrow 1 - \exp(-k_1 t) \tag{35}$$

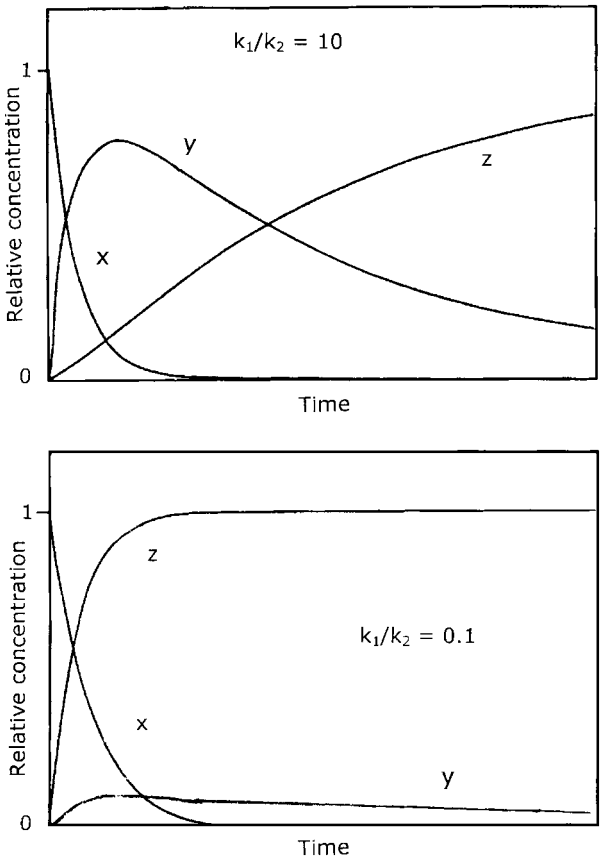

Fig. 2. Plots of $x(t) = [A(t)]/[A_0]$, $y(t) = [B(t)]/[A_0]$, and $z(t) = [C(t)]/[A_0]$ for the reaction sequence $A \rightarrow B \rightarrow C$ (with rate coefficients k_1 and k_2, respectively) where $k_1/k_2 = 10$ and 0.1.

and as $t_{max} \rightarrow 0$, $dy/dt \rightarrow 0$. This is the solution to the set of equations

$$-\frac{dx}{dt} = k_1 x \tag{36}$$

$$0 = k_1 x - k_2 y \tag{37}$$

$$\frac{dz}{dt} = k_2 y \tag{38}$$

This set of two differential equations and one algebraic equation replaces the original set of three differential equations. In practice, k_1/k_2 will not be infinitely small, but may nevertheless be small enough that $dy/dt \approx 0$, and

replacing dy/dt with 0 in the original set of equations will yield an approximate solution that will improve as k_2/k_1 decreases.

The formal kinetics $A \rightarrow B \rightarrow C$ occurs commonly in practice. Consider the reactivity of the free methyl radical, generated by azomethane pyrolysis, with an alkane, RH:

$$(CH_3)_3N \equiv N(CH_3)_3 \rightarrow 2CH_3 + N_2$$
$$CH_3 + RH \rightarrow CH_4 + R$$

If this reaction is carried out at a total pressure of 1 atm and at 700 K, $[RH] \approx 10^{19}$ molecules cm^3. Because of the high reactivity of CH_3, one expects $[RH] \gg [CH_3]$, and if the conversion of azomethane is small [RH] will be nearly constant over the course of the reaction. The bimolecular rate of the reaction of CH_3 with RH, $r = k_2[CH_3][RH]$, can be expressed as $k_2'[CH_3]$, where $k_2' = k_2[RH]$. The apparent kinetic order of this reaction is then 1, and with a constant concentration folded into the rate coefficient, is spoken of as pseudo-first order. This two-step reaction sequence is now formally equivalent to $A \rightarrow B \rightarrow C$. Using data from the literature, $k_2'/k_1 = 10^{-13}$ to 10^{-14}, and we expect the steady state approximation to be quite good. The above relationships from the formal $A \rightarrow B \rightarrow C$ sequence can be used in many practical situations to test the validity of the steady state approximation. For mechanisms of modest length, making the steady state approximation for the reactive intermediates frequently permits derivation of a closed form rate expression that aids greatly in the analysis of rate data. A common example is the reaction of H_2 and Br_2, which is given in many kinetic texts. For longer mechanisms, where numerical solution is required, applying the steady state approximation converts some of the differential equations to algebraic equations and reduces the computational effort. This is not necessary if one is only interested in reactions where the composition is uniform, for modern computers can handle even very large mechanisms without the assistance of the steady state approximation. However, in distributed parameter systems such as occurring commonly in reactive flows, applying the steady state approximation may facilitate the numerical solution.

2.10 Microscopic reversibility and detailed balance

Microscopic reversibility and detailed balance are important kinetic concepts. The former provides a mechanical argument for the reversibility of chemical reactions, while the latter shows a connection between kinetics and thermodynamics, and provides an important principle that must be applied in writing mechanisms.

It is well known that all chemical reactions have an equilibrium state where the concentrations of reactants and products are time invariant, and that this state is reached regardless of whether one starts the reaction by contacting the reactants or by contacting the products. This is true of both elementary reactions and stoichiometric reactions. Thus, all reactions are said to be reversible, and the chemical composition at equilibrium depends solely on thermodynamic state functions. The description of reaction equilibria can be found in many texts on thermodynamics.

Microscopic reversibility is a non-thermodynamic argument for the reversibility of elementary chemical reactions. This principle derives from the fact that the equations of motion for atoms and molecules are invariant under time reversal. The momenta of a pair of atoms or molecules on a particular collision trajectory change as a result of the collision. If, in the final state after the collision, all of the momenta of the translational, rotational, and internal motions of the collision products are reversed, then the trajectory is exactly retraced and a state similar to the initial state is reached, except that the momenta are reversed. This will be true irrespective of whether classical or quantum mechanics are used to describe the equations of motion, and is a consequence of the fact that the equations of motion have the same form when t is replaced by $-t$. It is true of both unreactive collisions (energy transfer) and reactive collisions. Thus, we see that reactions are required to be reversible when the time dependent behavior of the energy states is considered.

The application of microscopic reversibility to each molecular reactive collision in a chemical reaction system consisting of a statistically large assembly of molecules with a distribution of momenta and internal energy states is called the principle of detailed balance. Detailed balance requires one to write all elementary reactions as reversible, and it permits one to rule out some types of mechanisms, such as the cyclic sequence of the following equation:

(39)

Although it is possible to envision starting with pure A and reacting until a cyclic equilibrium is obtained, this cannot occur as written because detailed balance is not satisfied. Detailed balance requires each of the three steps to be reversible, as in the following equation:

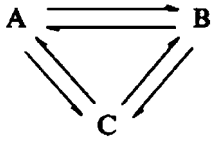

(40)

In developing mechanisms, one must be careful not to include sequences of reactions that lead to unallowable cyclic processes because of a failure to observe detailed balance. Such sequences may inadvertently creep in. Frequently it is computationally advantageous to reduce the number of reactions by omitting the reverse steps of reactions that go very nearly to completion before equilibrium is established. This is a permissible approximation only if it does not lead to unallowable cyclic equilibria.

Detailed balance gives a connection between kinetics and thermodynamics. In a reaction at chemical equilibrium, the concentrations of reactants and products are time invariant, but microscopic reversibility informs us that reactive collisions must still be occurring. The conclusion is that at equilibrium both the forward and the reverse reactions must occur at the same rate. If we consider a reversible reaction, such as

$$A + B \Leftrightarrow C + D$$

and if this is an elementary reaction the rate of the forward reaction, r_f, and the rate of the reverse reaction, r_b, may be written by inspection as

$$r_f = k_f[A][B] \tag{41}$$

$$r_b = k_b[C][D] \tag{42}$$

At equilibrium, $r_f = r_b$, so that we may write

$$\frac{k_f}{k_b} = \frac{[C]_E[D]_E}{[A]_E[B]_E} \tag{43}$$

From thermodynamics we know that the concentration equilibrium constant is given by

$$K_C = \frac{[C]_E[D]_E}{[A]_E[B]_E} \tag{44}$$

from which it is seen that

$$K_C = \frac{k_f}{k_b} \tag{45}$$

Equation (45) is always valid for elementary reactions, and will also be true for stoichiometric reactions if the kinetic order with respect to each reactant and product is equal to its stoichiometric coefficient.

For stoichiometric reactions in general the relationship between forward and reverse rate coefficient and the equilibrium constant given above for elementary reactions must be expressed as

$$\frac{k_f}{k_b} = K_C^n \tag{46}$$

where n is a number that may have any positive value, and must be determined from the stoichiometric coefficients and the kinetic order in both the forward and the reverse directions [1]. This relationship holds for stoichiometric reactions that have rate expressions of the form $r = k_f\Pi[A_i]^{ai} - k_b\Pi[A_k]^{ak}$, where subscript i is for reactants and subscript k is for products. For empirical rate expressions having other forms, equation (46) should not be used.

If the mechanism of a stoichiometric reaction is not known, serious errors can be made in the application of equation (45). For example, suppose the mechanism of the stoichiometric reaction $A \leftrightarrow B$ is given by the following two reactions:

$$A \leftrightarrow X$$

$$X \leftrightarrow B$$

By application of detailed balance it is found that $K_{C1} = k_{f1}/k_{b1} = [X]_e/[A]_e$, $K_{C2} = k_{f2}/k_{b2} = [B]_e/[X]_e$, and $K_C(\text{overall}) = (k_{f1}/k_{b1})(k_{f2}/k_{b2}) = [B]_e/[A]_e$. In fact, it is true that for any sequence of elementary reactions $K_C(\text{overall}) = \Pi k_{fi}/k_{bi}$. However, if the participation of X in the reaction is unknown, as might be the case if the kinetics are determined from initial reaction rates, the rate expressions would be found to be $-d[A]_{t=0}/dt = k_{1f}[A]_{t=0}$, starting from pure A. Starting the reaction from pure B, $-d[B]_{t=0}/dt = k_{2b}[B]_{t=0}$ would be found. If it is assumed that the mechanism of conversion of A to B is given by $A \leftrightarrow B$, then detailed balance predicts that $K_C = k_{f1}/k_{b2}$, which is incorrect.

Equation (45) is a powerful and useful relationship for it allows the calculation of one of the rate coefficients of an elementary reaction, either k_f or k_b, from thermodynamic data if the other one is known. The relationship is given by

$$K_C = \frac{k_f}{k_b} = \prod_{i=1}^{S}[A_i]^{v_i} \tag{47}$$

where the concentration equilibrium constant, K_C, it must be emphasized, differs from the thermodynamic equilibrium constant, $K(T)$, which is given by

$$K(T) = \exp\left(\frac{-\Delta G_T^0}{RT}\right) \tag{48}$$

where ΔG_T^0 is the standard Gibbs free energy change of the reaction at the absolute temperature T. For reactions between ideal gases the relationship between concentration equilibrium constant and the

thermodynamic equilibrium constant is

$$K_C = K(T)(RT)^{-\Delta v} \tag{49}$$

Here $\Delta v = \sum v_i$. For reactions in ideal solutions it is given by

$$K_C = K(T)(c^0)^{\Delta v} \tag{50}$$

where c^0 is the standard state concentration, usually taken to be $1\,\mathrm{mol\,l^{-1}}$. Ref. [1, pp. 138–145, 290–299], the former for gases and the latter for solutions, gives a thorough discussion of these relationships and also their temperature dependence.

3 POTENTIAL ENERGY

The potential energy of interaction between atoms, molecules, ions, and free radicals, $V(\mathbf{r})$, where the vector $\mathbf{r}$ gives the interparticle separation and orientation, plays a central role in determining the chemical reactivity of these species. Chemical reactions must, at some fundamental level, be describable in terms of forces operating between atoms or groups of atoms as the transformation takes place. The force, $F(\mathbf{r})$, is given by the negative gradient of the potential, $F(\mathbf{r}) = -\mathrm{d}V(\mathbf{r})/\mathrm{d}\mathbf{r}$, so the rate coefficients of elementary reactions and the microscopic rate coefficients of state-to-state processes will depend on $V(\mathbf{r})$ in any dynamical model.

3.1 The Born–Oppenheimer approximation

In atoms and molecules the speed of the electrons is much faster than the motions of the heavy nuclei, and it is possible to mathematically separate the motion of the electrons from the motions of the nuclei. That is, the electrons are considered to adjust instantaneously to changes in relative positions of the nuclei, permitting the potential energy to be expressed as a function only of nuclear positions. This is known as the Born–Oppenheimer approximation. The Born–Oppenheimer approximation predicts that each electronic quantum state of a molecule is characterized by a potential energy function, if the electronic states are sufficiently separated in energy that their potential energy functions do not interact with one another. Non-interacting potential energy functions are referred as adiabatic potentials. In most cases in this book, only the adiabatic potential of the lowest energy or ground electronic state is considered, because at the reaction temperatures we are interested in higher electronic states for the vast majority of cases have negligible

populations. However, there are cases where the Born–Oppenheimer approximation fails, causing transitions to occur between electronic states during the course of a reaction. When this happens the reaction is called a non-adiabatic reaction, and it must be treated by special means.

3.2 *Long-range potentials*

The asymptotic behavior of the potential is $V(\mathbf{r}) \to 0$ as $\mathbf{r} \to \infty$. As particles approach one another the interaction increases. Interactions that occur over a few atomic radii are called long-range interactions. For some types of long-range interactions the potential is well known. For example, the interaction between two ions is described by the Coulomb potential, with the vector $\mathbf{r}$ replaced with the scalar r because the potential is independent of orientation in this case

$$V(r) = \frac{z_1 z_2 e^2}{r} \tag{51}$$

where z_1 and z_2 are the number of charges on each ion, including the plus or minus sign, and e the electronic charge. For oppositely charged ions $V(r)$ is negative and the ions attract, and for like charges they repel one another. For the interaction of ions with neutrals there are two cases, depending on whether or not the uncharged particle has a permanent dipole moment. An ion interacting with a molecule having no permanent dipole moment will induce a moment, and the orientation independent potential is given by

$$V(r) = -\frac{\alpha(ze)^3}{2r^4} \tag{52}$$

where the neutral species has polarizability α. The potential between an ion and a species with a permanent dipole moment depends on both r and the angle θ between the direction of the dipole, μ_D, and r

$$V(r, \theta) = \frac{-ze\mu_D \cos\theta}{r^2} \tag{53}$$

3.3 *Short-range repulsive forces*

For interactions between neutrals, both long- and short-range interactions have to be accounted for. At long range van der Waals dispersion forces or incipient chemical bonding are operative, and at short range the Pauli exclusion principle ensures a strong repulsive force. Empirical potentials have been extensively used to describe binary

interactions to avoid the difficult problem of determining $V(\mathbf{r})$ from first principles. For non-bonded species the Lennard–Jones expression provides a reasonably realistic empirical potential. Spherical particles are assumed, so $\mathbf{r}$ is replaced by the scalar r. The inverse 6th

$$V(r) = 4\varepsilon_{LJ}\left[\left(\frac{\sigma_{LJ}}{r}\right)^{12} - \left(\frac{\sigma_{LJ}}{r}\right)^{6}\right] \tag{54}$$

power term represents attraction (the minus sign), due to dispersion forces, the inverse 12th power term gives a steep short-range repulsion, and as a result the potential curve has a minimum at r_e where the two species exist as a non-bonded pair. The parameter σ_{LJ} is the value of r when $V = 0$ in the repulsive region, and ε_{LJ} is the value of V at $dV/dr = 0$. Typically the well depth is of order $1\,\mathrm{kJ\,mol^{-1}}$ and dimers only exist at low temperatures.

3.4 Bonding interactions

Of particular interest is the situation where chemical bonds are formed as a result of interactions between atoms, atoms and molecules, and molecules. The simplest of these is the formation of a diatomic molecule from two atoms where $V(r)$ is only a function of the internuclear distance, r. A typical potential curve is shown in Fig. 3. The potential

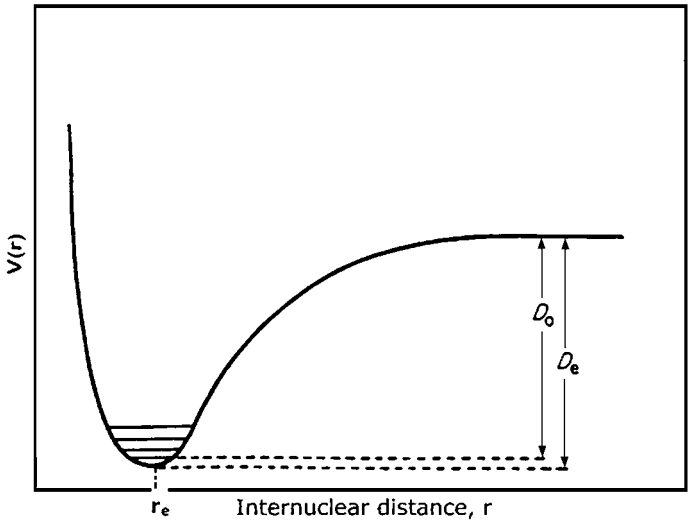

Fig. 3. Typical potential energy curve for a diatomic molecule. D_0 and D_e are bond dissociation energies measured from the vibrational zero point energy and the bottom of the potential well, respectively, and r_e is the equilibrium bond distance.

energy as a function of internuclear distance can be estimated by quantum chemistry methods, or by a combination of empiricism and vibrational spectroscopy. An empirical potential that has been extensively used is the Morse function

$$V = D_e[\exp(-2\beta R) - 2\exp(-\beta R)] \tag{55}$$

It consists of an attractive part to describe the forces driving formation of the bond, and a short-range repulsion required by the Pauli exclusion principle. The attractive term dominates over a range of r values where the diatomic molecule is stable. D_e is the bond dissociation energy measured from the bottom of the potential well, D_0 the dissociation energy measured from the vibrational zero point energy level, $R = r - r_e$ the displacement from the potential minimum, and $\beta = \nu(\mu/2D_e)^{1/2}$, where ν is the fundamental vibrational frequency and $\mu = m_1 m_2/(m_1 + m_2)$, where m_1 and m_2 are the masses of the two particles, the reduced mass. It is seen that $V(r)$ is described by quantities that can be obtained from experiment.

3.5 Potential energy surfaces

For polyatomic molecules the electronic potential is a function of more than one internuclear distance. It cannot be graphically represented in the plane of $V(r)$ and r, but requires a space of higher dimensionality. For a molecule of N atoms, $3N$ Cartesian coordinates are required to specify the position of each atom. The electronic potential energy is independent of location in space and depends only on the relative positions of the atoms, which for any pair x and y is given by the vector $\mathbf{R}_{xy}$. Thus, only $N-1$ vector distances, or $3N-3$ Cartesian coordinates, are required, the discarded three Cartesian coordinates being those that locate the (unnecessary) position of the molecule in space.

Consider a stable triatomic molecule consisting of the atoms A, B, and C. Six Cartesian coordinates are required to specify their relative positions. If B is the central atom, specifying $\mathbf{R}_{AB}$ and $\mathbf{R}_{BC}$ gives $\mathbf{R}_{AC}$ because $\mathbf{R}_{AC} = \mathbf{R}_{AB} - \mathbf{R}_{BC}$, and the six Cartesian coordinates are three for $\mathbf{R}_{AB}$ and three for $\mathbf{R}_{BC}$. An alternative description would be to specify three scalar distances, either R_{AB}, R_{BC}, and R_{AC}, or R_{AB}, R_{BC}, and the ABC bond angle, plus three coordinates to give the spatial orientation of the plane of the three atoms. Because the potential energy does not depend on spatial orientation, but only on the relative separations of the atoms, three scalar coordinates suffice to give the potential energy as a function of their relative positions.

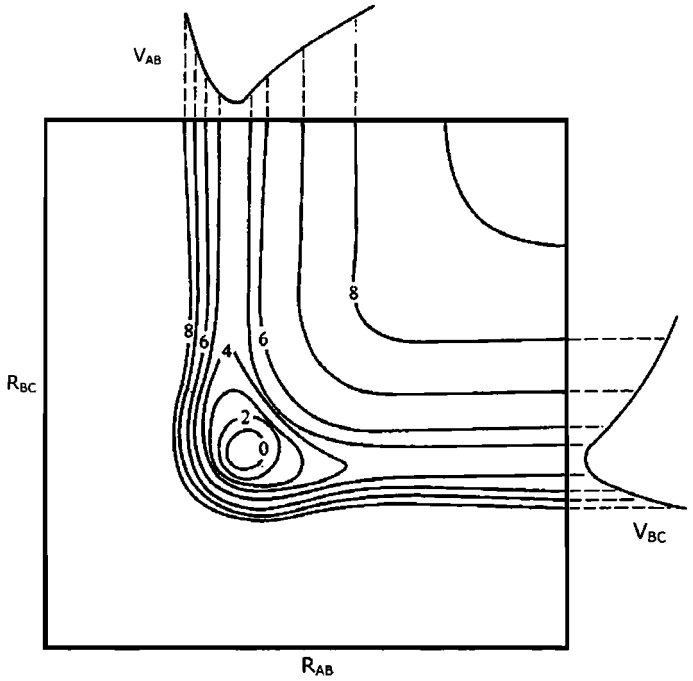

Fig. 4. Potential energy surface for a stable triatomic molecule, ABC, showing dissociation to A and C atoms.

If the ABC bond angle is held constant, the potential energy as a function of R_{AB} and R_{BC} can be plotted in three Cartesian dimensions, R_{AB}, R_{BC}, and energy, to yield a visualizable potential energy surface (PES). The surface is conventionally plotted with the bond lengths as the x and y coordinates and energy as the z coordinate. Figure 4 shows how a projection of contour lines of constant potential energy onto the plane of R_{AB} and R_{BC} might look. The minimum of potential energy gives the bond lengths of the stable molecule at the fixed bond angle. Other bond angles would give other, similar, surfaces. The plateau in the upper right hand corner gives the energy of the atoms at large separation corresponding to complete dissociation. Starting at the potential minimum and moving parallel to either R_{AB} or R_{BC} describes dissociation into an atom and a diatomic molecule. It is apparent that the PES contains information not only on molecular structure, but also on chemical reactivity.

Now consider a reaction between an atom and a diatomic molecule, $A + BC = AB + C$, where a stable triatomic molecule ABC does not exist. The PES can be described with the same coordinates used for the stable triatomic, but it will have a different shape because the minimum

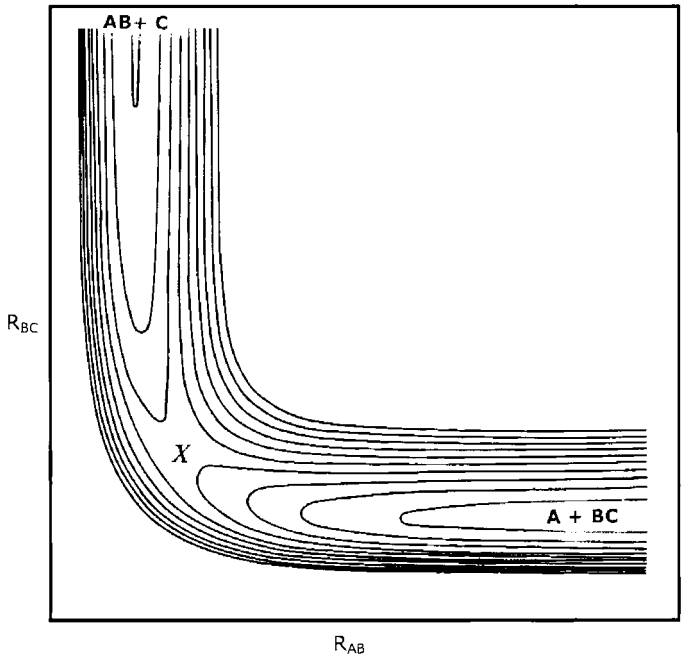

Fig. 5. Potential energy surface for triatomic ABC reaction system where a stable triatomic molecule is not formed.

will be absent. Figure 5 shows a typical PES for this type of reaction where the potential energy shows a maximum in the region of close ABC interaction. The region of close interaction between A, B, and C looks, to an observer standing at x, like a mountain pass, with energy decreasing from the summit, at x, in the direction of increasing R_{AB} and also in the direction of increasing R_{BC}, and increasing steeply for symmetric extension and compression of both R_{AB} and R_{BC}. This clearly shows the instability of ABC with respect to dissociation into an atom (either A or C), and its relative stability with respect to complete dissociation into three atoms. A picture of the reaction emerges by starting at large R_{AB} and following the path of lowest energy as R_{AB} decreases. At first one climbs the grade to the pass if the reactants have enough energy to surmount the pass, and then ABC either redissociates by retreating along the same path or continues down the other side to form diatomic AB and atom C. The pass is a potential energy barrier which causes this reaction to have an activation energy (but note that the vertical height of the barrier is not numerically equal to the activation energy (see equation (26)), and plays a critical role in determining the numerical value of the reaction rate coefficient. PESs of this type resemble a saddle, and

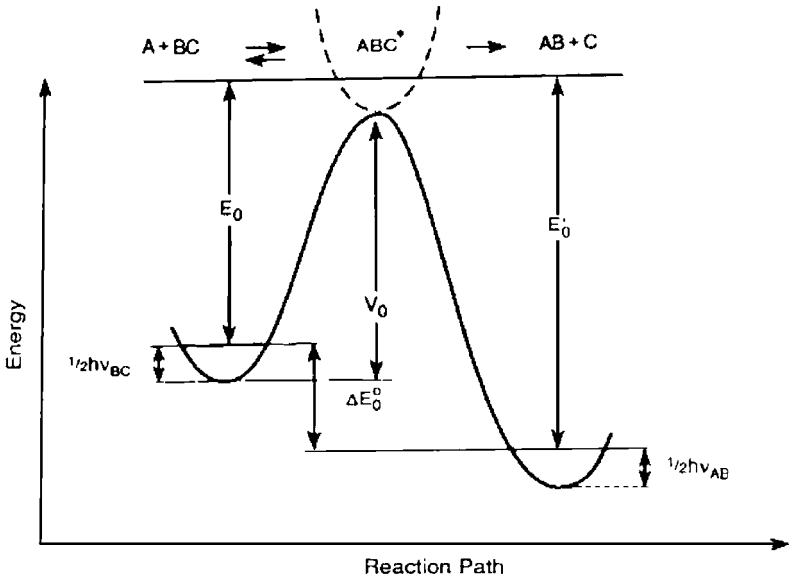

Fig. 6. Reaction path profile for the reaction of A with diatomic molecule BC.

point x, the summit of the pass, is commonly referred as a *saddle point*. The relative motions of A, B, and C as they proceed toward either AB or BC along the minimum energy path is called the *reaction coordinate.*

Figure 6 shows a reaction path profile, the trace of the path of lowest potential energy over a surface with a single electronic barrier, as in Fig. 5. This is a useful construction, although the bond distances are lost in making it. The path shows the potential energy minima of the reactant and product diatomic molecules, and the potential energy maximum, V_0. Also shown are the vibrational zero point energies of the diatomic molecules, and the zero point vibrational energy of the symmetric stretch motion of ABC in the potential well of the steep side walls at the top of the pass. The bending vibration cannot be represented because the path is derived from a surface with a fixed ABC bond angle. Also shown is ΔE_0°, the standard internal energy change of the reaction, and E_0 and E_0', which are the activation energies of the forward and reverse reactions, respectively, at the absolute zero of temperature. Reaction path profiles are frequently used to represent the energetics of reactions involving four or more atoms, although in these cases it must be remembered that the dimensionality of the PES is greater than 3, and so the representation merely facilitates our visualization of how the reaction proceeds. Nevertheless, the two-dimensional representation is extremely useful for this purpose, and can be thought of as a reaction path in which the

important changes involve only three atoms, the remainder of the atoms present being assumed not to influence the potential energy changes in the reaction coordinate, so the reaction profile can be thought of in terms of the triatomic case. PESs may have considerable complexity, with multiple maxima and minima if they describe the potential energy changes accompanying a sequence of elementary reactions. The reaction path profiles for multistep reactions will then have multiple maxima and minima. The chapter on pressure dependent reactions shows some reaction path profiles for such reaction systems, and illustrates the usefulness of reaction path profiles for visualization.

Electronic potentials for polyatomic molecules which have not been constrained for presentation in three dimensions require higher dimensionality, and are termed potential energy *hypersurfaces*. There will be many hypersurfaces for each molecule, each corresponding to a different electronic state. There also will be many hypersurfaces over which a chemical reaction can occur. When a reaction occurs on a single hypersurface connecting the reactant(s) to the product(s) the reaction is said to be electronically adiabatic, and when a transition between hypersurfaces occurs during reaction the reaction is said to be non-adiabatic. Most thermal chemical reactions occur adiabatically on the electronic ground state hypersurface. Reactions involving electronically excited reactants, whether they are formed thermally or photochemically, require consideration of the role of electronically excited hypersurfaces.

The hypersurface plays a critical role in determining the reaction rate and the mechanism by which a reaction occurs, as is apparent from the simple triatomic example above. It is enormously useful to know the surface, both for understanding how the reaction proceeds and for estimation of the rate parameters. Qualitative information on the nature of the surface can be obtained from kinetic experiments. It can be determined if there is a potential barrier between reactant(s) and product(s) as evidenced by an activation energy, or if a potential energy minimum exists, which would be indicated by a pressure dependent apparent rate coefficient. While obtaining quantitative information on the surface is possible from spectroscopy, it is not a practical matter to do so. Most of the available information on PESs has been obtained from electronic structure calculations. In recent years methods for performing calculations of high accuracy have become available and are the method of choice for investigating PESs. Chapter 2 discusses methods for computing thermochemical data for stable molecules, i.e., for chemical species existing at a potential energy minimum. Potential energy minima are stationary points where $\partial V(\mathbf{r})/\partial \mathbf{r} = 0$ and where the curvature of the surface is positive in all directions. A saddle point on a PES for a

chemical reaction is also a stationary point, but the curvature is negative for one of the internal coordinates that corresponds to atomic motion leading to reaction products. This motion is called the *reaction path*, and these structures are called *transition states*. The computational methods described in Chapter 2 for stable molecules can also be applied to transition states. Chapter 5 discusses the use of computational chemistry for transition state structures and energies.

4 BIMOLECULAR REACTION RATE THEORY

4.1 Simple collision theory

Simple collision theory (SCT) is an early theory of bimolecular reactions that was developed in the first decades of the twentieth century. Although SCT oversimplifies collision dynamics, and is of limited predictive power, it provides a beginning point for the collision dynamics approach to bimolecular reactions, and the beginnings of insight into factors that affect chemical reactivity. SCT also permits estimates to be made of the upper limit expected for the value of the bimolecular gas phase reaction rate coefficients from the rate of gas phase collisions. For these reasons SCT is worthy of examination.

The SCT model considers reaction between chemical species A and B, each considered to be structureless, spherical masses that interact according to the hard sphere potential: $V(r) = 0,\ r > d_{AB};\ V(r) = \infty,\ r = d_{AB}$, and all collisions result in reaction. The last may be restated as a reaction probability: the probability of chemical reaction, $P(r)$, is 1 when $r = d_{AB}$ and 0 otherwise. The collision diameter, $d_{AB} = (d_A + d_B)/2$, where d_A and d_B are the molecular diameters of A and B, respectively, defines the interaction distance for these billiard ball-like collisions. The collision rate, Z_{AB}, is

$$Z_{AB} = \pi d_{AB}^2 \left(\frac{8k_B T}{\pi\mu}\right)^{1/2} n_A n_B \tag{56}$$

and if the reaction is not between different chemical species, but rather between the same chemical species, say A, the collision rate is

$$Z_{AA} = \pi d_{AA}^2 \left(\frac{4k_B T}{\pi m}\right)^{1/2} n_A^2 \tag{57}$$

In these equations, $\mu = m_A m_B/(m_A + m_B)$ is the reduced mass of the collision pair, m the species molecular mass, k_B the Boltzmann constant, T the absolute temperature, and n_A and n_B the molecular densities. The

derivation of these equations can be found in any text on physical chemistry or kinetic theory of gases, and in most texts on chemical kinetics. Tabulations of molecular diameters, mostly obtained from gas viscosity measurements, can be found in texts on transport phenomena, such as Hirschfelder *et al.* [14], and in handbooks. The appropriateness of using transport data may be questioned, since interactions leading to chemical reaction might reasonably be expected to be different from the physical interactions governing transport properties. However, simple collision theory is based on a very elementary collision model, and this subtlety can be ignored.

For an elementary reaction of species A with species B, the rate of disappearance of A is given by the kinetic rate expression

$$\frac{-\mathrm{d}n_{\mathrm{A}}}{\mathrm{d}t} = kn_{\mathrm{A}}n_{\mathrm{B}} \tag{58}$$

If reaction occurs on every hard sphere collision, the rate of disappearance of A is equal to the collision rate, Z_{AB}. Comparison of equations (56) and (58) shows that the SCT expression for the rate coefficient, k_{SCT}, for reaction between A and B is

$$k_{\mathrm{SCT}} = \pi d_{\mathrm{AB}}^2 \left(\frac{8k_{\mathrm{B}}T}{\pi\mu}\right)^{1/2} \tag{59}$$

For reaction between identical species k_{SCT} is given by

$$k_{\mathrm{SCT}} = \pi d_{\mathrm{AA}}^2 \left(\frac{4k_{\mathrm{B}}T}{\pi m}\right)^{1/2} \tag{60}$$

In equation (59), πd_{AB}^2 is the area projected by A such that all trajectories of B passing within d_{AB} of A result in collision with A, and all trajectories passing outside of d_{AB} result in no collision. Thus, πd_{AB}^2 is the collision cross-sectional area, and in SCT it is also the reaction cross-section. Also, in equation (59), $(8k_{\mathrm{B}}T/\pi\mu)^{1/2}$ is the average relative speed of A and B, and we see that the rate coefficient can be written as the product of the cross-section, σ, and the average speed, $\langle v \rangle$

$$k_{\mathrm{SCT}} = \sigma\langle v\rangle \tag{61}$$

Similar considerations are obtained starting from equation (59) for collisions of the same species.

If the molecular diameters of A and B are 4×10^{-8} cm, typical numbers for modest sized gases, and the average speed is $5 \times 10^{4}\,\mathrm{cm\,sec^{-1}}$, also typical for temperature in the vicinity of 300 K, then $k_{\mathrm{SCT}} \sim 2.5 \times 10^{-10}\,\mathrm{cm^3\,molecule^{-1}\,sec^{-1}}$ is predicted. This is an approximate upper limit for the bimolecular rate coefficient for reaction between

two neutral reactants. There is some uncertainty in this upper limit because collision diameters are uncertain. For reactions between oppositely charged ions, and for ion–molecule reactions, the long-range attraction gives rise to larger cross-sections and somewhat larger bimolecular rate coefficients than for neutrals. However, bimolecular rate coefficients for reactions between neutral species that are reported to be significantly larger than the SCT prediction may be confidently rejected for use in kinetic models.

When a reaction has an activation energy the bimolecular rate coefficient will be smaller than the upper limit estimate. In SCT it is assumed that the relative kinetic energy of two reactants, which are treated as though they are structureless point masses, along their line of centers must be greater than V_0 (see Fig. 5) for particles obeying classical mechanics to cross the barrier. The simplest assumption is that reaction occurs at every collision for collision pairs with energy greater than V_0. That is, the reaction probability, $P(r)$, is unity for such pairs. If the relative kinetic energy is less than E_0 the barrier cannot be crossed and $P(r) = 0$. The fraction of reactants having energy greater than V_0 is $\exp(-V_0/RT)$, so with these assumptions the rate coefficient is given by

$$k = k_{\mathrm{SCT}} \exp\left(\frac{-V_0}{RT}\right) \tag{62}$$

This expression is formally similar to the Arrhenius equation, but not equivalent to it because V_0 is not the activation energy, which is given by equation (26), and because k_{SCT}, the pre-exponential factor, is not independent of temperature as the Arrhenius equation requires. However, the $T^{1/2}$ dependence of k_{SCT} anticipates the temperature dependent pre-exponential factors that are predicted by other more sophisticated molecular theories of reaction rate coefficients. Because barrier heights for real reactions have been found to range from very low values, near $1\,\mathrm{kcal\,mol^{-1}}$, to chemical bond strengths in the vicinity of $100\,\mathrm{kcal\,mol^{-1}}$, the exponential term can reduce bimolecular rate coefficients to many orders of magnitude below the SCT upper limit estimate, and we see that the possible range of bimolecular rate coefficients is extremely wide.

The activation energy is defined by $E_{\mathrm{a}} \equiv -R\,\mathrm{d}\ln k(T)/\mathrm{d}(1/T)$. Substituting the rate coefficient expression of equation (60), collision theory predicts that $E_{\mathrm{a}} = V_0 + 1/2RT$, and in addition, from equation (58) it predicts that $A = (8\pi k_{\mathrm{B}}T/\mu)^{1/2} d_{\mathrm{AB}}^2 \exp(1/2)$. Thus, the SCT model predicts that both the activation energy and the pre-exponential factor are temperature dependent quantities. To test collision theory, experimentally determined values of E_{a} and A can be compared with the above

predictions. Although it is now possible to calculate V_0 by the methods of modern computational chemistry, in the past this was not so, and it was common practice to only compare pre-exponential factors when an experimental activation energy was available. Pre-exponential factors predicted by SCT are all of order $10^{-10}\,\mathrm{cm}^3\,\mathrm{sec}^{-1}$, and from reaction to reaction are only predicted to vary with d_{AB}^2, i.e., by about an order of magnitude. Some experimental A-factors for relatively small reactants are of about the predicted order of magnitude. For example, the SCT predicted rate coefficient for $CH_3 + CH_3 = C_2H_6$ (there is no energy barrier for this reaction) differs by only a factor of 2 from experiment. However, experimental A-factors show far wider variability than can be accounted for by collision theory. They are typically found to be smaller than the SCT prediction, frequently by orders of magnitude (in some cases as much as 10^{-5} times smaller), and to decrease with increasing number of atoms in the reactants. In collision theory it was argued that the discrepancy between theory and experiment could be accounted for by the effect of molecular orientation. In collision theory all approach orientations of the two reactants are assumed to lead to reaction, but it seems reasonable that in real molecules there should be some approach directions that do not lead to a close enough interaction between reactive centers or functional groups for reaction to occur. This led to the introduction of the steric factor, p, an empirical multiplier where $p \leq 1$, applied to the pre-exponential factor to force agreement with experiment. This simple orientation correction is reasonable, but unsatisfying because no quantitative theoretical treatment was available until recently. Smith [15] has modified collision theory to account for both orientation and collision energetics. The modified theory predicts steric factors between 0.1 and 0.01, but cannot account for the smaller values of p that are frequently required to reconcile collision theory with experiment.

The SCT models bimolecular reactions as occurring between structureless, spherical molecules without long-range interactions, and for which only kinetic energy along the line of centers plays a role in surmounting an energy barrier. It is perhaps surprising that such a simple model has any success at all, yet it gets the right order of magnitude for the rate coefficients and pre-exponential factors for some reactions between small gaseous molecules. Numerous kinetic texts provide comparisons of SCT predictions with experiment. The failure of collision theory to predict even an order of magnitude rate coefficient for larger polyatomics is due in part to the simplified potential and in part to the structureless, spherical point masses that serve as a surrogate for real molecules.

4.2 *Bimolecular collision dynamics*

Collision theory has been extended to include the influence of realistic interaction potentials on reactions between two entities assumed to be point masses, and where only their relative kinetic energy is taken into account. The potential is spherically symmetric, so orientation (steric) effects are not included. This approach has had some success in predicting rate coefficients for reactions involving ions, and also the combination of atoms and small free radicals, when there is no energy barrier. In the case of ions the strength of the long-range interaction, which is large enough to overcome the energetics of breaking and reforming chemical bonds, may justify the assumption of structureless point masses [15].

In SCT the thermal rate coefficient is the product of the cross-section and average speed, $k_{\mathrm{SCT}} = \sigma \langle v \rangle$, where the reactive cross-section is $\sigma = \pi d_{\mathrm{AB}}^2$. This result can also be obtained from the microscopic rate coefficient, $k(g)$, for an initial specific collision speed, g, given by $k(g) = \sigma(g)g$, and averaging over all speeds, as shown in equation (63), where $f(g)$ is the Maxwell–Boltzmann velocity distribution

$$k(T) = \int_0^\infty \sigma(g) f(g) g \, \mathrm{d}g \tag{63}$$

Similarly, the rate coefficient for a thermal reaction occurring with the influence of a spherically symmetric potential $V(r)$ can be calculated from equation (63) by relating the cross-section to the potential. A useful relationship from classical scattering dynamics [16] is found in terms of the impact parameter, b. The impact parameter is the distance of closest approach between two particles in the absence of an interparticle force. At large separation, the collision trajectories of two particles will be parallel straight lines, and the impact parameter is the perpendicular distance between the trajectories. The cross-section is given by equation (64),

$$\sigma(g) = \pi b_{\mathrm{max}}^2 \tag{64}$$

where b_{max}, the cut-off impact parameter, is the largest impact parameter for which a reaction occurs (or can be observed experimentally) for a given speed. Larger impact parameters result in interactions where the point of closest approach between the reactive centers is sufficiently large that no chemical reaction is possible. For simple hard spheres, $b_{\mathrm{max}} = d_{\mathrm{AB}}$. For interacting particles, b_{max} depends on g and the interparticle interaction. When there are attractive forces, b_{max} increases because the attraction is able to pull collision partners close enough that reaction can take place. Analysis of collision trajectories shows that when

angular momentum is taken into account, b_{max} is given by the following equation for attractive potentials expressed as $V(r) = -C/r^n$ when $n > 2$:

$$b_{max}^2 = \left[\frac{C(n-2)}{\mu g^2}\right]^{2/n} \frac{n}{n-2} \tag{65}$$

4.3 Ion–molecule reactions

A simple model for the reaction of ions with neutrals that do not have a permanent dipole moment is known as the Langevin model [17]. The potential for ion-induced dipole interactions is given by equation (52), from which we see that $n = 4$, and $C = \alpha z^2 e^2/2$, so the reactive cross-section, $\sigma = \pi b_{max}^2$, is given as

$$\sigma = 2\pi\left\{\frac{\alpha z^2 e^2}{\mu g^2}\right\} \tag{66}$$

The Langevin rate coefficient, $k_L = \sigma \langle v \rangle$, is given by

$$k_L = 2\pi z e \left(\frac{\alpha}{\mu}\right)^{1/2} \tag{67}$$

Note that k_L is independent of the kinetic energy of the reactants. For ion–molecule reactions without an energy barrier, and in the absence of a permanent dipole moment, the Langevin model gives reasonably good estimates of rate coefficients. For example, the rate coefficient for the reaction of Ar^+ ions with H_2 is predicted to be $1.5 \times 10^{-9}\,cm^3\,molecule^{-1}\,sec^{-1}$, and the experimental value is reported to be $1.7 \times 10^{-9}\,cm^3\,molecule^{-1}\,sec^{-1}$ [18]. Other cases for which there is better agreement of the model prediction with experiment can be found, many of them listed in kinetic texts referenced here. The predicted rate coefficients are significantly larger (by approximately an order of magnitude) than those predicted by SCT. This can be attributed to the influence of the attractive potential. Although the Langevin model gives agreement for many cases where comparisons have been made, it fails for reactions having an activation energy. Also, some reservations about reliability have been expressed by Smith [19].

If the neutral has a permanent dipole moment, the potential for the interaction of an ion with the dipole will be given by equation (53). The ion–dipole rate coefficient, k_{ID}, averaged over $\cos\theta$, is given by equation (68). Su and Bowers [20] have tabulated values of $\langle \cos\theta \rangle$

$$k_{ID} = \langle \cos\,\theta \rangle \frac{\mu_D z}{\mu g^2}\left[\frac{2}{\pi \mu k_B T}\right]^{1/2} \tag{68}$$

During the ion–dipole interaction, polarization of the neutral must also occur. The reaction rate coefficient may be considered to be composed of contributions from both the ion–dipole and the ion-induced dipole interactions. An estimate of the total rate coefficient may be made as the sum of the Langevin and the ion–dipole rate coefficients.

4.4 Ion–ion reactions

The approach to deriving the rate coefficient for ion–molecule reactions is limited to attractive potentials expressed as $V(r) = -C/r^n$, where $n > 2$. For the Coulomb potential, $n = 1$, and to derive an expression for the rate coefficient a different approach must be taken. For ions with like charges the interaction is repulsive and at collision energies typical of thermal reactions the ions will not approach closely enough for any chemical change to take place. For oppositely charged ions, we start with the equation for the total collision energy of a trajectory, ε_0

$$\varepsilon_0 = \frac{\mu(\mathrm{d}r/\mathrm{d}t)^2}{2} + \frac{\varepsilon_0 b^2}{r^2} + \frac{z_1 z_2 e^2}{r} \tag{69}$$

where the three terms are kinetic energy, centrifugal energy, and potential energy, respectively. At point of closest approach of the two particles, $\mathrm{d}r/\mathrm{d}t = 0$, the first term vanishes, and $r = r_\mathrm{m}$, the minimum distance. If there is some critical minimum distance, $r_\mathrm{m} = R$, such that reaction does not occur at closest approaches longer than R, the corresponding impact parameter is b_max. The cross-section, expressed in terms of b_max and R, is given by

$$\sigma = \pi b_\mathrm{max}^2 = \pi R^2 \left(1 - \frac{z_1 z_2 e^2}{\varepsilon_0 R}\right) \tag{70}$$

The rate constant, obtained by averaging over all initial kinetic energies, is given by

$$k(T) = \pi R^2 \left(\frac{8k_\mathrm{B}T}{\pi\mu}\right)^{1/2} \left(1 - \frac{z_1 z_2 e^2}{R k_\mathrm{B} T}\right) \tag{71}$$

It is immediately apparent that the rate coefficient is larger than the SCT expression for neutrals by the last factor in parentheses. Unlike the ion–molecule rate coefficient, the critical distance R appears in the rate coefficient expression for ion–ion reactions. Because the value of R for a particular reaction is not a directly measurable quantity equation (71) is not predictive, but R can be estimated by using an experimentally determined value for $k(T)$. For oppositely charged ions the values of R are found to be in the vicinity of 1–3 nm, or up to a factor of 10 greater

than hard sphere collision diameters. Since the cross-section and the rate coefficient depend on R^2 the predicted and measured thermal rate coefficients are ~1000 times larger than the equivalent hard sphere rate coefficients. In reactions between oppositely charged ions the critical distance R may be interpreted as the distance at which an electron jumps from the negatively charged ion to form neutral products.

4.5 Bimolecular association of free radicals

The association of two free radicals occurs on an attractive PES without an energy barrier. Considering just the bond being formed by pairing the electrons, and ignoring the remaining internal degrees of freedom, the potential energy becomes one dimensional and can be represented by a curve such as the one in Fig. 5. At large separation the total energy of the two radicals is the potential energy at the asymptote of the curve, plus relative kinetic energy and internal energy. As the radicals approach each other, potential energy decreases, internal energy increases, and total energy remains constant. The two radicals will fly apart unless they lose energy by collision(s) with third bodies while they are in the vicinity of r_e and thereby fall into the potential well. Otherwise no reaction will be observed. The bimolecular collision dynamics model considers only structureless masses with a superimposed potential. We can estimate the rate coefficient for free radical association by this model by assuming that all collisions between the radicals where a bond can be formed lead to reaction. This amounts to tacitly calculating the bimolecular rate coefficient at the high pressure limit, the limit of infinite collision rates.

Assuming that the long-range attraction between two free radicals can be described by the attractive part of the Lennard–Jones potential, $V(r) = -4\varepsilon(\sigma/r)^6$, and applying equation (65),

$$\sigma(g) = \pi b_{\max}^2 = \frac{3}{2}\left[\frac{16\varepsilon_{LJ}\sigma_{LJ}^6}{\mu g^2}\right]^{1/3} \tag{72}$$

This cross-section can be inserted into equation (63), and the integral evaluated in terms of gamma functions. The rate coefficient is given by

$$k(T) = \frac{8.47(4\varepsilon\sigma^6)^{1/3}(kT)^{1/6}}{\mu^{1/2}} \tag{73}$$

This equation predicts rate coefficients that are significantly greater than the SCT predictions from equations (59) and (60) because the effect of the attractive potential is to increase the reactive cross-section. For the combination of methyl radicals to form ethane, equation (60), with

$d_{AA} = 5.9 \times 10^{-9}$ cm (the diameter of methane obtained from gas viscosity measurements), predicts $k_{SCT} = 3.3 \times 10^{-10}\,cm^3\,molecule^{-1}\,sec^{-1}$, and equation (73) (with Lennard–Jones parameters for methane) predicts $k_{LJ} = 9.9 \times 10^{-10}\,cm^3\,molecule^{-1}\,sec^{-1}$, an increase of a factor of 3. So the effect of an attractive potential can be quite large. The experimental value of this rate coefficient at high pressure is smaller than the estimate by either model, $k_{exp} = 6 \times 10^{-11}\,cm^3\,molecule^{-1}\,sec^{-1}$.

One factor contributing to the overestimate is the omission of electronic degeneracy from the calculation. The predicted rate coefficient for association reactions between open shell species, those species with unpaired electrons, will be smaller than the estimate given by equations (59), (60), or (73) because only a fraction of the total number of collisions can result in the formation of a new bond. Many of the electronically degenerate states resulting from the association will be incapable of forming a stable bond because of the Pauli exclusion principle. For example, in the case we are considering the CH_3 radicals are doublet states with spin quantum number $+1/2$ or $-1/2$. The combination of two CH_3 radicals will have a rate coefficient that is only 1/4 of the collision theory estimate. This is because if, in a given collision, the two electron spins are parallel a triplet state which has a degeneracy of 3 ($2S+1$, where $S = |s_1 + s_2| = 1$) results, and no reaction is possible. If the spins are paired, $|s_1 + s_2| = 0$, and reaction is allowed. Furthermore, $S = 1$, in this case, so in every collision there are four electronic states possible, only one of which can result in reaction. A useful discussion of electronic degeneracy has been given by Smith [21].

Applying a statistical factor of 1/4 to both the SCT and the LJ predictions gives corrected rate coefficients of 8.3×10^{-11} and $2.5 \times 10^{-10}\,cm^3\,molecule^{-1}\,sec^{-1}$, respectively. The SCT prediction is now only 40% more than experiment, and the LJ prediction is a factor of 4 larger. It should not be concluded that SCT is better than LJ, because LJ includes attractive forces, and is more realistic. However, it is not clear that the $-C/r^6$ attraction is correct, or for that matter what attraction should be used. Further discussion of this issue has been given by Johnston [22].

4.6 Classical trajectory calculations

The development of the collision dynamics approach to bimolecular reactions has for the most part departed from models that seek analytical expressions for rate coefficients, and has centered on trajectory calculations, a method made possible by the development of high speed computers.

The classical trajectory method employs Hamilton's equations, $H = V + E$, where V is the potential energy and E the kinetic energy [23], to calculate trajectories for pairs of molecules undergoing bimolecular collisions. The trajectories start at large separation of the pair (essentially zero interaction between them), continue through the collisional interaction and on to large separation of the scattered products. The potential energy comes from the PES for the colliding pair, and thus requires the availability of a PES at the outset. The kinetic energy comes from the translational energy plus internal energies of the pair. A single trajectory requires specification of the impact parameter, b, the initial relative kinetic energy, ε_0 (i.e., at large separation), the initial vibrational energy and phase, and the initial rotational energy and orientation of each reactant. Monte Carlo procedures are used to select a set of these parameters for each trajectory so that the actual distribution of initial energy states and impact parameters are closely approximated for a relatively small set of trajectories. The minimum number of trajectories that must be calculated for the results to be statistically significant is at least 1000, and may be as many as 10,000 or more. Molecular dynamics studies by means of trajectory calculations are large scale computations requiring substantial computer resources. Examination of the long time asymptotes (after the interaction) of the trajectories shows that some trajectories result in the formation of new chemical species (the reaction products). The remaining trajectories consist of reactants in altered energy states, and therefore describe inelastic or elastic collisions. The probability of reaction, P_R, as a function of the initial conditions can then be obtained as the fraction of total collisions that result in reaction

$$P_R(E_0, J, v, b) = \lim_{N\to\infty} \frac{N_R(g, J, v, b)}{N_{TOTAL}(g, J, v, b)} \tag{74}$$

Here J and v represent the initial rotational and vibrational conditions, respectively, N_R is the number of trajectories resulting in reaction, and N_{TOTAL} the total number of trajectories. The reactive cross-section is obtained by integrating over the impact parameters,

$$\sigma_R(g, J, v) = 2\pi \int_0^{b_{max}} P_R(g, J, v, b) b \, db \tag{75}$$

and microscopic rate coefficients for each vibration/rotation level are obtained by averaging the cross-sections over the Maxwell–Boltzmann distribution

$$k(J, v) = \int_0^{\infty} \sigma(g, J, v) g f(g) dg \tag{76}$$

It is evident from these equations that trajectory calculations give microscopic, or state-to-state, information for a reaction. Finally, the thermal rate coefficient for the elementary reaction can be obtained by summing the $k(v, J)$ over each weighted level

$$k(T) = \sum k(v, J) f(v, J) \tag{77}$$

The validity of this approach depends on whether classical mechanics provides an adequate representation of what, strictly speaking, are quantum mechanical events. It is possible to restrict the initial vibrational energy to allowed vibrational quantum states. When this is done, the method is referred as the quasiclassical trajectory method. Full quantum mechanical scattering calculations are more demanding than classical ones, and they can be done for reaction systems consisting of only a few atoms, up to six at present [24]. Quantum trajectory calculations may be used to evaluate the goodness of classical and quasiclassical trajectory calculations. The goodness of the results obtained from any trajectory calculation depends critically on the accuracy of the PES. PESs are constructed using the methods of modern computational chemistry described in Chapter 1. However, trajectory calculations require, in addition to the stationary points where stable molecules and transition states are found, all parts of the PES that contribute to the scattering. Fortunately, some methods for electronic structure calculations yield energies to chemical accuracy. Surfaces are obtained by calculating, in addition to the stationary points, the potential at as many other points as feasible, given constraints of time and money, over the regions of the potential that are energetically accessible, and connecting the points with splines or by other numerical methods. Note that special methods are needed to calculate the potential at points other than the stationary points [25].

Trajectory calculations have supplanted collision theory, which has severe limitations for predicting rate coefficients except in a few special cases. While classical trajectory calculations do not have the limitations of collision theory, and are capable of providing calculated bimolecular rate coefficients that may be quite good, they are computationally intensive and time consuming. Because they require significant effort they may be of limited interest for predicting rate coefficients for use in a DCKM, although the method is certainly worth considering if an important rate coefficient cannot be reliably estimated by other means. In the chemical kinetics/chemical dynamics research community classical trajectory calculations are a very important tool for the detailed information they can give about reaction products and product states, cross-sections and dynamical insights into chemical reactivity.

4.7 Transition state theory

Transition state theory (TST) was introduced in the 1930s [26,27]. It has since been extensively developed and successfully applied to many chemical reactions. TST is called a statistical theory, in contrast with the dynamical approaches above, because statistical thermodynamics is used to derive an expression for the rate coefficient. It is used primarily for bimolecular elementary reactions occurring over simple adiabatic electronic potential barriers, such as the one in Fig. 6, and unimolecular reactions at the high pressure limit. The theory can be conveniently described as the solution to a barrier crossing problem, where the barrier maximum is at the saddle point on the adiabatic PES over which the reaction occurs. The passage from reactants to products occurs through a dividing surface, which is the surface separating the phase space of the reactants from the phase space of the products. The dividing surface is orthogonal to the lowest energy reaction path, and is conventionally and historically located at the saddle point. Other dividing surface locations are possible (see next section), and to make the distinction clear, the theory developed below is nowadays referred as conventional transition state theory (CTST). However, in the past, this distinction has not been made, so the remainder of this section, what is strictly speaking CTST, will be referred simply as TST. The chemical entity that exists at the moment of crossing the dividing surface is called the transition state, denoted by $A^{\dagger}$, and is formed directly from the reactant(s). The case of a bimolecular reaction between reactants R_1 and R_2 is written as follows:

$$R_1 + R_2 \rightarrow A^{\dagger} \rightarrow \text{products}$$

The rate of the reaction is given by the classical rate of crossing the dividing surface. The crossing rate is expressed as the product of the transition state concentration, $[A^{\dagger}]$, the frequency of crossing, υ^*, and a transmission coefficient, κ

$$r = \kappa \upsilon^* [A^{\dagger}] \tag{78}$$

In this equation the transition states are considered to be formed only when their total energy is equal to or greater than E_0. The transmission coefficient provides a correction factor for quantum effects. It may be necessary to correct the classical rate coefficient for quantum mechanical tunneling through the barrier for reactants with total energy less than V_0, or for non-adiabatic reactions. The transition state concentration, $[A^{\dagger}]$, refers to only those transition states that are moving toward product formation, and does not include those that may come from the

reverse reaction. If the reaction were at chemical equilibrium, transition states would be passing over the barrier in both the forward and the reverse directions, and $[A^{\dagger}]$ would be one-half of the equilibrium concentration of transition states. For a bimolecular reaction with reactants R_1 and R_2 we can write $[A^{\dagger}] = 1/2K_C^{\dagger}[R_1][R_2]$, where $K_C^{\dagger}$ is the equilibrium constant for the hypothetical equilibrium between the reactants and the transition state. The reaction rate becomes

$$r = \frac{1}{2}\kappa \upsilon^* K_C^{\dagger}[R_1][R_2] \tag{79}$$

Although a chemical equilibrium argument is used to arrive at this equation, it can be applied to reactions that are far from equilibrium. This conclusion can be reached by considering the molecular energy distribution of the reactants and the transition state. At chemical equilibrium the system will be at thermal equilibrium, and the reactants and transition state will have Maxwell–Boltzmann energy distributions. If the reaction is far from chemical equilibrium, but the energy distributions of the reactants and transition state are Maxwell–Boltzmann, or do not vary significantly from Maxwell–Boltzmann equation (79) can be used. Energy distributions that are nearly Maxwell–Boltzmann will be maintained if the rate of the reaction is slower than the rate of collisional energy redistribution. So we may expect deviations from the TST prediction for very fast reactions, or for reactions occurring at very low pressure. In these cases a different approach, which is covered in Chapter 4, must be taken. Equation (79) requires that all transition states for the forward reaction proceed to products, and that recrossing of the dividing surface does not occur. If recrossing actually occurs, TST gives an upper limit value for the reaction rate.

If the Born–Oppenheimer approximation is valid for both the reactants and the transition state, the equilibrium constant, $K_C^{\dagger}$, is related to molecular partition functions, $K_C^{\dagger} = Q^{\dagger}/\prod Q_i$, as shown in almost any text on statistical thermodynamics. The rate coefficient can be expressed by the following equation.

$$k(T) = \kappa \frac{k_B T}{h} \frac{Q^{+}}{\Pi Q_i} \exp\left(\frac{-E_0}{k_B T}\right) \tag{80}$$

Here Q is the zero point energy-corrected molecular partition function per unit volume for each species, k_B the Boltzmann's constant, T the absolute temperature, h the Planck constant, and $E_0 = V_0^{\dagger} + \sum \varepsilon_0$, where $\sum \varepsilon_0$ is the zero point energy of the transition state minus the sum of the zero point energies of the reactants. Details for the calculation of

partition functions can be found in most kinetic texts, and in statistical mechanics texts, for example, those of Davidson [28], Hill [29], and McQuarrie [30]. The transition state has one less internal degree of freedom (df) than "normal" molecules, $3N-6$df for linear transition states, and $3N-7$df for non-linear transition states. This arises because the TS is unstable in the direction of the reaction path, and an internal df is "lost" by transformation to a one-dimensional (1D) translation. The atomic motion(s) undergoing this transformation is (are) called the reaction coordinate. The motion along the reaction coordinate is assumed to be a separable df, so a 1D translational partition function, $(2\pi m^{\dagger}k_{\mathrm{B}}T/h^2)^{1/2}\delta x$, is factored out of the transition state partition function. The barrier crossing frequency is considered to be a molecular speed, $v^{\dagger} = (2k_{\mathrm{B}}T/\pi m^{\dagger})^{1/2}$. These factors give rise to the $k_{\mathrm{b}}T/h$ factor that appears in equation (80). More detail on the derivation of equation (80) can be found in almost any text on kinetics.

4.8 The statistical factor

The rotational partition functions are divided by a symmetry number which counts the number of ways that a molecule can be rotated to give a different but equivalent arrangement of its atoms when identical atoms are labeled to make them distinguishable. For example, the symmetry number of molecular hydrogen, H_1–H_2, is 2. In TST the use of rotational partition functions for reactant(s) and the transition state including their symmetry numbers leads to correct results in the majority of cases, but there are some anomalous situations where the symmetry numbers lead to incorrect rate coefficients (Ref. [31] gives a concise discussion of this point). A procedure that avoids these errors has been advanced by Bishop and Laidler [32]. In this method, the symmetry numbers are omitted from the rotational partition functions, and the right hand side of equation (80) is multiplied by a statistical factor, sometimes called the reaction path degeneracy, which counts the number of ways that the reaction product(s) can arise when identical atoms are labeled to make them distinguishable. For example, in the reaction of atomic hydrogen with methane, $H_1 + CH_2H_3H_4H_5$, there are four identical paths for the formation of molecular hydrogen, and the statistical factor is 4. In the majority of cases, the statistical factor is numerically equal to the ratio of symmetry numbers obtained from the ratio of rotational symmetry numbers, but we can avoid errors altogether by always using the statistical factor, and this procedure is recommended.

4.9 Tests of transition state theory

TST predicts the trend of decreasing Arrhenius pre-exponential factor with increasing reactant size and molecular complexity that is revealed by experimental measurements of rate coefficients, and that SCT explained away by invoking the steric factor. This trend arises in TST through the internal degrees of freedom, which are accounted for in the partition functions, and which are not present in the structureless point masses of SCT. If electronic, vibrational, rotational, and translational dfs are independent, the molecular partition function factors into electronic, vibrational, rotational, and translational contributions, i.e., $Q = q_e q_v q_r q_t$. The orders of magnitude of the partition functions per df are: $q_e \sim 1$, $q_v \sim 1$–10 per vibrational or internal rotational df, $q_r \sim 10$–10^3 per overall rotational df, and $q_t \sim 10^{31}$–$10^{32}\,\mathrm{cm}^{-3}$. For a bimolecular reaction between two structureless point masses, A and B, the partition factor ratio of equation (80) becomes a ratio of translational partition functions, $q^{\dagger}/q_{t,A}q_{t,B}$, and k_{TST} becomes equal to k_{SCT} given by equation (59). For this case TST and SCT are equivalent. For other reaction partners, working out the partition function ratio and putting in the above orders of magnitude predicts that the pre-exponential factor is significantly reduced by factors that can range down to as low as 10^{-10} for non-linear, polyatomic reactants (see, e.g., Ref. [33] for this kind of calculation). The decrease, which is in qualitative agreement with experimental observations, is caused by the contributions of internal degrees of freedom, as expressed through the partition functions. This is a significant improvement over SCT, emphasizing the role molecular structure has on chemical reactivity, and overcoming a principal limitation of SCT and other simple collision dynamics models where the reactants are considered to be structureless point masses. These simple order of magnitude estimates of A-factors can be done quickly, and are extremely useful as a first check of suspect kinetic data, discarding results that are significantly out of line.

The above estimates show that TST is at least qualitatively correct, but they do not address the question of whether the theory is capable of providing useful estimates of rate coefficients for modeling purposes. A limitation of TST is that it cannot, by itself, provide any information on barrier heights. Historically, tests of the theory have been limited to comparison with experimental rate coefficients when a reliable experimentally determined activation energy is available. Because E_0 in equation (80) is not the activation energy, some manipulation is necessary to relate theoretical quantities with the observed pre-exponential factor. See, for example, Pilling and Seakins [34] for appropriate relationships. The partition functions for the reactants can be evaluated from

experimental molecular spectroscopy, where much data are available, or otherwise from electronic structure calculations, which give quite adequate accuracy for vibrational frequencies and moments of inertia. In contrast, evaluation of $Q^{\dagger}$ presents a problem. The transition state is a species with a fleeting existence, because its lifetime is determined by the atomic motions that occur during its transformation into reactants as it crosses the dividing surface. The transition state "lifetime" is expected to be less than a vibrational period, which is $\sim 10^{-12}$ to 10^{-13} sec. Because transition states are inherently unstable they cannot be isolated, and because their very short lifetime means very low concentration they are extraordinarily difficult to detect by ultrafast spectroscopy. Thus, experimental data for transition states are non-existent. In the past it has been necessary to estimate $Q^{\dagger}$ by intuiting a reaction coordinate, and estimating the partition functions for the remaining degrees of freedom by analogy with stable molecules. A reasonable reaction coordinate can usually be deduced by consideration of the atomic rearrangements that result in formation of products from reactants. For example, in dissociation of a molecule by simple bond scission the reaction coordinate may be considered to be the transition of the bond stretching vibration to the relative translation of the two groups that result. If the remaining degrees of freedom of the transition state after factoring out the 1D translation are considered to be bound states the frequencies and moments of inertia may be estimated from properties of similar molecules. This approach leaves much room for adjustment of the transition state model, and it is usually possible to fit experimental data without doing violence to what are reasonable values for transition state frequencies and moments of inertia. Many instances in the literature where reasonable fits have been obtained give confidence that the theory has at least most of the essential features necessary for a quantitative rate constant model. The TST model has been tested by calculating the effect of isotopic substitution on rate coefficients. Because substitution of an atom in a molecule by one of its isotopes does not change the electronic potential, a test of theory that is independent of the electronic barrier height can be done by calculating a rate coefficient ratio. For example, a number of hydrogen and deuterium atom transfer reactions have been studied, and reasonable agreement between $(k_H/k_D)_{exp}$ and $(k_H/k_D)_{TST}$ has been found [35] (see also Ref. [12], chapter 10). Tests such as these have provided confidence in the validity of TST.

The obvious ambiguity of the historical approach is eliminated by employing modern electronic structure calculations, which are capable of giving stationary points to chemical accuracy, and reliable vibrational frequencies and moments of inertia not only for the reactants, but also

for the transition state. Early calculations on scaled semi-empirical surfaces showed that TST is capable of giving quite good agreement with experiment. For example, Shavitt [36] did TST calculations for the reactions $D + H_2$ and $H + D_2$ that are in excellent agreement with experimental rate coefficients from 250 to 1000 K. More recently the development of composite methods for electronic structure calculations has permitted chemical energies to be calculated to "chemical accuracy," usually stated to be within 1–2 kcal mol^{-1} of experiment. These methods have made it possible to use TST to successfully predict rate coefficients solely from statistical mechanics and quantum mechanics. For example, Wu and Carr [37] have used the G2 method to compute the electronic barrier height for elimination of HCl from the CH_2ClO radical, and calculation of the transition state properties

$$CH_2ClO \rightarrow CHO + HCl$$

The results are in excellent agreement with experiment [38].

4.10 Microcanonical transition state theory

CTST can also be described as a canonical rate theory because a central assumption is that the thermal equilibrium distribution of energy is maintained for reactants and transition states during the course of the reaction. Thus, it is a canonical theory in the statistical mechanics sense of canonical ensembles being systems in thermal equilibrium with their surroundings. In microcanonical TST the rate coefficient $k(T)$ is calculated from microcanonical rate coefficients, $k(\varepsilon)$, which are the rate coefficients for reactant(s) at a fixed energy, ε, by integrating over the normalized energy distribution $f(\varepsilon)$

$$k(T) = \int_0^\infty k(\varepsilon) f(\varepsilon) \mathrm{d}\varepsilon \tag{81}$$

The $k(\varepsilon)$ are microcanonical in the statistical mechanical sense of isolated systems at constant energy. Marcus [39] showed how to relate microcanonical rate coefficients to TST in the context of unimolecular reactions, but the same principles apply to bimolecular reactions. The microcanonical approach is extensively developed in Chapter 4, and so it will not be discussed further here.

4.11 Variational transition state theory

Trajectory calculations have revealed that some trajectories, after crossing the saddle point, actually recross it, to the reactant side, and

result in no reaction. The CTST assumes that recrossing does not occur, but that all transition states formed from the reactants continue to form products. Therefore, in situations where recrossing occurs, CTST overestimates reaction rate coefficients. It is possible to correct CTST by relocating the dividing surface from the potential maximum to a position where recrossings of the dividing surface are minimal (not zero, since in general it may not be possible to find a location where recrossings are totally absent). Keck [40] first introduced the idea of varying the position of the dividing surface to improve TST and reduce, but not eliminate, the overestimation of $k(T)$. Procedures for accomplishing this have been devised, and are classified as variational transition state theories (VTST), since they have in common the use of calculus of variations for the minimization of the rate coefficient (minimization of recrossings). Canonical VTST minimizes the thermal rate coefficient, $k(T)$, with respect to $x^{\dagger}$, a coordinate corresponding to the reaction path, and provides a better upper bound estimate than does CTST

$$\frac{\mathrm{d}k(T)}{\mathrm{d}x^{\dagger}} = 0 \tag{82}$$

The equilibrium constant, $K_{\mathrm{C}}^{\dagger}$, is related through equations (48)–(50) to the Gibbs free energy change on forming the transition state from the reactants, and it can be readily seen from equation (82) that $k(T)$ is minimized at the maximum of the Gibbs free energy along the reaction path. In fact, Steel and Laidler [41] suggested that the transition state should be located at the maximum of the Gibbs free energy, rather than the maximum of potential energy, along the reaction path. With this criterion, the optimum location of the transition state depends on both energetic and entropic considerations, in contrast with CTST, where the only consideration for locating the transition state is at the potential energy maximum.

Microcanonical VTST minimizes the microcanonical rate coefficients, $k(E)$, and takes into account that the dividing surface location is most likely energy dependent

$$\frac{\mathrm{d}k(\varepsilon)}{\mathrm{d}x^{\dagger}} = 0 \tag{83}$$

This defines a different transition state for each energy, and is an improvement over canonical VTST, which does not incorporate any energy dependence of recrossing. CTST gives very good estimates of rate coefficients for many reactions. For some types of reactions, most notably reactions without energy barriers, it is not very accurate. In these cases VTST should be used. Implementation of VTST requires a computer, as

there is more computational effort required than there is for CTST. Truhlar and Garrett [42–44] have done extensive work on VTST. Details of VTST calculations are given in Ref. [45].

4.12 The transmission coefficient

The transmission coefficient, κ, is a factor to correct the TST rate coefficient, which treats the barrier crossing problem classically, for quantum mechanical effects when they are important. For reactants whose total energy is lower than the classical barrier height, there is a probability that the system wave function will be found with finite amplitude on the product side of the barrier. This is referred to as quantum mechanical tunneling. Also, if the PES of another electronic state exists in the vicinity of the ground state surface, there is a probability for a transition from the ground state to the excited electronic state, possibly with the formation of different reaction products, or the same products, but in different electronic states. This is referred to as a non-adiabatic reaction. When tunneling is important the reaction goes faster than predicted by TST, and $\kappa > 1$. (The quantum mechanical treatment of tunneling also predicts that reactants with energy greater than the barrier height have a finite probability of being reflected, but the contribution of these higher energy states to the total quantum correction is reduced because of the Maxwell–Boltzmann energy distribution and they are not enough to make $\kappa < 1$.) When non-adiabatic reactions are important the rate of the ground state reaction is diminished, and $\kappa < 1$ for reaction on the adiabatic surface. Corrections for tunneling and non-adiabatic reactions are made independently of one another. Both phenomena present complicated problems when examined in detail, but simplified models have been developed and are briefly discussed next.

4.13 Tunneling

Quantum tunneling through an electronic barrier is favored for light atoms, primarily hydrogen and deuterium, low temperature, and thin barrier widths. Tunneling can make a non-negligible contribution to the reaction rate in these situations, and its possible importance may need to be checked in other situations. The quantum mechanical probability for penetration of an electronic barrier by reactants of specified energy can be estimated by solution of the 1D Schrodinger equation

$$\frac{-h^2}{8\pi^2\mu}\frac{\mathrm{d}^2}{\mathrm{d}x^2}\psi = [E - V(x)]\psi \tag{84}$$

Analytical expressions for the contributions of tunneling to the transmission coefficient have been obtained for some model barriers, $V(x)$, notably the Eckart potential, for which the solution is exact [46], and the truncated parabola, for which an approximate, but accurate, solution has been found [47]. These references should be consulted for details of the calculations and tabulations of tunneling corrections. A first approximation to tunneling through a barrier of arbitrary shape is given by the following equation [48]:

$$\kappa = \frac{1 + h|v^*|}{k_B T} \tag{85}$$

where v^* is the imaginary frequency of the transition state in the direction of negative curvature of the barrier. This expression may be used as a convenient and easy to use check on whether tunneling is important enough to warrant further computational effort, but should not be used as a reliable tunneling correction when accuracy is needed. The 1D calculations that can be reasonably readily done with these models may provide a satisfactory tunneling correction when high accuracy is not needed. They assume no or minimal curvature of the reaction path, adiabaticity of the internal degrees of freedom of the transition state, and co-linear transition states. They will be best at lower temperatures where the minimum energy path dominates, but they do not account for reaction paths other than the minimum energy path through the saddle point. Referring to Fig. 4 it is apparent that reaction paths of higher energy crossing wider parts of the surface adjacent to the saddle point are possible and may contribute to κ. Johnston and Rapp [49] approached this problem by doing tunneling corrections for several parallel reaction paths across 1D cuts through a PES in the vicinity of the saddle point, and where the potential energy profile along the cuts is described by the Eckart potential. They showed that tunneling through wider portions of the surface can be important. Calculations of tunneling corrections based on the Eckart potential have been tabulated by Johnston [50]. Consultation of these tables will indicate if tunneling is likely to be important for a reaction of interest. The tunneling corrections in these tables are overestimates, but they can be readily applied, and are satisfactory if the rate coefficient for the reaction in question does not need to be known to high accuracy in the mechanism in which it appears.

If accurate tunneling corrections are required, the situation rapidly becomes more complicated. Issues related to separability of motion along the reaction coordinate, curvature of the reaction coordinate, and multidimensional tunneling arise and must be dealt with. Marcus and Coltrin [51] found that reaction path curvature forces the reaction to cut

through a shorter tunneling path, which consequently gives a higher tunneling probability. Tunneling corrections which deal with curvature and other factors are computationally intensive, and should be implemented for reactions in kinetic models only if absolutely necessary. Fernández-Ramos et al. [52] has recently discussed a number of approaches to tunneling corrections that summarize the current state of affairs. Allison and Truhlar [53] have shown that a microcanonical multidimensional method [54] gives transmission factors for atom–diatom reactions that are accurate enough for almost all practical work. However, if the time and resources to carry out a numerical study of a reaction of interest are lacking, and if the rate coefficient of interest need not be known with high accuracy, then the Eckart potential is an efficient way to estimate the importance of tunneling. Tunneling will generally only be appreciable for light atoms, low temperatures, and "thin" barriers. Because tunneling increases in importance as temperature decreases, it may cause non-linearity of Arrhenius plots at low temperatures. Tunneling predicts that the plot of $k(T)$ vs. $1/T$ will be concave upward at low temperatures in cases where it is important. There are experimental examples of such behavior, and they may indicate the importance of tunneling. We have previously noted that concave upward curvature of Arrhenius plots at high temperatures may be caused by the temperature dependence of the pre-exponential factor.

4.14 Electronically non-adiabatic reactions

All the reactions we have considered so far have been adiabatic, by which we mean that they occur on a single adiabatic PES that is unperturbed by other electronic states. In addition, we have assumed that the surface is the lowest (ground) electronic state connecting the reactants and products. If, for a specified reaction, there is an excited state PES near enough to the ground state for the two to interact, it is possible for the reaction to occur on both surfaces. Reactions that can occur on more than one PES are called non-adiabatic reactions. The reaction on one surface may give different products, or the same products but in different electronic states, than does reaction on another surface. When a reaction involves reactants and/or products in electronically excited states, non-adiabatic reactions must be considered.

Generally speaking, for non-adiabatic reactions to be important, there must be a region where PESs converge or intersect. Considerations from quantum mechanics tell us that interacting electronic states do not cross one another. In regions where the energy ordering of surfaces changes there is no actual crossing of the surfaces; instead there is an avoided

crossing region forming lower and upper PESs linking reactants to products. The transition from reactants to products occurring on both the upper and the lower branches can occur with changes in electronic state. There is a probability that a reaction that starts, for example, on a ground state surface will stay on the lower branch of the avoided crossing and that the reaction products will correlate with the excited state rather than the ground state. There is also a probability that a transition from the lower branch to the upper branch will occur as the avoided crossing region is traversed. The probability of staying on the lower branch increases as the energy gap between the lower and the upper branches increases. For two states corresponding to the "same species," which means states with the same symmetry, electronic angular momentum, and spin, the energy separation is large (perhaps several kcal mol^{-1}) and the probability of a transition from the lower branch to the upper branch is small. On the other hand, for "different species," states which do not have the same symmetry, orbital angular momentum, and spin, the energy separation may be small (perhaps only a few cal mol^{-1}) and the probability of a transition to the upper branch can be appreciable. Laidler [55] and Nikitin [56] have excellent summaries of non-adiabatic reactions.

An example of this behavior is provided by the thermal decomposition of CO_2 to CO and O atoms. In the absence of perturbation by an excited state adiabatic dissociation of the ground state, $CO_2(^1\Sigma_g^+)$ would result in formation of singlet ground state CO and an excited $O(^1D)$ atom as required by the Wigner–Witmer spin conservation rule [21]

$$CO_2\left(^1\Sigma_g^+\right) \rightarrow CO\left(^1\Sigma^+\right) + O(^1D),$$
$$\Delta H_{298}^0 = 172 \text{kcal mol}^{-1}$$

Several different experimental studies of the kinetics of CO_2 thermal decomposition report activation energies from ~90 to 110 kcal mol^{-1} [57], considerably smaller than the 172 kcal mol^{-1} endothermicity of this path. The observed activation energy compares more favorably with the 127 kcal mol^{-1} endothermicity of the dissociation of $CO_2(^1\Sigma_g^+)$ to ground state O atoms, $O(^3P)$, than with the formation of $O(^1D)$, and the reported activation energies suggest that ground state CO_2 decomposition occurs with violation of spin conservation. An excited state path leading to $O(^3P)$ could be written as follows:

$$CO_2\left(^3\Pi\right) \rightarrow CO\left(^1\Sigma^+\right) + O(^3P)$$

A reaction path following the lower branch of an avoided crossing between the ground state singlet PES and the excited state triplet PES

would explain the experimental results. Eremin *et al.* [58] observed that at high temperatures $O(^1D)$ atoms are formed from the thermal decomposition of CO_2, and found that $E_a = 148.7\,\text{kcal}\,\text{mol}^{-1}$ for this path. The path forming $O(^1D)$ atoms can then be attributed to a transition from the lower branch of the avoided crossing to the upper branch.

The minimum potential energy difference, ε_{12}, between the upper and the lower surfaces at the avoided crossing depends on whether the unperturbed electronic states are "same species" or "different species." The former gives rise to large splitting, several $\text{kcal}\,\text{mol}^{-1}$, and the latter to small splitting of a few $\text{cal}\,\text{mol}^{-1}$. A simple 1D model of non-adiabatic reactions for "different species" was introduced by Landau and Zener in the 1930s [59,60]. The model predicts that the probability of a transition from the lower to the upper curve at the avoided crossing is given by

$$P_{12} = \exp\left[\frac{-4\pi^2\varepsilon_{12}^2}{hv|s_1 - s_2|}\right] \tag{86}$$

where v is the classical velocity at the hypothetical crossing point of the unperturbed potential curves, s_1 and s_2 the slopes of the unperturbed curves, and h the Planck constant. The probability of staying on the lower surface is $p = 1 - P_{12}$. A correction, κ, to the TST rate coefficient can be calculated by averaging over the velocities

$$\kappa = \frac{\int_0^\infty p\ \exp[-\mu v^2/2k_B T]\mathrm{d}v}{\int_0^\infty \exp[-\mu v^2/2k_B T]\mathrm{d}v} \tag{87}$$

The Landau–Zener model illustrates the important variables influencing the probability of non-adiabatic transitions, but as a 1D model it is only applicable to bimolecular reaction of two atoms. For most reactions of interest it is too simple to provide accurate results. For reactions involving more than two atoms the PESs are multidimensional, as we have seen above, and the avoided crossing region on a multidimensional surface is described as a conical intersection [61]. The best method for handling this complex multidimensional reactive scattering problem is trajectory calculations. Fernández-Ramos et al. [52] has discussed approaches to this problem as part of a recent review of bimolecular reaction rate theory. It is fortunate that the vast majority of chemical reactions occur adiabatically. It will only be necessary to delve into the theory of non-adiabatic reactions when a non-adiabatic reaction is present in a reaction model, experimental data are not available, and the reaction rate influences the overall rate appreciably.

5 TERMOLECULAR REACTIONS

Some elementary chemical reactions follow a third order rate expression at all normally accessible experimental conditions, and according to the definitions of molecularity must be classified as termolecular. The most common example is the combination of two atoms in the presence of a third species. The rate expression is $r = k(T)[A]^2[M]$ for combination of like atoms, A, in the presence of the collider or heat bath species M. These reactions do not occur by the simultaneous collision of all three species, which is a very rare event, but by two bimolecular steps that take place within $\sim$1 psec of one another. An energy transfer mechanism of the reaction may be written as follows:

$$A + A \underset{k_{-1}}{\overset{k_1}{\Leftrightarrow}} A_2^*$$

$$A_2^* + M \xrightarrow{k_2} A_2 + M$$

In the first step the two atoms combine to form a diatomic molecule, A_2^*, where the asterisk denotes non-thermal internal excitation energy. The excitation energy comes from the bond energy of the newly formed molecule plus thermal energy carried by the atoms. A_2^* will redissociate in one vibrational period unless energy is removed by collisions with M. Applying a steady state, $d[A_2^*]/dt = 0$, gives the rate expression

$$\frac{d[A_2]}{dt} = \frac{k_1 k_2 [A]^2[M]}{k_{-1} + k_2[M]} \tag{88}$$

The order of magnitude of k_{-1} is given by the vibration frequency of the diatomic, $\sim 10^{12}$–$10^{13}\,\text{sec}^{-1}$, because there are no other vibrational degrees of freedom among which the internal energy can be shared, and unless energy is removed during one vibrational period, redissociation of A_2^* will occur. The collision frequency of M with A_2^* is $k_2[M]$, and if enough energy is removed from A_2^* at every gas kinetic collision to bring A_2^* below the bond dissociation energy, then $k_2[M]$ is the rate of collisional stabilization. Applying SCT to estimate k_2 at say, 300 K ($\sim 10^{-10}$ molecule $\text{cm}^{-1}\,\text{sec}^{-1}$), and if the partial pressure of M is 1 atm, then $k_2[M] \sim 10^{10}\,\text{sec}^{-1}$. Unless the pressure is very high, $k_{-1} \gg k_2[M]$, and the rate expression becomes

$$\frac{d[A_2]}{dt} = \frac{k_1 k_2}{k_{-1}}[A]^2[M] \tag{89}$$

This rate expression is kinetically third order, and will describe atom combination at all pressures of interest. Deviation from third order behavior will only become apparent if the total pressure approaches

1000 atm. If the pressure is high enough to cause condensation, the situation would be completely different, and it would have to be modeled as a diffusion limited reaction. The observed third order rate coefficient is composed of the rate coefficients for the three elementary reactions, $k(T) = k_1 k_2 / k_{-1}$. Simple models of these rate coefficients permit an estimate to be made of the expected magnitude of $k(T)$. There is no potential barrier for the association of two atoms to form A_2^*, so k_1 can be estimated to be $\sim 10^{-10}$ molecule $\mathrm{cm}^{-3}\,\mathrm{sec}^{-1}$ by SCT if the association occurs at each collision. We have already estimated k_2 and k_1, so $k(T) \sim 10^{-33}\,\mathrm{cm}^{-6}\,\mathrm{molecule}^{-2}\,\mathrm{sec}^{-1}$ is the expected order of magnitude for the third order rate coefficient. Experimentally determined third order rate coefficients for many atom combination reactions are of this order of magnitude.

Atoms may also combine by a mechanism called the bound complex mechanism, in which an atom, A, forms a van der Waals cluster, AM, followed by reaction of the cluster with another atom

$$\mathrm{A} + \mathrm{M} \underset{k_4}{\overset{k_3}{\Leftrightarrow}} \mathrm{AM}$$

$$\mathrm{AM} + \mathrm{A} \xrightarrow{k_5} \mathrm{A}_2 + \mathrm{M}$$

The rate of formation of diatomic molecules is given by

$$\frac{\mathrm{d}[\mathrm{A}_2]}{\mathrm{d}t} = k_5[\mathrm{AM}][\mathrm{A}] \tag{90}$$

Because the atoms are normally present in a large excess of M the AM complexes can be considered to be in chemical equilibrium. The equilibrium constant is

$$K_\mathrm{C} = \frac{[\mathrm{AM}]}{[\mathrm{A}][\mathrm{M}]} \tag{91}$$

And the overall rate expression is third order

$$\frac{\mathrm{d}[\mathrm{A}_2]}{\mathrm{d}t} = k_5 K_\mathrm{C}[\mathrm{A}]^2[\mathrm{M}] \tag{92}$$

For this mechanism the third order rate coefficient $k(T) = k_5 K_\mathrm{C}$ can be estimated by evaluating K_C from statistical mechanics and using SCT for k_5. For weakly bound AM complexes where the interaction is expressed by a Lennard–Jones potential, Bunker and Davidson [62] expressed K_C by

$$K_\mathrm{C} = \sqrt{\pi}\left(\frac{\varepsilon}{k_\mathrm{B}T}\right)^{1/2}\left[\frac{8}{3} + \frac{32\varepsilon}{45k_\mathrm{B}T}\right]\sigma^3 \tag{93}$$

where ε and σ are the Lennard–Jones parameters for the A–M interaction (see equation (54)). With this expression for K_C, and a SCT estimate of k_5, this mechanism leads to an order of magnitude estimate of $\sim 10^{-32}\,\mathrm{cm}^6\,\mathrm{molecule}^{-2}\,\mathrm{sec}^{-1}$ for $k(T)$. Experimental data for first row atoms combining in the presence of atomic and diatomic M species show that $k(T)$ is within a factor of ~ 2 of this estimate. For more strongly bound complexes $k(T)$ can be considerably larger. For example, third order rate coefficients for the combination of iodine atoms increase from $4 \times 10^{-33}\,\mathrm{molecule}^{-2}\,\mathrm{cm}^{-6}\,\mathrm{sec}^{-1}$ for M = He to $1.1 \times 10^{-30}\,\mathrm{molecule}^{-2}\,\mathrm{cm}^{-6}\,\mathrm{sec}^{-1}$ for M = trimethyl benzene. Iodine is known to form charge transfer complexes with aromatic compounds.

For weakly bound complexes the energy transfer and the bound complex mechanisms give similar order of magnitude estimates for $k(T)$, so that it is difficult to distinguish which mechanism predominates. In fact, in these cases probably both mechanisms are simultaneously operative. If experimental rate coefficient data are not available, the simple modeling approach provides a rapid method of estimating overall termolecular rate coefficient from the contributions of each mechanism that will usually be satisfactory, because atom combination reactions are usually relatively slow, and even if the rate coefficient is not accurately known only minor errors will be made. If the A–M interaction is stronger, however, it may be necessary to estimate the lifetime of the complex by other means if rate data are not available.

Termolecular rate coefficients possess a "negative temperature dependence," increasing with decreasing temperature, as do other association reactions where the PES is attractive during the entire course of the reaction (no potential barrier). This can be rationalized for the bound complex mechanism in terms of the temperature dependence of K_C for the exothermic association of A with M, but it is more difficult to explain for the energy transfer mechanism. If Arrhenius plots are made for termolecular reactions, they have positive slopes, which according to the Arrhenius equation give a negative number for E_a. Termolecular reactions are frequently said to have negative activation energies, but it is not possible to attach any physical significance to such a concept.

REFERENCES

[1] K.G. Denbigh, *The Principles of Chemical Equilibrium*. Cambridge University Press, 1964, pp. 442–447.

[2] S.L. Freiss, E.S. Lewis, A. Weissburger eds., Investigation of Rates and Mechanisms of Reactions, *Technique of Organic Chemistry*, Volume VIII, Parts I and II. Interscience, New York, 1962, 1963.

[3] C.H. Bamford, C.F.H. Tipper, *Comprehensive Chemical Kinetics*, Volume 1. Elsevier, Amsterdam, 1969.
[4] J.H. Espenson, *Chemical Kinetics and Reaction Mechanisms*. McGraw-Hill, New York, 1981.
[5] K.J. Laidler, *Chemical Kinetics*, 3rd ed., Harper and Row, New York, 1987.
[6] J.I. Steinfeld, J.S. Francisco, W.L. Hase, *Chemical Kinetics and Dynamics*, 2nd ed., Prentice Hall, Upper Saddle River, NJ, 1999.
[7] R.D. Levine, R.B. Bernstein, *Molecular Reaction Dynamics and Chemical Reactivity*. Oxford University Press, Oxford, 1987.
[8] S. Arrhenius, *Z. Phys. Chem.*, **4** (1889) 226.
[9] K.J. Laidler, *J. Chem. Educ.*, **61** (1984) 494.
[10] R.H. Fowler, E.A. Guggenheim, *Statistical Thermodynamics*. Cambridge University Press, Cambridge, 1939.
[11] W.G. Mallard, F. Westley, J.T. Herron, R.F. Hampson, D.H. Frizzell, *NIST Chemical Kinetics Database: NIST Standard Reference Database17*. National Institute of Standards and Technology, Cambridge, 2005.
[12] H.S. Johnston, *Gas Phase Reaction Rate Theory*. Ronald, New York, 1966.
[13] G. Szabo, in: C.H. Bamford, C.F.H. Tipper (Eds.), *Comprehensive Chemical Kinetics*, Volume 2. Elsevier, Amsterdam, 1961, Chapter 2.
[14] J.O. Hirschfelder, C.F. Curtiss, R.B. Bird, *Molecular Theory of Gases and Liquids*. Wiley, New York, 1954.
[15] I.W.M. Smith, *Kinetics and Dynamics of Elementary Gas Reactions*. Butterworths, London, 1980, pp. 81–84.
[16] R.E. Weston, H.A. Schwartz, *Chemical Kinetics*. Prentice Hall, Englewood Cliffs, NJ, 1972, Chapter 3 contains a very useful description.
[17] P. Langevin, *Ann. Chem. Phys.*, **5** (1905) 245.
[18] V. Cermak, A. Dalgarno, E.E. Ferguson, L. Friedman, E.W. McDaniel, *Ion Molecule Reactions*. John Wiley and Sons, New York, 1970.
[19] I.W.M. Smith, *Kinetics and Dynamics of Elementary Gas Reactions*. Butterworths, London, 1980, pp. 189–190.
[20] T. Su, and M. T. Bowers, *J. Chem. Phys*., **58** 3027 (1973); Int. J. Mass Spectrom. Ion Phys., **17** 211 (1975).
[21] I.W.M. Smith, *Kinetics and Dynamics of Elementary Gas Reactions*. Butterworths, London, 1980, pp. 51–57.
[22] H.S. Johnston, *Gas Phase Reaction Rate Theory*. Ronald, New York, 1996, pp. 151–154.
[23] H. Goldstein, C.P. Poole, J.L. Safco, *Classical Mechanics*, 3rd ed., Addison-Wesley, New York, 2002.
[24] S.C. Althorpe, D.C. Clary, *Annu. Rev. Phys. Chem.*, **54** (2003) 493.
[25] G.C. Schatz, *Rev. Mod. Phys.*, **61** (1989) 669.
[26] H. Eyring, *J. Chem. Phys.*, **3** (1935) 107.
[27] M.G. Evans, M. Polanyi, *Trans. Faraday Soc.*, **31** (1935) 875.
[28] N. Davidson, *Statistical Mechanics*. Harper and Row, New York, 1973.
[29] T.L. Hill, *Introduction to Statistical Mechanics*. Addison-Wesley, Reading, MA, 1972.
[30] D.A. McQuarrie, *Statistical Mechanics*. Harper Collins, New York, 1976.
[31] K.J. Laidler, *Chemical Kinetics*, 3rd ed., Harper and Row, New York, 1987, pp. 98–105.
[32] D.M. Bishop, K.J. Laidler, *J. Chem. Phys.*, **42** (1965) 1688.

[33] K.J. Laidler, *Chemical Kinetics*, 3rd ed., Harper and Row, New York, 1987, pp. 106–109.
[34] M.J. Pilling, P.W. Seakins, *Reaction Kinetics*. Oxford University Press, Oxford, UK, 1995, p. 75.
[35] R.E. Weston, H.A. Schwartz, *Chemical Kinetics*. Prentice-Hall, Inc., Englewood Cliffs, New Jersey, 1972, pp. 109–113.
[36] I. Shavitt, *J. Chem. Phys.*, **44** (1968) 4048.
[37] F. Wu, R.W. Carr, *J. Phys. Chem. A*, **106** (2002) 5832.
[38] F. Wu, R.W. Carr, *J. Phys. Chem. A*, **105** (2001) 1423.
[39] R.A. Marcus, *J. Chem. Phys.*, **20** (1952) 359.
[40] J.C. Keck, *J. Chem. Phys.*, **32** (1960) 1035.
[41] C. Steel, K.J. Laidler, *J. Chem. Phys.*, **34** (1961) 1827.
[42] B.C. Garrett, D.G. Truhlar, *J. Chem. Phys.*, **70** (1979) 1593; *ibid*., **76** (1982) 1380.
[43] B.C. Garrett, D.G. Truhlar, *J. Phys. Chem.*, **83** (1979) 1052; *ibid.*, **87** (1983) 4553(E).
[44] D.G. Truhlar, B.C. Garrett, *Annu. Rev. Phys. Chem.*, **35** (1984) 159.
[45] D.G. Truhlar, A.D. Isaacson, B.C. Garrett, in: M. Baer ed., *Theory of Chemical Reaction Dynamics*, Volume 4. CRC Press, Boca Raton, FL, 1985, pp. 56–137.
[46] H.S. Johnston, J. Heicklen, *J. Phys. Chem.*, **66** (1966) 532.
[47] R.P. Bell, *Trans. Faraday Soc.*, **55** (1959) 1.
[48] E.P. Wigner, *Z. Phys. Chem. B*, **19** (1932) 203.
[49] H.S. Johnston, D. Rapp, *J. Am. Chem. Soc.*, **83** (1961) 1.
[50] H.S. Johnston, *Gas Phase Reaction Rate Theory*. Ronald, New York, 1966, pp. 190–196.
[51] R.A. Marcus, M.E. Coltrin, *J. Chem. Phys.*, **67** (1977) 2609.
[52] A. Fernández-Ramos, J.A. Miller, S.J. Klippenstein, D.G. Truhlar, *Chem. Rev.*, **106** (2006) 4518.
[53] T.C. Allison, D.G. Truhlar, in: D.L. Thompson (Ed.), *Modern Methods for Multidimensional Dynamics Computations in Chemistry*. World Scientific, Singapore, 1998, pp. 618–712.
[54] Y.-P. Liu, D.-h. Lu, A. Gonzalez-Lafont, D.G. Truhlar, B.C. Garrett, *J. Am. Chem. Soc.*, **115** (1993) 7806.
[55] K.J. Laidler, *The Chemical Kinetics of Excited States*. Clarendon Press, Oxford, 1955, pp. 28–36.
[56] E. E. Nikitin, *Theory of Elementary Atomic and Molecular Processes in Gases*. Translated by M. J. Kearsley. Clarendon Press, Oxford, 1974.
[57] NIST Chemical Kinetics Database.
[58] A.V. Eremin, V.S. Ziborov, V.V. Shumera, D. Voicki, P. Roth, *Kinet. Catal. (English Trans.)*, **38** (1997) 1.
[59] L. Landau, *Physik Z. Sowjetunion*, **2** (1932) 46.
[60] C. Zener, *Proc. Roy. Soc. Lond. A*, **137** (1933) 696; **A140** (1930) 660.
[61] C.A. Mead, *J. Chem. Phys.*, **70** (1979) 2276.
[62] D.L. Bunker, N. Davidson, *J. Am. Chem. Soc.*, **80** (1958) 1285.

This page intentionally left blank

Chapter 4

The Kinetics of Pressure-Dependent Reactions

Hans-Heinrich Carstensen and Anthony M. Dean

1 INTRODUCTION

Commonly used reaction mechanisms for atmospheric or combustion systems contain a significant fraction of unimolecular and chemically activated reactions. Each of these reactions is in principle both temperature and pressure dependent, although the pressure dependence might vanish under certain conditions. Consequently, in order to achieve accurate kinetic predictions of complex chemical systems, it is necessary to incorporate this pressure and temperature dependence into kinetic models. This leads to the need to develop tools which allow the kineticist to analyze these types of reactions and which yield apparent time-independent rate constants that can be used in modeling studies.

Among the reaction types that display pressure dependence are radical–radical recombination reactions, addition reactions of radicals to multiple bonds, insertions of species with empty orbitals (e.g., carbenes) into single bonds, elimination reactions, dissociation reactions (e.g., β-scission), and isomerization reactions. All these reactions can be thought of as a sequence of at least two steps with one of them being an excitation process followed either by a deactivation step, in which excess energy has to be removed by the bath gas to stabilize a molecule, or by a reaction producing generally[1] two or more products. We shall clarify this in the following section and note for the moment that it is energy transfer to or from a molecule or intermediate that distinguishes a pressure-dependent reaction from a pressure-independent one.

In this chapter we will first review the underlying theory of unimolecular and recombination reactions, starting with single-channel single-well systems and then considering complex multi-well systems. We then briefly discuss a few program packages, which allow a kinetic analysis of

[1]Pure isomerization reactions are an exception, because only one product (the isomer) is formed per reaction channel.

Comprehensive Chemical Kinetics, Volume 42, 101–184

ISSN: 0069-8040/doi:10.1016/S0069-8040(07)42004-0

pressure-dependent reactions, and also describe some methods to obtain the required input parameters. Finally, we present results of the kinetic analysis of several example reactions. These detailed calculations allow a comparison of the predictions with experimental data and a discussion of the accuracy of different methods and the input parameters they need. We conclude with an outlook of anticipated future research directions.

2 REVIEW OF PRESSURE-DEPENDENT REACTIONS

2.1 Unimolecular reactions

In this section we try to provide a short introduction of unimolecular reactions to set the stage for the practical applications that are discussed later in this chapter. For a more detailed discussion, the reader is referred to kinetics textbooks, e.g., those by Holbrook *et al.* [1] or Gilbert and Smith [2], which served as a guide for the following discussion.

Consider the unimolecular reaction $AB \rightarrow A + B$, which designates either a dissociation or an elimination reaction. The simplest model to qualitatively describe this reaction was proposed by Lindemann. It splits the overall process into two steps:

$$AB + M \underset{k_{-1}}{\overset{k_1}{\rightleftharpoons}} AB^* + M$$

$$AB^* \xrightarrow{k_2} A + B$$

The first step, a ''strong'' collision between a bath gas molecule (M) and a reactant AB, transfers enough energy to AB to reach a state above the reaction barrier (excitation step). This energized state AB^* then either rearranges to the products $A + B$ (reaction) or it loses energy in a subsequent collision to re-form AB (deactivation). After a short time, formation and consumption of AB^* will be in balance, or in other words the concentration of AB^* (symbolized as $[AB^*]$) reaches a constant value, called the steady-state concentration. At this time the condition $d[AB^*]_{ss}/dt = 0$ holds. If we assume that the time required to achieve the steady-state condition is negligible compared to the total reaction time, then the apparent unimolecular rate constant, k_{uni}, for the reaction $AB \rightarrow A + B$ can be derived as follows:

$$\frac{d[AB^*]_{ss}}{dt} = k_1[M][AB] - \{k_{-1}[M] + k_2\}[AB^*]_{ss} = 0 \qquad (1)$$

$$[AB^*]_{ss} = \frac{k_1[M]}{k_{-1}[M] + k_2} \; [AB] \tag{2}$$

$$-\frac{d[AB]}{dt} = \frac{d[A]}{dt} = \frac{d[B]}{dt} \equiv k_{uni}[AB] = k_2[AB^*] \cong k_2[AB^*]_{ss} \tag{3}$$

$$k_{uni} = \frac{k_1 k_2[M]}{k_{-1}[M] + k_2} \tag{4}$$

The two limiting cases of low ($[M] \to 0$) and high ($[M] \to \infty$) collider concentrations lead to expressions for the low-pressure rate constant k_0 and the high-pressure rate constant k_∞:

$$[M] \to 0, \quad k_{uni} \to k_{uni,0} \equiv k_0 = k_1[M] \tag{5}$$

$$[M] \to \infty, \quad k_{uni} \to k_{uni,\infty} \equiv k_\infty = \frac{k_1 k_2}{k_{-1}} \tag{6}$$

Fig. 1 schematically shows a double logarithmic plot of k_{uni} as a function of the total pressure, a so-called fall-off plot. If we use the low-pressure region as reference point, we observe that k_{uni} departs at a certain pressure from the linear relationship and "falls off" to the high-pressure limit. The transition region, in which k_{uni} switches from the low-pressure to the high-pressure rate regime, is called the fall-off region.[2] Its location may be characterized by the pressure $p_{1/2}$, at which k_{uni} equals $1/2k_\infty$. By substituting k_∞ in equation (4) with $1/2k_\infty$ and substituting k_∞ with the expression in equation (6) it follows after rearranging that at $p_{1/2}$ the condition $k_2 = k_{-1}[M]_{1/2}$ holds. This relationship allows one to determine how the location of the fall-off region shifts as a function of temperature. Typically k_2 grows faster with temperature than k_{-1} does; hence, with increasing temperature a larger concentration $[M]_{1/2}$ is required to fulfill the $k_2 = k_{-1}[M]_{1/2}$ condition. Further, since $[M]_{1/2} = p_{1/2}/RT$, the pressure required to maintain the same $[M]_{1/2}$ concentration scales with T. Both effects cause the fall-off region to shift with increasing temperature toward higher pressure. The magnitude of shift when going from low to high temperature conditions can be substantial, e.g., a reaction which at room temperature is at or near its high-pressure limit might be deep in the fall-off region at combustion temperatures. This explains why the pressure dependence of rate constants is especially important for the modeling of combustion systems.

[2] An alternative definition of the fall-off is possible by choosing the high-pressure limit as reference point. In the high-pressure regime, $k_{uni}/k_\infty = 1$. Some authors refer the fall-off region as the pressure range for which this ratio declines ("falls off"). According to this definition a rate is in a fall-off region as long as the high-pressure limit is not reached.

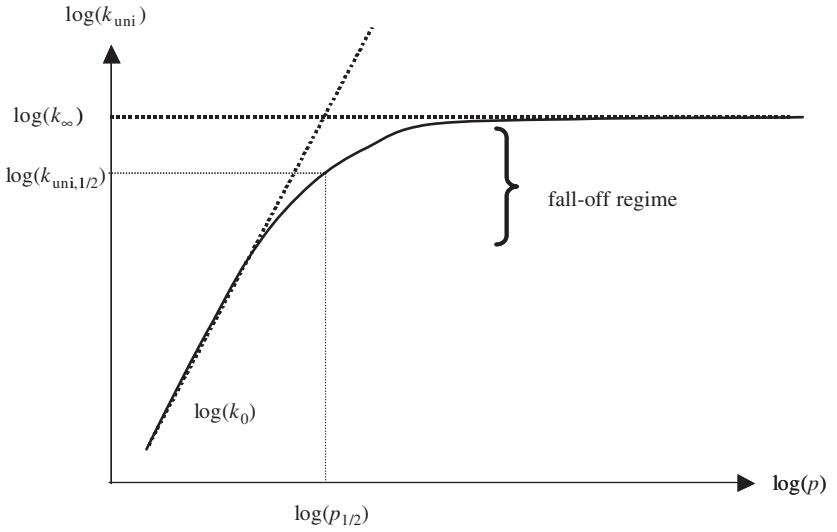

Fig. 1. A schematic fall-off plot for a unimolecular rate constant as function of pressure.

The unimolecular rate constant k_{uni} is usually expressed in terms of k_0 and k_∞, or, alternatively, in terms of the reduced pressure p_{r}, defined as

$$p_{\text{r}} = \frac{k_0[\text{M}]}{k_\infty} \tag{7}$$

$$k_{\text{uni}} = k_\infty \frac{p_{\text{r}}}{1 + p_{\text{r}}} \tag{8}$$

In the simplest form, the Lindemann mechanism assumes that the rate constants for the activation and deactivation steps, k_1 and k_{-1}, do not depend on energy and can directly be calculated from kinetic collision theory. With the probability for the AB species to obtain energy $\geqslant E_0$ being $\exp(-E_0/RT)$, we obtain

$$k_1 = Z_{\text{col}}\, \text{e}^{-E_0/RT} \tag{9}$$

$$k_{-1} = Z_{\text{col}} \tag{10}$$

The rate constant k_2 was initially also assumed to be independent of the energy in AB* and its value should be comparable to or smaller than a vibrational frequency ($10^{13}\,\text{sec}^{-1}$). For cases in which the high-pressure rate constant k_∞ is known from experiments one can calculate k_2 by rearranging equation (6),

$$k_2 = \frac{k_\infty k_{-1}}{k_1} \tag{11}$$

Although the Lindemann model can explain the occurrence of a fall-off region, it predicts its location to occur at several orders of magnitude higher pressures than experimentally observed. Related to this, calculated k_2 rate constants from experimental high-pressure rate constants were found to be unrealistically large. One major cause of these problems is the inherent assumption that AB and AB* can be treated as different species. If so, then we obtain with $\Delta G \approx E_0$

$$\frac{k_1}{k_{-1}} = K_{\text{eq}} = \text{e}^{-E_0/RT} \tag{12}$$

which leads to equation (9). In reality, AB* is the same species as AB with the difference that it contains additional internal energy, mainly stored in vibrational modes. A given amount of excess energy can be stored in many different combinations of vibrations (states) and the number of states increases rapidly with energy. Since AB* therefore exists in many different states, the probability to excite AB to AB* increases (it scales with the number of states). Hinshelwood derived an expression for this probability[3] based on the assumption that all vibrations are classical oscillators at equilibrium:

$$f(E) = \frac{(E/kT)^{s-1}}{(s-1)!}\text{e}^{-E/kT} \tag{13}$$

If this probability is incorporated into equation (9), one obtains

$$k_1 = Z_{\text{col}}\frac{(E_0/kT)^{s-1}}{(s-1)!}\text{e}^{-E_0/kT} \tag{14}$$

The ratio $(E/kT)^{s-1}/(s-1)!$ is usually significantly larger than unity; hence, k_1 increases compared to the initial Lindemann model. k_{-1} remains unchanged, because within the "strong" collision assumption every collision will still deactivate AB*. From equation (11) we see that an increase of k_1 leads to a smaller k_2 rate constant, which in turn reduces the bath gas density $[\text{M}]_{1/2}$ required to fulfill $k_2 = k_{-1}[\text{M}]_{1/2}$, our definition of the location of the fall-off region. Therefore, this modification improves both issues with the original model: it moves the fall-off regime to a lower pressure range and it leads to a more realistic value for k_2.

An important consequence of the Hinshelwood–Lindemann treatment is that the probability to find AB at the energy E depends now on the number of oscillators, s, or in other words on the size of the reacting

[3]We are using three different symbols for the energy distribution function: f(E) denotes the Boltzmann (equilibrium) distribution function, g(E) refers to an unspecified distribution function, and h(E) describes the overall energy distribution of reactants in chemically activated systems.

molecule AB. Larger species are more easily activated to energies above E_0 than small molecules.

In general, the Hinshelwood–Lindemann model reproduces the location of the fall-off region well, though the shapes of experimental fall-off curves are still not accurately captured. To further improve the theory, a modified reaction scheme proves to be helpful:

$$\mathrm{AB} + \mathrm{M} \underset{k_{-1}}{\overset{k_1}{\rightleftharpoons}} \mathrm{AB}^* + \mathrm{M}$$

$$\mathrm{AB}^* \xrightarrow{k_2} \mathrm{AB}^{\#}$$

$$\mathrm{AB}^{\#} \rightarrow \mathrm{A} + \mathrm{B}$$

The conversion of AB^* to products is now thought to proceed *via* a critical geometry $\mathrm{AB}^{\#}$. AB^* and $\mathrm{AB}^{\#}$ have the same energy, E, with $E \geqslant E_0$, but in AB^* this energy is randomly distributed among all oscillators, while in $\mathrm{AB}^{\#}$ an amount $E_m \geqslant E_0$ is localized in the reactive mode. This is the basic idea of the RRK theory (Rice–Ramsperger–Kassel). The assumption of random energy distribution among all modes allows the calculation of statistical weights for AB^* and $\mathrm{AB}^{\#}$. To do so, Kassel assigned—in the quantum version of this theory—a single average frequency, v, to all oscillators of AB. Now, the total distributable energy E is made up by n quanta and the threshold energy E_0 by m quanta ($n \geqslant m$) of v. Statistically, the probability w to distribute n quanta of energy among s oscillators is given by

$$w(\mathrm{AB}^*) = \frac{(n+s-1)!}{n!(s-1)!} \tag{15}$$

In the case of $\mathrm{AB}^{\#}$ only n–m quanta are freely distributable, which leads to

$$w(\mathrm{AB}^{\#}) = \frac{(n-m+s-1)!}{(n-m)!(s-1)!} \tag{16}$$

The rate constant k_2 is proportional to the ratio of these probabilities

$$k_2(E) \sim \frac{w(\mathrm{AB}^{\#})}{w(\mathrm{AB}^*)} = \frac{(n-m+s-1)!/\{(n-m)!(s-1)!\}}{(n+s-1)!/\{n!(s-1)!\}} \tag{17}$$

$$k_2(E) = A_{2,\infty} \frac{n!(n-m+s-1)!}{(n-m)!(n+s-1)!} \tag{18}$$

Now, k_2 is a function of the total energy E stored in AB*. The proportionality constant, $A_{2,\infty}$, can be identified as the high-pressure pre-exponential factor of $k_{2,\infty}$. The single frequency model also leads to a description of the ratio between $k_1(E)$ and k_{-1}:

$$\frac{k_1(E = nhv)}{k_{-1}} = \frac{(n + s - 1)!}{n!(s - 1)!}(1 - e^{-hv/kT})^s e^{-nhv/kT} \tag{19}$$

Written in this way, $k_2(E)$ and $k_1(E)/k_{-1}$ are step functions because n is an integer. This problem can easily be overcome by replacing $n!$ with the gamma function $\Gamma(n+1)$, which transforms them into continuous functions.

The single frequency versions of RRK and QRRK[4] theories predict experimental fall-off curves in most cases reasonably well if s is identified with the number of "effective" oscillators, which is often about one-half of the number of actual oscillators. Several ways to calculate the number of effective oscillators s are suggested in the literature. For example, Troe and Wagner [3] use

$$s = \frac{E_{\text{vib}}}{kT} \tag{20}$$

and Golden *et al.* [4] recommend

$$s = \frac{C_{\text{vib}}}{R} \tag{21}$$

A related question is how to determine the representative frequency. Investigations by, e.g., Weston [5] revealed that results obtained by using the geometric mean frequency agree "invariably better" with exact rate calculations compared to results from calculations employing the average mean frequency. Nevertheless, rate expressions obtained with RRK theory in its single frequency version often deviate substantially from experimental data. Kassel already pointed out that it is possible to extend RRK theory to a multi-frequency version, and Schranz *et al.* [6] demonstrated that a two-frequency model leads to improved accuracy. Later Chang *et al.* [7] reported the implementation of a three-frequency QRRK model with non-integer degeneracies of the representative frequencies. This method is useful for cases in which the complete sets of frequencies of the reacting species are not available, but their thermodynamic properties can be estimated *via*, e.g., group additivity methods. The representative frequencies are then obtained from fits to the $C_p(T)$ values [8].

[4]The name QRRK is not clearly defined. Here, we use QRRK to denote the quantum version of RRK theory, also referred as quantum Kassel theory.

Marcus modified the RRK theory to what is known as *RRKM* theory. RRKM theory is the microcanonical[5] version of transition state theory, and $AB^{\#}$ is identified as the transition state of the reaction. A transition state is defined as the "dividing surface" between reactants and products, and its location is determined by the condition that every trajectory (flux), which passes this surface, will form the products without recrossing. The second major assumption of RRKM theory, the ergodicity assumption, requires fast and complete randomization of the available freely distributable energy among all active modes after excitation. This assumption recognizes that only a part of the internal energy can freely be distributed among different modes. Examples of contributions to the internal energy that are assigned to a particular mode and hence not distributable are (1) the zero-point energy of vibrations and (2) a fraction of the rotational energy, which is bound to rotational modes due to the conservation law of total angular momentum. Hence, the distributable energy is mainly vibrational energy (excluding the zero-point energy) stored in oscillators and to a small extent rotational energy. It is common to consider all vibrations and one rotation (the so-called K-rotor) as active modes.

The rate constant $k_2(E)$ will depend on the transition frequency ($\nu^{\#}$) with which a trajectory passes through the transition state, $\nu^{\#} = kT/h$, and the probability (statistical weight ratio) to form the transition state geometry from all AB^*. This probability can be determined from the sum of states, $W(E)$ of $AB^{\#}$, and the number of states of AB^* at the energy E. Because the number of states of AB^* is generally enormously high, it is expressed *via* its density of states ($\rho(E)$, number of states per energy interval). The final expression[6] for $k_2(E)$ in the RRKM theory is

$$k_2(E) = \frac{kT}{h}\frac{W^{\#}(E - E_0)}{\rho(E)kT} = \frac{W^{\#}(E - E_0)}{h\rho(E)} \tag{22}$$

The unimolecular rate constant is obtained by integrating over all energy levels above E_0, weighted by the population distribution, $g(E)$:

$$k_{\text{uni}} = \int_{E_0}^{\infty} \frac{k_2(E)k_1(E)/k_{-1}}{1 + k_2(E)/k_{-1}[\text{M}]} g(E)\,\mathrm{d}E \tag{23}$$

[5]A microcanonical system is characterized by the number of particles (N), its volume (V), and the energy (E). Therefore, a microcanonical rate constant is a function of energy. On the other hand, a system defined by its temperature instead of its energy is called a canonical system and consequently, canonical rate constants are functions of T.

[6]For a detailed derivation of the RRKM theory, please refer to textbooks on chemical kinetics.

The ratio $k_1(E)/k_{-1}$ is easily evaluated for the condition of equilibrium

$$\frac{k_1(E)}{k_{-1}} = K_{eq} = \frac{Q_{AB^*}(E)}{Q_{AB}} \tag{24}$$

By applying the definition of a partition function Q,

$$Q = \sum_{i=0}^{\infty} g_i \, e^{-E_i/kT} \tag{25}$$

to a "species" existing only at the energy E (more precisely in the range E, $E + dE$),

$$Q(E) = \left(\sum_{E}^{E+dE} g(E) \right) e^{-E/kT} = \rho(E) e^{-E/kT} \tag{26}$$

we obtain

$$\frac{k_1(E)}{k_{-1}} = \frac{\rho(E)}{Q_{AB}} e^{-E/kT} \tag{27}$$

This points to the key role of the density of states, $\rho(E)$, in RRKM theory, as it is not only needed to calculate k_2, but also for the ratio between the activation and the deactivation rate constants.

At the high-pressure limit, equation (23) can be integrated analytically and it can be shown that $k_{uni}(T)$ obtained from RRKM theory as described here is similar but not equal to the high-pressure rate obtained *via* canonical transition state theory[7]

$$k_{uni,[M]\to\infty} = \frac{kT}{h} \frac{Q^{\#}_{vib}}{Q_{vib}} e^{-E_0/kT} \tag{28}$$

$$k_{TST} = \frac{kT}{h} \frac{Q^{\#}_{rot} Q^{\#}_{vib}}{Q_{rot} Q_{vib}} e^{-E_0/kT} \tag{29}$$

Equations (28) and (29) differ in that latter contains contributions from the rotational partition functions. This contribution is lost in a RRKM analysis unless one includes the total angular momentum, J, and thus formulates the microcanonical rate constants as $k(E, J)$. In many cases, the geometries of the transition state and the reactant are very similar and consequently the ratio of the rotational partition functions is very

[7]The transition state theory developed by Eyring and by Evans and Polanyi yields high-pressure rate constants $k(T)$. Since it is based on the same assumptions as the RRKM theory (existence of a transition state and fast complete energy distribution), the results from both theories should coincide. See textbooks for more details on TS theory.

close to unity. Then equations (28) and (29) lead to the same result. Reactions with loose transition states, e.g., those involving ionic species, are examples for which a simple $k(E)$ treatment is not accurate and a $k(E, J)$ analysis required.

In summary, an adequate kinetic description of unimolecular reactions requires knowledge of the rate constants for the individual processes of activation, deactivation, and transformation to products. In addition, the population distribution function for the reactant as a function of the internal energy E is needed. Within the framework of the steady-state treatment and strong collisions, the key property describing the population distribution is the density of states, $\rho(E)$. Both QRRK and RRKM theories are statistical methods and assume that excess energy is rapidly distributed among all active modes. Besides the barrier height and the pre-exponential factor of the high-pressure rate constant, QRRK theory only requires knowledge of the representative frequency(ies) of the reacting molecule and its collision parameters. This information is easily obtained from the literature or estimation methods, so that QRRK calculations can be performed with comparatively little effort. In contrast, detailed frequency and rotational data for the stable species as well as for the transition state are needed as input for RRKM theory. If such information is available, however, RRKM theory is more fundamental and precise and the method of choice.

2.2 Chemically activated reactions

The recombination $A + B \rightarrow AB$ is the reverse reaction of the unimolecular dissociation of AB. The principle of detailed balancing ties both reactions together by the thermodynamic equilibrium constant

$$\frac{k_{\text{uni}}}{k_{\text{rec}}} = K_{\text{eq}} \tag{30}$$

Consequently, k_{rec} is—like k_{uni}—pressure dependent. This is obvious for the high-pressure limit when collisions with the bath gas quickly establish a Boltzmann distribution of the population, but Smith *et al.* [9,10] argue that equation (30) also holds for lower pressures.

In the introduction we characterized a pressure-dependent reaction as a process that is composed of an excitation step followed by either deactivation or reaction to (often multiple) products. A closer look at the recombination in terms of the underlying scheme of elementary reactions

$$A + B \underset{k_2}{\overset{k_{-2}}{\rightleftharpoons}} AB^*$$

$$AB^* + M \xrightarrow{k_{-1}} AB + M$$

reveals that these criteria are met. The excitation step is called *chemical activation*, since energized AB^* molecules are created when a new bond is formed during the recombination process. Previously we discussed excitation due to collisions with the bath gas or so-called thermal activation. The energy distribution of initially formed AB^* with respect to non-activated AB is determined by two contributions: (1) the energy released from the newly formed bond and (2) the thermal energy content in both reactants, which is commonly assumed to follow a Boltzmann distribution. Redissociation of the excited complex leads back to the reactants (hence special type of products) and collisions with the bath gas to stabilization. Thus, all elements of a pressure-dependent reaction are present.

Application of the steady-state assumption for $[AB^*]$ yields the apparent recombination rate constant for stabilization, defined as $d[AB]/dt = k_{rec}[A][B]$,

$$k_{rec} = \frac{k_{-1}k_{-2}[M]}{k_{-1}[M] + k_2} \tag{31}$$

$$[M] \to 0, \quad k_{rec} \to k_{rec,0} \equiv k_0 = \frac{k_{-1}k_{-2}}{k_2}\ [M] \tag{32}$$

$$[M] \to \infty, \quad k_{rec} \to k_{rec,\infty} \equiv k_\infty = k_{-2} \tag{33}$$

If we combine equations (4) and (31) we can show that equation (30) is obtained:

$$\frac{k_{uni}}{k_{rec}} = \frac{k_1k_2[M]/\{k_{-1}[M] + k_2\}}{k_{-1}k_{-2}[M]/\{k_{-1}[M] + k_2\}} = \frac{k_1k_2}{k_{-1}k_{-2}} = \frac{[AB][AB^*]}{[AB^*][A][B]} = K_{eq} \tag{34}$$

In other words, if a steady-state population of the energized complex AB^* is formed, then the recombination and corresponding dissociation reactions always obey detailed balancing. Deviations from this principle may only occur in situations in which the steady-state condition is not (yet) reached.

Building on our definition for pressure dependence one might wonder about the impact of additional product channels. Adding just one additional product channel leads to the following scheme:

$$A + B \underset{k_2}{\overset{k_{-2}}{\rightleftharpoons}} AB^*$$

$$AB^* + M \xrightarrow{k_{-1}} AB + M$$

$$AB^* \xrightarrow{k_3} C + D$$

An example for such a case is the reaction between C_2H_5 radicals and H atoms. The C + D channel would then refer to the products $CH_3 + CH_3$, and AB can be identified with C_2H_6. The expression for the steady-state concentration of AB^*

$$[AB^*]_{ss} = \frac{k_{-2}[A][B]}{k_{-1}[M] + k_2 + k_3} \tag{35}$$

contains one additional term ($+k_3$) in the denominator compared to the previous scheme. However, we now need two apparent rate constants to fully describe this chemically activated reaction: one to describe the stabilization step and the second one for the formation channel of the new products.

$$A + B \xrightarrow{k_{stab}} AB \Rightarrow \frac{d[AB]}{dt} = k_{stab}[A][B]$$

$$A + B \xrightarrow{k_{prod}} C + D \Rightarrow \frac{d[C]}{dt} = \frac{d[D]}{dt} = k_{prod}[A][B]$$

If we formulate the formation of AB or C + D in terms of $[AB^*]_{ss}$, we obtain expressions for k_{stab} and k_{prod}

$$\begin{aligned} &\frac{d[AB]}{dt} = k_{-1}[M][AB^*]_{ss} = k_{-1}[M]\frac{k_{-2}[A][B]}{k_{-1}[M] + k_2 + k_3} \\ &\Rightarrow k_{stab} = \frac{k_{-1}k_{-2}[M]}{k_{-1}[M] + k_2 + k_3} \end{aligned} \tag{36}$$

$$\begin{aligned} &\frac{d[C]}{dt} = \frac{d[D]}{dt} = k_3[AB^*]_{ss} = k_3\frac{k_{-2}[A][B]}{k_{-1}[M] + k_2 + k_3} \\ &\Rightarrow k_{prod} = \frac{k_3k_{-2}}{k_{-1}[M] + k_2 + k_3} \end{aligned} \tag{37}$$

By considering the limiting case of high pressure, we again find that the high-pressure rate constant for stabilization is independent of [M]. More interesting is to examine the pressure dependence of the apparent rate constant for the C + D product channel. This rate constant at its high-pressure limit is inversely proportional to pressure. This is also true for the redissociation reaction, which is just a special product channel.

$$\Rightarrow k_{redis} = \frac{k_2k_{-2}}{k_{-1}[M] + k_2 + k_3} \tag{38}$$

By combining equations (36)–(38) it is easy to show that the sum of all three apparent rate constants equals k_{-2}, or in other words that the rate for the formation of the excited complex equals the sum of all complex consuming rates (as it should be).

2.3 *Energy transfer models*

(*i*) *The modified strong collision assumption*

Before continuing the discussion of more complicated reaction systems we will consider the energy transfer process. So far the discussion was based on the assumption that all collisions are ''strong,'' meaning that a single collision with a collider species completely activates AB or deactivates AB*. This assumption leads to a bimodal energy distribution and ignores the fact that depending on the collision angle, relative velocities of the colliding species, and energy distribution in the colliders a wide range of interactions is possible. Certainly, in the real world, not each ''collision'' will lead to complete exchange of energy. In order to keep the simplicity of the strong collision assumption, the ''modified strong collision (MSC)'' approach was developed. It basically assumes that only a fraction of all collisions is ''strong'' while the remaining collisions are elastic (no transfer of internal energy). The collision parameter β_c describes the fraction of ''successful'' collisions as a function of collider properties and the temperature. If we express the collision frequency ω, defined as the number of collisions per time, in terms of the Lennard–Jones diameters σ_R and σ_M for a reactant R and bath gas M, we obtain

$$\omega_{LJ} = N_A \left(\frac{\sigma_R + \sigma_M}{2}\right)^2 \sqrt{\frac{8\pi kT}{\mu}}\, \Omega^{*(2,2)}(T)\,[M] \tag{39}$$

where N_A is the Avogadro number, μ the reduced mass, and $\Omega^{*(2,2)}$ the collision integral. In the framework of the MSC assumption, the stabilization rate constant is then given as

$$k_{MSC} = \beta_c \omega_{LJ} \tag{40}$$

Based on solutions of the master equation (ME) (see below) for model systems, Troe [11,12] developed a relationship between the collision efficiency parameter (β_c) and the average energy transferred per collision, $\langle \Delta E_{all} \rangle$

$$\frac{\beta_c}{1 - \sqrt{\beta_c}} \cong \frac{-\langle \Delta E_{all} \rangle}{F_E kT} \tag{41}$$

The ''energy-dependence factor'' of the density of states F_E is a function introduced by Troe [13] and it is defined for vibrational densities of

states as

$$F_E(T) = \frac{\int_{E_0}^{\infty} \rho_{\text{vib}}(E)\text{e}^{-E/kT}\,\text{d}E}{kT\rho_{\text{vib}}(E_0)\text{e}^{-E_0/kT}} \tag{42}$$

In this equation we explicitly write F_E as a function of temperature to emphasize that it is not a constant number. Evaluation of F_E requires knowledge of $\rho_{\text{vib}}(E)$ and in a later section we will describe methods to accurately calculate this function.

Gilbert *et al.* [14] showed that the approximation given by equation (41) leads to inaccurate results for high values of F_E and suggested the following alternative formulation:

$$\beta_{\text{c}} = \left(\frac{\alpha_{\text{c}}}{\alpha_{\text{c}} + F_E kT}\right)^2 \frac{1}{\Delta} \tag{43}$$

In this equation α_{c} represents the average energy transferred in deactivating ("down") collisions. α_{c} is related to $\langle \Delta E_{\text{all}} \rangle$ *via*

$$\langle \Delta E_{\text{all}} \rangle = \gamma_{\text{c}} - \alpha_{\text{c}} \tag{44}$$

and

$$\gamma_{\text{c}} = \frac{\alpha_{\text{c}} F_E kT}{\alpha_{\text{c}} + F_E kT} \tag{45}$$

where γ_{c} represents the average energy transferred in activating ("up") collisions. Notice that because the average energy transferred in down collisions is always larger than that for up collisions, $\langle \Delta E_{\text{all}} \rangle$ is defined as a negative property. This explains the negative sign in equation (41) to ensure $0 < \beta_{\text{c}} \leq 1$.

The property Δ in equation (43) can again be calculated if the functions F_E and $\rho_{\text{vib}}(E)$ are known:

$$\Delta = \Delta_1 - \left[\frac{F_E kT}{\alpha_{\text{c}} + F_E kT}\right]\Delta_2 \tag{46}$$

$$\Delta_1 = \frac{\int_0^{E_0} \rho_{\text{vib}}(E)\text{e}^{-E/kT}\text{d}E}{\Delta_N} \tag{47}$$

$$\Delta_2 = \frac{\int_0^{E_0} \rho_{\text{vib}}(E)\text{e}^{-E/kT}\,\text{e}^{-(E_0-E)/F_E kT}\,\text{d}E}{\Delta_N} \tag{48}$$

$$\Delta_N = \int_0^{\infty} \rho_{\text{vib}}(E)\text{e}^{-E/kT}\,\text{d}E \tag{49}$$

Although these integrals might look complicated, they can easily be evaluated if the density of states function is given in an analytic way as introduced by Whitten and Rabinovitch [15]. Essentially ρ_{vib} (E) is expressed as a polynomial in E and the above integrals have analytic solutions (see, e.g., Ref. [16]).

(*ii*) *The master equation*

A realistic description of energy transfer would include all possible states or energy levels of a molecule AB with AB* being a subset of AB. In a collision, energy can be transferred as translational, vibrational, and rotational energy. Since the rate constants of pressure-dependent reactions depend only on the energy content in active modes, we can ignore changes in translational energy in this context. Due to the restriction of total angular momentum conservation, only a small part of rotational energy is freely distributable and available for reaction. Consequently, the transfer of energy as vibrational energy is most important. In reality, vibrations and rotations are coupled, meaning that they are not completely independent of each other. However, a separation of modes is often a good assumption and generally internal modes are treated as independent harmonic oscillators and rigid rotors (HO–RR approximation).

A collision between two colliders will not depend on previous collisions if we assume rapid energy redistribution among all active modes in-between collisions. In other words, ''collisions'' are independent events, and they depend only on the initial states of the two colliding partners. Therefore, we can describe them as Markovian or ''random walk'' processes, and we can assign time-independent rate constants for the transition of a species AB from a state of energy E' to a state of energy E:

$$\frac{\mathrm{d}[\mathrm{AB}(E)]}{\mathrm{d}t} = k(E, E')[\mathrm{AB}(E')] \tag{50}$$

Looking at the evolution of the population of states of energy E with time t, we obtain

$$\frac{\partial \rho(E,t)}{\partial t} = \int_{E'} k(E, E')\rho(E', t)\mathrm{d}E' - \int_{E'} k(E', E)\rho(E, t)\mathrm{d}E' \tag{51}$$

$$\frac{\partial \rho(E,t)}{\partial t} = \sum_{E'} k(E, E')\rho(E', t) - \sum_{E'} k(E', E)\rho(E, t) \tag{52}$$

The first term of the right-hand side of either the continuous (51) or discrete (52) formulation describes the increase of $\rho(E, t)$ *via* transitions from levels E' to E while the second term represents depletion of $\rho(E, t)$ to states of energy E'. In the following, we will focus on the discrete

description since it is the basis for implementation into computer codes. $\rho(E', t)$ may also be thought of as a population density function (population per energy interval), in which case equations (51) and (52) are descriptions of the evolution of the population density with time. If the transfer of AB from a state E to E' is exclusively caused by collisions, we can define the collision frequency $\omega(E)$ as

$$\omega(E) = \sum_{E'} k(E', E) \tag{53}$$

and equation (52) becomes

$$\frac{\partial \rho(E,t)}{\partial t} = \sum_{E'} k(E, E')\rho(E', t) - \omega(E)\rho(E, t) \tag{54}$$

It is desirable to define a normalized transition probability $P(E, E')$

$$P(E, E') = \frac{k(E, E')}{\sum\limits_{E} k(E, E')} = \frac{k(E, E')}{\omega(E')} \tag{55}$$

which allows us to rewrite equation (54) to

$$\frac{\partial \rho(E,t)}{\partial t} = \omega(E') \sum_{E'} P(E, E')\rho(E', t) - \omega(E)\rho(E, t) \tag{56}$$

This latest transformation is only valid with the assumption that the collision frequency $\omega(E')$ is only a weak function of E and hence can be treated as a constant. This assumption holds well if, for example, Lennard–Jones collision frequencies are used.

The detailed balancing requirement puts a constraint on the reverse energy transfer rates ($f(E)$ is again the equilibrium distribution function):

$$k(E, E')f(E') = k(E', E)f(E) \tag{57}$$

or in terms of transition probabilities:

$$\omega(E')P(E, E')f(E') = \omega(E)P(E', E)f(E) \tag{58}$$

Again utilizing $\omega(E) \cong \omega(E')$, the detailed balancing requirement simplifies to

$$P(E, E')f(E') = P(E', E)f(E) \tag{59}$$

Numerous energy transfer models for $P(E, E')$ are discussed in the literature [17]; the most widely known and used one is the "exponential down model." It assumes that the probability to transfer energy in a single collision event depends exponentially on the energy amount that is transferred. Small amounts of energy are more likely transferred than

large quantities. If the probability is expressed as

$$P(E', E) = A(E')e^{-\alpha(E-E')}, \quad \text{for } E \geq E' \tag{60}$$

then we can identify the parameter α to be inversely proportional to the average energy transferred in deactivating collisions:

$$\alpha = \frac{1}{\langle E_{\text{down}} \rangle} \tag{61}$$

$\langle E_{\text{down}} \rangle$ values range from $\sim 100\,\text{cm}^{-1}$ to $200\,\text{cm}^{-1}$ for weak colliders such as He and can take values $> 1000\,\text{cm}^{-1}$ if the bath gas belongs to the group of very strong colliders. Equation (60) defines only the energy transfer probabilities of deactivating collisions. The complementary probability function for activating collisions,

$$P(E, E') = A(E')e^{-\alpha(E-E')}\frac{f(E)}{f(E')}, \quad \text{for} \quad E > E' \tag{62}$$

is obtained by substituting equation (60) into equation (59) and rearranging. Note that this time the condition $E > E'$ does not include equality of E and E' to avoid double-counting. Finally, the normalization factor $A(E')$ is determined *via* the criteria

$$\sum_E P(E', E) = 1 \tag{63}$$

Besides being a normalization factor, $A(E')$ can also be interpreted as the probability that a collision is elastic, or in other words it is the fraction of collisions that do not lead to energy transfer. This can be seen from equation (60) by setting $E = E'$.

Having specified the energy transfer probabilities $P(E', E)$, we notice that the right-hand side of equation (56) is linear in $\rho(E, t)$. This allows us to rewrite equation (56) as an eigenvalue problem

$$\frac{\partial \rho(E, t)}{\partial t} = \hat{M}\rho(E, t) \tag{64}$$

The operator $\hat{M}$ describes the collision and reaction terms. The solutions of eigenvalue problems are eigenvalues λ_i and the corresponding eigenfunctions ψ_i. A convenient way to define those is *via*

$$\rho(E, t) = \sum_i c_i \psi_i(E) e^{\lambda_i t} \tag{65}$$

The population distribution function is described as an expansion of the eigenfunctions and the eigenvalues define their exponential decays. The expansion coefficients c_i are given by the density distribution at $t = 0$ sec. The number of chosen energy intervals determines the number of

expansion terms. Since all density distributions are finite and the total mass is conserved, all eigenvalues λ_i must be real and of negative or zero value. They have the physical meaning of relaxation rates. At long times the energy distribution will reach thermal equilibrium. Hence, the largest eigenvalue for pure collision systems must be zero and the second largest eigenvalue describes the slowest relaxation rate. The eigenfunctions ψ_i are most conveniently chosen to be δ-functions. They then define the individual energy intervals of AB used in the discrete expressions of the ME.

2.4 The master equation approach for single-well systems

The review of pressure-dependent reactions, which so far was based on the strong collision assumption, is readily adapted to more sophisticated collision models. Here, we discuss the description of unimolecular reactions in form of the ME. Our initial scheme

$$\mathrm{AB} + \mathrm{M} \underset{P(E,E')}{\overset{P(E',E)}{\rightleftharpoons}} \mathrm{AB}^*$$

$$\mathrm{AB}^* \xrightarrow{k_2(E)} \mathrm{A} + \mathrm{B}$$

translates into the following ME (assuming ω is independent of E):

$$\frac{\partial \rho(E,t)}{\partial t} = \omega \sum_{E'} P(E,E')\rho(E',t) - \omega\rho(E,t) - k_2(E)\rho(E,t) \quad (66)$$

The rate constants k_1 and k_{-1} of the (modified) strong collision model have been replaced by state specific energy transitions as discussed above. The first right-hand term describes the increase of the population density $\rho(E, t)$ by collisions that transfer species which contain the energy E' to states of energy E. Note that the sum includes the case $E' = E$ although it does not increase $\rho(E, t)$. The second term describes the removal of species at energy E by collisions. Again, elastic collisions are included even though they do not lead to depletion of $\rho(E, t)$. The net effect is that the elastic collisions in both terms annihilate each other. Finally, the third term describes the consumption of $\rho(E, t)$ *via* chemical reaction (to form the products A + B). If we label discrete energy intervals with i and j, we can rewrite equation (66) to

$$\frac{\partial \rho_i(t)}{\partial t} = \omega \sum_{E'} P_{ij}\rho_j(t) - \omega\rho_i(t) - k_{2i}\rho_i(t) \quad (67)$$

Written as eigenvalue problem (see equation (64)) we can identify the matrix elements

$$\begin{aligned} M_{ij} &= \omega P_{ij} \\ M_{ii} &= \omega P_{ii} - \omega - k_{2i} \end{aligned} \tag{68}$$

As mentioned before, the solution of this eigenvalue problem provides a set of negative eigenvalues, which contain all kinetic and dynamic information. In most cases collisional relaxation is fast compared to chemical reactions, and if this is the case then the smallest negative eigenvalues will be clearly separated in magnitude from the remaining ones. Since the product formation is irreversible, no thermal equilibrium is reached and the smallest negative eigenvalue is less than zero. Its negative value represents the unimolecular rate constant for the chemical reaction.

The eigenvalues of this eigenvalue problem are found by diagonalizing the matrix $\hat{M}$. The situation is more complicated if collisional relaxation is not fast compared to chemical reaction. In that case, the solution will yield more than one small negative eigenvalues and the overall reaction will proceed on a non-exponential time scale. In other words, if collisional relaxation interferes with unimolecular reaction, the reaction process cannot be described by a time-independent rate constant k_{uni}.

We now take a look at the corresponding chemically activated reaction,

$$\begin{aligned} &\mathrm{A} + \mathrm{B} \underset{k_2(E)}{\overset{k_{-2}(E)}{\rightleftharpoons}} \mathrm{AB}^* \\ &\mathrm{AB}^* + \mathrm{M} \underset{P(E',E)}{\overset{P(E,E')}{\rightleftharpoons}} \mathrm{AB} + \mathrm{M} \end{aligned}$$

This system is described by the following ME:

$$\begin{aligned} \frac{\partial \rho(E,t)}{\partial t} = \omega \sum_{E'} P(E,E')\rho(E',t) - \omega\rho(E,t) \\ - k_2(E)\rho(E,t) + k_{-2,\infty} h(E)[\mathrm{A}][\mathrm{B}] \end{aligned} \tag{69}$$

Several features of this equation make the solution more challenging compared to the dissociation: (1) The last term on the right-hand side makes equation (69) non-linear, because [A] and [B] are both time dependent. (2) Often, the association or recombination rate is only known as high-pressure rate $k_{-2,\infty}(T)$. (3) The deactivation of energized AB is reversible so that stabilized AB can be reactivated. Starting with the second problem, it can be resolved by introducing a new function $h(E)$ to convert $k_{-2,\infty}(T)$ to an energy-dependent rate constant. This function

$h(E)$ is easily determined from considerations at equilibrium, with

$$\frac{k_{-2,\infty}}{k_{2,\infty}} = \frac{[\mathrm{AB}]}{[\mathrm{A}][\mathrm{B}]} = K_{\mathrm{eq}} \tag{70}$$

Under the same conditions, detailed balancing requires

$$k_{-2,\infty} h(\mathrm{E})[\mathrm{A}][\mathrm{B}] = k_2(\mathrm{E}) f(\mathrm{E})[\mathrm{AB}] \tag{71}$$

Both equations combined yield

$$k_{-2,\infty} h(E) = k_2(E) f(E) K_{\mathrm{eq}} \tag{72}$$

Hence

$$\frac{\partial \rho(E,t)}{\partial t} = \omega \sum_{E'} P(E,E')\rho(E',t) - \omega\rho(E,t) - k_2(E)\rho(E,t) + k_2(E) f(E) K_{\mathrm{eq}}[\mathrm{A}][\mathrm{B}] \tag{73}$$

An alternative would have been to substitute only $h(E)$ by

$$h(E) = \frac{k_2(E) f(E)}{\sum\limits_{E > E_0} k_2(E) f(E)} \tag{74}$$

which follows straightforwardly from equations (70) and (71) together with

$$k_2 = \sum_{E \geq E_0} k_2(E) f(E) \tag{75}$$

The first problem with equation (69) is also easily fixed by requiring $[\mathrm{B}] \gg [A]$. Now only the concentration of [A] will vary during the reaction and $[\mathrm{B}] = [\mathrm{B}]_0$ and the ME is linearized.

$$\frac{\partial \rho(E,t)}{\partial t} = \omega \sum_{E'} P(E,E')\rho(E',t) - \omega\rho(E,t) - k_2(E)\rho(E,t) + k_2(E) f(E)[\mathrm{B}]_0 K_{\mathrm{eq}}[\mathrm{A}] \tag{76}$$

If we consider $[\mathrm{A}](t)$ as an additional element in the population vector $\rho(E, t)$, equation (76) is again an eigenvalue problem and can be re-written in the same form as equation (64) with similar matrix elements, except for the additional source term.

There are several options to solve either (76) or (64): first, equation (76) may be integrated numerically. The results are time-dependent populations of all energy levels based on the initial conditions. If conditions change, a new integration is needed. The advantage of this method is that the population profiles are exact; however, it does not directly provide rate constants suitable for modeling. To obtain these

rate constants for the association reaction

$$A + B \rightarrow AB$$

one can evaluate the formation of AB at short reaction times, when the redissociation (the third problem discussed in connection with equation (69)) of AB is still insignificant, but relaxation of the individual energy levels is already complete. The reverse rate can be obtained from the final concentrations at long times when equilibrium is reached. This method will work well for systems with deep wells relative to the thermal energy. Under these conditions redissociation will occur on a long time scale that is clearly separated from the association process. Another but similar way to obtain the association rate constant is to prevent redissociation by making the stabilization process irreversible. AB molecules are "frozen out" when reaching a low-lying energy level. This technique is known as introducing an "absorbing boundary" to the system. The boundary will be located sufficiently below the barrier (for example, 10 kT below E_0). In general, this method works also for shallow wells for which a temporal separation of the reactions is not possible.

Both methods essentially rely on reaching steady-state concentrations for the energized AB molecules relative to the concentration of [A](t). Otherwise, the obtained rate constants would vary with time, because the population distribution would change. In terms of the eigenvalue approach of this reaction system, the smallest negative eigenvalues must be clearly separated from those that describe energy relaxation. As written above, the largest eigenvalue is obviously zero, because the system eventually reaches equilibrium. Thus, the second largest eigenvalue (the second smallest negative eigenvalue) will contain the desired kinetic information.

2.5 Complex pressure-dependent systems

So far, we only considered single-well and single-channel reactions. Often pressure-dependent reactions proceed *via* several isomerization steps and have many different product channels. In the following we will discuss such systems and the specific problems arising from them.

(*i*) *Two-well isomerization*

Consider the irreversible isomerization reaction

$$A \xrightarrow{k_A} B$$

The (modified) strong collision assumption allows us to separate this reaction into several steps

$$\mathrm{A} + \mathrm{M} \underset{k_{\mathrm{deact,A^*}}}{\overset{k_{\mathrm{act,A}}(E)}{\rightleftharpoons}} \mathrm{A^*} + \mathrm{M}$$

$$\mathrm{A^*} \underset{k_{\mathrm{BA}}(E)}{\overset{k_{\mathrm{AB}}(E)}{\rightleftharpoons}} \mathrm{B^*}$$

$$\mathrm{B^*} + \mathrm{M} \overset{k_{\mathrm{deact,B^*}}}{\longrightarrow} \mathrm{B} + \mathrm{M}$$

The steady-state assumption for $\mathrm{A^*}$ and $\mathrm{B^*}$ yields

$$\frac{\mathrm{d}[\mathrm{A^*}](E)}{\mathrm{d}t} = 0 = k_{\mathrm{act,A}}(E)[\mathrm{M}][\mathrm{A}] + k_{\mathrm{BA}}(E)[\mathrm{B^*}](E) - \{k_{\mathrm{deact,A^*}}[\mathrm{M}] + k_{\mathrm{AB}}(E)\}[\mathrm{A^*}](E) \tag{77}$$

$$\frac{\mathrm{d}[\mathrm{B^*}](E)}{\mathrm{d}t} = 0 = k_{\mathrm{AB}}(E)[\mathrm{A^*}](E) - \{k_{\mathrm{BA}}(E) + k_{\mathrm{deact,B^*}}[\mathrm{M}]\}[\mathrm{B^*}](E) \tag{78}$$

$$[\mathrm{B^*}](E) = \frac{k_{\mathrm{AB}}(E)}{k_{\mathrm{AB}}(E) + k_{\mathrm{deact,B^*}}[\mathrm{M}]}[\mathrm{A^*}](E) \tag{79}$$

$$[\mathrm{A^*}](E) = \frac{k_{\mathrm{act,A}}(E)[\mathrm{M}]}{k_{\mathrm{deact,A^*}}[\mathrm{M}] + k_{\mathrm{AB}}(E) - k_{\mathrm{BA}}(E)((k_{\mathrm{AB}}(E))/x}\ [\mathrm{A}] \quad \text{where } x = (k_{\mathrm{BA}}(E) + k_{\mathrm{deact,B^*}}[\mathrm{M}]) \tag{80}$$

Note that we treat the species $\mathrm{A^*}$ and $\mathrm{B^*}$ in energy-resolved form but deal with A and B as bulk species. This allows us to consider the deactivation steps as energy independent. With the steady-state concentrations of $\mathrm{A^*}$ and $\mathrm{B^*}$ determined, the rate constant $k_{\mathrm{iso,A}}$ is given by

$$\frac{\mathrm{d}[\mathrm{B}]}{\mathrm{d}t} \equiv k_{\mathrm{iso,A}}[\mathrm{A}] = \sum_E k_{\mathrm{deact,B^*}}[\mathrm{M}][\mathrm{B^*}](E) = \sum_E k_{\mathrm{deact,B^*}}[\mathrm{M}] \frac{k_{\mathrm{AB}}(E)}{k_{\mathrm{BA}}(E) + k_{\mathrm{deact,B^*}}[\mathrm{M}]} \times \frac{k_{\mathrm{act,A}}(E)[\mathrm{M}]}{k_{\mathrm{deact,A^*}}[\mathrm{M}] + k_{\mathrm{AB}}(E) - k_{\mathrm{BA}}(E)[k_{\mathrm{AB}}(E)/x]}\ [\mathrm{A}] \quad \text{where } x = (k_{\mathrm{BA}}(E) + k_{\mathrm{deact,B^*}}[\mathrm{M}]) \tag{81}$$

At the high-pressure limit ($[\mathrm{M}] \to \infty$) the pressure dependence cancels out and we obtain the same result as for unimolecular reactions forming

products, namely

$$k_{\mathrm{iso,A},\infty} = \sum_E k_{\mathrm{AB}}(E) \frac{k_{\mathrm{act,A}}(E)}{k_{\mathrm{deact,A^*}}} \tag{82}$$

For [M]$\rightarrow$0 we find a linear dependence of the low-pressure rate constant on [M]

$$k_{\mathrm{iso,A},0} = \sum_E \frac{k_{\mathrm{AB}}(E)}{k_{\mathrm{BA}}(E)} \frac{k_{\mathrm{act,A}}(E)}{k_{\mathrm{deact,A^*}}} k_{\mathrm{deact,B^*}}[\mathrm{M}] \tag{83}$$

but this time an additional term $k_{\mathrm{AB}}(E)/k_{\mathrm{BA}}(E)$ takes into account that the overall population of excited molecules is divided between [A*] and [B*]. This makes sense because at low pressures the reversible isomerization A$^* \rightleftharpoons$ B* leads to a partially equilibrated distribution among the excited states. Although collisions with M are required to produce A* and deactivate B*, we find only a linear dependence on [M]. This can be explained with the fact that collisions with [M] also deactivate A* and thus reduce the rate of production of B. Having obtained the rate constant for the irreversible isomerization of A to B, we could either repeat this procedure for B isomerizing to A or, alternatively, use the thermal equilibrium constant to calculate the reverse rate constant.

It should be clear at this point that all required elementary rate constants $k(E)$ for activation, deactivation, and isomerization can be obtained with either (Q)RRK or RRKM theory as discussed earlier.

We will now analyze the same isomerization reaction using the ME approach [18] to demonstrate differences and similarities. For the population densities of isomer A, $\rho^{\mathrm{A}}(E, t)$, we construct the ME

$$\begin{aligned} \frac{\partial}{\partial t}\rho^{\mathrm{A}}(E,t) = \omega \sum_{E'} P(E,E')\rho^{\mathrm{A}}(E',t) - \omega\rho^{\mathrm{A}}(E,t) \\ - k_{\mathrm{AB}}(E)\rho^{\mathrm{A}}(E,t) + k_{\mathrm{BA}}(E)\rho^{\mathrm{B}}(E,t) \end{aligned} \tag{84}$$

It contains two $\rho^{\mathrm{A}}(E, t)$ producing terms (either from different energy levels of A, term 1, or from $\rho^{\mathrm{B}}(E, t)$, term 4) and two consuming terms, in which $\rho^{\mathrm{A}}(E, t)$ is lost to other energy levels of A (term 2) or to B (term 3). For the population density of B an analogous ME exists. Both populations are coupled by the mass conservation requirement and therefore the set of coupled differential equations contains both species. We can define a new vector $\rho(E, t)$ which contains the populations of both isomers. This leads to the same eigenvalue equation as discussed earlier,

$$\frac{\partial}{\partial t}\rho(E,t) = \hat{M}\rho(E,t) \tag{85}$$

However, the matrix elements of the operator $\hat{M}$, which describes the evolution of the combined states, are different for each problem and distinguish one reaction system from the other. Provided that energy relaxation is fast compared to the reaction time or in other words that reaction takes place on a much longer time scale than energy transfer between individual levels, the solution of this eigenvalue problem will yield two chemically relevant eigenvalues which are much larger than and well separated from all other eigenvalues. The largest eigenvalue is zero reflecting that this reaction system will finally reach equilibrium. The second largest eigenvalue determines the approach to equilibrium and can be shown [19] to be equal to

$$-\lambda_2 = k_{\text{iso,A}} + k_{\text{iso,B}} \tag{86}$$

Since at equilibrium

$$K_{\text{eq}} = \frac{k_{\text{iso,A}}}{k_{\text{iso,B}}} \tag{87}$$

we obtain for the phenomenological rate constants

$$k_{\text{iso,A}} = \frac{-\lambda_2}{1 + 1/K_{\text{eq}}} \tag{88}$$

$$k_{\text{iso,B}} = \frac{-\lambda_2}{K_{\text{eq}} + 1} \tag{89}$$

The condition that the largest two eigenvalues must be well separated from all others implies that steady state is reached. Otherwise the isomerization reaction would depend on several eigenvalues describing the interaction between energy relaxation and chemical reaction. This would lead to time-dependent ''rate constants'' or non-exponential behavior.

(*ii*) *Multi-well, multi-channel systems*

Consider as an example for a multi-well, multi-channel problem the following chemically activated reaction system:

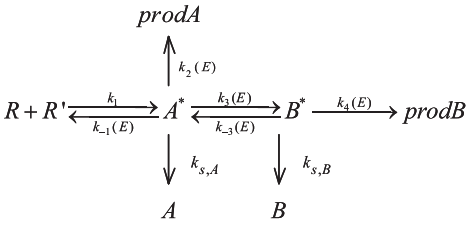

It describes the reaction of two reactants R and R′ to form the excited species A^*, which can stabilize *via* collisions with bath gas molecules M, react to products (prodA), or isomerize to B^*. Similarly, B^* can undergo

collisional stabilization, isomerize back to A^*, or form other products named prodB. If R and R′ were radicals, this scheme could represent a recombination reaction (e.g., $C_2H_5 + O_2$ if one considers O_2 as biradical, or $CH_3 + C_2H_3$), while if R′ were a molecule with multiple bonds, this scheme would represent an addition reaction (e.g., $CH_3 + C_2H_4$). R′ could also be a species with an empty orbital and then this example could describe an insertion reaction (e.g., $^1CH_2 + H_2O$).

(*a*) *The modified strong collision approach* In the following we will present the steady-state analysis of this system based on the MSC assumption. All product channels and stabilization reactions are treated as irreversible processes, and thermal dissociation of either A or B is considered as a separate process. Hence, the implicit assumption is made that the overall reaction system can be divided into two independent additive steps: (a) reactions originating directly from the reactants as shown in the scheme and (b) thermal dissociation reactions originating from stabilized intermediates.

The chemically activated reaction R + R′ yields four different products: A, B, prodA, and prodB. The goal is to obtain apparent[8] rate constants for these four channels, defined as

$$\frac{d[A]}{dt} = k_{stab,A}[R][R'] \tag{90}$$

$$\frac{d[B]}{dt} = k_{stab,B}[R][R'] \tag{91}$$

$$\frac{d[prodA]}{dt} = k_{prod,A}[R][R'] \tag{92}$$

$$\frac{d[prodB]}{dt} = k_{prod,B}[R][R'] \tag{93}$$

By applying the steady-state condition for A^* and B^* at all energy levels

$$\begin{aligned}\frac{d[A^*(E)]_{ss}}{dt} &= 0 \\ &= k_1 h(E)[R][R'] + k_{-3}(E)[B^*(E)]_{ss} \\ &\quad - \{k_{-1}(E) + k_2(E) + k_{s,A} + k_3(E)\}[A^*(E)]_{ss}\end{aligned} \tag{94}$$

$$\begin{aligned}\frac{d[B^*(E)]_{ss}}{dt} &= 0 = k_3(E)[A^*(E)]_{ss} \\ &\quad - \{k_{-3}(E) + k_4(E) + k_{s,B}\}[B^*(E)]_{ss}\end{aligned} \tag{95}$$

[8]The rate constants are called "apparent" because they refer to complex reactions. In contrast, "regular" rate constants correspond to elementary (one-step) reactions.

$$[\mathrm{B}^*(E)]_{\mathrm{ss}} = \frac{k_3(E)}{k_{-3}(E) + k_4(E) + k_{s,\mathrm{B}}}[\mathrm{A}^*(E)]_{\mathrm{ss}} \tag{96}$$

we obtain the steady-state concentrations of $[\mathrm{A}^*(E)]_{\mathrm{ss}}$ and $[\mathrm{B}^*(E)]_{\mathrm{ss}}$

$$[\mathrm{A}^*(E)]_{\mathrm{ss}} = \frac{k_1 h(E)}{k_{w1}(E) - k_{-3}(E)k_3(E)/k_{w2}(E)}[\mathrm{R}][\mathrm{R}'] \tag{97}$$

$$[\mathrm{B}^*(E)]_{\mathrm{ss}} = \frac{k_3(E)}{k_{w2}(E)}\frac{k_1 h(E)}{k_{w1}(E) - k_{-3}(E)k_3(E)/k_{w2}(E)}[\mathrm{R}][\mathrm{R}'] \tag{98}$$

with $k_{w1}(E)$ and $k_{w2}(E)$ defined as

$$k_{w1}(E) = k_{-1}(E) + k_2(E) + k_{s,\mathrm{A}} + k_3(E) \tag{99}$$

$$k_{w2}(E) = k_{-3}(E) + k_4(E) + k_{s,\mathrm{B}} \tag{100}$$

In this derivation the rate constant k_1 presents the temperature-dependent high-pressure rate constant for the addition reaction and the function $h(E)$ is used (as before) to calculate the energy distribution of the initial complex AB(E).

The apparent rate constants are given as:

$$\frac{\mathrm{d}[\mathrm{A}(E)]}{\mathrm{d}t} = k_{s,\mathrm{A}}[\mathrm{A}^*(E)]_{\mathrm{ss}} = k_{s,\mathrm{A}}\frac{k_1 h(E)}{k_{w1}(E) - k_{-3}(E)k_3(E)/k_{w2}(E)}[\mathrm{R}][\mathrm{R}'] \tag{101}$$

$$\frac{\mathrm{d}[\mathrm{prodA}(E)]}{\mathrm{d}t} = k_2(E)[\mathrm{A}^*(E)]_{\mathrm{ss}} = k_2(E)\frac{k_1 h(E)}{k_{w1}(E) - k_{-3}(E)k_3(E)/k_{w2}(E)}[\mathrm{R}][\mathrm{R}'] \tag{102}$$

$$\frac{\mathrm{d}[\mathrm{B}(E)]}{\mathrm{d}t} = k_{s,\mathrm{B}}[B^*(E)]_{\mathrm{ss}} = k_{s,\mathrm{B}}\frac{k_3(E)}{k_{w2}(E)}\frac{k_1 h(E)}{k_{w1}(E) - k_{-3}(E)k_3(E)/k_{w2}(E)}[\mathrm{R}][\mathrm{R}'] \tag{103}$$

$$\frac{\mathrm{d}[\mathrm{prodB}]}{\mathrm{d}t} = k_4(E)[\mathrm{B}^*(E)]_{\mathrm{ss}} = k_4(E)\frac{k_3(E)}{k_{w2}(E)}\frac{k_1 h(E)}{k_{w1}(E) - k_{-3}(E)k_3(E)/k_{w2}(E)}[\mathrm{R}][\mathrm{R}'] \tag{104}$$

Finally, integration (or summation in the discrete form) over all energy levels above the energy threshold for reaction (E_0) yields the total

apparent rate constants, e.g., for $k_{\mathrm{stab,A}}$:

$$k_{\mathrm{stab,A}} = k_1 \int_{E_0}^{\infty} \frac{k_{s,\mathrm{A}}}{k_{w1}(E) - k_{-3}(E)k_3(E)/k_{w2}(E)} h(E)\mathrm{d}E \qquad (105)$$

The normalized distribution function $h(E)$ is calculated similar to equation (74)

$$h(E) = \frac{k_{-1}(E)f(E)}{\int_{E_0}^{\infty} k_{-1}(E)f(E)\mathrm{d}E} \qquad (106)$$

Total apparent rate expressions for $k_{\mathrm{stab,B}}$, k_{prodA}, and k_{prodB} are obtained in an analogous way.

$$k_{\mathrm{prodA}} = k_1 \int_{E_0}^{\infty} \frac{k_2(E)}{k_{w1}(E) - k_{-3}(E)k_3(E)/k_{w2}(E)} h(E)\mathrm{d}E \qquad (107)$$

$$k_{\mathrm{stab,B}} = k_1 \int_{E_0}^{\infty} \frac{k_{s,\mathrm{B}}k_3(E)/k_{w2}(E)}{k_{w1}(E) - k_{-3}(E)k_3(E)/k_{w2}(E)} h(E)\mathrm{d}E \qquad (108)$$

$$k_{\mathrm{prodB}} = k_1 \int_{E_0}^{\infty} \frac{k_4(E)k_3(E)/k_{w2}(E)}{k_{w1}(E) - k_{-3}(E)k_3(E)/k_{w2}(E)} h(E)\mathrm{d}E \qquad (109)$$

In equations (105) and (107)–(109), the terms $k_{s,\mathrm{A}}$, $k_{s,\mathrm{B}}$, k_{w1}, and k_{w2} depend linearly on [M]. All other rates $k_i(E)$ are pressure independent. This allows us to analyze the pressure dependence of the four apparent rates. In the high-pressure limit we obtain

$$[\mathrm{M}] \to \infty \Rightarrow k_{\mathrm{stab,A}} \to k_1 \qquad (110)$$

$$[\mathrm{M}] \to \infty \Rightarrow k_{\mathrm{prodA}} \to k_1 \int_{E_0}^{\infty} \frac{k_2(E)}{k_{s,\mathrm{A}}} h(E)\mathrm{d}E \qquad (111)$$

$$[\mathrm{M}] \to \infty \Rightarrow k_{\mathrm{stabB}} \to k_1 \int_{E_0}^{\infty} \frac{k_3(E)}{k_{s,\mathrm{A}}} h(E)\mathrm{d}E \qquad (112)$$

$$[\mathrm{M}] \to \infty \Rightarrow k_{\mathrm{prodB}} \to k_1 \int_{E_0}^{\infty} \frac{k_3(E)k_4(E)}{k_{s,\mathrm{A}}k_{s,\mathrm{B}}} h(E)\mathrm{d}E \qquad (113)$$

The important point to notice is that the pressure dependence of the apparent rate constants at their high-pressure limits depends on the "distance" of the channels from the entrance channel (reactants). With "distance" we mean the number of isomerization steps needed to form the isomer, which then reacts to the products described by the apparent rate constant. With respect to our example system, all product channels originating from B are one isomerization step further away from the initial complex than products formed from A (the initial complex). Thus,

the corresponding apparent rate constant of the product channel of B exposes a different order of pressure dependence than that of the product channel of A. The same general conclusions can be drawn for the stabilization rate constants.

A look at the equations (110)–(113) clarifies this conclusion: the apparent high-pressure rate constant for stabilization of A is obviously pressure independent and the high-pressure rate constant for product formation from A^* is inversely proportional to [M] (due to $k_{s,A}$). This is reasonable because product formation competes with collisional stabilization. The high-pressure stabilization rate constant for B formation ($k_{stab,B}$) also depends inversely on [M] for the same reason and thus its dependence of [M] differs from $k_{stab,A}$ by $[M]^{-1}$. The same $[M]^{-1}$ difference is observed between k_{prodA} and k_{prodB}, since latter high-pressure rate constant shows a quadratic inverse dependence on [M].

It is also interesting to look at the low-pressure limits:

$$[M] \to 0 \Rightarrow k_{stab,A} \to k_1 \int_{E_0}^{\infty} \frac{k_{s,A}}{k_{-1}(E) + k_2(E) + k_3(E) - (k_{-3}(E)k_3(E)/(k_{-3}(E) + k_4(E))} h(E)\mathrm{d}E \tag{114}$$

$$[M] \to 0 \Rightarrow k_{prodA} \to k_1 \int_{E_0}^{\infty} \frac{k_2(E)}{k_{-1}(E) + k_2(E) + k_3(E) - (k_{-3}(E)k_3(E)/(k_{-3}(E) + k_4(E))} h(E)\mathrm{d}E \tag{115}$$

$$[M] \to 0 \Rightarrow k_{stab,B} \to k_1 \int_{E_0}^{\infty} \frac{k_{s,B}k_3(E)/(k_{-3}(E) + k_4(E))}{k_{-1}(E) + k_2(E) + k_3(E) - k_{-3}(E)k_3(E)/(k_{-3}(E) + k_4(E))} h(E)\mathrm{d}E \tag{116}$$

$$[M] \to 0 \Rightarrow k_{prodB} \to k_1 \int_{E_0}^{\infty} \frac{k_4(E)k_3(E)/(k_{-3}(E) + k_4(E))}{k_{-1}(E) + k_2(E) + k_3(E) - k_{-3}(E)k_3(E)/(k_{-3}(E) + k_4(E))} h(E)\mathrm{d}E \tag{117}$$

Within their low-pressure limits both stabilization rate constants depend linearly on [M] (incorporated in $k_{s,A}$ and $k_{s,B}$), while the rate constants for product formation are both pressure independent under these conditions.

The discussion so far dealt with apparent product formation and stabilization rates for $R + R'$ and we ignored the fact that the stabilized intermediates can thermally dissociate. We now briefly look at the latter

process. The underlying reaction system for the dissociation of the intermediate A looks very similar to the chemical activation part:

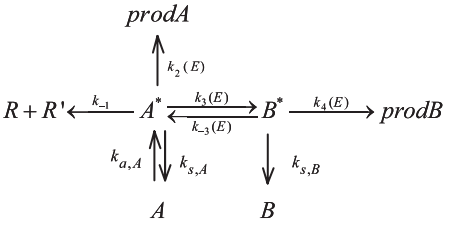

There are only two changes compared to the association part: first, collisional activation of the intermediate A is included, and second, the production of the former reactants R and R′ is now an irreversible channel. Apparent rate constants are expressed by analogy to those for the chemically activated reaction, e.g.,

$$\frac{\mathrm{d[R]}}{\mathrm{d}t} = k_{\mathrm{react,A}}[\mathrm{A}] \tag{118}$$

$$\frac{\mathrm{d[prodA]}}{\mathrm{d}t} = k_{\mathrm{prodA,A}}[\mathrm{A}] \tag{119}$$

and similar expressions can be derived if steady-state assumptions for A^* and B^* are made. The thermal dissociation of B can be treated in the same way.

If we compare the schemes for the chemically activated part ($R + R'$) and the thermal dissociation parts (unimolecular reactions of A and B), we will notice that several apparent rate constants are defined twice. For example, we obtain apparent rate constants not only for $R + R' \xrightarrow{k_{\mathrm{stab,A}}} A$, but also for $A \xrightarrow{k_{\mathrm{react,A}}} R + R'$. The principle of detailed balancing requires that both rate constants must be thermodynamically consistent and this can be used as internal check of the kinetic analysis.

A generalization of this example to multi-well and multi-channel systems is straightforward and easily implemented in kinetic software (discussed later). All integrals are replaced by finite sums and energy graining will be one important input parameter to such codes.

(*b*) *The master equation approach* There are several ways to extract apparent time-independent rate constants from the solution of the ME for a multi-channel, multi-well system. Based on the earlier discussion of the isomerization reaction $A \rightleftharpoons B$, one could use the "absorbing layer" method to make the formation of intermediates irreversible if they occupy energy levels significantly below the lowest reaction barrier. The thermal dissociations of stabilized intermediates could then be treated as

separate processes similar to the discussion above of the steady-state MSC approach.

Alternatively, apparent rate constants can be obtained by analyzing the results of the ME at short reaction times. Based on the starting conditions, the rate constants for the consumption of the reactants or for the thermal dissociation of intermediates can be found. A realization of this concept is described by Klippenstein and Miller [20,21], and we will discuss this method now for the two-well, two-channel example. To simplify the analysis, we assume that pseudo-first-order conditions apply ($[R'] \gg [R]$, where R is the minor reactant) and further lump all products together. The reaction scheme thus is:

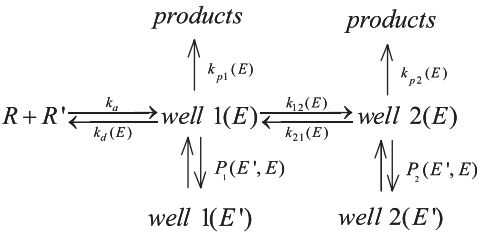

The corresponding MEs are

$$\frac{\partial n_{\mathrm{R}}}{\mathrm{d}t} = \sum_{i=1}^{M} \int_{E_{0i}}^{\infty} k_{\mathrm{d}i}(E) n_i(E) \mathrm{d}E - n_{\mathrm{R}} n_{\mathrm{R}'_0} \sum_{i}^{M} K_{\mathrm{eq},i} \int_{E_{0i}}^{\infty} k_{\mathrm{d}i}(E) f_i(E) \mathrm{d}E \tag{120}$$

for the minor reactant and

$$\begin{aligned} \frac{\partial n_i(E)}{\mathrm{d}t} = {} & \omega \int_{E_{0i}}^{\infty} P_i(E, E') n_i(E') \mathrm{d}E' - \omega n_i(E) \\ & + \sum_{j \neq i}^{M} k_{ij}(E) n_j(E) - \sum_{j \neq i}^{M} k_{ji}(E) n_i(E) \\ & + K_{\mathrm{eq},i} k_{\mathrm{d}i}(E) f_i(E) n_{\mathrm{R}} n_{\mathrm{R}'_0} - k_{\mathrm{p}i}(E) n_i(E) \end{aligned} \tag{121}$$

for the *isomer i*. Here, $n_i(E)$ is the concentration of *isomer i* at energy E, n_{R} the concentration of the minor reactant R, $n_{\mathrm{R}'_0}$ the time-independent concentration of the excess reactant R′, $k_{ij}(E)$ the microcanonical rate constants for isomerization from *well i* to *well j*, $K_{\mathrm{eq},i}$ the equilibrium constant for the system $\mathrm{R} + \mathrm{R}' \rightleftharpoons$ isomer i, $k_{\mathrm{p}i}(E)$ and $k_{\mathrm{d}i}(E)$ the energy-dependent rate constants for the product and reactant channels, respectively, and $f_i(E)$ the equilibrium energy distribution for *well i*. For our particular two-well example it follows that $M = 2$ and that all $k_{\mathrm{d}2}(E)$ rates are zero. The integrals can be replaced by sums if we divide the

continuous energy distribution into discrete energy "bins" of width δE. By doing so and by envisioning a vector $|w(t)\rangle$, which contains the population of isomer 1 in its first N_1 components, those of isomer 2 in its elements N_1+1 to N_1+N_2, and so on, and the population of n_R in its last element, we can formulate the eigenvalue problem

$$\frac{d|w(t)\rangle}{dt} = G\big|w(t)\big\rangle \tag{122}$$

Here, G is the transition matrix and is formed from the kinetic and energy transfer rates expressions in equations (120) and (121). It is a square matrix with $N = 1 + \sum_{i=1}^{M} N_i$ elements, if N_i is the number of discrete energy levels of *isomer i*. One possible solution to equation (122) is

$$|w(t)\rangle = \sum_{j=1}^{N} e^{\lambda_j t}\ \big|g_j\big\rangle\big\langle g_j\big|w(0)\big\rangle \tag{123}$$

which introduces the eigenvalues λ_j and eigenvectors $\big|g_j\big\rangle$. This definition of the eigenvectors $\big|g_j\big\rangle$ has the advantage that the population vector can now easily be calculated from the initial conditions stored in $\big|w(0)\big\rangle$. However, the solution is independent of the initial conditions and equation (123) can be used for any starting conditions. This allows one to use equation (123) to calculate apparent rate constants.

As mentioned earlier, apparent rate constants are only defined if energy relaxation processes are completed before chemical transformations become significant. This means that most of the eigenvalues are very small and clearly separated from the few chemically relevant ones. After a small lag time, all energy levels of the same isomer are relaxed (equilibrated) and contributions of the corresponding eigenvalues to the sum vanish. Assuming that the eigenvalues are sorted in decreasing order, we obtain

$$|w(t)\rangle = \sum_{j=1}^{N_{\text{chem}}} e^{\lambda_j t}\big|g_j\big\rangle\big\langle g_j\big|w(0)\big\rangle, \quad \text{for } t > t_{\text{energy relaxation}} \tag{124}$$

or, if we only consider the lth component of the population vector,

$$w_l(t) = \sum_{j=1}^{N_{\text{chem}}} e^{\lambda_j t}\ g_{jl}\big\langle g_j\big|w(0)\big\rangle \tag{125}$$

In order to obtain the desired apparent rate constants we choose the appropriate initial conditions and evaluate the formation rate at $t = 0$

(actually at a time that is short on the chemical time scale but long enough to allow complete energy relaxation). The number of independent apparent rate constants N_R needed to describe a multi-well, multi-channel system completely depends on the number of distinguishable "species", S. A system with N_W wells (intermediates), N_P *different* product channels, and one reactant channel has $S = 1 + N_W + N_p$ species. For our example with $N_P = 1$ and $N_W = 2$ we calculate $S = 4$. With this information we can calculate N_R:

$$N_R = \frac{S(S-1)}{2} - \frac{N_P(N_P-1)}{2} \tag{126}$$

which yields $N_R = 6$ for the example.[9] These six independent reactions and apparent rate constants are

$$\mathrm{R} \rightarrow \text{well 1} : \frac{\mathrm{d}[\text{well 1}]}{\mathrm{d}t} = k_{\text{stab1}}[\mathrm{R}]$$

$$\mathrm{R} \rightarrow \text{well 2} : \frac{\mathrm{d}[\text{well 2}]}{\mathrm{d}t} = k_{\text{stab2}}[\mathrm{R}]$$

$$\mathrm{R} \rightarrow \text{products} : \frac{\mathrm{d}[\text{products}]}{\mathrm{d}t} = k_{\text{prod,R}}[\mathrm{R}]$$

$$\text{well 1} \rightarrow \text{well 2} : \frac{\mathrm{d}[\text{well 2}]}{\mathrm{d}t} = k_{\text{iso12}}[\text{well 1}]$$

$$\text{well 1} \rightarrow \text{products} : \frac{\mathrm{d}[\text{products}]}{\mathrm{d}t} = k_{\text{prod,1}}[\text{well 1}]$$

$$\text{well 2} \rightarrow \text{products} : \frac{\mathrm{d}[\text{products}]}{\mathrm{d}t} = k_{\text{prod,2}}[\text{well 2}]$$

To obtain rates for the first three reactions, we select the $|w(0)\rangle$ such that all states are unpopulated with exception of the reactant R. We indicate this initial condition as $|w^{\mathrm{R}}(0)\rangle$. Similarly, $|w^1(0)\rangle$ stands for the initial condition at which all population is Boltzmann distributed in *well* 1, and so on. The total population of R is given in a single vector element $(N_1 + N_2 + 1)$, but the total population of wells 1 and 2 has to be calculated by adding the populations of all individual energy levels. For well 1 as example,

$$w^1(t) = \sum_{l=1}^{N_1} w_l(t) = \sum_{l=1}^{N_1} \sum_{j=1}^{N_{\text{chem}}} \mathrm{e}^{\lambda_j t}\, g_{jl} \langle g_j | w(0) \rangle \tag{127}$$

[9] Klippenstein *et al.* derived the simpler equation $N_R = S(S-1)/2$, because they considered chemically activated systems with just one product channel so that the second term vanishes.

Differentiation with respect to time yields

$$\frac{\mathrm{d}w^{1}(t)}{\mathrm{d}t} = \sum_{l=1}^{N_1} \frac{\mathrm{d}w_l(t)}{\mathrm{d}t} = \sum_{l=1}^{N_1} \sum_{j=1}^{N_{\mathrm{chem}}} \lambda_j \, \mathrm{e}^{\lambda_j t} \, g_{jl} \langle g_j | w^{\mathrm{R}}(0) \rangle$$
$$\equiv \mathrm{const} \cdot k_{\mathrm{stab1}} | w^{\mathrm{R}}(0) \rangle \tag{128}$$

The vector $|w^{\mathrm{R}}(0)\rangle$ in equation (128) indicates that we start with pure reactant $w^{\mathrm{R}}(0) = 1$, so that

$$k_{\mathrm{stab1}} = \frac{1}{\mathrm{const}} \sum_{l=1}^{N_1} \sum_{j=1}^{N_{\mathrm{chem}}} \lambda_j \, \mathrm{e}^{\lambda_j t} \, g_{jl} \langle g_j | w^{\mathrm{R}}(0) \rangle \tag{129}$$

Note that since all λ_j are negative but rate constants are defined to be positive, it follows that

$$\langle g_j | w^{\mathrm{R}}(0) \rangle \sum_{i=1}^{N_1} g_{jl} = -\Delta w_j^{1,\mathrm{R}} \tag{130}$$

where $\Delta w_j^{1,\mathrm{R}}$ is a positive number and it is a measure of the formation of w^1 *via* the relaxation process described by λ_j if the reaction started with pure R. The validity of equation (130) can be assured by evaluating equation (125) for $t = 0$ and ∞ and equating the difference to $\Delta w_j^{1,\mathrm{R}}$.

Equation (129) allows the calculation of the apparent rate constant k_{stab1} from the calculated chemically significant eigenvectors and eigenvalues. The constant "const" was introduced because the population vector does not contain concentrations, so that the rate constant defined in (128) is only proportional to the apparent rate constant defined above. In an analogous way, k_{stab2} and the total rate of consumption of R can be obtained. Since the product channel is not a part of the population vector, $k_{\mathrm{prod,R}}$ is calculated as the difference between the total rate and the rates to form stabilized intermediates. Apparent rate constants for the reactions of *wells* 1 and 2 are obtained with the same strategy. For a more detailed derivation and for a discussion of a second method see Klippenstein and Miller [20]. More details on the strategy to numerically solve the eigenvalue problem may be found in Bedanov *et al.* [22], who essentially use the same strategy as Klippenstein and coworkers.

To complete the discussion of techniques to obtain time-independent rate constants for complex reaction systems, the "virtual components" approach of Knyazev and Tsang [23] should be mentioned. This approach is based on earlier work by Schranz and Nordholm [24] and Smith *et al.* [9]. It envisions the total population of an isomer being partitioned into ("virtual") components from each eigenvector/eigenvalue pair of the solution of the ME. Each component will be in steady state and can be described by time-independent rate constants for

formation and consumption into different channels. The total rate constants are the sums of these rate constants for all virtual components. Knyazev *et al.* have demonstrated that this approach can be used for very complex systems in which activated complexes do not just undergo unimolecular but also bimolecular consumption reactions.

(*c*) *The stochastic approach* Stochastic simulations of complex reaction systems address the basic physical problem that chemical reactions are not continuous and that they may not be describable in a deterministic way. Instead, on a molecular level, reactions depend on randomly occurring collisions and the events can be seen as a ''random walk'' from one state to another. The most accurate method to describe complex chemical reactions in this way is to use a stochastic approach. Gillespie [25] developed algorithms that—in the limit of infinite trials—describe these systems exactly by statistical probing of random events. Two different approaches are possible: in the first case [26], a swarm of molecules is initially placed in a set of energy bins and at each time step one molecule is moved to a different bin. The vector of all populations is updated for each time step and the evolution of the distribution is followed. This approach is feasible for linear and non-linear problems. If the ME contains only linear terms, a second method [27] is beneficial. Here, a single molecule per trial is followed in time, and snapshots of its properties are taken at defined time intervals. This reduces the memory requirements, because only averaged results are stored. The final results of a stochastically solved ME are temporal distribution functions and derived information such as time profiles of average vibrational energy and time-dependent stochastic rate constants.

The Gillespie method requires two random numbers. One random number, r_1, defines the next time step, τ, *via*

$$\tau = \frac{-\ln(r_1)}{k_{\text{total}}} \tag{131}$$

where k_{total} is the sum of all first-order rate coefficients. The second random number, r_2, is used to select the direction of the transition

$$\sum_{i=1}^{j-1} k_i < r_2 \cdot k_{\text{total}} \leq \sum_{i=j}^{n} k_i \tag{132}$$

In this equation the *j*th path is selected by r_2 among a total of n different reaction paths. After each time step the rate coefficients need to be updated because either the transition leads to isomerization and different rate constants apply or the isomer is now in a different energy level and the $k(E)$ values change.

The time requirements for a stochastic analysis depend on the pressure (collision frequency), molecule parameters, unimolecular rate constants, reaction time, and the desired accuracy. Due to the central role of random numbers, the quality of the random number generator is crucial and its range of numbers as well as its randomness strongly influences the quality of the results.

A major advantage of stochastic solutions of MEs for multi-well and multi-channel systems is that they provide time-resolved distribution functions without the need to diagonalize a large matrix and interpret the eigenvalues. The distribution functions provide direct insight into the behavior of the system, especially the energy transfer part. A severe drawback is that stochastic calculations spanning a large time range require a substantial amount of CPU time. Deterministic methods are generally orders of magnitude faster than stochastic calculations.

(*d*) *Conclusions*

Chemically activated and unimolecular reactions are on a fundamental level very complicated because they are governed by energy transfer and chemical processes that can proceed on many different time scales. The most fundamental and precise results are obtained by numerically solving the time-dependent ME. Such solutions, however, have the disadvantage that they cannot easily be incorporated into kinetic models for large reaction systems. A second approach is to solve the eigenvalue problem of the ME. This leads to a huge number of eigenpairs, which again is not a feasible result if one is only interested in the chemical kinetics part. Only if one can separate the eigenvalues describing energy relaxation from those few that are chemically relevant, it is possible to extract a set of apparent rate constants that describe the chemistry of the systems accurately for all but very short reaction times. Essentially, waiting for the energy relaxation to be completed means to assume steady-state conditions. This raises the question of why one would want to solve the time-dependent ME in the first place if the solutions will anyway later be reduced to time-independent rate constants. One good reason is that it is frequently not clear under which conditions a steady-state analysis is sufficiently accurate to describe the kinetic behavior. The discussion of the thermal decomposition of ethoxy radicals later in this chapter will hopefully make this point clearer.

By applying the steady-state assumption prior to solving the ME, finding its solutions becomes a straightforward and easy task if a so-called ''absorptive boundary'' is introduced. This means that all channels except for the source are made irreversible. The entire reaction system is separated into several processes including association (in case

of a chemical activation process) and isomerization reactions of all isomers. An even more drastic simplification is to describe the energy transfer process in terms of MSCs, which further simplifies the analysis. The main justification to use this approach is that our knowledge of the energy transfer process is very limited and hence the required parameters for the more detailed models are not readily available. Computational speed, which was a limiting factor 10–20 years ago, does not restrict the use of any method except, perhaps, the stochastic approach.

3 PRACTICAL METHODS TO ANALYZE PRESSURE-DEPENDENT REACTIONS

To perform a kinetic analysis of pressure-dependent reactions is in practice a straightforward task, since many codes are available. The major problem is to obtain the required input parameters. The following sections give short descriptions of several programs that allow the calculation of pressure-dependent rate constants, followed by a discussion of methods to obtain the input data.

3.1 Software for the calculation of pressure-dependent rate constants

We provide a description of computer programs for the kinetic analysis of pressure-dependent reaction systems. This list is by no means complete and certainly subject to the choice of the authors. Nevertheless, we hope that it is useful for readers who begin to work in this field.

1. Unimol: The Unimol [28] suite of programs from Gilbert and Smith [2] was provided to complement their textbook on unimolecular and recombination reactions. It consists of four program codes: (1) the program RRKM calculates $k(E)$ and generates the input file for ME analysis, (2) the ME solver MASTER, (3) the program named GEOM calculates moments of inertia, and (4) the program BRW estimates the average energy transferred in collisions based on the ''biased random walk'' model [29]. This code can be used to calculate unimolecular dissociation or recombination rate constants of one-well systems. The RRKM and ME codes can optionally calculate/utilize $k(E, J)$ data and thus are suitable for reactions with loose transition states.
2. ChemRate: ChemRate is software running under Windows developed by Mokrushin *et al.* [30] and allows the user to create molecule and kinetic databases, calculate elementary high-pressure reaction rate constants with TST theory, and perform a

RRKM-based ME analysis of pressure-dependent reaction systems consisting of multiple wells and channels. The ME is either solved time dependent or by imposing the steady-state approximation. A general description and application of this code is published [31]. The short manual warns any potential user that this software is only intended for experienced kineticists. At the time of writing, the homepage for ChemRate was accessible at http://www.nist.gov/kinetics/chemrate/chemrate.html

3. MultiWell: Written and distributed by Barker [32], MultiWell is a program package created to analyze pressure-dependent unimolecular reaction systems based on Gillespie's stochastic method. It contains four programs: "Thermo" calculates thermodynamic properties, "MomInert" calculates moments of inertia, "DenSum" calculates densities and sums of states as a function of energy, and "MultiWell" calculates—among other things—species and energy distribution profiles as function of time. The package and its application to the isomerization of 2-methylhexyl radicals have been described in the literature [33,34].
4. CARRA: CARRA, for *chemically activated reaction rate analysis*, calculates apparent rate constants for multi-well, multi-channel systems based on QRRK theory. It uses either the MSC (CARRA_MSC) or the steady-state ME (CARRA_ME) approach. The original concept was based on a single frequency representation of the active modes of each isomer [35,36]. Later, the code was updated to handle three representative frequencies. Descriptions of these earlier versions as well as applications can be found in Refs. [7,37]. CARRA is a modified version of these older codes, which is currently still under development [38].
5. Other program packages: There are many other well-known packages known in literature, e.g., Klippenstein *et al.*'s "VARIFLEX" [39], "TheRate" by Truong *et al.*, or the program suite "CHARMMRATE" [40] by Truhlar *et al.* In addition, reaction engineering platforms such as the "OpenChem Workbench" [41] project or the "CSEO" [42] project by Truong *et al.* contain RRKM and other kinetic applications.

3.2 Getting input data for the calculations

Input data are needed to calculate $k(E)$ values, density of states functions, collision frequencies, and so on. The specific type of required parameters depends on the selected method. If the goal is to do a "back

of the envelope'' calculation with emphasis of getting a quick answer rather than the most accurate prediction, a good choice would be a QRRK-based program since it requires only representative frequencies for the isomers, high-pressure rate constants for the individual reaction steps, and collision parameters. All this information can easily be obtained from estimation methods such as group additivity or rate estimation rules. The other extreme would be to perform a very detailed kinetic analysis with the most accurate and specific input data possible. This calls for a RRKM ME analysis and requires detailed molecular information for isomers as well as for the transition states. Although detailed information is nowadays often available from *ab initio* quantum mechanical calculations, such an approach is more time consuming and not feasible for every reaction in large mechanisms. Whatever the choice of analysis method will be, one should keep in mind that the results from both, QRRK and RRKM theories strongly depend on the energy transfer parameters employed, and a significant part of the remaining uncertainty from either analysis can be attributed to an inadequate description of the energy exchange processes during collisions.

A general strategy to obtain the required input parameters could involve the following sequence:

1. Maybe the best resource for input parameters are original publications, because these provide not just the data *per se* but also the context in which they were obtained and often an estimate of their uncertainties. Obvious sources for input data are, for example, kinetic studies (high-pressure rate expressions) and spectroscopic measurements (molecular properties)
2. If original papers are not available, consider the use of reviews, compilations, reference books, etc., which summarize and organize results from original publications. Thermodynamic data may, for example, be obtained from JANAF tables [43] or the NIST webbook [44]; high-pressure rate constants can be retrieved from recommendations (e.g., the UIPAC sponsored evaluation of rate expressions for atmospheric chemistry [45]) or web-based databases such as the NIST kinetic database [46], and a good source for transport properties is, for example, the reference book by Poling *et al.* [47]. Chemkin [48], a well-known modeling software, provides thermodynamic and transport databases for a set of frequently used molecules.
3. After all literature sources for input data are exhausted, consider estimating the missing parameters. This can be done intuitively by relating the unknown parameters to related data, or one can use

estimation methods and rules. We will discuss this approach in more detail in the following section.

4. Finally, use theoretical methods to calculate missing parameters. The most powerful tool in this regard are *ab initio* calculations, which provide all basic molecular parameters needed to calculate thermodynamic properties (*via* statistical mechanics methods) and kinetic data (*via* transition state theory). Some aspects of this approach will be outlined further below.

(*i*) *Input data based on estimation methods*
(*a*) *Thermodynamic data from group additivity* The basic assumption of group additivity is that certain properties, Φ, of a molecule are given as a sum of contributions of all the groups, ϕ_i, that form this molecule

$$\Phi = \sum_{i=1}^{n} \phi_i \tag{133}$$

If the contributions of all groups (defined as polyvalent atoms with its ligands) are known, the property for the entire molecule can be calculated. Ethanol, C_2H_6O, might serve as a simple example to illustrate this concept. Written as CH_3–CH_2–OH, we notice three polyvalent atoms (two C and one O) and hence three groups. The first group can be symbolized as {C/C/H3}, with the left part "{C/" presenting the central polyvalent atom and the following entries "C/" and "H3}" indicating the type of atoms, to which the central carbon is connected. Similarly, {C/C/H2/O} and {O/C/H} are representations of the other two groups. In order to get an estimate of thermodynamic properties of ethanol, we need to find the contributions of these three individual groups from tables as they can be found, e.g., in the textbook by Benson [49], who developed a group additivity scheme that is widely used in kinetics to estimate $\Delta_f H^{298}$, S^{298}, and $C_p(T)$ data. For example, we find in a database for the heat of formation the following contributions (in kcal/mol):

{C/C/H3}: −10.20
{C/C/H2/O}: −8.10
{O/C/H}: −37.90

This leads to an estimated heat of formation value for ethanol of −56.20 kcal/mol, which is essentially identical with the value found in the NIST webbook [44]. The estimations of entropies and heat capacities

are done similarly, although additional symmetry corrections make the estimation of entropies slightly more challenging.

Initially the group additivity concept was only used to estimate properties of stable molecules. Later the database was expanded to allow estimates for radicals [50,51] and transition states [52–54] as well. A widely distributed program called Therm [50] makes such estimates an easy task on a PC.

(*b*) *Representative frequencies from heat capacities* Usually molecular geometry and frequency information of a given species is used to calculate thermodynamic properties. However, it is possible to reverse this process. Estimated heat capacities as function of the temperature can serve as input to calculate representative frequencies [8] of that molecule. The basic theory for this process is as follows: from statistical mechanics we know how much one oscillator with the frequency ν (or wavenumber $\tilde{\nu}$) contributes to the heat capacity:

$$c_v^{\text{vib}} = R\left(\frac{\theta}{T}\right)^2 \exp\left(\frac{\theta}{T}\right)\left[\exp\left(\frac{\theta}{T}\right) - 1\right]^{-2}, \quad \text{with } \theta = \frac{h\nu}{k} = \frac{hc\tilde{\nu}}{k} \tag{134}$$

Hence, if a species has s "effective" oscillators and if we wish to represent the internal modes with, let us say, three representative frequencies, the total heat capacity is given by

$$\begin{aligned} c_v(T) = {} & c_v^{\text{trans}}(T) + c_v^{\text{rot}}(T) + \alpha_1 c_{v,1}^{\text{vib}}(T) \\ & + \alpha_2 c_{v,2}^{\text{vib}}(T) + \{s - \alpha_1 - \alpha_2\} c_{v,3}^{\text{vib}}(T) \end{aligned} \tag{135}$$

The contributions from translation ($3/2R$) and external rotation ($3/2R$ for non-linear and $1R$ for linear species) are known, which leaves five adjustable parameters ($\alpha_1, \alpha_2, \tilde{\nu}_1, \tilde{\nu}_2,$ and $\tilde{\nu}_3$) that are determined *via* non-linear regression. Note that in this formulation α_1 and α_2 are not restricted to integer values. The same is true for n, which can take half-integer values, because each vibrational mode that represents an internal (hindered) rotation is counted as 1/2 oscillator. The representative frequencies together with their degeneracies are needed as input parameters for multi-frequency QRRK codes.

(*c*) *Estimation methods for high-pressure rate constants* Many research groups have provided estimation rules, which allow a quick calculation of an approximate high-pressure rate constant for a certain reaction family or class. A recent review of some methods can be found in

Ref. [55], and a widely used reference book for rate constant estimations was authored by Benson [49].

The basic idea behind estimation rules is to generalize experimentally obtained or calculated rate constants. This can be done by simply averaging a set of rate constants, or by developing systematic correlations to kinetic or thermodynamic properties.

Let us first look at C–H bond fission reactions as an example problem. To obtain an estimate of the rate constant we would use the following strategy: (1) Get a good estimate for the reverse reaction, the recombination of alkyl radicals with H atoms. (2) Calculate K_{eq} for the reactants and products. (3) Use the microscopic reversibility condition to calculate the C–H fission rate constant. Steps (2) and (3) are straightforward, if all thermodynamic data and the recombination rate constant are available. Therefore, only step (1) needs further discussion. We chose the recombination of H atoms with alkyl radicals as starting point, because we expect that the rate constant is independent of the alkyl radical. This is verified in Table 1, which contains a compilation of data for several H + alkyl recombination reactions found in the NIST kinetics database [46]. When several entries for a reaction are available, we selected those that appeared most reliable and averaged them. Except for the H + *n*-C_4H_9 reaction, nearly all rate constants are within a factor of 2 and even the rate constant for H + *n*-C_4H_9 is within a factor of 10 to most of the data.

Therefore, the average of all entries can serve as an estimate for the entire family of reactions. This average rate constant hardly changes with temperature, so that we can use a value of $\sim$1.3E14 $cm^3/(mol\,sec)$ for all temperatures. The rate constant for the reverse reaction (the C–H fission) is not constant but depends *via* K_{eq} on the C–H bond strength.

Dean [35] provided a detailed discussion of this approach not only for bond fission, but also for β-scission reactions. Updated results of the

TABLE 1
Averaged high-pressure rate constants (in $cm^3/(mol\,sec)$) for H + *n*-alkyl recombination reactions obtained from selected entries in the NIST Kinetics Database [46]

Reaction	300 K	500 K	1000 K	1500 K	2000 K	2500 K
$H + CH_3 \rightarrow CH_4$	1.99E14	1.89E14	1.80E14	1.66E14	1.66E14	1.39E14
$H + C_2H_3 \rightarrow C_2H_4$	1.21E14		3.27E14			
$H + C_2H_5 \rightarrow C_2H_6$	1.0E14					
$H + C_3H_5 \rightarrow$ products	1.85E14	1.99E14	1.99E14	1.99E14	1.99E14	1.99E14
$H + C_3H_7 \rightarrow C_3H_8$	1.5E14					
$H + C_4H_9 \rightarrow$ products	3.01E13	3.01E13	3.01E13	3.01E13	3.01E13	3.01E13
Average	1.31E14	1.39E14	1.84E14	1.32E14	1.32E14	1.23E14

TABLE 2
Estimation rules for the addition of H or CH_3 to olefins on a per site basis

Reaction class	A (cm^3/(mol sec))	N	E (kcal/mol)
Recombination reactions			
$H + R \rightarrow R\text{-}H$	1.60×10^{14}	0.0	0.10
$CH_3 + R \rightarrow R\text{-}CH_3$	1.40×10^{13}	0.0	−0.47
$R' + R \rightarrow R\text{–}R'$	1.32×10^{13}	0.0	−0.10
Addition reactions			
$H + C_2H_4 \rightarrow C_2H_5$	1.69×10^{08}	1.61	1.0
H + olefin → primary R	1.26×10^{12}	0.29	2.8
H + olefin → secondary R	1.29×10^{15}	−0.55	3.0
H + olefin → tertiary R	1.29×10^{15}	−0.55	1.9
H + aromatics →	8.00×10^{12}	0.0	4.0
$CH_3 + C_2H_4 \rightarrow n\text{-}C_3H_7$	1.63×10^{11}	0.0	7.7
CH_3 + olefin → primary R	8.0×10^{10}	0.0	7.7
CH_3 + olefin → secondary R	8.0×10^{10}	0.0	7.0
CH_3 + olefin → tertiary R	8.0×10^{10}	0.0	6.0
CH_3 + aromatics →	8.0×10^{10}	0.0	7.5

Also provided are approximate data H or R + R recombination rate expressions.

evaluation of recombination and addition reactions for hydrocarbons yielded the estimation rules given in Table 2. We notice that—as expected—barriers for recombination reactions are very small or even negative, while addition reactions have a small positive barrier. For the recombination reactions we see that H atoms recombine about one order of magnitude faster than alkyl radicals. This can be explained with the size difference, which gives H atoms more flexibility while approaching the radical site or with the loss of active degrees of freedom[10] while the new bond is formed.

The addition reactions shown in Table 2 have small barriers that correlate roughly with the stability of the produced alkyl radical. Such correlations are more obvious for other types of reactions, e.g., abstraction reactions. They are known as linear free-energy relationships (LFER), and the most prominent correlation is the Evans–Polanyi relationship

$$\ln(k) = \ln(k_{\text{ref}}) + m(\Delta H_{\text{rxn}} - \Delta H_{\text{rxn,ref}}) \tag{136}$$

[10]The three translational degrees of freedom of a H atom are converted to three vibrations in the alkane. For methyl radicals, three translations and three rotations are lost and five vibrational and one internal rotation modes are formed. If one assumes that the vibrational modes contribute less to the total entropy than translations and rotations, the loss of entropy is larger for CH_3 than for H and the A-factor will be smaller.

Given $\ln(k) = \ln(A) - E/RT$, and assuming that the A-factor of a reaction family is constant, then this equation translates to

$$E_A = E_{A,\text{ref}} + \alpha\,\Delta H \tag{137}$$

The significance of this equation is that it provides an estimation method for the activation energy of a reaction based on a reference system and the difference in reaction enthalpies between both. α is positive and normally in the range 0–1 (often ~0.5). Its value can be determined for a family of reactions if kinetic data for two reactions of different exothermicity are available. From equation (137) it is clear that the barrier for a reaction within a reaction family increases with decreasing exothermicity.

Isomerization reactions may serve as an example to show how rate constants can be estimated based on analogy or correlations. Let us assume we are interested in a rough estimate for the 1,3-H shift reaction

$$\bullet CH_2CH_2CH_2CH_3 \rightleftharpoons CH_3CH_2CH\bullet CH_3$$

We notice that one H atom is transferred from a secondary C atom (a CH_2 group) to a primary radical site.[11] We also notice that the transition structure for this migration reaction is cyclic and that the ring contains four atoms (the three C atoms and the migrating H atom). Assuming that we have some information about bimolecular H abstraction reactions, then a possible strategy to approximate this unknown rate expression could involve the following steps: (1) identify a bimolecular reaction that is similar to our 1,3-H shift reaction and use the activation energy of this reaction as starting point; (2) estimate the pre-exponential factor (A-factor) based on a simple analysis of the reaction mechanism; (3) correct the A-factor and activation energy for ring strain effects.

Step 1: A good choice of a bimolecular reaction resembling our target reaction is the H abstraction from a CH_2 moiety by ethyl radicals.

$$C_2H_5\bullet + \text{R-CH}_2\text{-R}' \rightleftharpoons C_2H_6 + \text{R-CH}\bullet\text{-R}'$$

An evaluation of abstraction reactions by Dean (unpublished) leads to the following Arrhenius parameters:

$$K(T) = AT^n \exp\left(-\frac{E}{RT}\right) \tag{138}$$

[11]The terms primary, secondary, and tertiary distinguish in this context C atom with one, two, or three C–C bonds. The type of a C atom determines the strength of the C–H bonds it forms.

where

$$A = 6.6E3\ \mathrm{cm}^3/(\mathrm{mol\ sec});\quad n = 2.51;\quad E = 9.9\ \mathrm{kcal/mol}$$

Since we wish to express the rate constant for the example reaction in simple Arrhenius form

$$k(T) = A \exp\left(-\frac{E_\mathrm{A}}{RT}\right) \tag{139}$$

we need to transform the parameters of the modified Arrhenius expression to the corresponding E_A value. By applying the definition for "activation energy," E_A

$$E_\mathrm{A} = RT^2 \frac{\mathrm{d}\ln k}{\mathrm{d}T} \tag{140}$$

to equation (138), we obtain the activation energy for a given temperature,

$$E_\mathrm{A} = E + nRT \tag{141}$$

Assuming we were interested in a value for the rate constant at $\sim$1000 K we calculate

$$E_\mathrm{a} = 9.9\ \mathrm{kcal/mol} + 2.51 \times 0.001987\ \mathrm{kcal/(mol\ K)} \times 1000\ \mathrm{K} \approx 14.9\ \mathrm{kcal/mol}$$

Before concluding with step 1, we should reflect on the rather high value for n in the rate expression of the reference reaction ($n = 2.51$). This indicates strong non-Arrhenius behavior. Our attempt to describe the intramolecular H migration in form of a simple Arrhenius rate equation is therefore only valid within the small temperature range around—in this example—1000 K.

Step 2: The pre-exponential factor of the reference reaction used in step 1 describes a bimolecular reaction and is therefore of no use. To get an initial estimate for the pre-exponential factor, we compare the transition state rate expression

$$k_\mathrm{TST}(T) = \frac{kT}{h} \mathrm{e}^{\Delta S^\#/R}\, \mathrm{e}^{-\Delta H^\#/RT} \tag{142}$$

with the Arrhenius expression. Using again the definition for activation energy we find

$$E_\mathrm{A} = RT^2 \frac{\mathrm{d}k_\mathrm{TST}(T)}{\mathrm{d}T} = RT + \Delta H^\# \tag{143}$$

and we obtain

$$k(T) = A \exp\left(-\frac{RT + \Delta H^{\#}}{RT}\right) = eA \exp\left(-\frac{\Delta H^{\#}}{RT}\right) \tag{144}$$

By comparing equations (142) and (144) we finally get

$$A = \frac{ekT}{h} e^{\Delta S^{\#}/R} \tag{145}$$

During the migration process of the H atom, one C–H bond is breaking while the new bond starts to build. The partially broken (weakened) C–H bond leads to an increase of the entropy of the transition state relative to the reactant, but this increase is counterbalanced by the new partially formed C–H bond, which reduces the entropy. It is therefore reasonable to assume as a first approximation that all things considering the entropy of the transition state will be very similar to that of the reactant. Setting $\Delta S^{\#} = 0$ and focusing again on a temperature of $T = 1000\,\mathrm{K}$ we calculate $A \sim 6\mathrm{E}13\,\mathrm{sec}^{-1}$.

Step 3: Finally we apply corrections to the A-factor and activation energy that reflect the cyclic nature of the transition state. The formation of a cyclic transition state has two consequences: (1) In non-cyclic molecules, groups that are connected *via* C–C single bonds can rotate against each other. These internal rotations contribute significantly to the total entropy of a molecule. In cyclic structures, all internal rotations of C–C bonds that are part of the ring system are "frozen," which means that they do not longer behave as rotations but are converted to low-frequency vibrations. In our example, two initially "free" rotors are transformed to wagging modes (vibrations). Since these vibrations contribute less to the entropy than the rotations, it follows that a cyclic transition state will be lower in entropy than a corresponding non-cyclic transition state. The amount of entropy change depends obviously on the ring size or the number of frozen rotors. Table 3 lists approximate correction factors for transition states with up to four frozen rotors. For our example, we find that $\Delta S^{\#}$ is expected to be lower by $\sim 6.0\,\mathrm{cal/(mol\,K)}$, which translates to a correction factor of $\exp(-6.0/R)$. (2) A cyclic transition state also experiences ring strain, which is caused by less than optimal bond angles and distances. Table 3 provides approximate ring strain corrections for different ring sizes. A four-member ring is

TABLE 3
Correction values for ring strain and entropy loss in cyclic hydrocarbon transition [56]

Ring size	Ring strain (kcal/mol)	Number of frozen rotors	$\Delta S^{\neq}$ (cal/(mol K))	Reduction factor for A
3 (1,2-H shift)	25	1	–3.6	6
4 (1,3-H shift)	25	2	–6.0	20
5 (1,4-H shift)	8.0	3	–12.7	600
6 (1,5-H shift)	1.0	4	–17.3	6000

~25 kcal/mol higher in energy than the corresponding non-cyclic transition state and this energy adds to the activation energy from step 1.

Putting all corrections together, we obtain our final rate constant estimate (per H atom)

$$A = 6\text{E}13\ \text{sec}^{-1} \times 0.05 = 3\text{E}12\ \text{sec}^{-1}$$
$$E_a = 14.9 + 25.0\ \text{kcal/mol} = 39.9\ \text{kcal/mol}$$

The rate estimation method discussed above might appear very rough. But even though such rate constants estimates are sometimes only accurate to one order of magnitude, they are nevertheless useful for at least two reasons: (a) they allow modelers to incorporate reactions with unknown rate constants into mechanism. By including these reactions in modeling studies and performing a rate and/or sensitivity analysis, it is possible to identify important reactions and study these later in more detail. (b) Estimation rules are also very helpful in providing a quick validation of calculated or experimentally observed rate constants and in providing a selection criterion for scattered or conflicting data.

In recent years rate estimation techniques gained substantial interest because they are needed for automated mechanism generation algorithms and new estimation approaches and improved "rate rules" are still currently developed. The example discussed above is only intended to provide a first glance of how such estimations can be made with rather little knowledge of the reaction details.

(*d*) *k(E) from high-pressure rate constants* High-pressure rate constants are not only useful for QRRK calculations, but can also be used in RRKM programs. In the latter case, the $k(T)$ rate constants need to be converted to microcanonical $k(E)$ rate constants. This can be achieved with the inverse Laplace transformation (ILT) technique. The temperature-dependent high-pressure rate constant is given by integrating the

$k(E)$ contributions for all E weighted by the Boltzmann distribution:

$$k(T) = \int_{E_0}^{\infty} k(E) \frac{\rho(E)}{Q_{\text{vib,rot}}(T)} \mathrm{e}^{-E/RT} \, \mathrm{d}E \tag{146}$$

This equation is known as a Laplace transformation of $k(E)$ to $k(T)$. The inverse transformation (ILT) produces $k(E)$ if $k(T)$ is given. Forst [57] has shown that if $k(T)$ can be expressed in simple Arrhenius form $k(T) = A_\infty \exp(-E_\infty/RT)$, then the ILT yields

$$k(E) = A_\infty \frac{\rho_{\text{vib,rot}}(E - E_\infty)}{\rho_{\text{vib,rot}}(E)} \tag{147}$$

In other words, knowledge of the A-factor of a high-pressure rate constant and the density of states function allows us to calculate $k(E)$ without the need to know any further detail of the transition state.

(*e*) *$\rho(E)$ based on estimated representative frequencies* If only estimated thermo data and representative frequencies are available for stable species (isomers) that are involved in pressure-dependent reactions, the corresponding density of states function can also only be calculated with limited accuracy. This is done with a modified version of the Kassel expression, in which the factorials are replaced by the gamma function to allow for continuity. The single frequency formula for $\rho(E)$ is

$$\rho(E) = N(n,s) \frac{1}{hv} = \frac{\Gamma(n+s)}{\Gamma(n+1)\Gamma(s)} \frac{1}{hv} \tag{148}$$

Here, $n = E/(hv)$ is the number of quanta and s the number of oscillators. In Ref. [7] a detailed discussion of the function $N(n, s)$ for a multifrequency case can be found.

(*f*) *Estimation of collision parameters* Lennard–Jones parameters for stable species can be estimated if their critical properties (T_c, V_c, P_c) and dipole moment are known (see, for example, the method by Brokaw [58], as described in Ref. [47]). For polyaromatic hydrocarbons, Wang and Frenklach [59] proposed a group contribution method for the prediction of Lennard–Jones parameters. All these methods are restricted to stable molecules. To the best of our knowledge more general estimation methods, which are also applicable for radicals, are not available. The same is true for energy transfer parameters ($-\langle E_{\text{all}} \rangle$ or $\langle E_{\text{down}} \rangle$) Therefore, the common procedure is to identify a molecule of similar size or composition for which these data are available and use the same values for the species of interest.

(*ii*) *Input data based on ab initio results*

A basic description of electronic structure calculations is outside of the scope of this chapter. Instead we will restrict ourselves to a discussion of how to use such calculations to get some of the required parameters needed for pressure-dependent rate analysis.

(*a*) *Thermodynamic properties* Basic results from *ab initio* calculations include the electronic energies (E_e or with zero-point energy E_0), the optimized geometric properties of a species, the principal rotational constants, and the frequencies of molecular vibrations approximated as harmonic oscillators. Statistical mechanics [60] allow us to calculate thermal contributions to the enthalpy, the entropy, and heat capacities directly from this information within the HO–RR approximation. However, if low-frequency modes corresponding to internal rotations are present, then the entropy and $C_p(T)$ values obtained with the HO–RR method are not accurate. Instead these modes must be treated as hindered rotors. Several methods for this treatment are reported in the literature [52,61–64]. We will not discuss this issue any further except to mention that recent versions of the *ab initio* package Gaussian [65] provide an option for an automatic hindered rotor treatment (see Ref. [64] for details).

Although only relative energies are needed for an analysis of a pressure-dependent reaction system, the final goal of modelers is to incorporate these results into a reaction mechanism and perform simulations. In this case thermodynamic data of all species are needed, so we need to convert the absolute electronic energies to heats of formation. Two conversion methods are widely used: (1) atomization energies [66–68] and (2) isodesmic reactions [68,69]. The atomization method is based on the decomposition of a species into its atoms. For a species $C_xH_yO_z$ this reaction is

$$C_xH_yO_z^{(g)} \rightarrow xC^{(g)} + yH^{(g)} + zO^{(g)}$$

The reaction energy for this process can be calculated *via ab initio* calculations. With the use of literature values for the enthalpies of all involved atoms we are able to calculate the enthalpy of the species $C_xH_yO_z$ *via*

$$\begin{aligned}\Delta H^{0K}(C_xH_yO_z) = {} & E_0(C_xH_yO_z) - xE_0(C) - yE_0(H) \\ & - zE_0(O) + x\,\Delta_f H^{0K}(C) \\ & + y\,\Delta_f H^{0K}(H) + z\,\Delta_f H^{0K}(O) \end{aligned} \quad (149)$$

If spin–orbit coupling is not incorporated in the *ab initio* method, an additional SOC correction term should be added. To convert $\Delta H^{0\,K}(C_xH_yO_z)$ values to the heats of formation at 298.15 K, thermal

enthalpy corrections for the elements in standard state and the species of interest are applied:

$$\begin{aligned}\Delta_f H^{298\ K}(C_xH_yO_z) = \Delta H^{0\ K}(C_xH_yO_z) + \Delta\Delta H^{298\ K}(C_xH_yO_z) \\ - x\Delta\Delta H^{298\ K}(C_{(s)}) - y\Delta\Delta H^{298\ K}(H_2) \\ - z\Delta\Delta H^{298\ K}(O_2)\end{aligned} \quad (150)$$

The $\Delta\Delta H^{298}(i)$ values in this equation are given on per atom basis.

Isodesmic reactions such as

$$CH_4 + C_2H_5OH \rightarrow CH_3OH + C_2H_6 \quad \Delta_R H^{298}$$

have the property that the reactants and products have the same number of bonds of all bond types. For example, we have nine C–H bonds, one C–O bond, one O–H bond, and one C–C bond on both the left- and right-hand sides. If the heats of formation of all but one species in the reaction are known, the unknown value can be calculated *via*

$$\begin{aligned}\Delta_f H^{298}(CH_3OH) = \Delta_R H^{298} - \Delta_f H^{298}(C_2H_6) + \Delta_f H^{298}(CH_4) \\ + \Delta_f H^{298}(C_2H_5OH)\end{aligned} \quad (151)$$

The heat of reaction is calculated from *ab initio* results,

$$\begin{aligned}\Delta_R H^{298} = E_0(CH_3OH) + E_0(C_2H_6) - E_0(CH_4) - E_0(C_2H_5OH) \\ + \Delta\Delta H^{298}(CH_3OH) + \Delta\Delta H^{298}(C_2H_6) \\ - \Delta\Delta H^{298}(CH_4) - \Delta\Delta H^{298}(C_2H_5OH)\end{aligned} \quad (152)$$

In this equation $E_0(i)$ is zero-point corrected energy for species i and $\Delta\Delta H^{298}(i)$ the change of enthalpy for species i when the temperature is raised from 0 K to 298 K.

Both methods have advantages and disadvantages. The atomization method is well defined and can directly be used for all species including transition states. The strength of using isodesmic reactions is that they—unlike the atomization method—implicitly correct for systematic bond errors which are inherent in *ab initio* calculations. Some drawbacks of isodesmic reactions are that they are not uniquely defined and that they might contain a large number of species, which reduces the accuracy due to error propagation. By introducing bond additivity (BAC) [70,71] or atom-based [72] correction terms to the atomization method, systematic errors of atomization energies can be reduced and their accuracy significantly improved.

(*b*) *High-pressure rate constants* Given that the molecular and thermodynamic properties of all involved species (including the transition state)

are known it is straightforward to calculate the high-pressure rate constant of a reaction:

$$k_{\mathrm{TST}}(T) = \kappa(T)\frac{kT}{h}\frac{Q_{\#}}{\prod_i Q_i}\mathrm{e}^{-E_0/kT} \tag{153}$$

$$k_{\mathrm{TST}}(T) = \kappa(T)\frac{kT}{h}V_{\mathrm{mol}}^{\Delta n-1}\,\mathrm{e}^{-\Delta G^{\#}/RT} \tag{154}$$

Here, $\prod_i Q_i$ is the product of partition functions for all reactants involved, V_{mol} the molar volume, and Δn the molecularity of the reaction. All other symbols have been introduced earlier. The expressions (153) and (154) are equivalent. The appropriate equations to calculate, e.g., the partition function Q from basic molecular properties can be found in standard textbooks of statistical thermodynamics [60]; however, this information is often provided as part of the results of *ab initio* calculations. The program packages ChemRate, Unimol, and MultiWell do or can perform TST rate calculations, but sometimes external software with special features, e.g., to deal with hindered rotor modes, yield more accurate results. Equations (153) and (154) contain the function $\kappa(T)$, which corrects for contributions from quantum mechanical tunneling. The simplest correction function

$$\kappa(T) = 1 + \frac{1}{24}\left(1.44\frac{\nu_{\mathrm{imaginary}}}{T}\right)^2 \tag{155}$$

is based on the work of Wigner [73], but more sophisticated corrections are also known [74–76].

High-pressure rate constants for reactions with no pronounced barrier such as recombination reactions or bond fissions are more difficult to calculate theoretically. Part of the problem is due to the fact that the corresponding transition state or better transition state region is located at large bond distances. Most commonly used *ab initio* methods are optimized for regular (short) bonds and will lose accuracy when applied to long distance interactions. Related is the difficulty to define the exact transition state location. In tight transitions states all but the reacting mode remain well defined. Loose transition states on the other hand contain several weakened internal modes, which are difficult to describe accurately. In addition, the conservation of angular momentum becomes significant and the rate constant thus must be treated as $k(E, J)$. In short, reliable rate constants for reactions without a barrier still present a challenging task though the basic theory, variational transition state theory, is well established. Truhlar and co-workers [76–78] investigated

in many studies the use of combinations of *ab initio* methods and interpolation techniques to obtain a suitable potential energy surface (PES). The PES is then used as basis for variationally localizing the transition state. Other methods, going back to a simple model, were proposed by Gorin and later extended by Benson [49] and others [79]. In this model the transition state is assumed to be closely related to the final products. This allows the use of frequencies of the completely separated products for the TS. The remaining five (for the case of two non-linear fragments) missing frequencies or modes are estimated based on geometric constrains. One of these five modes can be approximated as an internal rotation around the breaking bond and the other four might be approximated as two-dimensional restricted rotors.

Recently, Harding *et al.* [80] and Klippenstein *et al.* [81] published calculations for the barrierless association of H atoms to alkyl radicals and for the combination of two alkyl radicals. Studies like these show that such calculations are possible but that they required significant efforts if high accuracy is required.

Programs such as Variflex [39], CHARMMRATE [40], or ChemRate [30] have the capability to calculate rate constants for reactions with no barrier, though both contain adjustable parameters and appear to work best if the rate constants can be anchored to experimental data.

(*c*) *The density of states function* $\rho(E)$ A key function required in any analysis of pressure-dependent reactions is the density of states $\rho(E)$. Related important functions are the sum of states $W(E)$ and the number of states $N(E)$. The Beyer–Swinehart (BS) algorithm allows the calculation of these functions by ''directly counting'' all states. The results are therefore exact within the framework of the given theory that determines the states. A second formalism to calculate the density of states function was developed by Whitten and Rabinovitch. This analytic method was widely used prior to the BS algorithm and it is still useful for theoretical derivations. For example, Troe's formula to calculate the collision efficiency factor for the MSC approach is based on the Whitten–Rabinovitch density of states function. We will present both methods in the following sections.

The Whitten–Rabinovitch formula [15] for the vibrational density of states function is

$$\rho_{\text{vib}}(E) = \frac{(E_0 + aE_z)^{S-1}}{(s-1)!\prod_{i=1}^{S} h\nu_i} \tag{156}$$

where E_z is the zero-point energy and a is given as

$$\begin{aligned} a &= 1 - \beta_v w \\ \log(w) &= -1.0506\left(\frac{E}{E_z}\right)^{0.25}, \quad \text{for } E > E_z \\ w &= \left[5.00\frac{E}{E_z} + 2.73\left(\frac{E}{E_z}\right) + 3.51\right]^{-1}, \quad \text{for } E < E_z \\ \beta_v &= \frac{S-1}{S}\frac{\langle v^2\rangle}{\langle v\rangle^2} \end{aligned} \tag{157}$$

This method is still used in the CARRA codes and it was until very recently an option in MultiWell.

The BS algorithm [82] was published in 1973 and in the same year extended by Stein and Rabinovitch [83]. The latter algorithm is more flexible (e.g., in addition to harmonic oscillators it can be applied to anharmonic oscillators and hindered rotors as well) and more accurate (rounding errors in the energy discretization step are reduced), but it requires one additional array to store intermediate results. The algorithm may be described as follows:

1. Set the energy range (0–$E_{\max}$) and the step size (ΔE) based on the problem requirements and the lowest vibrational mode. Set the integer value M such that $M\,\Delta E = E_{\max}$.
2. Declare two arrays T and TA of size $M+1$. Indexing is from 0 to M. The array element $T(j)$ with $j>0$ contains the number of states with energy $(j-0.5)\Delta E$ to $(j+0.5)\Delta E$.
3. Initialize $T(0)$ and TA(0) with 1 and all other elements with 0. This reflects that just one state exists with $E = E_0$.
4. For any given vibrational mode with energy levels E_k, set the integer value R_k to $R_k = \mathrm{MOD}((E_k - E_0)/\Delta E, 1)$. E_0 is the zero-point energy of this mode. Also set n to the largest integer for which $E_n < E_{\max}$ holds.
5. for $k = 1$ to n do
   for $j = 0$, M-R_k do
   $\mathrm{TA}(R_k + j) = \mathrm{TA}(R_k + j) + T(j)$
   end
   end
   for $j = 1$ to M do
   $T(j) = \mathrm{TA}(j)$
   end
6. Repeat step 5 for any mode.

After all iterations are done, $T(j)$ will contain the number of states in the corresponding energy interval, $N(E)$. The sum of states, $W(E)$, is calculated by adding all $T(j)$ with energies less than or equal to E. Finally, the density of states $\rho(E)$ can be calculated *via* $N(E)/\Delta E$.

How does this algorithm work? Let us assume that we have a certain state distribution (stored in the T vector) among all energy bins realized with the first $j-1$ oscillators and we add contributions from the jth oscillator. If the jth oscillator is in its ground state, it does not contribute, because the ground state corresponds to the zero-point energy. If the vibration is single excited (its quantum number $k = 1$), then it provides additional energy $R_k\Delta E$ to the system. This means that if $T(j)$ states were at energy $R_k\Delta E$ before we added this new oscillator mode, then these states will now be at energy $(j + R_k)\Delta E$. The total number of states at energy $(j + R_k)\Delta E$ is therefore given by those states which were realized without the jth oscillation, $\mathrm{TA}(j + R_k)$, plus the new contributions involving one quanta of the jth oscillator, $T(j)$. The updated total number of states is stored in TA until all overtone contributions of the jth vibration are dealt with. Then the new populations are transferred to the T vector and the $(j + 1)$th vibration is considered.

For cases in which the K-rotor contributes to the density of states, only the initialization step of above outlined algorithm needs to be changed. Both vectors are now initialized with $W_{\text{K-rotor}}$, the sum of states due to the K-rotor within 0–ΔE. This initialization is based on the assumption that the rotational energy of this rotor is significantly smaller then ΔE. Anharmonic vibrations, hindered rotors, and so on are easily incorporated since above algorithm is not restricted to equally spaced energy levels.

Utility programs to explicitly calculate the density of states function with either the BS algorithm or the Whitten–Rabinovitch formula are provided with the MultiWell program package. In addition (due to the central role of the density of states function in QRRK and RRKM theories), these calculations are integral parts of all programs that analyze pressure-dependent systems. If the energy is significantly higher than E_0 the densities of states calculated with either of the methods are very similar; agreement is generally better than a factor of 2. Only for energies that are within a few $100\,\mathrm{cm}^{-1}$ to a few $1000\,\mathrm{cm}^{-1}$ of E_0, clear deviations can be found. This is mainly because the Whitten–Rabinovitch formula is a steady function while the direct counting method leads to non-steady, stepwise behavior. This is shown in Fig. 2 for ethoxy radicals as an example.

(*d*) *Collision parameters* Following a review by Cambi *et al.* [84], electronic structure calculations can be used to estimate Lennard–Jones

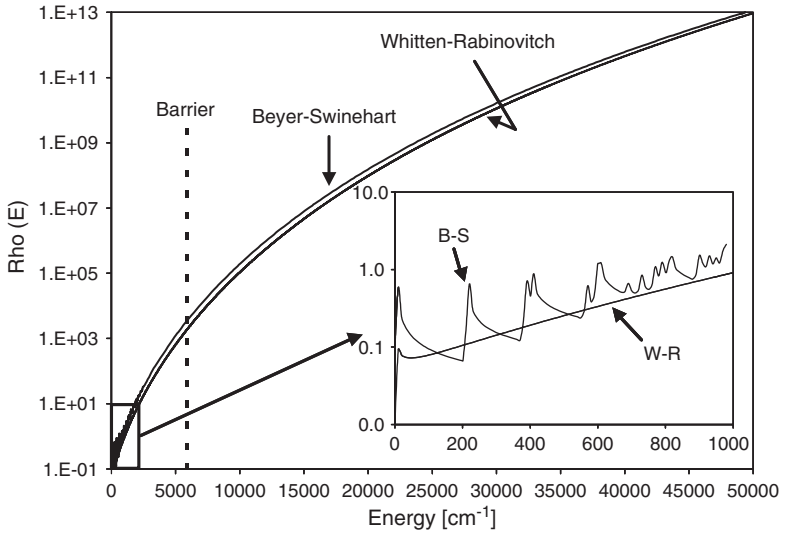

Fig. 2. Densities of states as function of the freely distributable energy for ethoxy radicals calculated with the Beyer–Swinehart (B–S) algorithm or the Whitten–Rabinovitch (W–R) equation. Calculations were done with DenSum from the MultiWell distribution.

parameters of radicals or molecules for which literature data are not available. The basic molecular property required is the average polarizability (α). In Fig. 3, we present a plot of calculated versus experimental polarizabilities for a variety of H/C/O compounds. The calculations were done at the B3LYP/6-311 + + G(3df,3pd) level of theory with geometries optimized at the B3LYP/6-31 + G(2d,p) level. Nearly all data pairs are close to the line resembling $\alpha_{exper} = \alpha_{calc}$, which shows the polarizabilities of these species can be accurately predicted with *ab initio* calculations.

Cambi *et al.* relate the LJ parameter σ_{LJ} directly to the polarizability (in $Å^3$) of a species. For the general case of two species A and B the following relation is recommended:

$$\sigma_{LJ} = 1.767 \frac{\alpha_A^{1/3} + \alpha_B^{1/3}}{(\alpha_A \alpha_B)^{0.095}} \text{ [A]} \tag{158}$$

The numerator in this equation is a measure of the molecule sizes and the product of polarizabilities in the denominator relates to the attraction of two species. The factor 1.767 and the exponent 0.095 are optimized values.

With σ_{LJ} determined and the observation that ε_{LJ} is (approximately) proportional to the product $\sigma_{LJ}^{-6}\, C_6^{eff}$, it is possible to estimate ε_{LJ}, if we know the long-range interaction term C_6^{eff} or if we can estimate its value.

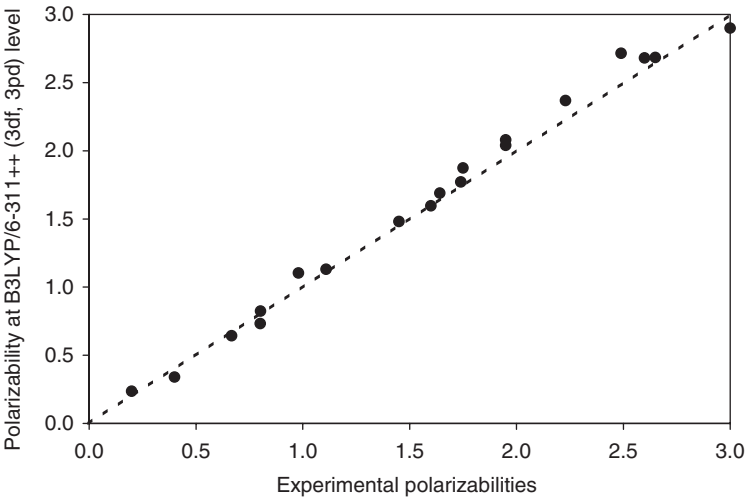

Fig. 3. Comparison between calculated and observed polarizabilities of organic compounds. The calculated polarizabilities were obtained at the B3LYP/6-311++G(3df,3pd)//B3LYP/6-31+G(2d,p) level of theory.

The C_6^{eff} parameter is usually related to the polarizability by the Slater–Kirkwood equation [85]

$$C_6^{\text{eff}} = 15.7 \times 10^3 \frac{\alpha_A \alpha_B}{\sqrt{\alpha_A/N_A} + \sqrt{\alpha_B/N_B}} \text{ [meV Å}^6\text{]}$$
$$= 1.82 \times 10^5 \frac{\alpha_A \alpha_B}{\sqrt{\alpha_A/N_A} + \sqrt{\alpha_B/N_B}} \text{ [K Å}^6\text{]} \quad (159)$$

The unknown "effective number of valence electrons," N_i, can be found with the following recipe proposed by Cambi:

$$\text{for atoms:} \quad N = N_{\text{ext}} \left\{ 1 + \left(1 - \frac{N_{\text{ext}}}{N_{\text{int}}} \right) \left(\frac{N_{\text{int}}}{N_{\text{tot}}} \right)^2 \right\} \quad (160)$$

where N_{ext} is the valence electrons, N_{int} the core electrons, $N_{\text{tot}} = N_{\text{int}} + N_{\text{ext}}$.

$$\text{for molecules:} \quad N = N_{\text{tot}} \left\{ 1 - \frac{N_b N_{nb}}{N_{\text{tot}}^2} \right\} \quad (161)$$

where N_b is the bond electrons, N_{nb} the lone-pair electrons, $N_{\text{tot}} = N_b + N_{nb}$.

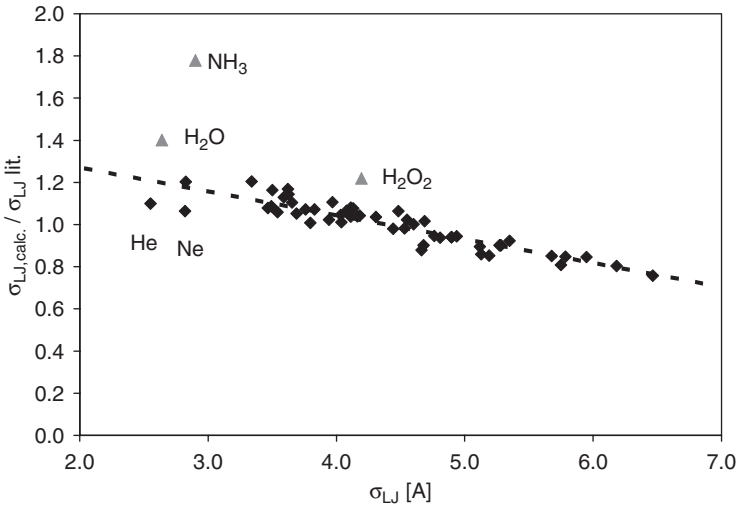

Fig. 4. Comparison of calculated and experimental σ_{LJ} values. See text for calculation details.

The final relation for the well depth is

$$\varepsilon_{LJ} = 0.720\frac{C_6^{eff}}{\sigma_{LJ}^6}[\text{meV}] = 8.36\frac{C_6^{eff}}{\sigma_{LJ}^6}\ [\text{K}] \tag{162}$$

It should be mentioned that the review by Cambi *et al.* is mainly based on atoms and small radicals. Though the relations are formulated in a general way, we are not aware of any comprehensive studies that validate their usefulness for large molecules or radicals. However, preliminary results of the calculations of σ_{LJ} suggest a generally good agreement with experimental data, although small systematic deviations, which scale with σ_{LJ} (Fig. 4), are observed. The agreement between calculated and tabulated ε_{LJ} values is at this point less satisfying. But it might be possible to improve this situation in future by, e.g., redefining the number of effective electrons.

A further improvement appears to be necessary if at least one of the colliding species has a permanent dipole moment. Paul and Warnatz [86] investigated correction methods in the context of transport properties. Although we will not discuss details of these corrections, the basic effect is that permanent dipole moments decrease the collision diameter slightly, while the attractive energy is strongly increased. Because the value of the collision integral $\Omega^{*(2,2)}$ depends *on* ε_{LJ}, the overall effect at low temperatures is an increase of the collision frequency.

In addition to the Lennard–Jones collision parameters, we need a measure of the energy transfer probability to describe the energy transfer

in collisions. Lim and Gilbert [2,87] published a method called the ''biased random walk'' model that calculates the average energy transferred per collision, $\langle \Delta E_{all} \rangle$. A corresponding program (BRW) is provided in the ''Unimol'' package. The program requires readily available input data: LJ parameter, the mass, specification of the composition, and so-called local LJ parameters. According to the authors, this source of energy transfer data should be used with caution since the theory for energy transfer is still in its infancy. Often, a generic value for $\langle \Delta E_{down} \rangle$ is a better choice at this stage.

4 WORKED-OUT EXAMPLES OF THE ANALYSIS OF PRESSURE-DEPENDENT REACTIONS

To complete the discussion of pressure-dependent reactions we present and discuss in this section worked-out examples for the following four reaction systems:

1. The thermal dissociation of C_2H_5O radicals to $CH_3 + CH_2O$.
2. The reversible isomerization of n-C_3H_7 to i-C_3H_7.
3. The reaction of C_2H_5 with O_2.
4. The reaction of $C_2H_3 + O_2$.

The selected examples will be used to demonstrate specific aspects of the kinetic analysis discussed earlier.

4.1 Example 1: the thermal dissociation $C_2H_5O \rightarrow CH_3+CH_2O$

Ethoxy radicals (C_2H_5O) are rather unstable and dissociate even at temperatures as low as 400 K in less than a millisecond. Therefore, the thermal dissociation of ethoxy is suitable to demonstrate the performance of different reaction analysis programs including MultiWell. The reaction channel leading to CH_3 and CH_2O, $\Delta_R H^{298} \approx 10.5$ kcal/mol, has the lowest barrier and dominates over the second most important channel ($CH_3CHO + H$, $\Delta_R H^{298} \approx 13.8$ kcal/mol) up to at least 500 K as shown by Caralp *et al.* [88] in a recent experimental and theoretical study. Under these circumstances, the overall thermal dissociation might be thought of (in the Lindemann picture) as a two-step process:

$$C_2H_5O \overset{+M}{\rightleftharpoons} C_2H_5O^*$$
$$C_2H_5O^* \rightarrow CH_3 + CH_2O$$

We use for the high-pressure rate constant and collision parameters the following values, which are close to those given by Caralp *et al.*:

$$\sigma_{LJ}(C_2H_5O) = 4.53\text{Å}, \quad \sigma_{LJ}(He) = 2.55\text{Å}$$
$$\varepsilon_{LJ}(C_2H_5O) = 362.6\text{K}, \quad \varepsilon_{LJ}(He) = 10.0\text{K}$$
$$k_\infty = 1.0 \times 10^{13} \exp(-16.8\ \text{kcal/mol}/RT)\text{sec}^{-1}$$

Other molecular parameters are obtained from CBS-QB3 *ab initio* calculations. Since the *ab initio* data do not yield the observed *A*-factor, we adjusted the reaction path degeneracy in those applications that calculate the TST rates directly from molecular data (ChemRate, Unimol). Programs such as CARRA and MultiWell accept high-pressure rate constants in Arrhenius form as input and no adjustments were needed in these cases. The programs CARRA_MSC and CARRA_ME calculate the density of states from three characteristic frequencies instead of taking the complete set of frequencies, which we obtained with a separate fitting program.

We will present results of the thermal dissociation of ethoxy to address the following three questions:

(a) How do the predictions with the different programs compare (for an arbitrarily chosen $\langle E_{down} \rangle$ value)?
(b) How sensitive are these predictions to:
    the energy transfer treatment (MSC approach versus ME approach);
    the value for $\langle E_{down} \rangle$;
    the functional form for $P(E, E')$?
(c) Can the steady-state approximation be justified?

In Fig. 5 we present predictions of fall-off curves for the unimolecular dissociation of C_2H_5O in He with (a) Unimol, (b) ChemRate, (c) MultiWell, and (d) CARRA_ME. The $\langle E_{down} \rangle$ value was set to $200\,\text{cm}^{-1}$, which is a frequently used "standard" value for He as collider. It can be seen that the predictions with all programs are quite similar but not identical. The first two calculations slightly over-predict the unimolecular dissociation at low pressure, while MultiWell results in this region are on the low side. Finally, results obtained with CARRA_ME reproduce the data well. Since the $\langle \Delta E_{down} \rangle$ value was arbitrarily chosen, a good or bad agreement with the experimental data does not necessarily indicate that one program performs better than another. It only shows that the predictions are sensitive to specifics of the implementation of the theory in these programs. These include the treatment of internal rotations, the default energy grain size, differences in the calculation of $k(E)$, and so on. Everything else

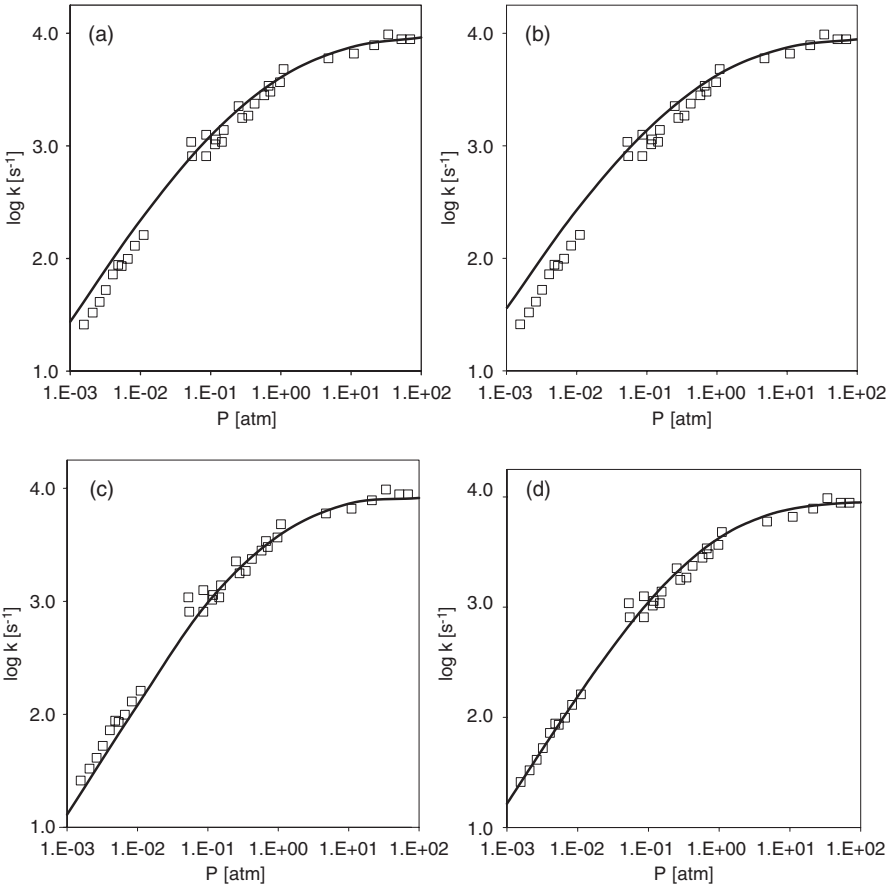

Fig. 5. Comparison of predicted fall-off curves for the thermal dissociation of C_2H_5O radicals forming $CH_3 + CH_2O$ at 406 K with experimental data. All calculations use the exponential down model with $\langle E_{down} \rangle = 200\,cm^{-1}$. (a) Unimol, (b) ChemRate (steady-state and time-dependent calculations yield similar results), (c) MultiWell, and (d) CARRA_ME.

being equal, results from CARRA_ME using QRRK theory and a three-frequency representation of the internal modes are expected to be less accurate, so the good agreement observed here is fortunate.

Next we compare collision parameters and models. In Fig. 6a, we present results obtained with CARRA_MSC and CARRA_ME. Except for the energy transfer values, all input data are identical. The CARRA_ME results are the same as shown in Fig. 5, using $\langle E_{down} \rangle = 200\,cm^{-1}$ (or 573 cal/mol). An equivalent $\langle E_{all} \rangle$ value of -273 cal/mol (or $95\,cm^{-1}$), calculated *via* equations (44) and (45), is used in CARRA_MSC. The results from both calculations compare well

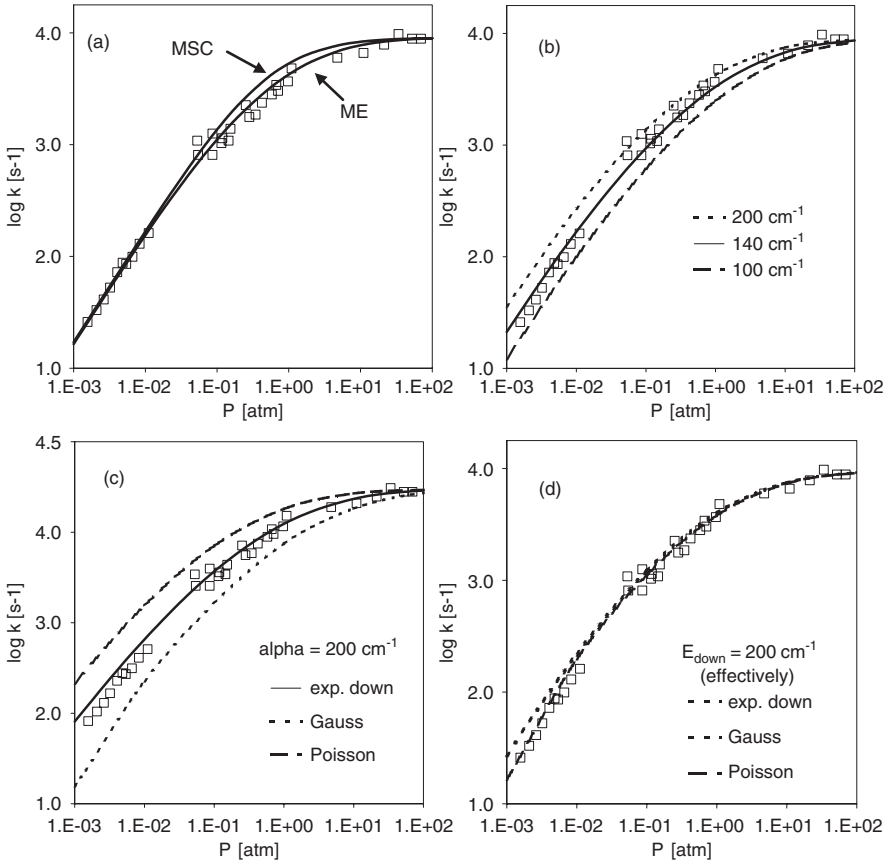

Fig. 6. Demonstration of the influence of collision parameters and energy transfer models on the fall-off prediction for the thermal dissociation of ethoxy at 406 K. (a) MSC (CARRA_MSC) versus ME (CARRA_ME) approach. (b) Impact of the $\langle E_{\text{down}} \rangle$ value (calculation done with ChemRate). (c) Impact of the energy transfer model for a given value of α (see text) (calculation done with Unimol). (d) Impact of the choice of the energy transfer model if α is adjusted to yield numerically $\langle \Delta E_{\text{down}} \rangle = 200\,\text{cm}^{-1}$ (calculation done with Unimol).

although the fall-off curve obtained with the ME treatment is somewhat flatter. At least for this example, the MSC formalism appears to provide a good alternative to the ME approach.

Fig. 6b contains results from ChemRate calculations with various $\langle \Delta E_{\text{down}} \rangle$ values. The relation between this parameter and the predictions is obvious: a larger $\langle \Delta E_{\text{down}} \rangle$ value leads to an increase in the unimolecular dissociation rate at low pressures and in the fall-off region. A consequence of this observation is that for each program an optimal $\langle \Delta E_{\text{down}} \rangle$ value can be found that leads to good agreement with the

data. For ChemRate this value is $\sim 140\,\mathrm{cm}^{-1}$ and for Unimol it is $\sim 150\,\mathrm{cm}^{-1}$. Another indication for the uncertainty of energy transfer parameters is that the original analysis by Caralp *et al.*—done in the framework of the Troe formalism—yielded a $\langle \Delta E_{\mathrm{all}} \rangle$ value of $-24\,\mathrm{cm}^{-1}$, which is—as the authors admit—surprisingly low. As discussed above, we used in our CARRA_MSC analysis a four times larger value for $\langle \Delta E_{\mathrm{all}} \rangle$ and obtained good agreement with the data.

Even if we restrict ourselves to a ME analysis, we still have the choice of many different collision models. In the review section we only discussed the exponential down model (60),

$$P(E, E') = \frac{1}{N(E')} \exp\left(-\frac{E' - E}{\alpha}\right), \quad \text{with } E < E' \text{(exponential down)}$$

but this is just one of many functional forms of $P(E, E')$ that are used in ME calculations.[12] Other models, for example, assume a Poisson or Gaussian distribution of the energy transfer probability. The corresponding expressions are

$$P(E, E') = \frac{1}{N(E')} \frac{E' - E}{\alpha} \exp\left(-\frac{E' - E}{\alpha}\right), \quad \text{with } E < E' \text{ (Poisson)}$$

$$P(E, E') = \frac{1}{N(E')} \exp\left(-\frac{(E' - E)^2}{\alpha^2}\right), \quad \text{with } E < E' \text{ (Gaussian)}$$

All these functions contain only one parameter, α, which in the case of the exponential down model equals $\langle E_{\mathrm{down}} \rangle$. In Fig. 6c, we compare fall-off curves for the ethoxy dissociation at 406 K calculated with each of these energy transfer models and a constant α value of $200\,\mathrm{cm}^{-1}$. At first glance we would conclude that the choice of the energy transfer model has a huge impact on the predictions. However, α has a different meaning in all three energy transfer models and thus it is not immediately clear that its value should be the same for all cases. Fortunately, the Unimol software, which was used for this subset of calculations, provides the average amount of energy transferred in a down collision (meaning a numerically obtained effective $\langle E_{\mathrm{down}} \rangle$ value) as part of the output. We find for our calculations effective $\langle E_{\mathrm{down}} \rangle$ values of $190.4\,\mathrm{cm}^{-1}$, $407\,\mathrm{cm}^{-1}$, and $108\,\mathrm{cm}^{-1}$, respectively,[13] for the exponential

[12] The current version of MultiWell handles 10 pre-defined collision models. See also the recent review by Barker *et al.* [17].

[13] The difference between the provided and effective $\langle \Delta E_{\mathrm{down}} \rangle$ values in the exponential down model can be explained with numerical errors due to the finite energy grain size.

down, Poisson, and Gaussian models. The calculated higher rate constant for the Poisson model is consistent with the earlier observation that a higher energy transfer value results in an increased rate constant in the low-pressure region. In Fig. 6d we adjusted the α parameters for all three cases in such a way that approximately the same numerical $\langle E_{\text{down}} \rangle$ value resulted. Now all predictions essentially overlap, proving that the specific choice of the model is of little impact.

Finally, we use MultiWell to study the change of the energy distribution function of ethoxy while it dissociates. To do so we carry out the following computer experiment: we assume that ethoxy is formed completely thermalized at 900 K and 1 atm and that it only dissociates to $CH_3 + CH_2O$. (It would be trivial to incorporate additional channels but we try to keep it simple.) The top of Fig. 7 depicts the distribution of ethoxy radicals with respect to the total amount of vibrational energy. At $t = 0$ sec the maximum population is found at $\sim 3000\,\text{cm}^{-1}$ (8.6 kcal/mol), but the long exponential tail in the energy distribution reveals that a significant fraction of ethoxy radicals possess substantially much more vibrational energy (up to and above $10{,}000\,\text{cm}^{-1}$). The barrier for dissociation is $\sim 5860\,\text{cm}^{-1}$ (16.8 kcal/mol), hence well inside the ethoxy population at this temperature. All profiles provided at longer times are clearly distinguished from the initial population in that the exponential tail is nearly completely depleted and only a very small fraction of ethoxy exists at energies above the barrier. The shapes of these later profiles are all similar and it appears as if only the area under the profiles diminishes. The bottom part of Fig. 7 depicts the integrated mole fractions versus time. Initially the mole fraction of ethoxy drops nearly instantaneously by 20%. This is followed by an exponential steady decay of the reactant and formation of the products. Since the time-dependent unimolecular rate constant is defined as $-\text{d}\ln(x)/\text{d}t$ at each point in time, we can qualitatively see that the rate constant is initially not independent of time. At later times, however, the rate constant becomes time independent and the populations are at steady state. More precisely, the distribution among different energy levels remains steady but the absolute amount of ethoxy declines due to reaction. MultiWell's output of the distributions visualizes the transition from a time regime where energy redistribution is important to the time domain where only chemically significant processes occur. The inset clarifies that the ethoxy decay is exponential after some time and a truly time-independent rate constant is defined.

Although Fig. 7 clearly shows that we can assign a time-independent rate constant for the thermal dissociation of ethoxy, it is also obvious that the initial fast decay is ignored. This is a consequence of waiting

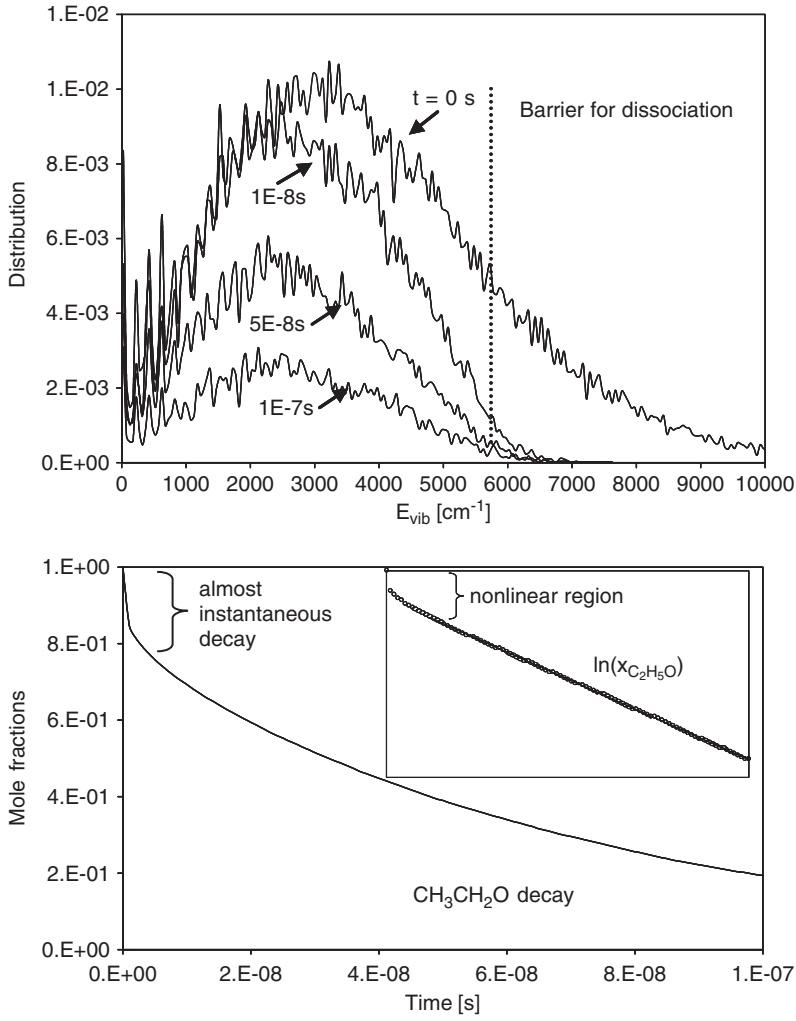

Fig. 7. Study of the unimolecular dissociation of ethoxy to $CH_3 + CH_2O$ at 900 K and 1 atm with MultiWell. (Top) Change of the distribution and population of vibrational energy levels as a function of time. (Bottom) Integrated C_2H_5O profiles versus time; (inset) $\ln(C_2H_5O)$ versus time. Notice the statistical noise inherent to all stochastic calculations.

until steady state is achieved. In this example, ~20% of the decay is not captured if we only use the apparent rate constant. Since the initial dissociation proceeds more or less instantly, this decay would have to be accounted for in the description of the formation reaction of ethoxy by assigning 20% of the yield directly to the products. For example, if we

envision that ethoxy is formed *via*

$$C_2H_5OH + F \rightarrow C_2H_5O + HF$$

we could assign an 80% yield to this channel and include

$$C_2H_5OH + F \rightarrow CH_3 + CH_2O + HF$$

as a 20% channel to account for the initial fast decay.

4.2 Example 2: the isomerization reaction n-C_3H_7 ⇌ i-C_3H_7

Our second example is the unimolecular isomerization of propyl radicals. We have chosen this reaction to address the question of how well does a steady-state analysis describe isomerizations. This will be done in three steps: first, we perform a steady-state kinetic analysis with the CARRA software (ME and MSC) for 1200 K with Ar as collider. Next we repeat the analysis with the stochastic MultiWell program to understand which time scales are involved in the overall process. Finally we compare predicted species profiles from both approaches.

The two isomers *n*-C_3H_7 and *i*-C_3H_7 are separated by a barrier of ~37 kcal/mol (measured with respect to *n*-C_3H_7) and they can easily interconvert at sufficiently high temperatures. Although in reality both radicals dissociate to propene + H and ethylene + CH_3 (see Fig. 8), we will ignore these channels here and focus exclusively on the isomerization part. The steady-state analysis with CARRA yields one apparent pressure-dependent rate constant, since the rate constant for the reverse reaction is determined by the equilibrium constant. The predictions with both versions (MSC and ME) for $T = 1200$ K and various pressures are shown in Fig. 9. The results are very similar and show the expected fall-off behavior. The MSC treatment—despite its simplicity—captures the pressure dependence well.

Next, we look at the results from MultiWell. Instead of focusing at the population distribution function, as we did in the first example, we use this time the results for the average energy ($\langle E_{vib} \rangle$) stored in the vibrational modes of both isomers. The change of $\langle E_{vib} \rangle$ with time is a measure of the energy transfer during the isomerization. Fig. 10 presents $\langle E_{vib} \rangle$ as a function of time for three different pressures and $T = 1200$ K. Initially *n*-C_3H_7 is thermalized and $\langle E_{vib} \rangle$ is at $t = 0$ sec in equilibrium with the thermal energy. (Note that $\langle E_{vib} \rangle_{t=0\,sec} = \sim 8200\,cm^{-1}$, which means that on average ~23.5 kcal/mol of energy is stored in these modes.) Shortly thereafter we see a clear drop of $\langle E_{vib} \rangle$. The lower the pressure, the larger this drop. The reason is clear: part of the *n*-C_3H_7 population at high energies quickly isomerizes to *i*-C_3H_7 and

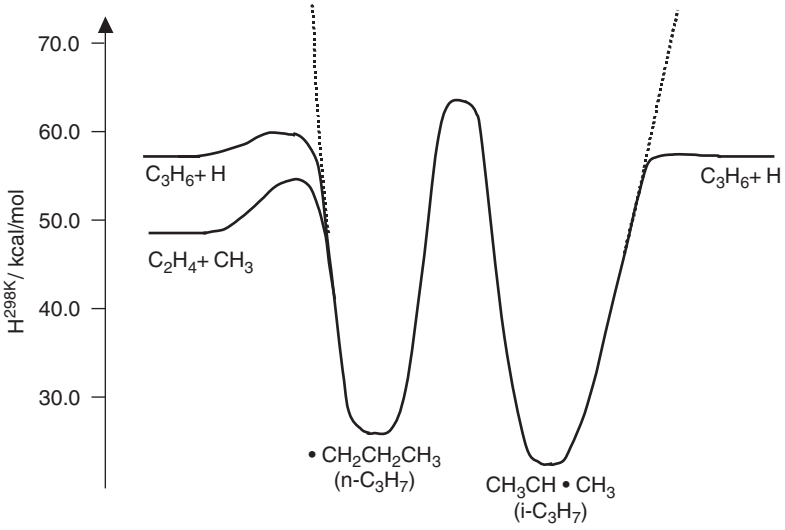

Fig. 8. PES surface for the isomerization of C_3H_7 radicals. The dotted lines indicate the cases in which the dissociation channels are ignored. The energies were calculated *ab initio* at CBS-QB3 level.

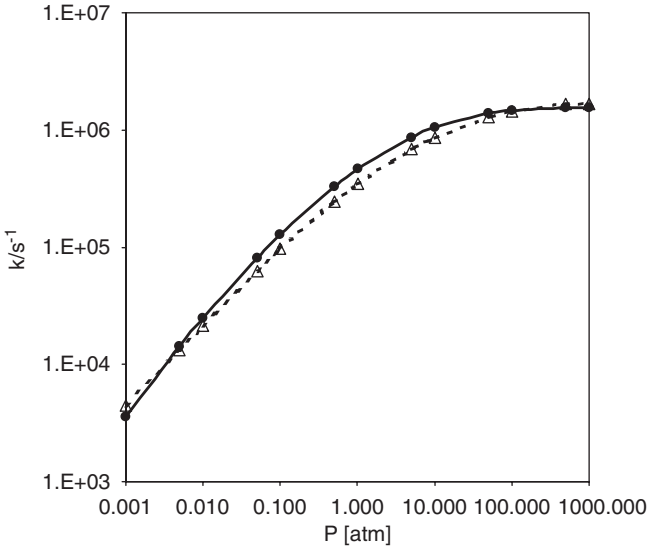

Fig. 9. Predicted rate constant for the isomerization of *n*-C_3H_7 to *i*-C_3H_7 as a function of pressure at 1200 K. Solid line with filled circles: QRRK/MSC prediction (with CARRA_MSC); broken line with open triangles: QRRK/ME predictions (with CARRA_ME).

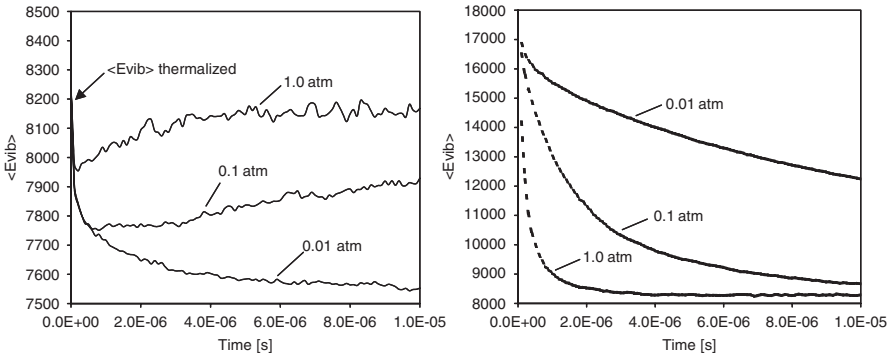

Fig. 10. Average vibrational energy E_{vib} of n-C_3H_7 (left) and i-C_3H_7 (right) as a function of reaction time. Conditions: 1 atm (Ar) and 1200 K; calculations with MultiWell. $\langle E_{vib} \rangle$ is given in cm^{-1}; 1 kcal/mol = 349 cm^{-1}.

thus is lost. If the pressure is high, the missing population is easily regenerated *via* collisions and the Boltzmann distribution is nearly maintained, while this is not possible at low pressures.

The barrier for isomerization is ~14,500 cm^{-1} (41.5 kcal/mol) above the zero-point energy of i-C_3H_7. Therefore, i-C_3H_7 is formed with a large amount of internal energy as seen in the right-hand side of Fig. 10. The initially formed highly excited i-C_3H_7 states are quickly deactivated (*via* collisions) so that the $\langle E_{vib} \rangle$ value decreases. Again, a lower pressure leads to a slower deactivation process. At equilibrium the $\langle E_{vib} \rangle$ values for both isomers should be very similar because they contain the same number of vibrations with similar frequencies. This can be seen for the results at 1 atm total pressure. At a reaction time of ~5E−6 sec the $\langle E_{vib} \rangle$ values for both, n-C_3H_7 (left) and i-C_3H_7 (right), have reached within the error limits their final values which can be seen to be ~8200 cm^{-1}. At the lower pressures the reaction is far from equilibrium and the $\langle E_{vib} \rangle$ values are far from the final value.

In Fig. 11 we compare predictions based on CARRA_MSC results with mole fraction profiles from MultiWell for two pressures at 1200 K. The steady-state code does not capture the initial drop seen at early times for the 0.01 atm profiles but agrees well at longer times. At 1 atm there is no initial drop apparent and steady-state rate constants could in principle describe the MultiWell data. The predicted profiles with both codes are rather close and small changes in the $-\langle E_{all} \rangle$ value used in CARRA_MSC can bring both plots even closer together. The major point to notice is again the characteristics of the steady-state assumption to ignore initial changes, which happen before the steady-state condition

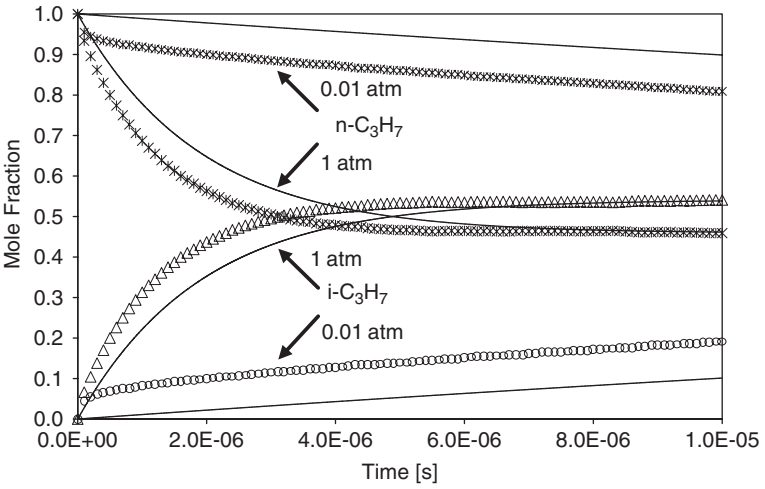

Fig. 11. Comparison of predicted MultiWell concentration profiles (symbols) for *n*-C_3H_7 and *i*-C_3H_7 with integrated profiles calculated from the CARRA_MSC results (lines) at 1 atm and 0.01 atm (Ar) and $T = 1200$ K.

is established. In this example the error is small, but one could imagine cases where the steady-state assumption is no longer a valid approach and time-dependent solutions to the ME must be used.

4.3 Example 3: the reaction $C_2H_5+O_2 \rightarrow$ products

The next example is a chemically activated reaction, the recombination of C_2H_5 radicals with O_2. This well-studied reaction [37,89–100] plays an important role in the low temperature oxidation of ethane. The underlying PES (Fig. 12) reveals that the initially formed ethyl peroxy complex, C_2H_5OO, can either undergo stabilizing collisions, react to bimolecular products such as ethylene and hydroperoxy or acetaldehyde and hydroxyl, isomerize to hydroperoxy ethyl, or redissociate back to the reactants. The isomerization product hydroperoxy ethyl, CH_2CH_2OOH, can also dissociate to ethylene and hydroperoxy or it can form ethylene oxide and hydroxyl radicals. Although this system appears to be a complex system, it is rather simple since—as we shall see—most of these channels are of minor importance. The barrier for the elimination of ethylene and hydroperoxy from ethyl peroxy is lower than the entrance channel but the corresponding rate constant has a significantly lower *A*-factor than the rate constant for the redissociation. The

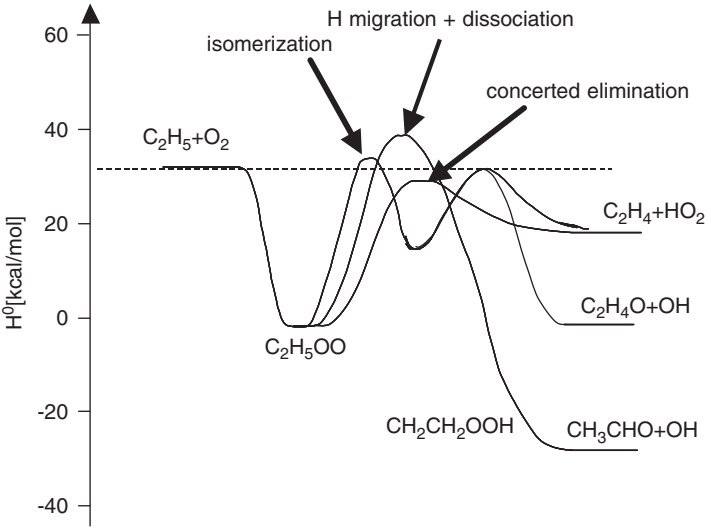

Fig. 12. PES for the reaction $C_2H_5 + O_2$.

barrier for the isomerization is slightly above the energy of the reactants and since this reaction has a low *A*-factor, too, it will be a minor channel under all conditions.

We will mainly use CARRA_MSC to analyze this system. Before looking at the results, we should address the question of how many apparent rate constants are required to fully describe this system. We have three sets of reactions: (a) reactions of $C_2H_5 + O_2$, (b) unimolecular reactions of stabilized C_2H_5OO, and (c) unimolecular reactions of CH_2CH_2OOH. These reactions are:

$$
\begin{aligned}
C_2H_5 + O_2 &\rightarrow CH_3CH_2OO \text{ (stabilization)} \\
&\rightarrow C_2H_4 + HO_2 \text{ (direct elimination)} \\
&\rightarrow CH_3CHO + OH \text{ (H migration to form } CH_3CHOOH, \\
&\quad \text{then rapid dissociation)} \\
&\rightarrow C_2H_4 + HO_2 \text{ (isomerization to form } CH_2CH_2OOH, \\
&\quad \text{then elimination)} \\
&\rightarrow C_2H_4O + OH \text{ (isomerization to form } CH_2CH_2OOH, \\
&\quad \text{then elimination)} \\
&\rightarrow CH_2CH_2OOH \text{ (isomerization to form } CH_2CH_2OOH, \\
&\quad \text{then stabilization)}
\end{aligned}
$$

$$
\begin{aligned}
CH_3CH_2OO &\rightarrow C_2H_5 + O_2 \text{ (reverse of recombination)}^* \\
&\rightarrow C_2H_4 + HO_2 \text{ (direct elimination)} \\
&\rightarrow CH_3CHO + OH \text{ (H migration to form } CH_3CHOOH, \text{ then rapid dissociation)} \\
&\rightarrow C_2H_4 + HO_2 \text{ (isomerization to form } CH_2CH_2OOH, \text{ then elimination)} \\
&\rightarrow C_2H_4O + OH \text{ (isomerization to form } CH_2CH_2OOH, \text{ then elimination)} \\
&\rightarrow CH_2CH_2OOH \text{ (isomerization to form } CH_2CH_2OOH, \text{ then stabilization)}
\end{aligned}
$$

$$
\begin{aligned}
CH_2CH_2OOH &\rightarrow C_2H_5 + O_2 \text{ (reverse of recombination)}^* \\
&\rightarrow C_2H_4 + HO_2 \text{ (direct elimination)} \\
&\rightarrow C_2H_4O + OH \text{ (direct elimination)} \\
&\rightarrow C_2H_4 + HO_2 \text{ (isomerization to form } CH_3CH_2OO, \text{ then elimination)} \\
&\rightarrow CH_3CHO + OH \text{ (isomerization to form } CH_3CH_2OO, \text{then H migration to form } CH_3CHO + OH, \text{ then dissociation)} \\
&\rightarrow CH_3CH_2OO \text{ (isomerization to form } CH_3CH_2OO, \text{ then stabilization)}^*
\end{aligned}
$$

Three out of these 18 apparent reactions are marked with an asterisk "*", because they are the reverse reactions of already listed ones and thus do not present independent rate constants. This leaves 15 independent reactions to describe this example reaction. This number could be further reduced if channels with insignificant contributions to the overall product spectrum were eliminated. One more word of clarification to the reaction list: reactions labeled with "isomerization …, then elimination" are different from those labeled with "direct elimination," because they follow a different reaction path. For example, the two $CH_2CH_2OOH \rightarrow C_2H_4 + HO_2$ product channels are:

1. $CH_2CH_2OOH \xrightarrow{\text{elimination barrier}} C_2H_4 + HO_2.$
2. $CH_2CH_2OOH \xrightarrow{\text{isomerization barrier}} CH_3CH_2OO^*$
   $CH_3CH_2OO^* \xrightarrow{\text{elimination barrier}} C_2H_4 + HO_2.$

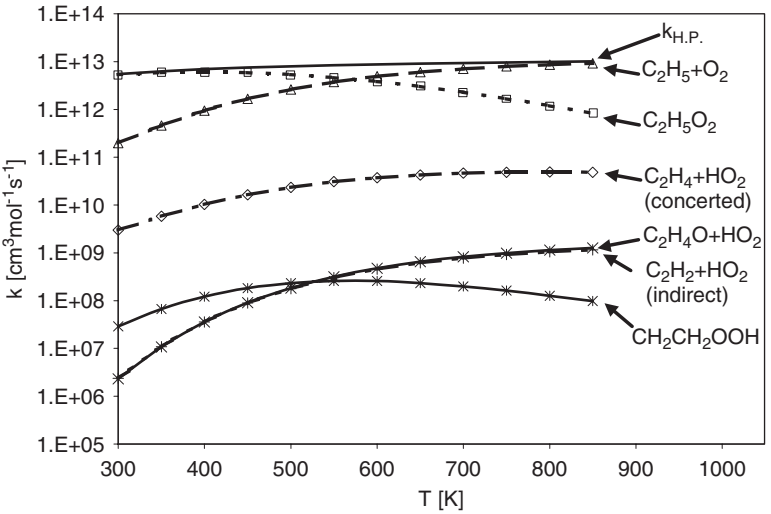

Fig. 13. Temperature-dependent apparent rate constants for chemically activated reactions of the $C_2H_5 + O_2$ system ($CH_3CHO + OH$ channel is not included). In addition, the redissociation channel (formally $C_2H_5 + O_2 \Rightarrow C_2H_5 + O_2$) and the high-pressure rate constant (k_{HP}) are shown. The calculations were done at 1 atm He.

The second apparent rate constant is different from those for CH_3CH_2OO because the $CH_3CH_2OO^*$ is not stabilized.

In Fig. 13 we present results for the chemically activated reactions at 1 atm (He) as a function of temperature. In addition to the apparent rate constants (the unimportant $CH_3CHO + OH$ channel is omitted), the redissociation rate constant and the high-pressure rate constant are plotted. At low temperatures, stabilization to ethyl peroxy dominates all other channels. With increasing temperature, the redissociation rate constant becomes increasingly more important and at 850 K this channel is more than one order of magnitude faster than stabilization. Effectively this means that the observable $C_2H_5 + O_2$ rate decreases drastically with temperature under these conditions. Among the bimolecular products the concerted elimination channel has the highest yield, followed by the formation of $C_2H_4O + OH$ and $C_2H_4 + HO_2$ from the isomerization channel.

The initially stabilized ethyl peroxy adduct is not stable at higher temperatures. Predictions of its unimolecular reactions for the same conditions are presented in Fig. 14. The major dissociation channel leads to $C_2H_5 + O_2$ and the only other important reaction path produces $C_2H_4 + HO_2$. Due to the higher A-factor, the dominance of the redissociation channel increases with temperature. For the dissociation

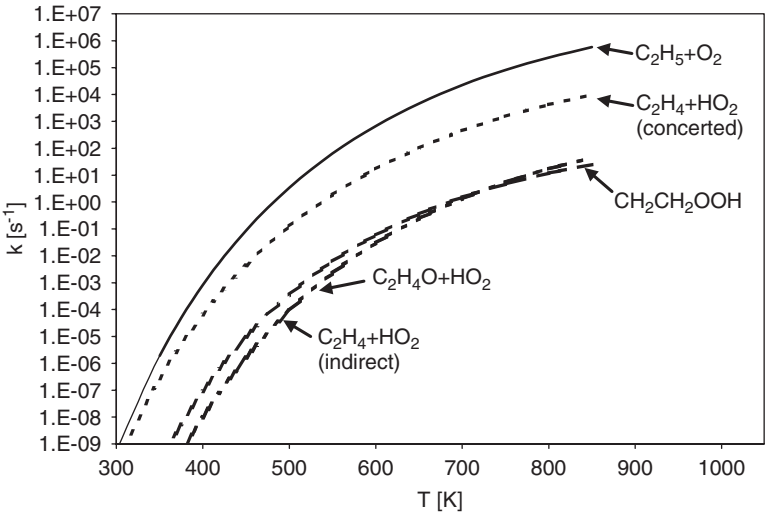

Fig. 14. Apparent rate constants for major channels of the unimolecular dissociation of ethyl peroxy at 1 atm (He).

of the second isomer, similar results are obtained, although they are not shown.

The work by Sheng *et al.* [101] demonstrated that results obtained with the QRRK/ME approach are very similar to the predictions from this QRRK/MSC analysis. The separation of the $C_2H_5 + O_2$ reaction into two steps: (1) prompt chemically activated reactions and (2) delayed thermal dissociation reactions, might appear unphysical or arbitrary. A justification why this approach is reasonable can be obtained from time-dependent solutions of the ME. We use MultiWell to illustrate this for one specific case (700 K, 1 atm). The results are presented in Fig. 15. We can clearly see that $C_2H_5O_2$ is consumed on two very different time scales: ~90% of it dissociates very rapidly to $C_2H_5 + O_2$, thereby competing with collision stabilization. In contrast, the stabilized $C_2H_5O_2$ fraction dissociates several orders of magnitudes slower. The appearance of two completely separated time domains provides the justification to break the entire process down into two separate steps as it is done in the QRRK/MSC analysis presented before. Fig. 15 also shows the minor $C_2H_4 + HO_2$ channels (magnified by 100). Under these conditions, MultiWell predicts that $C_2H_4 + HO_2$ is nearly exclusively produced on the prompt time scale. However, the noise of the profile is too high to allow any conclusions as to whether small amounts of delayed $C_2H_4 + HO_2$ are being produced on longer time.

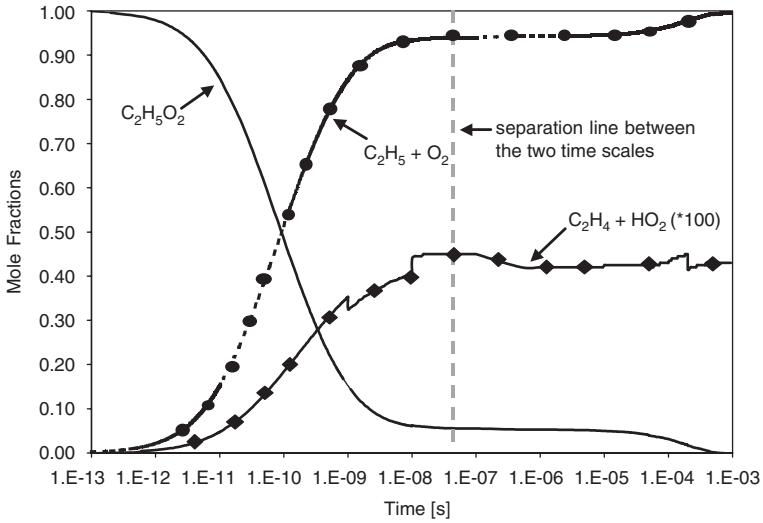

Fig. 15. MultiWell results of the decay of chemically activated ethyl peroxy at 700 K and 1 atm He. The separation line divides the time range into the "prompt" (left) and the "delayed" (right) regions.

4.4 Example 4: the reaction $C_2H_3+O_2 \rightarrow$ products

While the previous example is basically a single-well reaction (the isomerization and therefore reactions of the second well play only a very minor role), this final example deals with a multi-well multiple channel reaction. The reaction between vinyl radicals + O_2 was studied by several groups [102–104] and we will present here an analysis close to that provided by Bozzelli and Dean [102][14]. A schematic PES is shown in Fig. 16. It is characterized by the existence of several product and isomerization channels with barriers clearly below the entrance channel. If one considers only the energetic properties, the most favorable products would be CH_2O + HCO and OHCCOH (glyoxal) + H. However, these products can only be formed after two isomerization steps with relatively low *A*-factors.

In contrast, vinoxy ($\bullet CH_2CHO$) has the highest barrier but it is formed from the initial complex and the *A*-factor for this bond fission is expected to be high. Therefore, based on this qualitative analysis of the PES, one would expect a competition of these different channels.

[14]An improved surface is available in Klippenstein *et al.* [104]. Note that the use of a different PES will lead to different results.

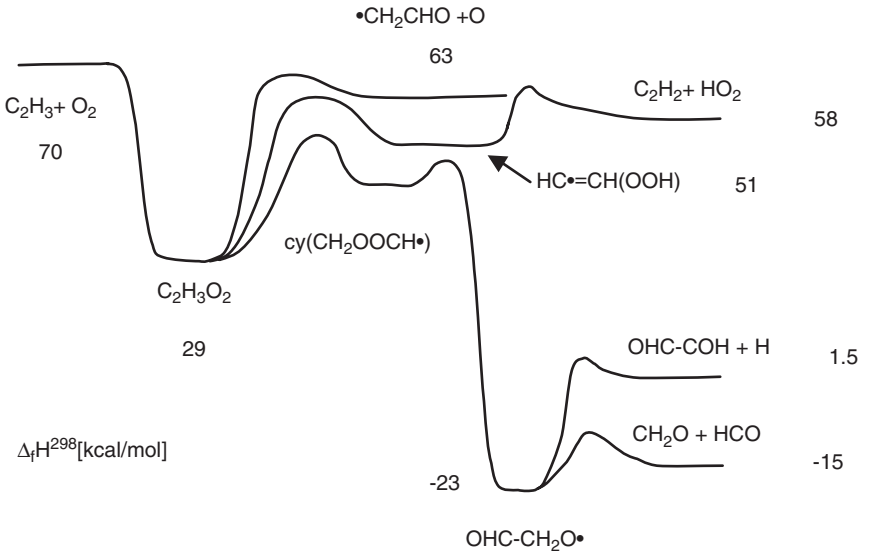

Fig. 16. Schematic representation of the PES for the reaction $C_2H_3 + O_2$ (taken from Bozzelli and Dean [102]).

Predicted apparent rate constants for various channels of the $C_2H_3 + O_2$ reaction are shown in Fig. 17. The plots at the top were calculated with CARRA_MSC for $T = 300\,K$. Apart from specific details about individual rate constants one can generally see two different types of profiles: (1) rate constants that decline with increasing pressure and (2) those that increase (at least over a certain pressure range) if the pressure rises. A closer look at the results reveals that all bimolecular product channels belong to the first category while stabilization channels form the second type. Since the $HC\bullet = CH(OOH)$ isomer is stabilized after isomerization from chemically activated $C_2H_3O_2$, this profile contains a maximum. At low pressures, a pressure increase leads to more collision stabilization of $HC\bullet = CH(OOH)$ and prevents it from further reaction to $C_2H_2 + HO_2$. This explains the initial increase of the production rate with pressure. At a certain pressure, a further pressure increase prevents the isomerization step from happening because the collisional stabilization of $C_2H_3O_2$ becomes too fast. Therefore, at this point a pressure increase leads to a reduction of the $HC\bullet = CH(OOH)$ formation rate.

The bottom part of Fig. 17 shows similar calculation results at 1300 K. As discussed earlier in the theory section an increase of the temperature shifts the fall-off region toward higher pressure. The magnitude of such a shift can be seen here: while the apparent rate constants at 300 K

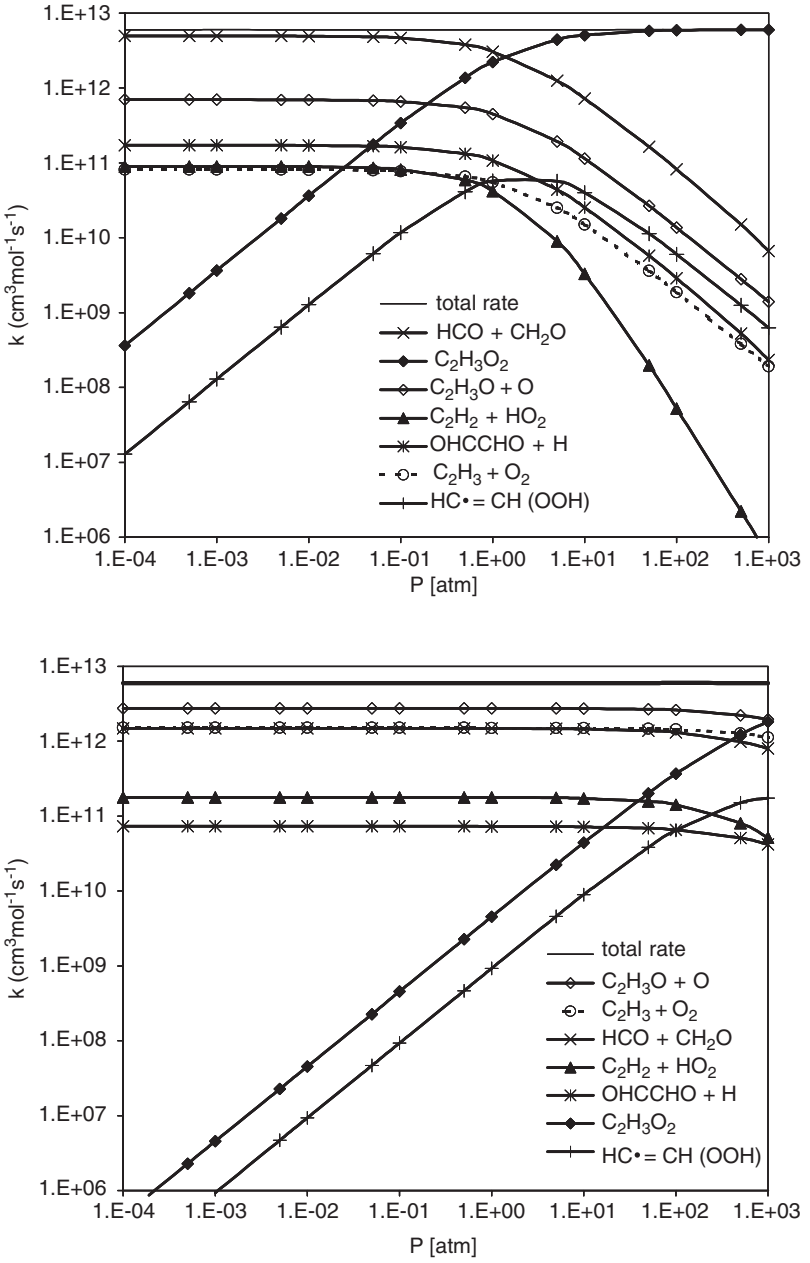

Fig. 17. Pressure dependence of the apparent rate constants for various channels in the reaction of C_2H_3 with O_2 at 300 K (top) and 1300 K (bottom).

approach the high-pressure limit somewhere ~100 atm, we notice that at 1300 K even a pressure of 1000 atm is too low to come close to the high-pressure limit[15]. Therefore, the 1300 K results are similar to the low-pressure results at 300 K. Now the nearest product channel (vinoxy + O) dominates. Another change is that the redissociation rate constant increased significantly compared to the results at 300 K.

We present only results from the chemically activated analysis, but the complete set of reactions would again include apparent rate constants for the thermal dissociation of all isomers as well.

5 REPRESENTATION OF $k(T, p)$ RATE COEFFICIENTS FOR MODELING

From the viewpoint of modeling, the ultimate goal of the kinetic analysis of pressure-dependent reaction systems is to provide reliable time-independent rate expressions $k(T, p)$ which can be incorporated into large kinetic models. The functional forms of these rate expressions can be rather complicated for multi-channel multiple wells systems, since—as we saw from the examples—the competition of product channels leads to strongly non-Arrhenius behavior. On the other hand, pressure-dependent rate constants for single-well single-channel reaction systems are comparably easy to describe. Therefore, we will divide this discussion into two sections going from simple fall-off systems to complex systems.

5.1 Single-well single-channel systems

Simple fall-off reactions are reasonably well described by Lindemann's collision activation model discussed in Section 2. It leads to an expression for the rate constant $k(T, p)$ based on k_0, k_∞, and [M] (see equation (8)). Improved treatments of single-well single-channel reactions differ only in details from the Lindemann model. Therefore, it seems natural to base a general fall-off description on an extension of equation (8):

$$k(T,p) = k_\infty(T)\frac{p_r}{1+p_r}F; \quad p_r = \frac{k_0(T)[M]}{k_\infty(T)} \tag{163}$$

Here, the "form or broadening factor" F is introduced. Both, k_0 and k_∞, are well-defined functions of the temperature and typically expressed in modified Arrhenius form. Thus, the role of the form factor is to correct

[15]At the high-pressure limit, the stabilization rate constant for $C_2H_3O_2$ is equal to the total rate constant.

the shape of the Lindemann fall-off curve to match the experimental data. Gilbert *et al.* [14] and Stewart *et al.* [105] provide parameterizations of this form factor that are implemented in modeling software such as Chemkin. Based on solutions of the MEs for a series of unimolecular reactions, Gilbert *et al.* define the broadening factor in terms of the so-called Troe formalism (or F_{cent} method) *via*

$$\log(F) = \frac{\log(F_{\text{cent}})}{1 + [(\log(p_{\text{r}}) + c)/(n - d(\log(p_{\text{r}}) + c))]^2} \tag{164}$$

with

$$c = -0.4 - 0.67\log(F_{\text{cent}})$$
$$n = 0.75 - 1.27\log(F_{\text{cent}})$$
$$d = 0.14$$

$$F_{\text{cent}} = (1 - a)\exp\left(-\frac{T}{T^{***}}\right) + a\exp\left(-\frac{T}{T^{*}}\right) + \exp\left(-\frac{T^{**}}{T}\right) \tag{165}$$

The approximation (165) contains four adjustable parameters (a, T^{***}, T^{*}, and T^{**}). Together with modified Arrhenius parameters (A, n, E_{a}) for both the low- and the high-pressure rate constants, the overall fall-off representation requires 10 parameters.

The second parameterization by Stewart *et al.* is commonly referred as the SRI formula. Here, the broadening factor F is given by

$$F = \left[a\exp\left(-\frac{b}{T}\right) + \exp\left(-\frac{T}{c}\right)\right]^{x} \tag{166}$$

which also contains four adjustable parameters (a, b, c, x). The implementation of this method in Chemkin provides even a fifth parameter, d, which scales F by d. In total 11 parameters are available to provide a good fit to the data.

In addition to the methods mentioned above, several other parameterizations to represent pressure-dependent rate constants based on k_0 and k_∞ are known; see, for example, the work by Wang and Frenklach [106], Gardiner [107], and Poole and Gilbert [108]. However, these methods did not find their way into modeling software such as Chemkin.

5.2 *Multi-well multi-channel systems*

Despite the rather large number of adjustable parameters, neither the Troe formalism nor the SRI method allows an adequate description of

the temperature and pressure dependences of apparent rate constants for multiple well, multiple channel systems [109,110]. A main reason for this is that these rate constants are not longer only determined by the physics that leads to the modified Arrhenius behavior of elementary rate constants or the simple fall-off predicted by the Lindemann concept. Instead, they are also strongly affected by the competition between different reaction channels. Since this competition can lead to a complicated function of temperature and pressure, the above methods fail.

Given that the apparent rate constants for complex reaction systems might strongly deviate from Lindemann-type rate expressions, the concept of correcting the Lindemann expression for $k(T, p)$ leads to problems.[16] Based on this conclusion, Venkatesh *et al.* [110] proposed the use of a purely mathematical approximation, Chebyshev polynomials, to represent the temperature and pressure dependences of apparent rate constants. Briefly, a Chebyshev polynomial of degree $i-1$ is defined as

$$\Phi_i(x) = \cos((i - l)\arccos(x)), \quad \text{with } x \in [-1, 1] \text{ and } i = 1, 2, \ldots \tag{167}$$

An arbitrary function $f(x)$ defined in the interval [–1, 1] can be well approximated *via*

$$f(x) \approx \sum_{k=1}^{N} c_k \Phi_k(x) \tag{168}$$

Provided $f(x)$ is known for certain values of x, the Chebyshev coefficients can be calculated analytically. Therefore, this approximation is not a fitting procedure. A second important feature is that the approximation is still good if only $M<N$ coefficients are used for the approximation.

For the representation of $k(T, p)$ data in terms of $1/T$ and $\log(P)$ we obtain the following relations:

$$\tilde{T} \leftarrow \frac{2T^{-1} - T_{\min}^{-1} - T_{\max}^{-1}}{T_{\min}^{-1} - T_{\max}^{-1}}, \quad \text{with } T_{\min} \le T \le T_{\max} \tag{169}$$

$$\tilde{p} \leftarrow \frac{2\log(p) - \log(p_{\min}) - \log(p_{\max})}{\log(p_{\max}) - \log(p_{\min})}, \quad \text{with } \log(p_{\min}) \le \log(p) \le \log(p_{\max}) \tag{170}$$

[16] However, Kazakov *et al.* [109] proposed a parameterization method, which is a generalization of the Lindemann formulation and which provides in many—though not all—cases a good description of $k(T, p)$.

$$\log(k(T,p)) = \log(k(\tilde{T},\tilde{p})) = \sum_{i=1}^{N_T}\sum_{j=1}^{N_p} \alpha_{ij}\Phi_i(\tilde{T})\Phi_j(\tilde{p}) \tag{171}$$

Equations (169) and (170) project the temperature ($1/T$) and pressure ($\log(p)$) to the required [−1, 1] interval. Equation (171) formulates the approximation as a double sum over N_T Chebyshev polynomials in T and N_p Chebyshev polynomials in p. This representation thus requires $N_T N_p$ coefficients. In practice, $N_T = 7$ and $N_p = 3$ often provide excellent approximations of $k(T, p)$ rate constants over large temperature (300–2000 K) and pressure (0.001–100 atm) ranges. The Chebyshev representation is implemented in recent Chemkin releases and the program CARRA provides rate expressions in form of Chebyshev polynomials as an output option. More details can be found in Naik *et al.* [111].

6 SUMMARY AND LOOK TO THE FUTURE

Successful modeling of complex reaction systems strongly depends on the availability of accurate temperature- and pressure-dependent rate constants. We discussed the well-known basic theory starting with single-well systems and expanding to complex multiple-channel multiwell problems. Different treatments of these systems may be distinguished by two points: (1) the method to calculate $k(E)$ and $\rho(E)$ and (2) the energy transfer model. This leads to two extreme cases of sophistication. The most accurate and physically fundamental analysis utilizes RRKM theory to calculate $k(E)$ and $\rho(E)$ and solves the time-dependent ME to describe the energy transfer process. The ME may be solved in a deterministic or stochastic way. To serve the modeling community, the results of these calculations must be translated into time-independent rate constants. Though the RRKM/ME approach is in principle the most accurate method, it comes with a price: it requires detailed knowledge of molecular properties of the reactants as well as of the transition states involved. In contrast, a QRRK/MSC analysis can yield $k(T, p)$ data based on estimated thermodynamic and kinetic data of the reactants alone. Such an approach can be very useful as a screening method to identify crucial pressure-dependent reactions in mechanism, which later may be reanalyzed more thoroughly with RRKM/ME programs. The main advantage of such a strategy is to be able to focus on crucial reactions while less important ones can still be treated in a pressure-dependent manner.

Having said this, one should note that the example cases presented here as well as several other comparisons in the literature indicated that

results from the QRRK/MSC analysis compare remarkably well with more sophisticated programs. Just because the method is simple, it does not have to give bad predictions.

Given that the theoretical background is well established one might ask what the future will bring. At least four areas that need improvements can be identified:

(1) Molecule parameters can now be obtained from *ab initio* calculations. These still have large error margins despite the enormous progress made in the last few decades. Such errors translate into large uncertainties of the kinetic input data, thus making the predictions unreliable. For example, a realistic error in the activation entropy, $\Delta S^{\#}$, of 1 entropy unit changes the corresponding rate constant by a factor of 2.7. Many factors, such as the neglect of anharmonicity effects due to the HO–RR assumption, the neglect of coupling between internal modes, the use of single determinant (HF)-based methods to calculate the electronic energy, and so on, contribute to these deficiencies. Further increases of CPU power and advances in algorithms will certainly lead to continued improvements of *ab initio* results, which in turn will improve kinetic calculations.

(2) A precise description especially of loose transition states requires the formulation of microcanonical rate constants as function of E and J, since the conservation laws for both energy and total angular momentum must be obeyed. Unimol can handle $k(E, J)$ rate constants but most kinetic studies neglect effects of the angular momentum. In the future we expect that more attention will be paid to this issue.

(3) The energy transfer process is not well understood and energy transfer values such as $\langle E_{\text{down}} \rangle$ are frequently treated as adjustable parameters and not as well-defined input data for rate prediction. Continued advances in experimental methods and more sophisticated simulations (e.g., trajectory studies) will steadily improve our basic knowledge of energy transfer mechanisms. New models such as the BRW model and similar concepts indicate that progress has been made in this field. Nevertheless, a lot of work needs to be done to make energy transfer processes truly predictable.

(4) Finally, there is clearly a need for guidelines or evaluation methods to determine the criteria a reaction system needs to fulfill in order to be described by time-independent apparent rate constants. Vice versa, it would be useful to have a list of criteria at

hand that would allow to determine under which circumstances constant rate expressions fail to provide an adequate description of the chemistry and therefore time-dependent rate expressions are needed. The example calculations presented earlier clearly demonstrate that apparent rate constants are often a very good approximation—especially if all other sources of errors are taken into account. On the other hand, the observation of incubation times in certain shock tube experiments makes clear that these systems can only be modeled with a time-dependent description of the reaction rates. Hence, it would be desirable to have tools or criteria in hand that allow a kineticist to decide for which cases conventional reaction mechanisms are appropriate or, vice versa, which problems can only adequately described by formulating and solving the underlying time-dependent ME.

Even though the kinetic analysis of pressure-dependent reactions can clearly be improved, even at this point the kineticist is already in the position to provide relatively accurate pressure-dependent rate constants. We hopefully showed that such calculations are straightforward to perform, and we anticipate that $k(T, p)$ data for many more important reactions will soon be available for modeling studies.

REFERENCES

[1] K.A. Holbrook, M.J. Pilling, S.H. Robertson, *Unimolecular Reactions*. Wiley, Chichester, 1996.
[2] R.G. Gilbert, S.C. Smith, *Theory of Unimolecular and Recombination Reactions*. Blackwell Scientific Publications, Oxford, 1990.
[3] J. Troe, H.G. Wagner, *Berichte der Bunsengesellschaft für physikalische Chemie*, **71** (1967) 937–979.
[4] D.M. Golden, R.K. Solly, S.W. Benson, *J. Phys. Chem.*, **75** (1971) 1333–1338.
[5] R.E. Weston Jr., *Int. J. Chem. Kinet.*, **18** (1986) 1259–1276.
[6] H.W. Schranz, S. Nordholm, N.D. Hamer, *Int. J. Chem. Kinet.*, **14** (1982) 543–564.
[7] A.Y. Chang, J.W. Bozzelli, A.M. Dean, *Zeitschrift fuer Physikalische Chemie*, **214** (2000) 1533–1568.
[8] J.W. Bozzelli, A.Y. Chang, A.M. Dean, *Int. J. Chem. Kinet.*, **29** (1997) 161–170.
[9] S.C. Smith, M.J. McEwan, R.G. Gilbert, *J. Chem. Phys.*, **90** (1989) 4265–4273.
[10] S.C. Smith, M.J. McEwan, J.I. Brauman, *J. Phys. Chem. A*, **101** (1997) 7311–7314.
[11] J. Troe, *J. Phys. Chem.*, **83** (1979) 114–126.
[12] J. Troe, *Berichte der Bunsengesellschaft für physikalische Chemie*, **87** (1983) 161–169.
[13] J. Troe, *J. Chem. Phys.*, **66** (1977) 4758–4775.
[14] R.G. Gilbert, K. Luther, J. Troe, *Berichte der Bunsengesellschaft für physikalische Chemie*, **87** (1983) 169–177.
[15] G.Z. Whitten, B.S. Rabinovitch, *J. Chem. Phys.*, **38** (1963) 2466–2473.

[16] I.S. Gradshteyn, I.M. Ryzhik, *Table of Integrals, Series, and Products*. Academic Press, New York, 1965.
[17] J.R. Barker, L.M. Yoder, K.D. King, *J. Phys. Chem. A*, **105** (2001) 796–809.
[18] M.J. Pilling, S.H. Robertson, *Annu. Rev. Phys. Chem.*, **54** (2003) 245–275.
[19] N.S. Snider, *J. Chem. Phys.*, **42** (1965) 548–555.
[20] S.J. Klippenstein, J.A. Miller, *J. Phys. Chem. A*, **106** (2002) 9267–9277.
[21] J.A. Miller, S.J. Klippenstein, *J. Phys. Chem. A*, **107** (2003) 2680–2692.
[22] V.M. Bedanov, W. Tsang, M.R. Zachariah, *J. Phys. Chem.*, **99** (1995) 11452–11457.
[23] V.D. Knyazev, W. Tsang, *J. Phys. Chem. A*, **103** (1999) 3944–3954.
[24] H.W. Schranz, S. Nordholm, *Chem. Phys.*, **87** (1984) 163–177.
[25] D.T. Gillespie, *J. Comput. Phys.*, **22** (1976) 403.
[26] D.T. Gillespie, *J. Phys. Chem.*, **81** (1977) 2340–2361.
[27] J.R. Barker, *Chem. Phys.*, **77** (1983) 301–318.
[28] R.G. Gilbert, M.F.T. Jordan, S.C. Smith, G.P. Knight, *UNIMOL*. School of Chemistry, Sydney University, NSW, Australia, 1994.
[29] K.F. Lim, R.G. Gilbert, *J. Chem. Phys.*, **84** (1986) 6129–6140.
[30] V. Mokrushin, V. Bedanov, W. Tsang, M. Zachariah, V. Knyazev, *ChemRate*. NIST, Gaithersburg, MD, 1996–2002.
[31] V.D. Knyazev, W. Tsang, *J. Phys. Chem. A*, **104** (2000) 10747–10765.
[32] J. R. Barker, N. F. Ortiz, J. M. Preses, L. L. Lohr, A. Maranzana, P. J. Stimac. MultiWell Program Suite. Department of Atmospheric, Oceanic and Space Sciences, Department of Chemistry, University of Michigan Ann Arbor, MI 48109-2143, USA.
[33] J.R. Barker, *Int. J. Chem. Kinet.*, **33** (2001) 232–245.
[34] J.R. Barker, N.F. Ortiz, *Int. J. Chem. Kinet.*, **33** (2001) 246–261.
[35] A.M. Dean, *J. Phys. Chem.*, **89** (1985) 4600–4608.
[36] A.M. Dean, J.W. Bozzelli, E.R. Ritter, *Combust. Sci. Technol.*, **80** (1991) 63–85.
[37] C.Y. Sheng, J.W. Bozzelli, A.M. Dean, A.Y. Chang, *J. Phys. Chem. A*, **106** (2002) 7276–7293.
[38] For inquiries on the status/availability of this code, please send an email to hcarsten@mines.edu
[39] S.J. Klippenstein, A.F. Wagner, R.C. Dunbar, D.M. Wardlaw, S.H. Robertson, J.A. Miller, *VARIFLEX*. 1999.
[40] M. Garcia-Viloca, C. Alhambra, J. Corchado, M.L. Sanchez, J. Villa, J. Gao, D.G. Truhlar. CHARMMRATE. Department of Chemistry and Supercomputer Institute, University of Minnesota, Minneapolis, MN 55455-0431, USA, 2002.
[41] J.T. McKinnon, G. Murray, MarkNimlos, D. Hodgson, Z. Zhang, P. Guzman, B. Scroggs, B. Vandermeer, D. Ward, *OpenChem Workbench*. Colorado School of Mines, Golden, CO 80401, USA, 2003.
[42] T.N. Truong, T. Cook, M. Nayak, C. Boonyasiriwat, L.-T.T. Tran, S. Zhang, *CSEO*. 2003.
[43] M.W. Chase, Jr., C.A. Davies, J.R. Downey Jr., D.J. Frurip, R.A. McDonald, A.N. Syverud, *J. Phys. Chem. Ref. Data* (Suppl. 14) (1985) 1.
[44] http://webbook.nist.gov/chemistry
[45] R. Atkinson, D.L. Baulch, R.A. Cox, J.N. Crowley, R.F. Hampson, R.G. Hynes, M.E. Jenkin, M.J. Rossi, J. Troe, *Atmos. Chem. Phys.*, **4** (2004) 1461–1738.
[46] http://kinetics.nist.gov/index.php
[47] B.E. Poling, J.M. Prausnitz, O'J.P. Connell, *The Properties of Gases and Liquids*. McGraw-Hill, New York, 2000.

[48] R.J. Kee, F.M. Rupley, J.A. Miller, M.E. Coltrin, J.F. Grcar, E. Meeks, H.K. Moffat, A.E. Lutz, G. Dixon-Lewis, M.D. Smooke, J. Warnatz, G.H. Evans, R.S. Larson, R.E. Mitchell, L.R. Petzold, W.C. Reynolds, M. Caracotsios, W.E. Steward, P. Glarborg, C. Wang, O. Adigun, *Chemkin Collection*. Reaction Design, Inc., San Diego, CA, 2000.
[49] S.W. Benson, *Thermochemical Kinetics*. Wiley, New York, 1976.
[50] E.R. Ritter, J.W. Bozzelli, *Int. J. Chem. Kinet.*, **23** (1991) 767–778.
[51] T.H. Lay, J.W. Bozzelli, A.M. Dean, E.R. Ritter, *J. Phys. Chem.*, **99** (1995) 14514–14527.
[52] R. Sumathi, H.-H. Carstensen, W.H. Green Jr., *J. Phys. Chem. A*, **105** (2001) 6910–6925.
[53] R. Sumathi, H.-H. Carstensen, W.H. Green Jr., *J. Phys. Chem. A*, **105** (2001) 8969–8984.
[54] R. Sumathi, H.-H. Carstensen, W.H. Green Jr., *J. Phys. Chem. A*, **106** (2002) 5474–5489.
[55] R. Sumathi, W.H. Green Jr., *Theor. Chem. Acc.*, **108** (2002) 187–213.
[56] H.-H. Carstensen, A.M. Dean, unpublished data, 2006.
[57] W. Forst, *J. Phys. Chem.*, **76** (1972) 342–348.
[58] R.S. Brokaw, *Ind. Eng. Chem. Prog. Des. Dev.*, **8** (1969) 240–253.
[59] H. Wang, M. Frenklach, *Combust. Flame*, **96** (1994) 163–170.
[60] D.A. McQuarrie, J.D. Simon, *Molecular Thermodynamics*. University Science Books, Sausalito, CA, 1999.
[61] A.L.L. East, L. Radom, *J. Chem. Phys.*, **106** (1997) 6655–6674.
[62] K.S. Pitzer, W.D. Gwinn, *J. Chem. Phys.*, **10** (1942) 428–440.
[63] R.B. McClurg, R.C. Flagan, W.A. Goddard III, *J. Chem. Phys.*, **106** (1997) 6675–6680.
[64] P.Y. Ayala, H.B. Schlegel, *J. Chem. Phys.*, **108** (1998) 2314–2325.
[65] M.J. Frisch, G.W. Trucks, H.B. Schlegel, G.E. Scuseria, M.A. Robb, J.R. Cheeseman, V.G. Zakrzewski, J.A. Montgomery Jr., R.E. Stratmann, J.C. Burant, S. Dapprich, J.M. Millam, A.D. Daniels, K.N. Kudin, M.C. Strain, O. Farkas, J. Tomasi, V. Barone, M. Cossi, R. Cammi, B. Mennucci, C. Pomelli, C. Adamo, S. Clifford, J. Ochterski, G.A. Petersson, P.Y. Ayala, Q. Cui, K. Morokuma, D.K. Malick, A.D. Rabuck, K. Raghavachari, J.B. Foresman, J. Cioslowski, J.V. Ortiz, A.G. Baboul, B.B. Stefanov, G. Liu, A. Liashenko, P. Piskorz, I. Komaromi, R. Gomperts, R.L. Martin, D.J. Fox, T. Keith, M.A. Al-Laham, C.Y. Peng, A. Nanayakkara, M. Challacombe, P.M.W. Gill, B. Johnson, W. Chen, M.W. Wong, J.L. Andres, C. Gonzalez, M. Head-Gordon, E.S. Replogle, J.A. Pople, *Gaussian 98*. Gaussian, Inc., Pittsburgh, PA, 1998.
[66] A. Nicolaides, A. Rauk, M.N. Glukhovtsev, L. Radom, *J. Phys. Chem.*, **100** (1996) 17460–17464.
[67] L.A. Curtiss, K. Raghavachari, P.C. Redfern, J.A. Pople, *J. Chem. Phys.*, **106** (1997) 1063–1079.
[68] L.A. Curtiss, K. Raghavachari, P.C. Redfern, B.B. Stefanov, *J. Chem. Phys.*, **108** (1998) 692–697.
[69] K. Raghavachari, B.B. Stefanov, L.A. Curtiss, *J. Chem. Phys.*, **106** (1997) 6764–6767.
[70] C.F. Melius, *Proc. Combust. Inst.*, **21** (1986) 1953.
[71] G.A. Petersson, D.K. Malick, W.G. Wilson, J.W. Ochterski, J.A. Montgomery Jr., M.J. Frisch, *J. Chem. Phys.*, **109** (1998) 10570–10579.

[72] M. Saeys, M.-F. Reyniers, G.B. Marin, V.V. Speybroeck, M. Waroquier, *J. Phys. Chem. A*, **107** (2003) 9147–9159.
[73] E. Wigner, *Zeitschrift fuer Physikalische Chemie B*, **19** (1932) 203–216.
[74] W.H. Miller, *J. Am. Chem. Soc.*, **101** (1979) 6810–6814.
[75] M. Schwartz, P. Marshall, R.J. Berry, C.J. Ehlers, G.A. Petersson, *J. Phys. Chem. A*, **102** (1998) 10074–10081.
[76] T.V. Albu, J.C. Corchado, D.G. Truhlar, *J. Phys. Chem. A*, **105** (2001) 8465–8487.
[77] B.J. Lynch, D.G. Truhlar, *J. Phys. Chem. A*, **106** (2002) 842–846.
[78] W.-P. Hu, Y.-P. Liu, D.G. Truhlar, *J. Chem. Soc., Faraday Trans.*, **90** (1994) 1715–1725.
[79] I.G. Pitt, R.G. Gilbert, K.R. Ryan, *J. Phys. Chem.*, **99** (1995) 239–247.
[80] L.B. Harding, Y. Georgievskii, S.J. Klippenstein, *J. Phys. Chem. A*, **109** (2005) 4646–4656.
[81] S.J. Klippenstein, Y. Georgievskii, L.B. Harding, *Phys. Chem. Chem. Phys.*, **8** (2006) 1133–1147.
[82] T. Beyer, D.F. Swinehart, *Commun. Assoc.*, **16** (1973) 379.
[83] S.E. Stein, B.S. Rabinovitch, *J. Chem. Phys.*, **58** (1973) 2438–2445.
[84] R. Cambi, D. Cappelletti, G. Liuti, F. Pirani, *J. Chem. Phys.*, **95** (1991) 1852–1861.
[85] J.C. Slater, J.G. Kirkwood, *Phys. Rev.*, **37** (1931) 682–697.
[86] P. Paul, J. Warnatz, *Proc. Combust. Inst.*, **27** (1998) 495–504.
[87] K.F. Lim, R.G. Gilbert, *J. Chem. Phys.*, **92** (1990) 1819–1830.
[88] F. Caralp, P. Devolder, C. Fittschen, N. Gomez, H. Hippler, R. Mereau, M.T. Rayez, F. Striebel, B. Viskolcz, *Phys. Chem. Chem. Phys.*, **1** (1999) 2935–2944.
[89] J.W. Bozzelli, A.M. Dean, *J. Phys. Chem.*, **94** (1990) 3313–3317.
[90] J.D. DeSain, S.J. Klippenstein, J.A. Miller, C.A. Taatjes, *J. Phys. Chem. A*, **107** (2003) 4415–4427.
[91] J.A. Miller, S.J. Klippenstein, S.H. Robertson, *Proc. Combust. Inst.*, **28** (2000) 1479–1486.
[92] J.A. Miller, S.J. Klippenstein, *Int. J. Chem. Kinet.*, **33** (2001) 654–668.
[93] E.W. Kaiser, T.J. Wallington, J.M. Andino, *Chem. Phys. Lett.*, **168** (1990) 309–313.
[94] E.W. Kaiser, I.M. Lorkovic, T.J. Wallington, *J. Phys. Chem.*, **94** (1990) 3352–3354.
[95] E.W. Kaiser, *J. Phys. Chem.*, **99** (1995) 707–711.
[96] E.W. Kaiser, *J. Phys. Chem. A*, **106** (2002) 1256–1265.
[97] T.J. Wallington, J.M. Andino, E.W. Kaiser, S.M. Japar, *Int. J. Chem. Kinet.*, **21** (1989) 1113–1122.
[98] I.R. Slagle, E. Ratajczak, D. Gutman, *J. Phys. Chem.*, **90** (1986) 402–407.
[99] A.F. Wagner, I.R. Slagle, D. Sarzynski, D. Gutman, *J. Phys. Chem.*, **94** (1990) 1853–1868.
[100] I.C. Plumb, K.R. Ryan, *Int. J. Chem. Kinet.*, **13** (1981) 1011–1028.
[101] C. Sheng, J.W. Bozzelli, A.M. Dean, Presented at *2nd Joint Meeting of the U.S. Sections of the Combustion Institute*, Oakland, CA, 2001.
[102] J.W. Bozzelli, A.M. Dean, *J. Phys. Chem.*, **97** (1993) 4427–4441.
[103] A.M. Mebel, E.W.G. Diau, M.C. Lin, K. Morokuma, *J. Am. Chem. Soc.*, **118** (1996) 9759–9771.
[104] S.J. Klippenstein, J. Georgievskii, J.A. Miller, J.A. Nummela, B.K. Carpenter, P.R. Westmoreland, Presented at *Joint Meeting of the U.S. Sections of the Combustion Institute*, 2003.
[105] P.H. Stewart, C.W. Larson, D.M. Golden, *Combust. Flame*, **75** (1989) 25–31.
[106] H. Wang, M. Frenklach, *Chem. Phys. Lett.*, **205** (1993) 271–276.

[107] W.C. Gardiner, Presented at *12th IMACS World Congress on Scientific Computations*, Paris, 1988.
[108] J.S. Poole, R.G. Gilbert, *Int. J. Chem. Kinet.*, **26** (1994) 273–281.
[109] A. Kazakov, H. Wang, M. Frenklach, *J. Phys. Chem.*, **98** (1994) 10598–10605.
[110] P.K. Venkatesh, A.Y. Chang, A.M. Dean, M.H. Cohen, R.W. Carr, *AIChE J.*, **43** (1997) 1331–1340.
[111] C. Naik, H.-H. Carstensen, A.M. Dean, Presented at *WSS 2002 Spring Meeting of the Combustion Institute*, San Diego, CA, 2002. An executable (DOS) converting k(P,T) data into Chebyshev polynomials can be found on the companion CD or requested by sending an email to hcarsten@mines.edu

Chapter 5

Constructing Reaction Mechanisms

Mark T. Swihart

1 INTRODUCTION

In this chapter, we focus on the development of detailed mechanisms of elementary chemical reactions. This is particularly important in cases where little of the chemistry may be known *a priori*, such as vapor-phase processing of inorganic materials. However, it is also relevant in areas such as combustion, where much of the chemistry and many reaction rate parameters are known, particularly when considering atypical reaction conditions, such as an unusual fuel or a catalytic combustion process that involves both surface and vapor-phase reactions. In constructing reaction mechanisms and computing species properties and reaction rate parameters, we will rely heavily on the tools developed in previous chapters, including group additivity, quantum chemistry, transition state theory, and specialized theories of unimolecular reactions. Detailed chemical kinetic modeling has been quite successful in making quantitative predictions about some systems, particularly for combustion and pyrolysis of small hydrocarbons and for atmospheric chemistry. Both these successes involve reactions of small molecules made up of light elements that are amenable to treatment by computational quantum chemistry and reaction rate theories. In addition, for both of these cases there is a substantial database of evaluated chemical kinetic data that can be used in constructing detailed reaction mechanisms [1–6].

There are many other systems, particularly those important in the processing of inorganic materials, that could potentially be modeled with similar success using detailed chemical kinetic modeling. However, in these cases we generally have very few experimentally measured rate parameters and may not even have experimentally determined thermochemical properties (enthalpy of formation, standard entropy, etc.) for many of the important chemical species. While experiments are still the most reliable source for most of the needed data, they are also in many

Comprehensive Chemical Kinetics, Volume 42, 185–242

ISSN: 0069-8040/doi:10.1016/S0069-8040(07)42005-2

cases prohibitively expensive and time-consuming. Therefore, we often turn to quantum chemistry calculations or more empirical estimation methods for much of these data. As a result, these reaction mechanisms will generally have greater uncertainties in rate parameters, and even in reaction paths, than those involving small hydrocarbons. In some cases, the number of possible species and reactions may become so large that it is not possible, or at least not reasonable, to construct the detailed reaction mechanism manually. In those cases, we may apply methods of automated reaction mechanism generation, in which the computer is used not only in the estimation or calculation of species properties and reaction rate parameters, but also in determining what reactions should be included in the mechanism.

The goal of the approach described in this chapter is to develop a detailed reaction mechanism, made up of elementary reactions, for some overall chemical transformation. The reaction mechanism consists of a list of elementary reactions occurring in the system under conditions of interest, along with rate parameters for those reactions and thermochemical properties of all the chemical species participating in the reactions. To illustrate the methodology used for doing this, we will consider some representative examples, including the thermal decomposition of the chlorosilanes and the thermal decomposition of aluminum chloride. We will consider primarily gas-phase reactions, though the methodology used is more general and can be applied with appropriate modifications in the liquid phase or at surfaces. Gas-surface reactions, in particular, are of great interest in many material processing contexts, but will not be explicitly considered here. The aluminum chloride chemistry illustrates many of the difficulties that can come up in the construction of reaction mechanisms where little of the chemistry is known *a priori*. Although this system will be used as an 'example problem' here, some aspects of it are actually quite complex. It was worked out over the course of several years and the results were presented in several publications [7–10]. While the presentation in this chapter focuses on what to do in the absence of substantial data, the same approaches are also applicable to the construction of new reaction mechanisms within systems for which there is a substantial amount of kinetic and thermochemical data available.

The overall process for constructing a detailed reaction mechanism is illustrated schematically in Fig. 1. As shown there, we can envision this process as a sequence of steps in which the primary information flow is from one step to the next, vertically downward in the figure. However, as indicated by the curved arrows in the figure, there is also feedback of information from later steps to earlier ones, such that the whole process can lead to iterative refinement of the reaction mechanism. There are

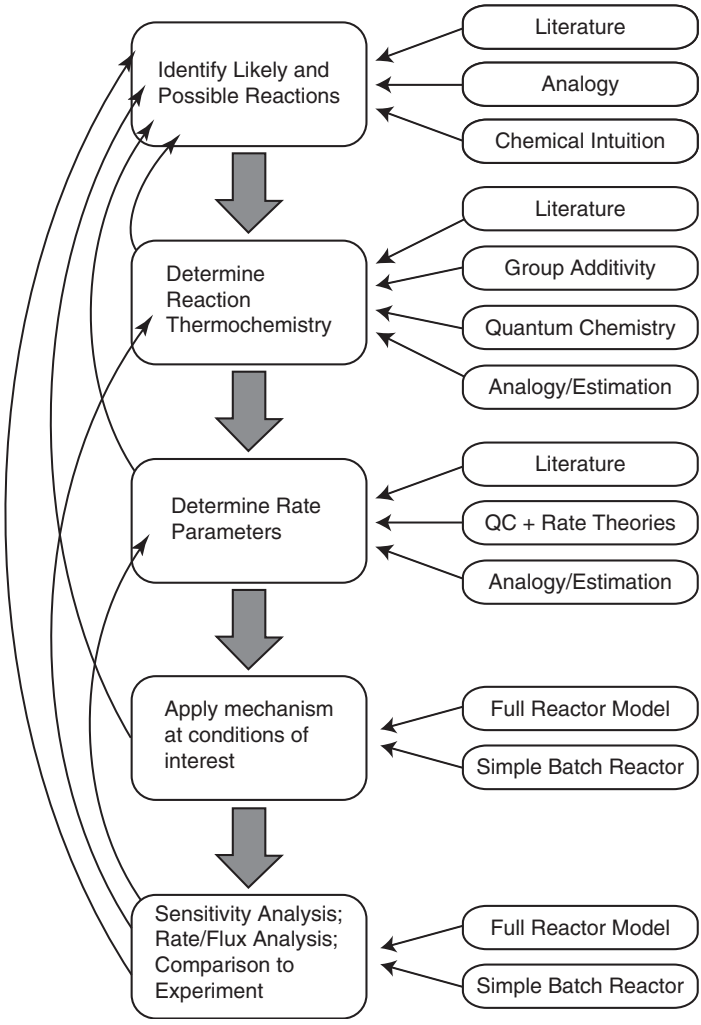

Fig. 1. Schematic illustration of the overall process of constructing a reaction mechanism. The structure of this chapter follows this schematic.

a range of different methods or levels of treatment that can be used for each step in this process, and often more than one of these methods or levels of treatment will be used in each step. The structure of the remainder of this chapter follows that of Fig. 1, with sections on identifying reactions, determining species thermochemistry, determining rate parameters, applying the reaction mechanism, and validating and refining the mechanism based on sensitivity analysis, rate or flux analysis, and comparison with any available experiments.

2 IDENTIFYING REACTIONS

The process of identifying or postulating the elementary reactions that may occur under given conditions or that may lead to a given overall chemical transformation is perhaps the most subjective and least algorithmic step in the entire process of constructing a reaction mechanism. It is also the most essential component, since if the correct reaction paths are not considered, then the rest of the process of determining thermochemistry, determining rate parameters, and so on is irrelevant. Because it is unlikely that one will identify all potentially important reactions and chemical species in the first attempt, it is essential that this step be repeated with feedback from the later steps. For example, one will often postulate reactions that turn out to be thermodynamically or kinetically unfavorable and which can therefore be eliminated after determination of the reaction thermochemistry or rate parameters. Likewise, application of the mechanism at conditions of interest may give unexpected results, such as a high concentration of a species expected to be a reactive intermediate, that lead one to postulate new reaction paths. Sensitivity analysis and reaction rate or flux analysis may demonstrate that some postulated reactions or chemical species are unimportant and can be eliminated. Comparison with experimental results on the overall chemical transformation may reveal deficiencies that lead one to introduce new reactions into the mechanism. As shown in Fig. 1, there are essentially three sources for identifying or postulating the elementary reactions that make up the reaction mechanism for some overall process: (1) the literature on the system of interest; (2) analogies with similar systems; and (3) one's own imagination or chemical intuition. Below, we briefly consider each of these.

2.1 Finding reactions and reaction mechanisms in the literature

A useful starting point for accessing the literature is the NIST Chemical Kinetics Database [11], available online at http://kinetics.nist.gov. According to the introduction to the database, it includes 'essentially all reported kinetics results for thermal gas-phase chemical reactions.' Thus, by searching this database, one can find references related to almost any gas-phase reaction for which reaction rate measurements have been made. Of course, it will not provide information about the vast number of reactions that have been observed and reported in the literature, but for which reaction rates have not been measured. As an example, suppose we are interested in the thermal decomposition of $AlCl_3$ or in the combustion of aluminum. We might expect the species AlCl to be an important

intermediate in both of these situations. Searching the NIST Chemical Kinetics Database for all reactions for which AlCl is either a reactant or a product gives the results shown in Table 1. Nine reactions were found for which AlCl is a reactant, and four reactions were found for which AlCl is a product. There is more than one report for the last two reactions shown in the table. For each reaction the temperature range of the study and the reported reaction order and rate expression are given. The final column, labeled 'squib,' gives an abbreviated reference to the original study. In addition, the rate expressions can be plotted and compared. Information on the type of measurement or calculation used in each study and the full journal citation are also available. In many cases, rate expressions for different reactions are reported in the same paper. In this case, the 16 rate expressions given in Table 1 come from just seven different papers.

A more comprehensive, but not always more useful, way to access the literature is through the databases provided by the Chemical Abstracts Service (CAS), which can be accessed through the SciFinder or STN fee-based services. In addition to the traditional Chemical Abstracts literature index (CAPLUS), these provide access to the CASREACT database, which allows searching for reactions directly. However, the CASREACT database focuses primarily on solution phase organic synthesis and it may be difficult to find gas-phase elementary reactions of interest in it. For example, if we were building a reaction mechanism for the thermal decomposition of $AlCl_3$, we might start by looking for reactions involving $AlCl_3$ itself. There are no reactions in the NIST Chemical Kinetics Database with $AlCl_3$ as a reactant or a product. So, the next step might be to look for reactions of $AlCl_3$ in the CAS databases. Using SciFinder Scholar, the academic version of the SciFinder interface to the CAS databases, a search for $AlCl_3$ returns 27,233 references to $AlCl_3$ in the databases. A search for reactions of $AlCl_3$ in the CASREACT database returns no reactions with $AlCl_3$ in the role of 'reactant' or 'product,' but returns 96,036 reactions with $AlCl_3$ in the role of 'reagent' and 15,271 reactions with $AlCl_3$ in the role of 'catalyst.' This reminds us that $AlCl_3$ is a very popular Lewis acid catalyst in organic chemistry, but it does not provide any information useful in constructing a gas-phase reaction mechanism for the formation or decomposition of $AlCl_3$. So, the next step is to try to refine the 27,233 literature references to $AlCl_3$ to pick out any that might be relevant to gas-phase reactions. Refining the search by research topic using the phrase 'reaction mechanism or reaction kinetics' leaves 1210 references, which is probably still too long a list to even read all the titles. Further refining the search by research topic using the phrase 'gas or vapor' yields a list of 125 references. A quick manual review of the titles of these 125 papers resulted in

TABLE 1
Results from NIST Kinetics Database for reactions involving AlCl

Reaction	Temperature range (K)	Rate expression[a]	Order	Squib
$AlCl + Cl \rightarrow Al + Cl_2$	300–1000	$6.08 \times 10^{-11}\, e^{-18.22/RT}$	2	1979GAR/TRU5207
$H\bullet + AlCl \rightarrow AlH + Cl$	300–1000	$7.37 \times 10^{-11}\, e^{-11.43/RT}$	2	1979GAR/TRU5207
$N_2O + AlCl \rightarrow$ Products	700–990	$5.6 \times 10^{-11}\, e^{-14.67/RT}$	2	1993FUT/FON7222-7227
$Cl_2 + AlCl \rightarrow AlCl_2 + Cl$	400–1020	$9.55 \times 10^{-11}\, e^{-1.22/RT}$	2	1989ROG/MAR1118
$O_2 + AlCl \rightarrow$ Products	490–1750	$1.14 \times 10^{-16}(T/298\,\mathrm{K})^{4.57}\, e^{0.61/RT}$	2	1988ROG/FON943
$HCl + AlCl \rightarrow H\bullet + AlCl_2$	1330–1610	$1.1 \times 10^{-11}\, e^{-26.03/RT}$	2	1990SLA/FON375
$SO_2 + AlCl \rightarrow$ Products	800–1100	$< 5.0 \times 10^{-14}$	2	1993FUT/FON7222-7227
$CO_2 + AlCl \rightarrow CO + OAlCl$	1180–1780	$2.51 \times 10^{-12}\, e^{-15.00/RT}$	2	1986ROG/FON413
$CO_2 + AlCl \rightarrow$ Products	900–1790	$1.16 \times 10^{-15}(T/298\,\mathrm{K})^{3.00}\, e^{-7.75/RT}$	2	1993FUT/FON7222-7227
$AlH + Cl \rightarrow H\bullet + AlCl$	1000–4000	$4.48 \times 10^{-13}\, e^{-1.40/RT}$	2	1967MAY/SCH837-844
$Al + BeCl \rightarrow Be + AlCl$	1000–4000	$1.66 \times 10^{-13}\, e^{-4.39/RT}$	2	1967MAY/SCH837-844
$Al + Cl_2 \rightarrow AlCl + Cl$	425–875	$7.85 \times 10^{-10}\, e^{-1.55/RT}$	2	1989ROG/MAR1118
	1000–4000	$2.82 \times 10^{-13}\, e^{-13.49/RT}$	2	1967MAY/SCH837-844
$Al + HCl \rightarrow H\bullet + AlCl$	475–1280	$1.52 \times 10^{-10}\, e^{-1.60/RT}$	2	1989ROG/MAR1118
	300–1000	$3.29 \times 10^{-10}\, e^{-36.76/RT}$	2	1979GAR/TRU5207
	1000–4000	$5.48 \times 10^{-13}\, e^{-7.79/RT}$	2	1967MAY/SCH837-844

[a]Pre-exponential factor is in cm^3/sec, for use with concentration units of molecules per cm^3. Activation energy is for R in kcal/mol and T in Kelvins.

TABLE 2
Relevant references to $AlCl_3$ found using SciFinder Scholar

1	Kohlschutter H.W., Hantelmann P., Diener K., Schilling H.: Basic aluminum chlorides. *Zeitschrift fuer Anorganische und Allgemeine Chemie* 1941, **248**:319–344
2	Blau M., Carnall W.T., Willard J.E.: The exchange reaction between hydrogen chloride and aluminum chloride. *J. Am. Chem. Soc.* 1952, **74**:5762–5763
3	Hirschwald W., Kacke O.: Velocity of the reaction $2Al + AlCl_3 \rightarrow 3AlCl$. *Zeitschrift fuer Erzbergbau und Metallhuettenwesen* 1958, **11**:99–104
4	Alder H.P., Geisser H., Baiker A., Richarz W.: The chlorination of alumina. A comparison of the kinetics with different reduction agents. *Light Met. (Warrendale, PA, United States)* 1979:337–352
5	Pauleau Y., Bouteville A., Hantzpergue J.J., Remy J.C., Cachard A.: Thermodynamics and kinetics of chemical vapor deposition of aluminum nitride films. *J. Electrochem. Soc.* 1980, **127**:1532–1537
6	Szabo I., Blickle T., Ujhidy A., Jelinko R.: Kinetics of aluminum oxide chlorination. 1. The mechanism and mathematical model. *Ind. Eng. Chem. Res.* 1991, **30**:292–298
7	Meeks E., Ho P., Buss R.: Modeling aluminum etch chemistry in high density plasmas. *Proc. Electrochem. Soc.* 1997, **97-9**:283–290
8	Nitodas S.F., Sotirchos S.V.: Co-deposition of silica, alumina, and aluminosilicates from mixtures of CH_3SiCl_3, $AlCl_3$, CO_2, and H_2. Thermodynamic analysis and experimental kinetics investigation. *Chemical Vapor Deposition* 1999, **5**:219–231
9	Schierling M., Zimmermann E., Neuschutz D.: Deposition kinetics of Al_2O_3 from $AlCl_3$–CO_2–H_2–HCl gas mixtures by thermal CVD in a hot-wall reactor. *Journal de Physique IV: Proceedings* 1999, **9**:85–91
10	Egashira Y., Tanaka H., Mina T., Mori N., Ueyama K.: Evaluation of gas phase reaction rate constant by deposition profile analysis for in-situ counter diffusion CVD. *Proc. Electrochem. Soc.* 2000, **2000-13**:97–104
11	Auger M.L., Sarin V.K.: A kinetic investigation of CVD mullite coatings on Si-based ceramics. *Int. J. Refractory Met. Hard Mater.* 2001, **19**:479–494
12	Sotirchos S.V., Nitodas S.F.: Effects of residence time and reaction conditions on the deposition of silica, alumina, and aluminosilicates from CH_3SiCl_3, $AlCl_3$, CO_2, and H_2 mixtures. *Chem. Vapor Deposition* 2001, **7**:157–166
13	Swihart M.T., Catoire L.: Reactions in the Al–H–Cl system studied by ab initio molecular orbital and density functional methods. *J. Phys. Chem. A* 2001, **105**:264–273
14	Catoire L., Swihart M.T.: High-temperature kinetics of $AlCl_3$ decomposition in the presence of additives for chemical vapor deposition. *J. Electrochem. Soc.* 2002, **149**:C261–C267
15	Nitodas S.F., Sotirchos S.V.: Homogeneous and heterogeneous chemistry models of the codeposition of silica, alumina, and aluminosilicates. *J. Electrochem. Soc.* 2002, **149**:C555–C566
16	Nitodas S.F., Sotirchos S.V.: Development and validation of a mathematical model for the chemical vapor deposition of alumina from mixtures of aluminum trichloride, carbon dioxide, and hydrogen. *J. Electrochem. Soc.* 2002, **149**:C130–C141
17	Heyman A., Musgrave C.B.: A quantum chemical study of the atomic layer deposition of Al_2O_3 using $AlCl_3$ and H_2O as precursors. *J. Phys. Chem. B* 2004, **108**:5718–5725
18	Baronov S.B., Berdonosov S.S., Melikhov I.V., Kuz'micheva Y.V.: Mechanism of the thermohydrolysis of aluminum chloride vapors. *Russ. J. Phys. Chem.* 2005, **79**:803–809

the list of 18 papers shown in Table 2, which would be a good starting point for constructing a reaction mechanism for $AlCl_3$ formation or decomposition.

Of course, there are many other useful literature indexes and databases that can be searched, including the Science Citation Index, the Beilstein and Gmelin databases, and others. However, searching for a few key species in the manner described above will provide a good entrance into

the literature. Starting from those papers, one can follow 'citation trails' forward and backward in time to uncover any paper not found in the initial search. In addition to looking up relevant references in the papers discovered in the initial search, one should use an index such as Chemical Abstracts or the Science Citation Index to find papers that have cited the most relevant sources already identified. By moving both forward and backward through the literature in this way, one can fairly quickly find whatever information is available on the system of interest.

2.2 Identifying reactions by analogy

In some cases where the chemistry of a particular system is not well known, the chemistry of a similar system may be better established. In these cases, it can be useful to construct a preliminary reaction mechanism based on known reactions in the similar system. Of course, there are cases where superficially similar systems undergo different types of reactions. An example of an analogy that should work well is the development of reaction mechanisms for the Sn–H–C–Cl system based on known reaction mechanisms for the Si–H–C–Cl system. High-level quantum chemistry calculations show that the bonding and the relative strength of different bonds to tin in the Sn–H–C–Cl system are very similar to those in the Si–H–C–Cl system [12]. Table 3 shows the computed bond energies for the Si–H–Cl [13] and Sn–H–Cl [12] systems. Comparing the bond strengths in the table shows that while the bonds to tin are uniformly weaker than those to silicon, many of the same patterns are present. In both cases, the bonds to chlorine are ~20% stronger than the bonds to hydrogen in the saturated (SiH_xCl_{4-x} or SnH_xCl_{4-x}) compounds. In both cases, the second H or Cl atom is much easier to remove than the first. That is, the bond strengths in the SiH_xCl_{3-x} and SnH_xCl_{3-x} are much smaller than in the corresponding SiH_xCl_{4-x} and SnH_xCl_{4-x} compounds. In both cases, this difference between the first and second bond dissociation energies increases with increasing chlorination, and in both cases the third bond dissociation energy is larger than the second and comparable to the first. As a result of this strong–weak–strong pattern of bond dissociation energies, the decomposition of silanes and chlorosilanes proceeds primarily through reactions of divalent silylenes (SiX_2) species, rather than silyl radicals (SiX_3) species. Based on the patterns of bond strengths seen in Table 3, we would expect this also to be the case for the corresponding stannanes and chlorostannanes. Thus, a natural starting point for constructing reaction mechanisms involving the chlorostannanes would be reaction mechanisms that have been developed for the chlorosilanes [14–16].

TABLE 3
BAC-MP4 bond strengths in Sn–H–Cl and Si–H–Cl compounds

Bond energy at 298 K (kcal/mol)[a]		Bond energy at 298 K (kcal/mol)[a]	
Sn–H bonds[b]		Si–H bonds[c]	
SnH_4	74.9	SiH_4	91.3
SnH_3Cl	74.2	SiH_3Cl	92.0
SnH_2Cl_2	72.3	SiH_2Cl_2	92.5
$SnHCl_3$	70.3	$SiHCl_3$	93.2
SnH_3	48.4	SiH_3	69.4
SnH_2Cl	38.6	SiH_2Cl	60.0
$SnHCl_2$	25.5	$SiHCl_2$	49.9
SnH_2	62.5	SiH_2	78.3
HSnCl	59.9	HSiCl	74.0
SnH	55.7	SiH	68.4
Sn–Cl bonds[b]		Si–Cl bonds[c]	
SnH_3Cl	90.3	SiH_3Cl	108.4
SnH_2Cl_2	90.3	SiH_2Cl_2	111.3
$SnHCl_3$	87.8	$SiHCl_3$	112.1
$SnCl_4$	84.2	$SiCl_4$	111.4
SnH_2Cl	64.5	SiH_2Cl	85.9
$SnHCl_2$	56.6	$SiHCl_2$	78.8
$SnCl_3$	43.0	$SiCl_3$	68.8
HSnCl	88.4	HSiCl	104.1
$SnCl_2$	91.0	$SiCl_2$	102.9
SnCl	84.2	SiCl	98.6

[a]Bond energy is defined as the standard enthalpy change at 298 K for the bond-breaking reaction.
[b]Bond energies for tin compounds are from Allendorf and Melius [12].
[c]Bond energies for silicon compounds were computed from heats of formation given in Ho and Melius [13].

Of course, such analogies do not always work out so well. A simple example of an analogy that would not work so well would be the construction of a reaction mechanism for the decomposition of silane (SiH_4) by analogy with methane (CH_4). Despite the fact that silicon is immediately below carbon in group 4 of the periodic table, it turns out that the reactivities of silane and methane are very different. Methane does not exhibit the alternating strong–weak–strong pattern of bond dissociation energies mentioned above for silanes and stannanes. Instead, removing a second hydrogen from methane is slightly more difficult than removing the first one. As a result, methyl radicals (CH_3) are the key reactive intermediates in methane chemistry, and their reactivity is much different than that of divalent silylenes (SiH_2) that are the key reactive intermediates in silane chemistry.

2.3 *Identifying reactions based on 'chemical intuition,' or just making it up*

For some systems there may not be sufficient information in the literature to construct a preliminary reaction mechanism, and there may not be any obviously analogous system on which to base a new reaction mechanism. In this case, one must simply guess or intuit the possible reactions that can occur and then refine the mechanism later based on feedback from subsequent steps. This can be regarded as a 'brainstorming' phase of problem solving in which it is best to err on the side of including unlikely possibilities that may be easily ruled out later. Continuing with the example of $AlCl_3$ decomposition, suppose we began with no information at all about the possible species and reactions involved. Suppose also that we will be decomposing $AlCl_3$ in the presence of H_2, so that the only elements involved are Al, Cl, and H. We could be considering an overall transformation such as

$$AlCl_3 + H_2 \rightarrow AlCl + 2HCl \tag{1}$$

or

$$AlCl_3 + \tfrac{3}{2}H_2 \rightarrow Al + 3HCl \tag{2}$$

or perhaps the reverse process, in which aluminum atoms react with HCl to yield $AlCl_3$. The overall $AlCl_3$ decomposition (equation (1) or (2)), which generates reactive aluminum-containing intermediates might be relevant to CVD of aluminum from $AlCl_3$. Under most conditions, some sink for the Al atoms, such as a surface reaction, would be required to make the above transformations proceed. However, for the moment we will only consider the possible reactions in the gas phase.

So, we begin with the reactant, $AlCl_3$, and imagine the possible reactions it might undergo. We can imagine $AlCl_3$ decomposing either by a simple bond-breaking reaction (3) or by Cl_2 elimination (4):

$$AlCl_3 \leftrightarrow AlCl_2 + Cl \tag{3}$$

$$AlCl_3 \leftrightarrow AlCl + Cl_2 \tag{4}$$

The Cl atoms produced in (3) could then abstract a Cl atom from $AlCl_3$, $AlCl_2$, or AlCl, or they could abstract an H from H_2:

$$AlCl_3 + Cl \leftrightarrow AlCl_2 + Cl_2 \tag{5}$$

$$AlCl_2 + Cl \leftrightarrow AlCl + Cl_2 \tag{6}$$

$$AlCl + Cl \leftrightarrow Al + Cl_2 \tag{7}$$

$$H_2 + Cl \leftrightarrow H + HCl \tag{8}$$

Reaction (8) provides H atoms, and these can also abstract Cl from $AlCl_3$, $AlCl_2$, or AlCl, as well as from Cl_2:

$$AlCl_3 + H \leftrightarrow AlCl_2 + HCl \quad (9)$$

$$AlCl_2 + H \leftrightarrow AlCl + HCl \quad (10)$$

$$AlCl + H \leftrightarrow Al + HCl \quad (11)$$

$$Cl_2 + H \leftrightarrow Cl + HCl \quad (12)$$

We should also include in our preliminary mechanism all the simple bond-breaking reactions we can think of, in addition to reaction (3):

$$AlCl_2 \leftrightarrow AlCl + Cl \quad (13)$$

$$AlCl \leftrightarrow Al + Cl \quad (14)$$

$$H_2 \leftrightarrow 2H \quad (15)$$

$$HCl \leftrightarrow H + Cl \quad (16)$$

$$Cl_2 \leftrightarrow 2Cl \quad (17)$$

Continuing in this manner, we realize that all the reactive aluminum species (Al, AlCl, $AlCl_2$) could conceivably react with H, H_2, and HCl to give all the species with the formula AlH_xCl_y with $0 \leq x \leq 3$, $0 \leq y \leq 3$. So, we should write all the possible bond-breaking, molecular elimination, and H and Cl abstraction reactions of these species as well. Furthermore, we have thus far only considered species containing a single aluminum atom. At room temperature, $AlCl_3$ actually exists in dimeric form, as Al_2Cl_6. So, perhaps we should also be considering species with two or more aluminum atoms. At this point, we might realize that this could quickly spin out of control. In fact, if we do not limit the number of aluminum atoms in the molecules to be considered, we could write an infinite number of species and reactions involving larger and larger clusters of aluminum. So, for the moment, we will limit ourselves to species containing at most one aluminum atom. Doing so, while adding the rest of the AlH_xCl_y species with $0 \leq x \leq 3$, $0 \leq y \leq 3$ and their decomposition and abstraction reactions, we arrive at the list of reactions shown in Table 4. Note that the reaction numbering in Table 4 differs from the numbering in the text above.

In Table 4, we have classified the reactions into four groups: (1) simple bond-breaking/forming reactions, (2) molecular elimination/insertion reactions, (3) abstractions involving H and Cl atoms, and (4) abstractions involving two Al-containing species. Even in this very simple system that involves only three different elements, only molecules containing four or

TABLE 4
Conceivable reactions in the Al–H–Cl system

Simple bond-breaking/forming reactions	
1	$AlCl_3 \leftrightarrow AlCl_2 + Cl$
2	$AlHCl_2 \leftrightarrow AlCl_2 + H$
3	$AlHCl_2 \leftrightarrow AlHCl + Cl$
4	$AlH_2Cl \leftrightarrow AlHCl + H$
5	$AlH_2Cl \leftrightarrow AlH_2 + Cl$
6	$AlH_3 \leftrightarrow AlH_2 + H$
7	$AlCl_2 \leftrightarrow AlCl + Cl$
8	$AlHCl \leftrightarrow AlCl + H$
9	$AlHCl \leftrightarrow AlH + Cl$
10	$AlH_2 \leftrightarrow AlH + H$
11	$AlCl \leftrightarrow Al + Cl$
12	$AlH \leftrightarrow Al + H$
13	$H_2 \leftrightarrow 2H$
14	$HCl \leftrightarrow H + Cl$
15	$Cl_2 \leftrightarrow 2Cl$
Molecular elimination/insertion reactions	
16	$AlCl_3 \leftrightarrow AlCl + Cl_2$
17	$AlHCl_2 \leftrightarrow AlH + Cl_2$
18	$AlHCl_2 \leftrightarrow AlCl + HCl$
19	$AlH_2Cl \leftrightarrow AlH + HCl$
20	$AlH_2Cl \leftrightarrow AlCl + H_2$
21	$AlH_3 \leftrightarrow AlH + H_2$
22	$AlCl_2 \leftrightarrow Al + Cl_2$
23	$AlHCl \leftrightarrow Al + HCl$
24	$AlH_2 \leftrightarrow Al + H_2$
Abstraction reactions involving H and Cl atoms	
25	$AlCl_3 + H \leftrightarrow AlCl_2 + HCl$
26	$AlCl_3 + Cl \leftrightarrow AlCl_2 + Cl_2$
27	$AlHCl_2 + H \leftrightarrow AlCl_2 + H_2$
28	$AlHCl_2 + H \leftrightarrow AlHCl + HCl$
29	$AlHCl_2 + Cl \leftrightarrow AlCl_2 + HCl$
30	$AlHCl_2 + Cl \leftrightarrow AlHCl + Cl_2$
31	$AlH_2Cl + H \leftrightarrow AlHCl + H_2$
32	$AlH_2Cl + H \leftrightarrow AlH_2 + HCl$
33	$AlH_2Cl + Cl \leftrightarrow AlHCl + HCl$
34	$AlH_2Cl + Cl \leftrightarrow AlH_2 + Cl_2$
35	$AlH_3 + H \leftrightarrow AlH_2 + H_2$
36	$AlH_3 + Cl \leftrightarrow AlH_2 + HCl$
37	$AlCl_2 + H \leftrightarrow AlCl + HCl$
38	$AlCl_2 + Cl \leftrightarrow AlCl + Cl_2$
39	$AlHCl + H \leftrightarrow AlCl + H_2$
40	$AlHCl + H \leftrightarrow AlH + HCl$
41	$AlHCl + Cl \leftrightarrow AlCl + HCl$
42	$AlHCl + Cl \leftrightarrow AlH + Cl_2$

Table 4. (*Continued*)

43	$AlH_2 + H \leftrightarrow AlH + H_2$
44	$AlH_2 + Cl \leftrightarrow AlH + HCl$
45	$AlCl + H \leftrightarrow Al + HCl$
46	$AlCl + H \leftrightarrow AlH + Cl$
47	$AlCl + Cl \leftrightarrow Al + Cl_2$
48	$AlH + H \leftrightarrow Al + H_2$
49	$AlH + Cl \leftrightarrow Al + HCl$
50	$Cl_2 + H \leftrightarrow Cl + HCl$
51	$HCl + H \leftrightarrow H_2 + Cl$
Abstraction reactions among AlH_xCl_y species	
52	$AlCl_3 + AlHCl \leftrightarrow AlCl_2 + AlHCl_2$
53	$AlCl_3 + AlH_2 \leftrightarrow AlCl_2 + AlH_2Cl$
54	$AlHCl_2 + AlHCl \leftrightarrow AlCl_2 + AlH_2Cl$
55	$AlHCl_2 + AlH_2 \leftrightarrow AlCl_2 + AlH_3$
56	$AlHCl_2 + AlH_2 \leftrightarrow AlHCl + AlH_2Cl$
57	$AlH_2Cl + AlH_2 \leftrightarrow AlHCl + AlH_3$
58	$AlCl_3 + AlCl \leftrightarrow 2AlCl_2$
59	$AlCl_3 + AlH \leftrightarrow AlCl_2 + AlHCl$
60	$AlHCl_2 + AlCl \leftrightarrow AlCl_2 + AlHCl$
61	$AlHCl_2 + AlH \leftrightarrow AlCl_2 + AlH_2$
62	$AlHCl_2 + AlH \leftrightarrow 2AlHCl$
63	$AlH_2Cl + AlCl \leftrightarrow 2AlHCl$
64	$AlH_2Cl + AlCl \leftrightarrow AlH_2 + AlCl_2$
65	$AlH_2Cl + AlH \leftrightarrow AlH_2 + AlHCl$
66	$AlH_3 + AlCl \leftrightarrow AlH_2 + AlHCl$
67	$AlH_3 + AlH \leftrightarrow 2AlH_2$
68	$AlCl_3 + Al \leftrightarrow AlCl_2 + AlCl$
69	$AlHCl_2 + Al \leftrightarrow AlCl_2 + AlH$
70	$AlHCl_2 + Al \leftrightarrow AlHCl + AlCl$
71	$AlH_2Cl + Al \leftrightarrow AlHCl + AlH$
72	$AlH_2Cl + Al \leftrightarrow AlH_2 + AlCl$
73	$AlH_3 + Al \leftrightarrow AlH_2 + AlH$
74	$AlCl_2 + AlH \leftrightarrow AlCl + AlHCl$
75	$AlH_2 + AlCl \leftrightarrow AlH + AlHCl$
76	$AlCl_2 + Al \leftrightarrow 2AlCl$
77	$AlHCl + Al \leftrightarrow AlCl + AlH$
78	$AlH_2 + Al \leftrightarrow 2AlH$

fewer atoms, and no molecules containing more than one aluminum atom, the number of possible reactions is substantial. It is important to remember that all the reactions listed are reversible, so the list is only half as long as it would be if they were written separately in each direction. Especially for reactions like those in group 4, involving two Al-containing species, one must be careful to avoid writing the same reaction twice (in both directions). Even at this 'brainstorming' stage, where we may include some

species and reactions that we do not really expect to end up in the final mechanism, we must exercise some discretion. For example, we do not include species with more than three atoms bound to aluminum, because we expect aluminum to be trivalent. Likewise, we do not invent any molecules with multiple bonds to chlorine or hydrogen, which are monovalent.

After conducting a 'brainstorming' exercise like that illustrated in Table 4, it is easy to see how a mechanism involving slightly larger species and more types of atoms could quickly become too large to construct manually. This led to the development of schemes for automated reaction mechanism generation, in which a computer generates a list of reactions following algorithms like those we were implicitly using in constructing Table 4. In such methods, one defines types of reactions that are expected to occur, in a manner similar to the way in which we classified the reactions in Table 4 into four categories. The computer then applies rules, much like the ones we intuitively used, to generate all the reactions of each type that a given list of chemical species can undergo. That then adds more species to the list, and those species can, in turn, undergo more reactions, and so on, *ad infinitum*. If some constraints are applied, such as a maximum allowable number of atoms in a molecule, then this process may eventually converge. That is, it will reach a point where no new species or reactions are possible. Finding suitable constraints or other means of limiting the mechanism size without excluding reactions that are important to the chemistry of interest is a key challenge in automated reaction mechanism generation. Further discussion of automated reaction mechanism generation is beyond the scope of the present chapter, but many good descriptions of this field's development and examples of its application are available in the literature [17–23].

3 DETERMINING SPECIES THERMOCHEMICAL PROPERTIES

While we are ultimately interested in the chemical kinetics of the system under consideration, we must first consider the thermodynamics. This is important not only because thermodynamic equilibrium constrains the overall system, but also because for each elementary reaction, the forward and reverse reaction rates are related *via* the equilibrium constant. To compute the equilibrium constant, we must know the Gibbs energy of each species participating in the reaction, at the reaction conditions. However, the Gibbs energy is not usually tabulated directly. Rather, the thermochemical properties are usually specified by the standard enthalpy of formation at 298 K, the standard entropy at 298 K and 1 bar (1 atm in some cases), and the heat capacity as a function of

temperature over some range that includes 298 K. This information, plus an equation of state, is adequate to obtain all the thermodynamic properties of a substance over the temperature range for which the heat capacity is given. Here, we will assume that the substance is an ideal gas. The most difficult piece of thermochemical information to determine is the enthalpy of formation, because it is the component that includes the energies of the chemical bonds in a given molecule. These must be obtained from calorimetry or from relatively high-level (computationally expensive) quantum chemistry calculations. In contrast, entropy and heat capacity depend primarily on molecular geometry and vibrational frequencies, which can be obtained spectroscopically or by relatively inexpensive quantum chemical calculations.

As illustrated in Fig. 1, there are essentially four methods for obtaining thermochemical data for the species in our reaction mechanism. The first choice is to find the needed data in databases or in the literature in general. This includes both published experimental data and published quantum chemical calculations, which can also be a reliable source of thermochemical data. If no information on a substance is available in the literature, one should consider whether it can be treated by group additivity methods. If a well-constructed group additivity method is available for the class of molecules of interest, the results, which can be obtained with minimal effort, will be comparable in accuracy to those from the best quantum chemistry calculations. If group additivity is not applicable to the molecules of interest, then we may want to carry out quantum chemistry calculations for them, as discussed in detail in an earlier chapter. In some cases, the effort required to carry out the quantum chemical calculations may not be warranted, and we may want to make coarser, empirical estimates of thermochemical properties.

3.1 Finding thermochemical properties in the literature

The first place that one should generally look for thermochemical data is in the *NIST Chemistry WebBook* [24], available at http://webbook.nist.gov. This database contains thermochemical properties for more than 7000 small organic and inorganic compounds, and includes the entire contents of several other databases. Table 5 shows the enthalpies of formation and standard entropies of the species from the reaction mechanism in Table 4 that are available in the *NIST WebBook*. These properties were available for 10 of the 15 species. The source cited in the *NIST WebBook* for all these species was the NIST-JANAF Themochemical Tables [25], which have long been the first choice for finding thermochemical data for inorganic and very small organic

TABLE 5
Thermochemical properties for species included in Table 4

		NIST WebBook		HiTempThermo	
		$\Delta H_f^\circ(298)$ (kJ/mol)	S (298 K, 1 bar) (J/(mol K))	$\Delta H_f^\circ(298)$ (kJ/mol)	S (298 K, 1 bar) (J/(mol K))
1	$AlCl_3$	−584.59	314.44	−592.04	315.35
2	$AlHCl_2$	X	X	−360.24	289.87
3	AlH_2Cl	X	X	−117.57	254.05
4	AlH_3	X	X	129.29	207.86
5	$AlCl_2$	−280.33	289.39	−219.24	290.29
6	AlHCl	X	X	20.92	258.53
7	AlH_2	X	X	268.19	213.72
8	AlCl	−51.46	227.95	−49.79	228.32
9	AlH	259.41	187.87	247.69	187.69
10	Al	329.70	164.57	335.14	155.60
11	Cl_2	0.00	223.08	0.00	222.76
12	HCl	−92.31	186.90	−92.47	186.36
13	H_2	0.00	130.68	0.00	129.96
14	Cl	121.30	165.19	121.34	158.82
15	H	218.00	114.72	217.99	114.60

molecules. Incorporation of data from these tables into the *NIST WebBook* has made them much easier to access.

Another online source of thermochemical data useful for high-temperature chemical kinetics is the HiTempThermo page maintained by Sandia National Laboratories at http://www.ca.sandia.gov/HiTempThermo/. In that database, Allendorf and co-workers have compiled the results of the large number of bond-additivity-corrected (BAC) quantum chemical calculations that they and their collaborators have carried out over the years. Roughly 1000 compounds are included, with particularly strong representation of light, inorganic elements such as aluminum, silicon, and boron as well as small organic compounds. The last two columns of Table 5 show the enthalpies of formation and standard entropies from the HiTempThermo database. The system that we have chosen as an example is one that Allendorf and co-workers have studied, so the database includes data for all the species appearing in the reaction mechanism of Table 4. For the most part, these values are consistent with those obtained from the *NIST WebBook*. However, there are exceptions. In particular, for $AlCl_2$ the value from HiTempThermo is more than 60 kJ/mol higher than that from the *NIST WebBook*. Further investigation of this discrepancy reveals that the experimentally based value in the *NIST WebBook*, from the JANAF tables, is rather uncertain

[26], and several computational studies have found values similar to those given in the HiTempThermo database and have suggested that the JANAF value is probably in error [8,27,28]. While uncertainty remains, it seems likely that the value from the HiTempThermo database is nearer to the truth. In cases like this, it is probably wisest to use a complete set of thermodynamic properties data from a single source in which all values were determined by the same methods (the HiTempThermo database in this case) rather than mixing and matching values from a variety of sources.

Another valuable source is the thermochemical property database assembled by Burcat and Ruscic [29], which is available online at ftp://ftp.technion.ac.il/pub/supported/aetdd/thermodynamics/. This collection is regularly updated by Prof. Burcat. It contains data for ~1500 species, presented in the form of polynomial coefficients that can be used to compute the enthalpy, entropy, and heat capacity as a function of temperature. While Burcat's tables include a number of aluminum–oxygen compounds, they do not happen to include the aluminum–chlorine species that we have been using as an example. Of course, there are many other handbooks and compilations of thermodynamic properties. However, the vast majority of these focus on organic compounds and/or condensed phase species. Standard handbooks, such as the *CRC Handbook of Chemistry and Physics*, rarely have any information not included in the sources cited above.

Of course, one can also go directly into the primary literature to look for these properties, though it can be time-consuming and not always fruitful. A large fraction of the reliable data from the literature for small gas-phase molecules has already been captured in the above cited databases. As an example, let us see what we can find for $AlCl_2$, for which the JANAF tables and *ab initio* calculations are not apparently in good agreement. The chemical abstracts databases are probably the most convenient means to carry out such a search, because they allow for searching by CAS number and subsequent refining of the search results. A search of SciFinder Scholar for $AlCl_2$ (CAS number 16603-84-2) yields only 63 references. A quick manual scan of the titles of these papers results in 19 that might possibly have useful thermodynamic data in them. These are listed in Table 6. This list could quickly be shortened further by reading the abstracts and by excluding papers that are likely to be inaccessible. Finally, one must actually look up the relevant articles, read them, and make a judgment about what values of the thermochemical properties are likely to be most reliable. On doing this, one quickly realizes the value of thermodynamic compilations like those described above: someone else has already made this judgment.

TABLE 6
Relevant references for $AlCl_2$ thermochemistry found using SciFinder Scholar

1	Chai B.J., et al.: Heat of formation and entropy of aluminum(II) chloride(g) and its dimer, Al_2Cl_4(g). *J. Phys. Chem.* 1967, **71**:331–6
2	Bahn G.S.: Finite-kinetics expansions of reaction products among aluminum or boron, hydrogen, chlorine, and fluorine. *Pyrodynamics* 1969, **6**:297–314
3	Farber M. and Harris S.P.: Mass spectrometric determination of thermodynamic properties of compounds in the aluminum–chlorine–fluorine system. *High Temperature Science* 1971, **3**:231–6
4	Farber M. and Buyers A.G.: Thermodynamic properties of some high temperature aluminum species. *Proc. Symp. Thermophys. Prop., 5th* 1970483-8
5	Chase M.W., et al.: JANAF [Joint-Army-Navy-Air-Force] thermochemical tables, 1974 supplement. *J. Phys. Chem. Ref. Data* 1974, **3**:311–480
6	Chase M.W., Jr., et al.: JANAF thermochemical tables, 1978 supplement. *J. Phys. Chem. Ref. Data* 1978, **7**:793–940
7	Olah G.A., et al.: Aluminum dichloride and dibromide. Preparation, spectroscopic (including matrix isolation) study, reactions, and role (together with alkyl(aryl)aluminum monohalides) in the preparation of organoaluminum compounds. *J. Am. Chem. Soc.* 1988, **110**:3231–8
8	Numata M., Sugiura M., and Fuwa A.: Standard Gibbs energies of formation for gaseous aluminum chloride AlCl(g) and $AlCl_2$(g) species at temperatures from 600 to 1300 K. *Materials Transactions, JIM* 1993, **34**:511–6
9	Petrie S.: Thermochemistry of aluminum halides: A theoretical appraisal. *J. Phys. Chem. A* 1998, **102**:7828–7834
10	Allendorf M.D. and Melius C.F.: G2 predictions of group III thermochemistry: compounds containing aluminum. *Proceedings—Electrochemical Society* 1999, **98-23**:28–33
11	Baeck K.K., Choi H., and Iwata S.: Theoretical study on spectroscopic properties of positive, neutral, and negative species of BCl_2 and $AlCl_2$: The stability of the negative species. *J. Phys. Chem. A* 1999, **103**:6772–6777
12	Allendorf M.D., Melius C.F., and Bauschlicher C.W., Jr.: Heats of formation and bond energies in group III compounds. *Journal de Physique IV: Proceedings* 1999, **9**:23–31
13	Nitodas S.F. and Sotirchos S.V.: Co-deposition of silica, alumina, and aluminosilicates from mixtures of CH_3SiCl_3, $AlCl_3$, CO_2, and H_2. Thermodynamic analysis and experimental kinetics investigation. *Chem. Vapor Deposition* 1999, **5**:219–231
14	Swihart M.T. and Catoire L.: Thermochemistry of aluminum species for combustion modeling from ab initio molecular orbital calculations. *Combust. Flame* 2000, **121**:210–222
15	Swihart M.T. and Catoire L.: Reactions in the Al–H–Cl system studied by ab initio molecular orbital and density functional methods. *J. Phys. Chem. A* 2001, **105**:264–273
16	Filipovic M. and Kilibarda N.: A study of the thermodynamic functions of the combustion products of composite propellants. *Hemijska Industrija* 2001, **55**:109–113
17	Allendorf M.D., et al.: BAC-G2 predictions of thermochemistry for gas-phase aluminum compounds. *J. Phys. Chem. A* 2002, **106**:2629–2640
18	Timoshkin A.Y. and Frenking G.: Low-valent group-13 chemistry. Theoretical investigation of the structures and relative stabilities of donor–acceptor complexes R_3E-E′R′ and their isomers R_2E-E′RR′. *J. Am. Chem. Soc.* 2002, **124**:7240–7248
19	Shukla P.K. and Ray N.K.: Density functional study of some aluminium radicals. *Theochem* 2005, **723**:131–134

3.2 Estimating thermochemical properties using group additivity

If thermochemical data for a given substance are not available in the compilations cited above or in easily accessible literature, then the next best approach is to use an experimentally based empirical estimation technique. The most common approach of this type is group additivity,

in which a molecule is considered to be made up of several groups, and the thermochemical properties are written as the sum of contributions from each group. The group contribution values are obtained by regression of experimental (and sometimes computed) thermochemical data. As a result, group additivity parameters (the group contributions) are available only for relatively well-studied classes of compounds. When group additivity is applicable, it usually performs quite well. However, it cannot be applied to molecules containing chemical bonds or combinations of chemical bonds that do not appear in other molecules with well-characterized thermochemistry.!

3.3 Estimating thermochemical properties using computational quantum chemistry

If needed thermochemical data are not available in the literature, and if group additivity methods are not applicable, then computational quantum chemistry is the next logical route to pursue. As computers become more powerful, and as quantum chemistry software becomes more user-friendly, this option is becoming available to a widening array of scientists and engineers and for application to a widening array of chemical species. However, when the number of possible chemical species is large, it still may not be realistic to carry out quantum chemical calculations for all the species of interest. One alternative in that case is to carry out calculations for a selected subset of species and then use the results to build a group additivity scheme. This approach allows one to generalize the results of a large but manageable set of quantum chemistry calculations to make good predictions for arbitrary chemical species within a class of compounds. We have recently done this for silicon–hydrogen species [30]. Because the determination of thermochemistry from quantum calculations has already been discussed in detail elsewhere in this volume, we omit any further discussion here.

3.4 Estimating thermochemical properties by analogy or educated guessing

When thermochemical data for a substance or group of substances are not available in the literature, group additivity is not applicable, and quantum chemistry calculations are not feasible, then one can start by simply making some educated guesses. Sometimes, this can be done using analogies to similar systems, often moving up the periodic table to smaller, better studied elements. In other cases, one can ‘interpolate’

between known values. Several straightforward approaches can be illustrated by example.

Suppose we knew heats of formation for the gaseous aluminum atom and chlorine atom and for $AlCl_3$, but had no information at all about AlCl or $AlCl_2$. Then we might simply guess that the bond strengths for all three Al–Cl bonds were equal. We could write the hypothetical reaction

$$AlCl_3(g) \rightarrow Al(g) + 3Cl(g) \tag{18}$$

for which the heat of reaction is

$$\begin{aligned} \Delta H_r^\circ &= \Delta H_f^\circ(Al(g)) + 3\,\Delta H_f^\circ(Cl(g)) - \Delta H_f^\circ(AlCl_3(g)) \\ \Delta H_r^\circ &= 329.70 + 3 \times 121.30 - (-584.59) = 1278.19\ \text{kJ/mol} \end{aligned} \tag{19}$$

Since this is the total enthalpy change for breaking all three Al–Cl bonds, the average enthalpy change for breaking an Al–Cl bond is $1278.19/3 = 426.06$ kJ/mol. If we assume that all three bonds are equivalent, then the reactions

$$AlCl_3(g) \rightarrow AlCl_2(g) + Cl(g) \tag{20}$$

and

$$AlCl_2(g) \rightarrow AlCl(g) + Cl(g) \tag{21}$$

would each have an enthalpy of reaction of 426.06 kJ/mol. Then, we can estimate the enthalpy of formation of $AlCl_2$ and AlCl by writing the enthalpies of reaction for the single bond-breaking reactions and solving for the unknown enthalpies of formation:

$$\begin{aligned} \Delta H_r^\circ[(13)] &= \Delta H_f^\circ(AlCl_2(g)) + \Delta H_f^\circ(Cl(g)) - \Delta H_f^\circ(AlCl_3(g)) \\ \Delta H_r^\circ[(13)] &= \Delta H_f^\circ(AlCl_2(g)) + 121.30 - (-584.59) = 426.06\ \text{kJ/mol} \\ \Delta H_f^\circ(AlCl_2(g)) &= 426.06 - 121.30 - 584.59 = -279.8\ \text{kJ/mol} \end{aligned} \tag{22}$$

and

$$\begin{aligned} \Delta H_r^\circ[(14)] &= \Delta H_f^\circ(AlCl(g)) + \Delta H_f^\circ(Cl(g)) - \Delta H_f^\circ(AlCl_2(g)) \\ \Delta H_r^\circ[(14)] &= \Delta H_f^\circ(AlCl(g)) + 121.30 - (-279.8) = 426.06\ \text{kJ/mol} \\ \Delta H_f^\circ(AlCl(g)) &= 426.06 - 121.30 - 279.83 = 24.9\ \text{kJ/mol} \end{aligned} \tag{23}$$

While these are obviously very coarse estimates, they are not ridiculously far off. In a case where one had no idea, *a priori*, whether such species might be important, something like this might be appropriate for generating a first

estimate. In this example, we have gone through the formal process of writing a series of bond-breaking reactions and computing their enthalpies of reaction. However, the end result is equivalent to simple linear interpolation of the enthalpies of formation of Al and $AlCl_3$. That is, the same results are obtained by simply writing

$$\Delta H_f^\circ(AlCl_2(g)) = \Delta H_f^\circ(AlCl_3(g)) + \tfrac{1}{3}(\Delta H_f^\circ(Al(g)) - \Delta H_f^\circ(AlCl_3(g)))$$
$$\Delta H_f^\circ(AlCl_2(g)) = -584.59 + \tfrac{1}{3}(329.7 - (-584.59)) = -279.8\ \text{kJ/mol} \quad (24)$$

and

$$\Delta H_f^\circ(AlCl(g)) = \Delta H_f^\circ(AlCl_3(g)) + \tfrac{2}{3}(\Delta H_f^\circ(Al(g)) - \Delta H_f^\circ(AlCl_3(g)))$$
$$\Delta H_f^\circ(AlCl(g)) = -584.59 + \tfrac{2}{3}(329.7 - (-584.59)) = 24.9\ \text{kJ/mol} \quad (25)$$

In practice, this method of carrying out the interpolation is simpler and does not involve the heat of formation of the Cl atom, which ultimately cancels out of the calculation.

A similar sort of linear interpolation can be done for estimating the properties of molecules with a mixture of ligands attached to a given center when enthalpies are known for the corresponding molecules with only one ligand or the other. For example, if we knew only the enthalpies of formation of AlH_3 and $AlCl_3$, we might very reasonably assume that each substitution of Cl for H causes the same increment in enthalpy of formation. Based on that assumption, we could estimate the enthalpies of formation for the species with 'mixed' ligands, $AlHCl_2$ and AlH_2Cl. The enthalpies of formation of AlH_3 and $AlCl_3$ are given in the HiTempThermo database as 129.29 and −592.04 kJ/mol, respectively. Since substituting all three hydrogens by chlorine decreases the enthalpy of formation by a total of 721.33 kJ/mol, we could assume that each Cl for H substitution decreases the enthalpy of formation by one-third of this amount, 240.44 kJ/mol. Then the interpolated enthalpies of formation for AlH_2Cl and $AlHCl_2$ would be −111.2 and −351.6 kJ/mol, respectively. These estimates compare extremely well with the values of −117.57 and −360.24 kJ/mol in the HiTempThermo database. The two compounds with mixed ligands (both H and Cl) deviate by less than 10 kJ/mol from this simple linear interpolation.

As a third example of this sort of estimation, let us consider the analogy between the Si–H–Cl and Sn–H–Cl systems that were introduced in Table 3. Above, we saw that linearly interpolating between the heats of formation of $AlCl_3$ and Al to estimate the heats of formation for

AlCl and $AlCl_2$ gave somewhat poor results. This simply reflects the fact that not all the bond strengths are equal. Similarly, we see from Table 3 that removing the first H or Cl from SiH_xCl_{4-x} requires more energy than removing a second one. Now, suppose we wanted to estimate heats of formation for the compounds in the Sn–H–Cl system and that we only had data for SnH_4, $SnCl_4$, and the Sn atom. As a first attempt, we could interpolate linearly between SnH_4 and Sn to get the heats of formation for SnH, SnH_2, and SnH_3 and interpolate linearly between $SnCl_4$ and Sn to get the heats of formation for SnCl, $SnCl_2$, and $SnCl_3$. The results of this approach are shown in the fifth column of Table 7, which also includes the heats of formation for the Si–H–Cl species and those for the Sn–H–Cl species that we are trying to estimate. The results of simple linear interpolation are not totally unreasonable. However, we do not really expect the heat of formation to vary linearly. Rather, we expect behavior like that in the analogous silicon compounds, where the first atom is harder to remove, the second is easier to remove, etc. So, we might improve the estimates for the Sn–H–Cl species using our knowledge of the Si–H–Cl species thermochemistry. One way to do that is to assume that the fraction of the total atomization enthalpy that is required to sequentially remove each ligand is the same for the tin species as for the silicon species. For example, for SiH_4, the total atomization enthalpy is 1286.9 kJ/mol. Of this total, 382.2 kJ/mol (29.7%), 290.7 kJ/mol (22.6%), 327.7 kJ/mol (25.5%), and 286.4 kJ/mol (22.3%) are required to remove the first, second, third, and fourth hydrogens, respectively. For SnH_4, the total atomization enthalpy is 1010.5 kJ/mol. Assigning 29.7, 22.6, 25.5, and 22.3% of this total to breaking the first, second, third, and fourth Sn–H bonds gives the results shown in the sixth column of Table 7 for the enthalpies of formation of SnH_3, SnH_2, and SnH. Doing the same thing to interpolate between $SnCl_4$ and Sn gives the results shown there for $SnCl_3$, $SnCl_2$, and SnCl. Finally, we can interpolate linearly between SnH_4 and $SnCl_4$, between SnH_3 and $SnCl_3$, and between SnH_2 and $SnCl_2$ to fill in the rest of the heats of formation for the other species. As shown in Table 7, the approach using information from the Si–H–Cl system provides better estimates than simple linear interpolation. However, the results are still not perfect. In fact, the strong–weak–strong pattern of bond energies becomes more pronounced as one moves down the periodic table, so that SnH_2 and $SnCl_2$ are even more stable than we predict by direct analogy with the Si–H–Cl species. If we also had information about the Ge–H–Cl system, we might try to project the differences between the Si and Ge systems onto the Sn system, to obtain even better estimates.

In the above examples, we assumed that we had at least some information about the most stable, saturated compounds in each system, as well

TABLE 7
Estimating Sn–H–Cl thermochemistry using Si–H–Cl thermochemistry

Species	ΔH_f° (kJ/mol) from Ref. [13]	Species	ΔH_f° (kJ/mol) from Ref. [12]	ΔH_f° (kJ/mol) using linear interpolation	ΔH_f° (kJ/mol) using Si–H–Cl information
Si	449.2	Sn	301.2		
SiH	380.8	SnH	286.2	266.6	294.4
SiH_2	271.1	SnH_2	242.7	232.0	255.1
SiH_3	198.4	SnH_3	258.2	197.4	244.8
SiH_4	34.3	SnH_4	162.8		
SiCl	158.0	SnCl	70.3	106.3	95.8
$SiCI_2$	−151.3	$SnCI_2$	−189.1	−88.7	−123.9
$SiCI_3$	−318.0	$SnCI_3$	−247.7	−283.7	−230.8
$SiCI_4$	−662.7	$SnCI_4$	−478.6		
SiH_3CI	−134.0	SnH_3CI	1.7	2.4	2.4
SiH_2Cl_2	−311.4	SnH_2Cl_2	−162.3	−157.9	−157.9
$SiHCI_3$	−490.1	$SnHCI_3$	−323.8	−318.3	−318.3
SiH_2CI	33.1	SnH_2CI	94.1	37.0	86.3
$SiHCI_2$	−142.2	$SnHCI_2$	−77.8	−123.3	−72.3
SiHCl	66.3	SnHCl	37.7	71.7	65.6
H	218.0				
Cl	121.3				

as the atoms. This gave us a reference point to establish a typical bond energy for a particular bond type. In other cases, we might have to find that information from a compound other than the simple ones used above, in which only one type of bond was present, or even by analogy with other compounds. For example, if we had no idea what the Sn–H bond strength was, we might guess it by comparison to other group 14 hydrides. In this case, we can find heats of formation for CH_4, SiH_4, and GeH_4 and for all the relevant atoms. This would allow us to compute the atomization enthalpies for CH_4, SiH_4, and GeH_4 as 1664, 1288, and 1153 kJ/mol, respectively. In this case, there is a clear trend of weakening X–H bond strength moving down the periodic table. We could use any of a variety of methods to 'project' this decreasing bond strength to SnH_4, and we would not be far off from the SnH_4 atomization enthalpy of 1011 kJ/mol. On the other hand, this would not work so well for estimating the strength of the Sn–Cl bonds. In that case, the atomization enthalpies for CCl_4 and $SiCl_4$ are ~1298 and 1598 kJ/mol, respectively. $GeCl_4$ is not included in the usual databases of thermochemical properties. However, there is an experimental value in the literature [31] that is supported by recent high-level quantum chemistry calculations [32]. Using that value gives an atomization enthalpy for $GeCl_4$ of ~1352 kJ/mol. Here, the trend in bond strength moving down the periodic table is not monotonic, with a large increase from C to Si, and a smaller decrease from Si to Ge. It is not clear how to project this trend to Sn, and doing so would be unlikely to produce an estimate near the actual atomization enthalpy of $SnCl_4$ (~1265 kJ/mol). Assuming the same fractional decrease in going from Ge to Sn as observed in going from Si to Ge would give an estimate of 1144 kJ/mol. This is 10% lower than the actual value, but is about as good as can be expected from such a coarse estimation method. One might also try to incorporate information on trends in bond strengths in neighboring columns of the periodic table, but at some point, one simply has to make an educated guess and move on. If, in subsequent analyses, it appears that species with coarsely estimated thermochemistry are important in the overall kinetic model, then it will probably be necessary to carry out quantum chemical calculations for those species to provide better estimates.

4 DETERMINING RATE PARAMETERS

Once we have established the thermochemical properties of all the chemical species in our reaction mechanism, we must determine rate parameters for all the reactions. Given the thermochemistry, we only have to find rate parameters for a given reaction in the 'forward'

direction, where our operational definition of 'forward' is the reaction direction for which we have the rate parameters. The rate parameters for the 'reverse' direction are then fixed by the forward rate parameters and thermochemistry. On the rare occasions when we find reliable rate parameters for a given reaction in both directions, we can use these to determine the equilibrium constant for the reaction and use this as a check of the thermochemical properties we are using to compute the equilibrium constant. Ultimately, the least certain of the parameters should be adjusted to make the system consistent. The approach to obtaining rate parameters is very similar to that taken in the previous sections. First, we find whatever is available in the literature. Second, to whatever extent is feasible, we use quantum chemical calculations and reaction rate theories to fill in the gaps. Finally, where no literature information is available and theoretical calculations are not feasible, we must make estimates based on whatever information we can find and analogies to other systems.

4.1 Finding rate parameters in the literature

In searching for rate parameters of individual reactions in the literature, we proceed just as we have done in the previous section. By far the most useful source of gas-phase reaction rate parameters is the NIST Chemical Kinetics Database [11], available online at http://kinetics.nist.gov. This database is regularly updated, and contains virtually all published results for gas-phase chemical kinetics, except for those published in the current calendar year. For example, in late 2005, the database contained no references to papers published in 2005, but almost 400 references to papers published in 2004. Thus, if an elementary gas-phase reaction is not in this database, you are unlikely to be able to find rate parameters for it in the literature, unless those results have been published within the past year or two. A search of the NIST Chemical Kinetics Database for the reactions of Table 4 yields entries for eight of them, but only four of the eight entries actually have an experimentally based rate expression. Among the other four, three give rate expressions based on transition state theory calculations using bond-energy-bond-order (BEBO) estimation methods, and one cites quantum chemical calculations that do not directly provide a rate expression. The four experimental rate expressions come from two papers [33,34] by the same research group, and were all made using the same method. This is a rather typical situation for gas-phase chemical kinetics of inorganic species, in that the experimental data are often sparse and sometimes are known only from experiments in a single laboratory. Beyond the NIST Chemical Kinetics Database, one can search the

primary literature using the same approaches and tools described in previous sections for identifying reactions and obtaining thermochemical properties.

4.2 Determining rate parameters using quantum chemical calculations and transition state theory

If, as is often the case, there are no rate parameters in the literature for most of the reactions that one has postulated in the reaction mechanism, it may be worthwhile to use quantum chemical calculations and reaction rate theories (transition state theory and related theories for unimolecular reactions) to obtain rate parameters for at least some of the reactions. The Al–H–Cl system that we have been using as an example is one for which we have done many of these calculations, and will therefore be used here to illustrate the approaches that can be taken. From the point of view of computing rate parameters, it is useful to categorize reactions into four general classes, based on whether they are bimolecular in both reaction directions or unimolecular in at least one direction, and based on whether they have a significant energetic barrier to reaction. Thus, the four classes are: (1) bimolecular reactions with an energetic barrier, (2) unimolecular reactions with an energetic barrier, (3) barrierless bimolecular reactions, and (4) barrierless unimolecular reactions. A typical example of class (1) is an abstraction reaction that is not very exothermic. A typical example of class (2) is a molecular elimination reaction. Class (3) includes abstraction reactions that are very exothermic, and class (4) is exemplified by simple bond dissociation reactions. In many cases, one cannot determine, *a priori*, whether a reaction has an energetic barrier. In such cases, computational quantum chemistry will be used to identify either an energetic maximum on the path from reactants to products or a barrierless path connecting reactants to products. In the remainder of this section, we will consider examples of the four classes of reaction listed above that arise in the Al–H–Cl mechanism introduced in Table 4.

(*i*) *Bimolecular reactions with an energetic barrier*

Bimolecular reactions with an energetic barrier are probably the easiest of the four classes of reaction to treat computationally, because conventional transition state theory (TST) can be applied to them. We do not provide any derivation of TST here, but simply present the final result, which is

$$k_f = \frac{k_B T}{h} \frac{q^\dagger}{q_A q_B} \exp\left(\frac{-E_0}{k_B T}\right) \tag{26}$$

where k_f is the forward rate constant (what we are trying to compute), k_B is Boltzmann's constant (1.381×10^{-23} J/K), T is the temperature, h is Planck's constant (6.626×10^{-34} J sec), q_A, q_B, and q are the partition functions, per unit volume, of reactant A, reactant B, and the transition state, respectively, and E_0 is the energetic barrier to reaction (energy of transition state minus energy of reactants). Derivations of this expression are available in many textbooks, including the one by Steinfeld *et al.* [35]. The partition functions are calculated using the standard formulae from statistical mechanics [36], except that in the partition function of the transition state, the vibrational frequency corresponding to motion along the reaction path is omitted. The transition state structure is a maximum in energy with respect to one normal mode motion of the atoms (which corresponds to motion along the reaction path), and a minimum in energy with respect to all others, whereas a stable molecule is an energetic minimum with respect to all its normal mode motions. One vibrational frequency corresponds to each normal mode motion. In a transition state, the vibrational frequency corresponding to motion along the reaction path is an imaginary number, often printed as a negative number by computational quantum chemistry codes. A transition state structure should have exactly one imaginary vibrational frequency, which is omitted in computing the partition function of the transition state. The same information that is required to calculate thermodynamic properties of an ideal gas molecule, namely molecular geometry and vibrational frequencies, is required to calculate these partition functions. In addition, the energies of the reactants and the transition state are needed to determine E_0. So, to apply equation (20), we must fully characterize, using computational quantum chemistry, the reactants and transition state. Considerations in choosing computational methods (levels of theory) will be much the same as described in the earlier chapter on obtaining molecular thermochemistry from calculations.

As an example of this type of reaction, we consider reaction (25) from Table 4:

$$AlCl_3 + H \leftrightarrow AlCl_2 + H_2 \tag{27}$$

While we cannot be sure, *a priori*, that this reaction will have an energetic barrier, it turns out that it does. Using the enthalpies of reaction from the HiTempThermo database as given in Table 5, we find that the enthalpy of reaction for this reaction is ~62 kJ/mol, which is much smaller than the enthalpy of reaction for breaking the Cl_2Al–Cl bond (494 kJ/mol) or the H–Cl bond (432 kJ/mol). Because the bond that is breaking and the bond that is forming in this abstraction reaction are fairly strong and are comparable in energy, we expect that the reaction may have an energetic

TABLE 8
Energies from quantum chemical calculations

Species	Total energy (hartrees)				Relative energy (kJ/mol)			
	B3LYP	CBS-Q	G-2	CBS-RAD	B3LYP	CBS-Q	G-2	CBS-RAD
$AlCl_3 + H$	−1623.861112	−1621.975342	−1621.948747	−1621.974753	0.0	0.0	0.0	0.0
$AlCl_2 + HCl$	−1623.848263	−1621.951529	−1621.925425	−1621.951053	33.8	62.6	61.3	62.3
$AlCl_3 + H \leftrightarrow AlCl_2 + HCl$ TS	−1623.837378	−1621.940108	−1621.912098	−1621.939547	62.4	92.6	96.3	92.5

barrier. The energies of the reactants, products, and transition state for this reaction have been calculated using computational quantum chemistry at various levels of theory, and are given in Table 8. Three relatively accurate and computationally expensive multi-step methods for calculating energies (CBS-Q, G-2, and CBS-RAD) are in good agreement, while the results from a more approximate but much less computationally expensive density functional theory method (B3LYP/6-311 + G(3df,2p)// B3LYP/6-31G(d)) are significantly different. Table 9 gives the corresponding vibrational frequencies and moments of inertia that are required to compute the partition functions in equation (20). For further details of these calculations, see the original publication [9]. The relative energies of reactant, transition state, and product, as well as the transition state geometry, are shown schematically in Fig. 2. Finding the transition state geometry can be a challenge, but any detailed discussion of strategies for doing so is beyond the scope of the present chapter.[1] Once a structure is found that appears to be the transition state, it is a good idea to follow the reaction path from the transition state in both directions to check that it connects the expected reactants and products. Automated methods for locating transition states and for following the reaction path are included in the popular Gaussian computational quantum chemistry package [37] and other similar codes. These methods are generally adequate for reactions among just a few atoms, like the one considered here, though more specialized methods may be necessary in some cases. Generally, one starts by optimizing the geometry of the reactants and products. Then one provides these, along with a manually constructed or computer-generated guess for the transition state to the computational quantum chemistry software. Once the transition state is located, one can follow the path of steepest descent on the potential energy surface away from the transition state in both directions. One direction should lead to the reactants, and the other should lead to the products. Note that although the path of steepest

[1]Input files needed to carry out the calculations whose results are presented in Tables 8 and 9, using the Gaussian package, along with a brief discussion of how to run them and what they do, are included in the CD accompanying this text.

TABLE 9
Vibrational frequencies and moments of inertia from quantum chemical calculations

Species	Vibrational frequencies (cm^{-1})									Moments of inertia (amu $Å^2$)		
$AlCl_2$	148	451	567							22.3	230	252
$AlCl_3$	146	146	198	376	612	612				226	226	452
$AlCl_3 + H \leftrightarrow AlCl_2 + HCl$ TS	1485*i*	92	120	169	294	362	429	540	584	233	255	478
HCl	2845									1.6		

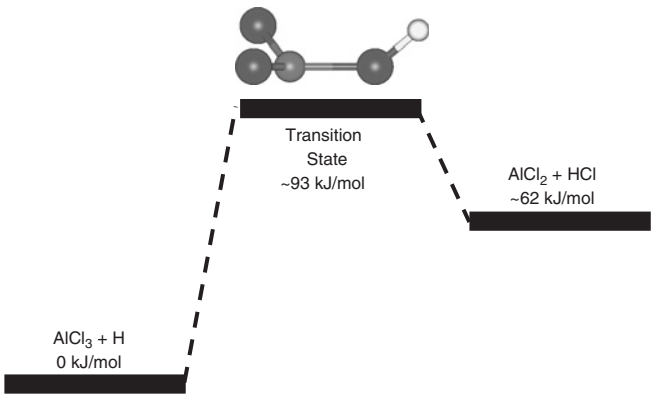

Fig. 2. Schematic representation of the reaction path for $AlCl_3 + H \leftrightarrow AlCl_2 + HCl$.

descent, starting from the transition state, is uniquely defined so that it is straightforward to follow the reaction path away from the transition state, there is no similarly straightforward means of following the reaction path *toward* the transition state from the reactants or the products.

Once the transition state structure has been located and its energy (relative to the reactants or products), geometry, and vibrational frequencies have been determined at an appropriate level of theory, it is straightforward to apply equation (20) to determine the rate constant at a given temperature. In equation (20), most of the temperature dependence is due to the exponential dependence on the energetic barrier to reaction, E_0. If this were the only temperature dependence, then the rate constant would give a perfectly straight line on an Arrhenius plot, with E_0 as the activation energy. However, there is additional temperature dependence in the 'universal prefactor,' kT/h, as well as in the partition functions. Rather than explicitly using equation (20) to compute the rate constant within a model containing many chemical reactions, it is usually preferable to evaluate equation (20) at several points over the temperature range of interest, and fit the results to a modified Arrhenius

form ($k = AT^{\beta}\exp(-E_a/RT)$).[2] The final results for the parameters in the modified Arrhenius form depend on the choice of temperatures at which the fitting is performed. In this example, over the temperature range from 300 to 5000 K, the TST results are fit to within 1% by the modified Arrhenius form with $A = 4.97 \times 10^{-15}$ cm^3/sec, $\beta = 1.47$, and $E_a = 89.98$ kJ/mol.

(*ii*) *Unimolecular reactions with an energetic barrier*

For reactions that are unimolecular in one or both directions, the reaction rate is expected to be pressure dependent, as discussed in detail in an earlier chapter of this text. In the high-pressure limit, conventional transition state theory as described in the previous section can be applied to estimate the rate constant. The only change in equation (20) is that only a single reactant partition function appears in the denominator. The pressure dependence can then be described at various levels of sophistication, from QRRK theory to RRKM theory, to full master equation treatments using microcanonical rate constants from RRKM theory, as described in the chapter by Carstensen and Dean. Because these approaches have been described in detail there, they are not treated in the present chapter.

(*iii*) *Bimolecular reactions without an energetic barrier*

The first challenge in treating barrierless bimolecular reactions is to identify them. From a practical point of view, one often cannot tell, *a priori*, whether a reaction has an energetic barrier. Often, one starts with the hypothesis that an energetic barrier exists, and then attempts to find this barrier using various transition state search strategies. When several of these searches fail, it may make sense to change strategies and attempt to identify a barrierless path connecting the reactants to the products. Perhaps the simplest example in this category from the Al–H–Cl mechanism we have been considering is reaction (47) of Table 4, rewritten in the exothermic direction as:

$$Al + Cl_2 \leftrightarrow AlCl + Cl \tag{28}$$

Using the heats of formation in Table 5, we can compute that this reaction is exothermic by ~263 kJ/mol. This represents the difference between the bond strength of the Al–Cl bond that forms (~506 kJ/mol) and the Cl–Cl bond that breaks (~243 kJ/mol). For a very exothermic abstraction reaction like this, the simultaneous formation of the stronger

[2] A Microsoft Excel spreadsheet that demonstrates the application of TST to calculate the rate constant for this example, as well as the fitting of the results to a modified Arrhenius form, is included in the CD that accompanies this text.

bond and breaking of the weaker bond may result in a path from reactants to products along which energy decreases monotonically. That is, at every point on the path, the energetic payoff associated with the forming bond is greater than the energetic cost associated with the breaking bond. For this simple reaction involving only three atoms, one can readily use computational quantum chemistry to scan the potential surface on which the reaction occurs. In such a calculation, the energy is computed for an array of lengths of the breaking and forming bonds. Other internal coordinates of the molecule can either be optimized (varied to minimize the energy) or held fixed. The potential surface computed for this example, holding the Al–Cl–Cl bond angle fixed at 180°, so the atoms are co-linear, is shown in Fig. 3.[3] This surface was computed using hybrid density functional theory, with the B3LYP functional and the 6-31G(d) basis set, but similar results were obtained with other methods and basis sets. There is clearly a monotonically decreasing barrierless path on this surface from $Al + Cl_2$ (upper right) to $AlCl + Cl$ (lower left). One can also carry out calculations in which only one bond length is constrained and all other internal coordinates are optimized. Such a search will sometimes allow direct identification of a barrierless reaction path. However, this approach does not always end up connecting the desired reactants and products. Similar potential energy surface scans can be carried out for more complex reactions, but at greater computational cost and with less certainty that a genuinely barrierless path can be found. In principle, if one constrains two internal coordinates to specify a point on the path, and then optimizes the remaining coordinates, it is possible that barriers could be missed. The coordinates that are optimized may jump discontinuously between adjacent pairs of constrained coordinates, and there may be a barrier to such a jump that is not observed. In practical calculations, one can constrain additional coordinates that are not involved in the reaction and that do not change much from reactants to products, which reduces the computational cost. One can also visualize the molecule at points along the path from reactants to products to manually look for discontinuous changes in the geometry.

Once it has been established that a reaction is barrierless, the next question is how to estimate the rate parameters. Conventional transition state theory cannot be applied to reactions without a well-defined energetic barrier along the reaction path. Variational transition state theory, which varies the structure of the transition state, or the position of the dividing

[3]An input file for carrying out this potential energy surface scan in the Gaussian programs is included in the CD accompanying this text, along with a Matlab plot file of the surface shown in Fig. 3, which can be loaded into Matlab and then rotated and manipulated.

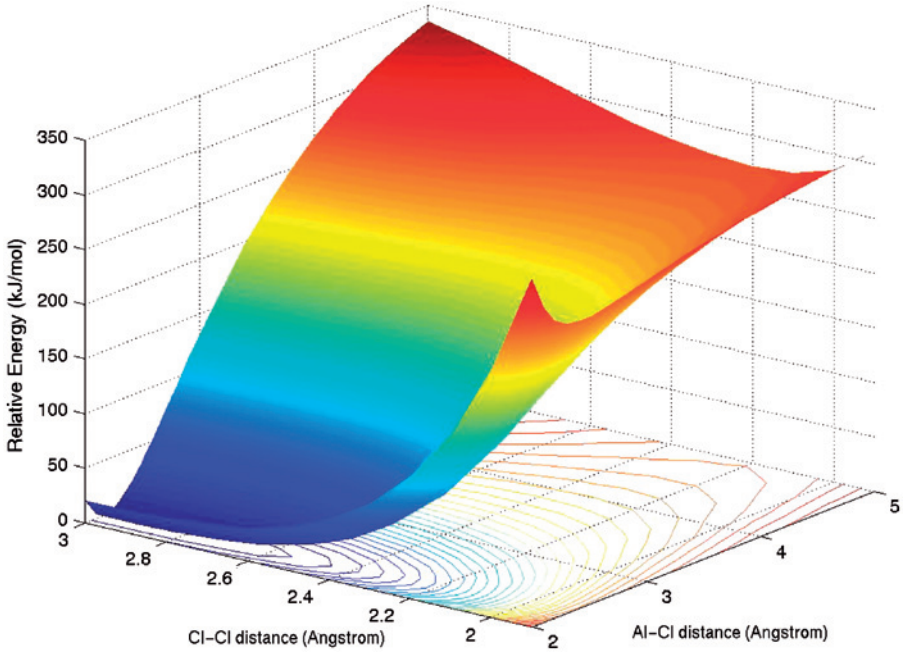

Fig. 3. Potential energy surface for the reaction $Al + Cl_2 \leftrightarrow AlCl + Cl$, with the atoms constrained to be collinear, computed at the UB3LYP/6-31G(d) level of theory.

surface that separates reactants from products, to minimize the rate constant is, in principle, applicable. However, its application is beyond the scope of the present chapter, and will be difficult when the reaction path is not well defined. Barrierless bimolecular reactions are generally expected to be fast, occurring at a significant fraction of the gas-kinetic collision rate, and to have zero or small negative activation energy. The temperature dependence of the rate constant can be roughly estimated from the nature of the reactants, with $T^{1.5}$ dependence expected for atom–molecule reactions, T^2 dependence for diatomic radical–molecule reactions, and T^3 dependence for polyatomic radical–molecule reactions [10,38]. As a first approximation, one can combine this expected temperature dependence with a pre-exponential factor from an analogous reaction to estimate the rate parameter. For example, in the Al–H–Cl system, the $Al + Cl_2$ reaction was studied experimentally by Rogowski *et al.* [33], whose results can be well fit by the expression $k = 7.43 \times 10^9 \times T^{1.5} \exp(+74/T)\,\mathrm{cm}^3/(\mathrm{mol\,sec})$ [10]. This is consistent with the expectation of near-zero activation energy other than the $T^{1.5}$ temperature dependence. In this case, there are two Cl atoms that can be abstracted by Al, so the pre-exponential factor is $\sim 4 \times 10^9$ per abstractable Cl atom. By analogy with this reaction,

we might write the rate parameters for all barrierless abstractions of Cl by Al as $k = m \times 4 \times 10^9 \times T^{1.5}$, where m is the number of abstractable Cl atoms in the molecule from which Cl is being abstracted.

(*iv*) *Unimolecular reactions without an energetic barrier*

Unimolecular reactions without an energetic barrier are fairly common, and are exemplified by simple bond-breaking reactions. In the Al–H–Cl system, an example is reaction (1) in Table 5

$$AlCl_3 \leftrightarrow AlCl_2 + Cl \tag{29}$$

For a simple bond-breaking reaction like this, we know *a priori* that there should be no energetic barrier beyond the heat of reaction. So, we are not faced with the problem of determining whether a barrier exists. It is also fairly straightforward to carry out a sequence of quantum chemistry calculations for different fixed lengths of the breaking bond, while optimizing the other internal coordinates at each step, to obtain a profile of energy vs. bond length. This can be used as input to a variational transition state theory calculation of the rate constant. Programs, such as Unimol [39], Variflex [40], and ChemRate [41], which have been discussed in the earlier chapter on unimolecular reactions, can be used to carry out such calculations. The most difficult aspect of such calculations is the treatment of the degrees of freedom in the transition state structure corresponding to the rotation of the two product fragments. Any detailed discussion of this is beyond the scope of the present chapter. To a first approximation, in the high-pressure limit, such reactions will simply have an activation energy approximately equal to the heat of reaction, and will have a 'large' pre-exponential factor, in the range of 10^{15}–10^{17} sec^{-1}.

4.3 Purely empirical estimation of rate parameters

Especially in the early stages of mechanism development, it is not likely to be practical to carry out quantum chemistry and transition state theory calculations for all the possible reactions in the mechanism. So, simpler empirical methods must be used to obtain initial estimates of the rate parameters. Perhaps the most useful description of these methods is found in the classic text, *Thermochemical Kinetics*, by Benson [42]. The following 'rules of thumb' for estimating rate parameters closely follow what is presented in more detail there. For different classes of reactions, the framework of transition state theory can be applied to aid in the estimation of rate parameters. This is most

often done using a thermodynamic formulation of transition state theory, which can be written as

$$k_f = \frac{k_B T}{h} \exp\left(\frac{\Delta S_0^\dagger}{R}\right) \exp\left(\frac{-\Delta H_0^\dagger}{RT}\right) \tag{30}$$

where $\Delta S_0^\dagger$ is the entropy of activation (the entropy difference between the reactants and transition state) and $\Delta H_0^\dagger$ the enthalpy of activation (the enthalpy difference between the reactants and transition state). Estimation methods for several classes of such reactions follow.

(*i*) *Unimolecular dissociation of one molecule into two by simple bond fission*

Examples : $C_2H_6 \leftrightarrow 2CH_3$, $AlCl_3 \leftrightarrow AlCl_2 + Cl$, $SiCl_4 \leftrightarrow SiCl_3 + Cl$

These reactions proceed by the breaking of a single bond, as discussed in the previous section. There is no energetic barrier beyond the heat of reaction, so the activation energy is approximately equal to the heat of reaction (ΔH_{rxn}). These reactions convert internal (vibrational) degrees of freedom to external (translational and rotational) degrees of freedom. The entropy of the products is therefore substantially greater than that of the reactants. Likewise, the transition state, which is on its way to losing the vibrational modes, is larger and 'looser' than the reactant, and the entropy of activation is positive. Transition states for reactions like this with no maximum in potential energy along the reaction path are called loose transition states. Since the entropy of the transition state is higher than that of the reactants, the factor $\exp(\Delta S_0^\dagger/R)$ is greater than 1, and the pre-exponential factor will be larger than the universal frequency factor, $k_B T/h$. Pre-exponential factors for simple bond fission reactions range from $\sim 10^{15}$ to $10^{17}\,\mathrm{sec}^{-1}$. Note that some reactions that might first appear to be simple bond fissions are not. For example, $C_2H_5 \leftrightarrow C_2H_4 + H$ involves breaking of the C–H bond, but also involves the formation of a bond between the carbon atoms (the C–C single bond becomes a C–C double bond). This reaction has a pre-exponential $\sim 10^{13.6}\,\mathrm{sec}^{-1}$, and an activation energy greater than the heat of reaction. Bond fission reactions will, in general, have pressure dependent rates. As a first approximation, the pressure dependence can be most easily treated using the QRRK approach described in the earlier chapter on pressure dependent reactions.

(*ii*) *Unimolecular isomerization reactions*

Examples : *cis*-butene $\leftrightarrow$ *trans*-butene, $H_3SiSiH \leftrightarrow H_2SiSiH_2$

In general, isomerization reactions have an entropy of activation near zero; the transition state will be about the same size and has about the same vibrational frequencies as the reactant. There may be a small negative entropy of activation since one vibrational mode in the reactant becomes the reaction coordinate in the transition state. Since there is almost no entropy of activation, pre-exponential factors for isomerizations are typically $\sim 10^{13}\,\mathrm{sec}^{-1}$. In general, there is no simple way to predict the activation energy of these reactions. However, for the particular class of *cis–trans* isomerizations, the activation energy is approximately equal to the energy needed to change the double bond into a single bond and a biradical (breaking the pi bond, but not the sigma bond joining the two atoms).

(*iii*) *Complex unimolecular dissociation reactions with cyclic transition states*

$$Si_2H_6 \leftrightarrow SiH_4 + SiH_2, \quad CH_3CH_2Cl \leftrightarrow C_2H_4 + HCl,$$
$$CH_3CH(NO)_2CH_3 \leftrightarrow CH_3CHCH_2 + HONO,$$
$$CH_3COOCH_2CH_2CH_3 \leftrightarrow CH_3COOH + CH_3CHCH_2$$

These four reactions proceed through transition states with three-, four-, five-, and six-membered rings, respectively, as illustrated schematically in Fig. 4. There is no simple way to predict the activation energy of these reactions. The best that one can usually do is to try to find a similar reaction and make a guess by analogy. The entropy of activation for these reactions can be positive or negative. The entropy of reaction is always positive, since we are forming two molecules from one (converting six vibrational degrees of freedom to rotational and translational degrees of freedom). This leads to an increase in entropy in going from reactant to transition state, as bonds become longer and looser (lower vibrational frequencies lead to more entropy contribution from those vibrations). However, there is entropy lost in forming the ring. In the transition state, some reactant bonds are replaced by a larger number of partial bonds. The pre-exponential factor is $\sim 10^{13.5}$ for many four-centered eliminations like the HCl elimination shown above. Pre-exponential factors for reactions with five- and six-center transition states range from 10^{11} (substantial negative entropy of activation) to 10^{15} (substantial positive entropy of activation).

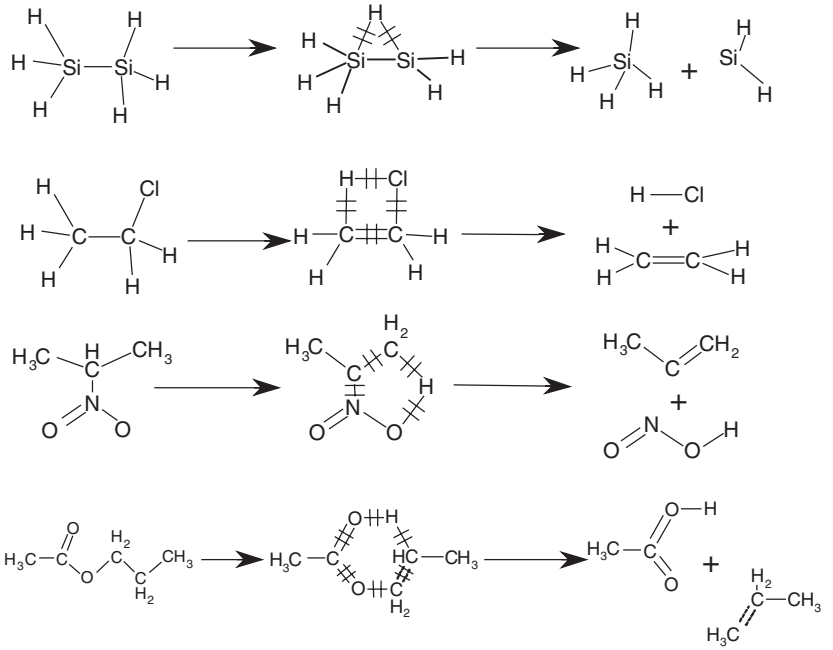

Fig. 4. Schematic illustration of reactions proceeding through three-, four-, five-, and six-membered cyclic transition states.

(*iv*) *Bimolecular association reactions*

$$\text{Examples :} \quad 2CH_3 \leftrightarrow C_2H_6, \quad AlCl_2 + Cl \leftrightarrow AlCl_3, \quad SiCl_3 + Cl \leftrightarrow SiCl_4$$

These are the reverse of unimolecular decomposition reactions. The decomposition reaction can be analyzed by the means discussed above, and then the rate constant for the association reaction can be obtained using the equilibrium constant. When doing this, it is important to check that the rate of the association reaction does not substantially exceed the gas-kinetic collision rate. If it does, then there is probably a problem with the decomposition rate constant, the equilibrium constant, or both.

(*v*) *Bimolecular abstraction reactions*

$$\text{Examples :} \quad H + C_2H_6 \leftrightarrow H_2 + C_2H_5, \quad AlCl_2 + Cl_2 \leftrightarrow AlCl_3 + Cl$$

For bimolecular reactions, the entropy of activation is always negative, since two reactants combine into one transition state (converting translational and rotational degrees of freedom into vibrations). For

atom + molecule reactions, only translational degrees of freedom are lost in going from the reactants to transition state. For many atom + molecule metathesis reactions, the pre-exponential factor is $\sim 10^{14}\,\mathrm{cm}^3/(\mathrm{mol\,sec})$. For molecule + molecule metathesis reactions, rotational degrees of freedom are also lost, and therefore the entropy of activation is more negative and the pre-exponential is smaller. One can also think of this as relating to the fact that a molecule + molecule reaction requires a certain orientation of both reactants, while a molecule + atom reaction requires no special orientation of the (spherically symmetric) atom. For many molecule + molecule reactions, the pre-exponential factor is $\sim 10^{11.5}\,\mathrm{cm}^3/(\mathrm{mol\,sec})$. There is no general means of estimating the activation energy for these reactions.

4.4 Linear free energy relationships and correlations for estimating activation energies

As we have seen above, there are some reasonable ways to go about estimating the thermochemistry of a reaction and the pre-exponential factor for certain types of reactions. Unfortunately, there are no similar methods for predicting the activation energies of chemical reactions. For certain classes of reactions, some correlations are available. Sometimes the activation energies of a series of reactions of the same type can be written as

$$E_a = \alpha\,\Delta H \tag{31}$$

where ΔH is the enthalpy of reaction and α a proportionality constant for a particular class of reactions. This is known as an Evans–Polanyi relationship or a linear free energy relationship. It is a simple, but not terribly accurate or widely applicable, means of correlating the activation energy with the heat of reaction. The value of α must be fit to whatever experimental activation energies are known. Broader or narrower definitions of reaction classes can be used, depending on the amount of data available. An example of this is the description of H-abstraction reactions presented by Blowers and Masel [43].

5 APPLYING THE MECHANISM AT CONDITIONS OF INTEREST

Once one has assembled an initial version of a reaction mechanism, the next step is to apply it under conditions representative of the original problem of interest. This can usually be done at a variety of levels of detail with respect to the other aspects of the problem. For example, if

one's aim was to model chemical vapor deposition of aluminum from $AlCl_3$ in the presence of hydrogen and/or HCl, then the reaction mechanism that we have been using as an example might provide a good representation of the relevant gas-phase chemistry. The real reactor of interest might have cooled walls and a heated substrate onto which an aluminum film is to be deposited. Thus, in the real physical system of interest, this gas-phase chemistry could be coupled in a complicated way to surface chemistry, fluid flow, and heat transfer by convection, conduction, and radiation. With modern computational fluid dynamics (CFD) software packages, it is possible to conduct simulations that include all this in detail, at least for a relatively small number of chemical species and reactions. However, it would probably not be prudent to do so with a preliminary version of the reaction mechanism being developed. At the other extreme, one could simply model the gas-phase reactions in isolation, at a fixed temperature, in a constant-volume or constant-pressure batch reactor. Doing this at a range of conditions (temperature, pressure, initial composition) similar to those expected in the situation of interest is probably the most efficient way to initially explore the behavior of a newly developed reaction mechanism. One can build from this point with simple simulations that incorporate surface reactions, perhaps initially still assuming uniform composition and a fixed surface-to-volume ratio, to begin to explore the coupling of surface and gas-phase chemistry. This is a logical next step for systems such as chemical vapor deposition where surface reactions are a key part of the process. Likewise, one can add an energy balance equation to the system of chemical species balances, for the simple batch reactor system, perhaps also with heat flows to or from the surroundings, to explore the behavior of the chemistry under non-isothermal conditions. This is a logical next step for systems where heat release is known to be large or important, such as combustion or propulsion systems. As the reaction mechanism is refined, one can increase the sophistication of the remainder of the model. Next steps might include simulations in one spatial dimension, such as a stagnation point flow or opposed jets geometry, or a boundary-layer model with one spatial dimension and one time-like spatial dimension in which diffusive processes are not considered.

Throughout this process, there will be tradeoffs between the levels of detail included in the different aspects of the model. For example, in a simple batch reactor model, one can include thousands of chemical species and reactions, whereas in a detailed three-dimensional fully coupled model of fluid flow, heat transfer, and chemical reactions, one might be limited to less than 20 chemical species and a similar number of reactions. With continuous advances in both computational hardware and

simulation software, these capabilities continue to expand. However, even if a fully coupled multi-dimensional model is computationally tractable, it may provide such an unmanageably large and detailed set of results that it provides less insight into the problem than a much simpler model. Thus, for purposes of mechanism development, it is usually wise to start from the simplest possible model relevant to the system of interest. This often means starting from a zero-dimensional batch reactor simulation where both the simulation itself and the analysis of results are considerably simpler than for models that include spatial distributions of temperature, fluid velocity, and species compositions. Thus, here we focus on the analysis of reaction mechanisms using simple zero-dimensional batch reactor simulations.

To illustrate the application and analysis of a reaction mechanism we will consider the thermal decomposition of $AlCl_3$ in an isothermal batch reactor in the presence of H_2. If the reactor is at fixed temperature and pressure, then we can take the rate constant for each of the reactions to be constant. Table 10 lists the reaction mechanism for this system with expressions for evaluating the forward rate parameters and numerical values (and units) of the forward and reverse rate constants at 1300 K and 0.1 bar total pressure. The expressions for the forward rate constants are from Swihart *et al.* [10]. The reverse rate constants were calculated based on equilibrium constants obtained using thermochemical data from the HiTempThermo database.[4] Note that this mechanism contains many fewer reactions than we had listed in the preliminary mechanism shown in Table 4. One reason for this is that none of the possible reactions involving multiple Al atoms have been included (reactions (52)–(78) of Table 4). In addition, after evaluating the thermochemistry and finding, estimating, or calculating rate parameters, many of the postulated reactions were found to be slower than competing reaction channels, in both directions. These reactions are not expected to be significant under any circumstance and can therefore be omitted. In many cases, the rate parameters were more easily computed or estimated for the reverse reaction, relative to the arbitrary direction in which reactions were written in Table 4, so many reactions in Table 10 are written in the reverse direction compared to Table 4. Finally, for one reaction, two different reaction channels (one direct and one chemically activated) with the same reactants and products are possible. As a result, this reaction is included twice, with two different expressions for the forward rate constant.

[4] A CHEMKIN input file containing the thermochemical data and rate expressions in the NASA polynomial form is included in the CD that accompanies this text. For details of this format, see the CHEMKIN documentation [44,45] and http://www.reactiondesign.com

TABLE 10
Al–H–Cl reaction mechanism with rate parameters

Reaction number	Table 4 number[a]	Reaction	$k(T, P)$[b]	k_f (1300 K, 0.1 bar)	k_r (1300 K, 0.1 bar)[c]
1	1	$AlCl_3 + (M) \leftrightarrow AlCl_2 + Cl + (M)$	$k_\infty = 1.7 \times 10^{15} \exp(-54788/T)$[d] $k_0 = 3.9 \times 10^{16} \exp(-43602/T)$ $F_c = 0.62 \exp(-T/309) + 0.38 \exp(-T/5695)$ $+ \exp(-7478/T)$	$4.23 \times 10\ \mathrm{sec}^{-1}$	$3.92 \times 10^{19}\ \mathrm{cm}^3/$ (mol sec)
2	4	$AlH_2Cl + (M) \leftrightarrow AlHCl + H + (M)$	$k_\infty = 2.08 \times 10^{15} \exp(-42523/T)$[d] $k_0 = 7.67 \times 10^{12} \exp(-40050/T)$ $F_c = 1.7$	$3.20 \times 10^{-1}\ \mathrm{sec}^{-1}$	$2.36 \times 10^{12}\ \mathrm{cm}^3/$ (mol sec)
3	7	$AlCl_2 + (M) \leftrightarrow AlCl + Cl + (M)$	$k_\infty = 1.92 \times 10^{14} \exp(-32291/T)$[d] $k_0 = 1.63 \times 10^{15} \exp(-26915/T)$ $F_c = 1.17 \exp(-T/1307) – 0.17 \exp(-T/376)$ $+ \exp(-2209/T)$	$1.54 \times 10^{6}\ \mathrm{sec}^{-1}$	$5.86 \times 10^{17}\ \mathrm{cm}^3/$ (mol sec)
4	8	$AlHCl + (M) \leftrightarrow AlCl + H + (M)$	$k_\infty = 4.94 \times 10^{15} \exp(-17284/T)$[d] $k_0 = 3.36 \times 10^{14} \exp(-14180/T)$ $F_c = 1.61 \exp(-T/642) – 0.61 \exp(-T/4609)$ $+ \exp(-250/T)$	$5.87 \times 10^{9}\ \mathrm{sec}^{-1}$	$9.78 \times 10^{15}\ \mathrm{cm}^3/$ (mol sec)
5	10	$AlH_2 + (M) \leftrightarrow AlH + H + (M)$	$k_\infty = 1.46 \times 10^{15} \exp(-23376/T)$[d] $k_0 = 9.68 \times 10^{14} \exp(-19962/T)$ $F_c = -4.1 \exp(-T/21.6) + 5.1 \exp(-T/493)$ $+ \exp(-942/T)$	$2.05 \times 10^{8}\ \mathrm{sec}^{-1}$	$1.97 \times 10^{16}\ \mathrm{cm}^3/$ (mol sec)
6	11R	$(Al + Cl + M \leftrightarrow AlCl + M)$[e]	$k_0 = 1.2 \times 10^{17}\ T^{-0.20}$	$2.61 \times 10^{10}\ \mathrm{cm}^3/$ (mol sec)	$5.44 \times 10^{-11}\ \mathrm{sec}^{-1}$

7	12R	$(Al + H + M \leftrightarrow AlH + M)^e$	$k_0 = 1.6 \times 10^{17}\, T^{-0.34}$	$1.28 \times 10^{10}\,cm^3/$ (mol sec)	$3.13 \times 10^{-3}\,sec^{-1}$
8	13	$(H_2 + M \leftrightarrow 2H + M)^e$	$k_0 = 2.23 \times 10^{14} \exp(-48350/T)$	$1.43 \times 10^{-8}\,sec^{-1}$	$1.13 \times 10^{9}\,cm^3/$ (mol sec)
9	14	$(HCl + M \leftrightarrow H + Cl + M)^e$	$k_0 = 9 \times 10^{13} \exp(-44000/T)$	$1.64 \times 10^{-7}\,sec^{-1}$	$3.91 \times 10^{10}\,cm^3/$ (mol sec)
10	15	$(Cl_2 + M \leftrightarrow 2Cl + M)^e$	$k_0 = 2.3 \times 10^{13} \exp(-23630/T)$	$2.68 \times 10^{-1}\,sec^{-1}$	$1.07 \times 10^{9}\,cm^3/$ (mol sec)
11	18	$AlHCl_2 + (M) \leftrightarrow AlCl + HCl + (M)$	$k_\infty = 1.63 \times 10^{12} \exp(-33016/T)^d$ $k_0 = 4.07 \times 10^{15} \exp(-29140/T)$ $F_c = 0.39 \exp(-T/1363) + 0.61 \exp(-T/189)$	$1.77 \times 10^{5}\,sec^{-1}$	$4.64 \times 10^{12}\,cm^3/$ (mol sec)
12	19	$AlH_2Cl + (M) \leftrightarrow AlH + HCl + (M)$	$k_\infty = 3.60 \times 10^{14} \exp(-37351/T)^d$ $k_0 = 1.96 \times 10^{15} \exp(-31774/T)$ $F_c = 0.35 \exp(-T/3323) + 0.65 \exp(-T/299)$ $+ \exp(-13590/T)$	$3.32 \times 10^{4}\,sec^{-1}$	$2.02 \times 10^{14}\,cm^3/$ (mol sec)
13	20	$AlH_2Cl + (M) \leftrightarrow AlCl + H_2 + (M)$	$k_\infty = 4.47 \times 10^{13} \exp(-37840/T)^d$ $k_0 = 1.95 \times 10^{15} \exp(-31774/T)$ $F_c = 0.01 \exp(T/951) + 0.99 \exp(-T/1613)$ $+ \exp(-187/T)$	$4.86 \times 10^{4}\,sec^{-1}$	$7.56 \times 10^{6}\,cm^3/$ (mol sec)
14	21	$AlH_3 + (M) \leftrightarrow AlH + H_2 + (M)$	$k_\infty = 1.48 \times 10^{13} \exp(-30756/T)^d$ $k_0 = 1.01 \times 10^{15} \exp(-27089/T)$ $F_c = 0.94 \exp(-T/885) + 0.06 \exp(-T/552)$ $+ \exp(-3807/T)$	$6.25 \times 10^{5}\,sec^{-1}$	$4.63 \times 10^{9}\,cm^3/$ (mol sec)
15	25	$AlCl_3 + H \leftrightarrow AlCl_2 + HCl$	$k = 7.76 \times 10^{8}\, T^{1.63} \exp(-10321/T)$	$3.29 \times 10^{10}\,cm^3/$ (mol sec)	$1.28 \times 10^{11}\,cm^3/$ (mol sec)
16	26R	$AlCl_2 + Cl_2 \leftrightarrow AlCl_3 + Cl$	$k = 10^{3}\, T^{3}$	$2.20 \times 10^{12}\,cm^3/$ (mol sec)	$9.45 \times 10^{3}\,cm^3/$ (mol sec)
17	27	$AlHCl_2 + H \leftrightarrow AlCl_2 + H_2$	$k = 1.25 \times 10^{8}\, T^{1.78} \exp(-318/T)$	$3.42 \times 10^{13}\,cm^3/$ (mol sec)	$7.13 \times 10^{9}\,cm^3/$ (mol sec)

Table 10. (*Continued*)

Reaction number	Table 4 number[a]	Reaction	$k(T, P)$[b]	k_f (1300 K, 0.1 bar)	k_r (1300 K, 0.1 bar)[c]
18	28	$AlHCl_2 + H \leftrightarrow AlHCl + HCl$	$k = 3.45 \times 10^8\, T^{1.64} \exp(-10610/T)$	1.26×10^{10} cm^3/(mol sec)	1.99×10^{11} cm^3/(mol sec)
19	29	$AlHCl_2 + Cl \leftrightarrow AlCl_2 + HCl$	$k = 1.6 \times 10^9\, T^{1.5}$	7.50×10^{13} cm^3/(mol sec)	5.18×10^9 cm^3/(mol sec)
20	30R	$AlHCl + Cl_2 \leftrightarrow AlHCl_2 + Cl$	$k = 10^3\, T^3$	2.20×10^{12} cm^3/(mol sec)	2.33×10^3 cm^3/(mol sec)
21	31	$AlH_2Cl + H \leftrightarrow AlHCl + H_2$	$k = 3.2 \times 10^9\, T^{1.5}$	1.50×10^{14} cm^3/(mol sec)	1.40×10^{10} cm^3/(mol sec)
22	32R	$AlH_2 + HCl \leftrightarrow AlH_2Cl + H$	$k = 5 \times 10^2\, T^3$	1.10×10^{12} cm^3/(mol sec)	1.73×10^{10} cm^3/(mol sec)
23	33	$AlH_2Cl + Cl \leftrightarrow AlHCl + HCl$	$k = 3.2 \times 10^9\, T^{1.5}$	1.50×10^{14} cm^3/(mol sec)	4.64×10^9 cm^3/(mol sec)
24	35	$AlH_3 + H \leftrightarrow AlH_2 + H_2$	$k = 4.8 \times 10^9\, T^{1.5}$	2.25×10^{14} cm^3/(mol sec)	1.74×10^{10} cm^3/(mol sec)
25	36	$AlH_3 + Cl \leftrightarrow AlH_2 + HCl$	$k = 4.8 \times 10^9\, T^{1.5}$	2.25×10^{14} cm^3/(mol sec)	5.75×10^9 cm^3/(mol sec)
26	37R	$AlCl + HCl \leftrightarrow AlCl_2 + H$	$k = 9.55 \times 10^4\, T^{2.55} \exp(-15970/T)$	3.85×10^7 cm^3/(mol sec)	2.41×10^{13} cm^3/(mol sec)
27	37R,CA	$AlCl + HCl \leftrightarrow AlCl_2 + H$	$k = 4.75 \times 10^{-2}\, T^{3.98} \exp(-7734/\mathrm{T})$	3.07×10^8 cm^3/(mol sec)	1.92×10^{14} cm^3/(mol sec)
28	38	$AlCl + Cl_2 \leftrightarrow AlCl_2 + Cl$	$k = 1.97 \times 10^7\, T^2 \exp(574/T)$	5.18×10^{13} cm^3/(mol sec)	5.42×10^{11} cm^3/(mol sec)
29	39	$AlHCl + H \leftrightarrow AlCl + H_2$	$k = 1 \times 10^{13}$	1.00×10^{13} cm^3/(mol sec)	2.11×10^2 cm^3/(mol sec)
30	41	$AlHCl + Cl \leftrightarrow AlCl + HCl$	$k = 1 \times 10^{13}$	1.00×10^{13} cm^3/(mol sec)	7.00×10^1 cm^3/(mol sec)
31	43	$AlH_2 + H \leftrightarrow AlH + H_2$	$k = 2 \times 10^{13}$	2.00×10^{13} cm^3/(mol sec)	2.44×10^4 cm^3/(mol sec)
32	44	$AlH_2 + Cl \leftrightarrow AlH + HCl$	$k = 2 \times 10^{13}$	2.00×10^{13} cm^3/(mol sec)	8.07×10^3 cm^3/(mol sec)

33	45R	$Al + HCl \leftrightarrow AlCl + H$	$k = 9.27 \times 10^8\, T^{1.5} \exp(326/T)$	$5.58 \times 10^{13}\,cm^3/$ (mol sec)	$2.76 \times 10^{10}\,cm^3/$ (mol sec)
34	46R	$AlH + Cl \leftrightarrow AlCl + H$	$k = 1 \times 10^{13}$	$1.00 \times 10^{13}\,cm^3/$ (mol sec)	$8.48 \times 10^{4}\,cm^3/$ (mol sec)
35	47R	$Al + Cl_2 \leftrightarrow AlCl + Cl$	$k = 7.43 \times 10^9\, T^{1.5} \exp(74/T)$	$3.69 \times 10^{14}\,cm^3/$ (mol sec)	$3.06 \times 10^{3}\,cm^3/$ (mol sec)
36	48	$AlH + H \leftrightarrow Al + H_2$	$k = 1 \times 10^{13}$	$1.00 \times 10^{13}\,cm^3/$ (mol sec)	$5.17 \times 10^{8}\,cm^3/$ (mol sec)
37	49	$AlH + Cl \leftrightarrow Al + HCl$	$k = 1 \times 10^{13}$	$1.00 \times 10^{13}\,cm^3/$ (mol sec)	$1.71 \times 10^{8}\,cm^3/$ (mol sec)
38	50	$Cl_2 + H \leftrightarrow Cl + HCl$	$k = 3.31 \times 10^{14} \exp(-1460/T)$	$1.08 \times 10^{14}\,cm^3/$ (mol sec)	$1.81 \times 10^{6}\,cm^3/$ (mol sec)
39	51R	$H_2 + Cl \leftrightarrow HCl + H$	$k = 2.88 \times 10^8\, T^{1.58} \exp(-1610/T)$	$6.94 \times 10^{12}\,cm^3/$ (mol sec)	$2.30 \times 10^{12}\,cm^3/$ (mol sec)

[a]The reaction number for this reaction in Table 4. R following the reaction number indicates that the reaction is written in the reverse direction, relative to the way it is written in Table 4. CA indicates a chemically activated reaction channel that competes with the same reaction occurring by a direct channel.

[b]Rate constant equation for use with units of K for temperature, sec for time, and mol/cm^3 for concentration, taken from Ref. [10].

[c]Rate constants for the reverse reactions were computed using the forward rate constant and the equilibrium constant based on the thermochemical properties from the HiTempThermo Database (http://www.ca.sandia.gov/HiTempThermo). Enthalpies of formation and standard entropies are given in Table 5.

[d]Rate expressions for pressure-dependent reactions are given in the 'Troe' form with up to seven parameters. Details of this parameterization of the pressure dependence are discussed elsewhere in this volume, and in the original papers by Troe and co-workers [47,48].

[e]As indicated by their units, rate parameters for these third-body-assisted reactions include the total concentration, [M], in the rate constant evaluated at this particular pressure.

For analyzing detailed reaction mechanisms, it is usually convenient to assign numerical indices to the species and reactions under consideration. Thus, we can write the reaction mechanism formally as

$$\sum_{k=1}^{K} \nu_{ki} A_k = 0, \quad i = 1, I \tag{32}$$

where A_k is the kth chemical species and ν_{ki} the net stoichiometric coefficient of the kth species in the ith reaction. By convention, the stoichiometric coefficients are negative for reactants and positive for products. The total number of chemical species is K and the total number of reactions is I. Thus, the stoichiometric coefficients form a sparse matrix with K rows and I columns. The change in species concentrations with time in a constant-volume batch reactor can be written as

$$\frac{\mathrm{d}[X_k]}{\mathrm{d}t} = \sum_{i=1}^{I} \nu_{ki} r_i \tag{33}$$

where r_i is the net rate (forward minus reverse) of the ith reaction (moles per volume per time) and $[X_k]$ the concentration of the kth species (moles per volume). If the reaction mechanism is made up of elementary reactions that obey the law of mass action, then the rate of the ith reaction will be given by

$$r_i = k_{\mathrm{f},i} \prod_{k=1}^{K} [X_k]^{\nu'_{ki}} - k_{\mathrm{r},i} \prod_{k=1}^{K} [X_k]^{\nu''_{ki}} \tag{34}$$

where $k_{\mathrm{f},i}$ and $k_{\mathrm{r},i}$ are the forward and reverse rate constants for the ith reaction, ν''_{ki} the forward stoichiometric coefficient of species k in reaction i, and ν''_{ki} the reverse stoichiometric coefficient of species k in reaction i. Thus, if ν_{ki} is negative, then $\nu'_{ki} = -\nu_{ki}$ and $\nu''_{ki} = 0$; if ν_{ki} is positive, then $\nu'_{ki} = 0$ and $\nu''_{ki} = \nu_{ki}$; and if $\nu_{ki} = 0$, then $\nu'_{ki} = \nu''_{ki} = 0$. With all these definitions, the equations governing the concentrations of the species in a constant-volume batch reactor can be written as

$$\frac{\mathrm{d}[X_k]}{\mathrm{d}t} = \sum_{i=1}^{I} \nu_{ki} \left(k_{\mathrm{f},i} \prod_{m=1}^{K} [X_m]^{\nu'_{mi}} - k_{\mathrm{r},i} \prod_{m=1}^{K} [X_m]^{\nu''_{mi}} \right), \quad \text{for } k = 1 \text{ to } K \tag{35}$$

This is a set of K ordinary differential equations that can readily be solved numerically. Doing so, for a given set of initial concentrations (at $t = 0$) and values of the rate parameters, provides the concentrations of all the species at a series of time points. The rate constants in the above

expression are, in general, functions of both temperature and pressure. Thus, for gas-phase reactions, they cannot be held strictly constant in a constant-volume batch reactor. If there is a change in the total number of moles due to reaction, then the temperature, pressure, and volume of the mixture cannot all remain constant. Nonetheless, the above approach (with constant values of k, evaluated at the initial pressure) is often a fine approximation for a constant-volume, isothermal system. Since the goal at this stage is only to analyze the overall behavior of the reaction mechanism, and not to model any particular physical system, it makes sense to proceed with this simple approach.

Returning to our example of the Al–H–Cl chemistry, we see that we have 39 reversible reactions ($I = 39$) among 15 chemical species ($K = 15$). The species will be indexed as in Table 5, and the reactions will be indexed as in Table 10. The resulting matrix of stoichiometric coefficients is shown in Table 11. The rate equations (equation (35)) were integrated using Matlab to yield the profiles of concentration vs. time shown in Fig. 5.[5] For these conditions, 0.1 bar, 1300 K, and initially 1% $AlCl_3$ in H_2, gas-phase equilibrium has been achieved by the final time of 10 sec, and integrating to longer times results in no further changes in the species concentrations. Examining the results, we see that the overall reaction that occurs on a macroscopic time scale is

$$AlCl_3 + H_2 \leftrightarrow AlCl + 2HCl \tag{36}$$

At equilibrium, the $AlCl_3$ concentration has decreased by ~17% from its initial value. Of course, this overall reaction does not happen in a single step, but results from a series of intermediate elementary reactions. Examination of the concentration profiles shown in Fig. 5 provides some initial insight into how it occurs. The first new species to appear are $AlCl_2$ and Cl. For the first 100 nsec or so, these are formed in equal amounts, which suggests that the only reaction occurring on such short time scales is

$$AlCl_3 \leftrightarrow AlCl_2 + Cl \tag{37}$$

After ~100 nsec, the $AlCl_2$ and Cl concentrations begin to differ, and the concentrations of H atoms and HCl exceed those of $AlCl_2$ and Cl. The AlCl concentration follows the H and HCl concentrations, but is

[5] A short Matlab function and an example of its use with built-in Matlab ODE solvers to produce the results shown in Fig. 5 are included in the CD that accompanies this text. Such calculations are also easily carried out using the SENKIN code [46] from the CHEMKIN family of codes (http://www.reactiondesign.com) or using elements of the Cantera suite of reacting flow tools (http://www.cantera.org).

TABLE 11
Matrix of stoichiometric coefficients for mechanism of Table 10[a]

	1	2	3	4	5	6	7	8	9	10	11	12	13	14	15	16	17	18	19	20	21	22	23	24	25	26	27	28	29	30	31	32	33	34	35	36	37	38	39
1	−1	0	0	0	0	0	0	0	0	0	0	0	0	0	−1	1	0	0	0	0	0	0	0	0	0	0	0	0	0	0	0	0	0	0	0	0	0	0	0
2	0	0	0	0	0	0	0	0	0	0	−1	0	0	0	0	0	−1	−1	−1	1	0	0	0	0	0	0	0	0	0	0	0	0	0	0	0	0	0	0	0
3	0	−1	0	0	0	0	0	0	0	0	0	−1	−1	0	0	0	0	0	0	0	−1	1	−1	0	0	0	0	0	0	0	0	0	0	0	0	0	0	0	0
4	0	0	0	0	0	0	0	0	0	0	0	0	0	−1	0	0	0	0	0	0	0	0	0	−1	−1	0	0	0	0	0	0	0	0	0	0	0	0	0	0
5	1	0	−1	0	0	0	0	0	0	0	0	0	0	0	1	−1	1	0	1	0	0	0	0	0	0	1	1	1	0	0	0	0	0	0	0	0	0	0	0
6	0	1	0	−1	0	0	0	0	0	0	0	0	0	0	0	0	0	1	0	−1	1	0	1	0	0	0	0	0	−1	−1	0	0	0	0	0	0	0	0	0
7	0	0	0	0	−1	0	0	0	0	0	0	0	0	0	0	0	0	0	0	0	0	−1	0	1	1	0	0	0	0	0	−1	−1	0	0	0	0	0	0	0
8	0	0	1	1	0	1	0	0	0	0	1	0	1	0	0	0	0	0	0	0	0	0	0	0	0	−1	−1	−1	1	1	0	0	1	1	1	0	0	0	0
9	0	0	0	0	1	0	1	0	0	0	0	1	0	1	0	0	0	0	0	0	0	0	0	0	0	0	0	0	0	0	1	1	0	−1	0	−1	−1	0	0
10	0	0	0	0	0	−1	−1	0	0	0	0	0	0	0	0	0	0	0	0	0	0	0	0	0	0	0	0	0	0	0	0	0	−1	0	−1	1	1	0	0
11	0	0	0	0	0	0	0	0	0	−1	0	0	0	0	0	−1	0	0	0	−1	0	0	0	0	0	0	0	−1	0	0	0	0	0	0	−1	0	0	−1	0
12	0	0	0	0	0	0	0	0	−1	0	1	1	0	0	1	0	0	1	1	0	0	−1	1	0	1	−1	−1	0	0	1	0	1	−1	0	0	0	1	1	1
13	0	0	0	0	0	0	0	−1	0	0	0	0	1	1	0	0	1	0	0	0	1	0	0	1	0	0	0	0	1	0	1	0	0	0	0	1	0	0	−1
14	1	0	1	0	0	−1	0	0	1	2	0	0	0	0	0	1	0	0	−1	1	0	0	−1	0	−1	0	0	1	0	−1	0	−1	0	−1	1	0	−1	1	−1
15	0	1	0	1	1	0	−1	2	1	0	0	0	0	0	−1	0	−1	−1	0	0	−1	1	0	−1	0	1	1	0	−1	0	−1	0	1	1	0	−1	0	−1	1

[a]The first row of the table gives the column numbers, which correspond to reaction numbers in Table 10. The first column of the table gives the row numbers, which correspond to the species numbers in Table 5.

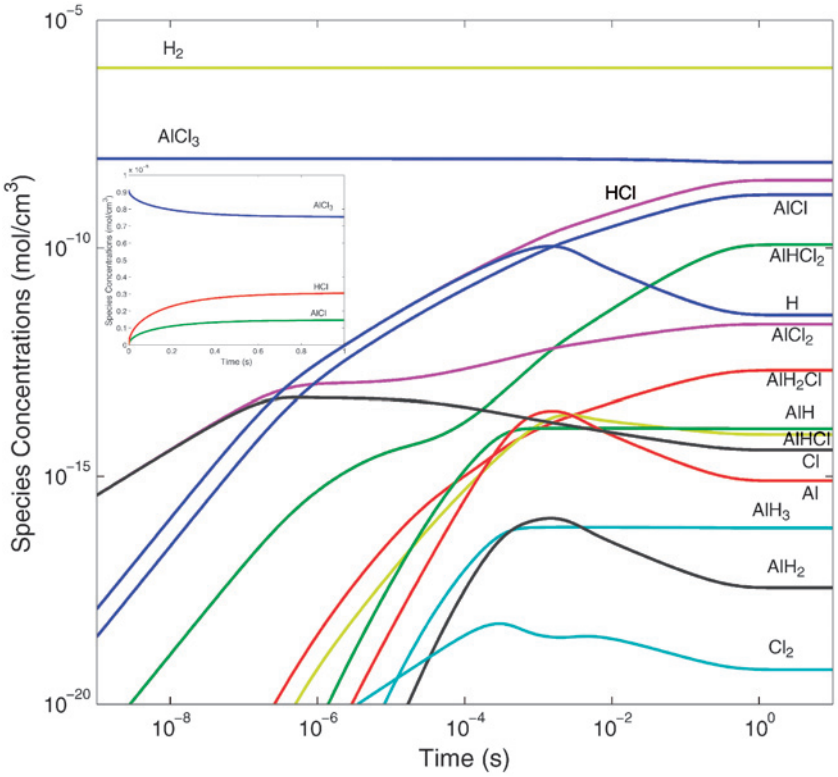

Fig. 5. Profiles of species concentrations vs. time predicted by the mechanism and rate parameters of Table 10 (at 1300 K and 0.1 bar), for an initial composition of 99% H_2, 1% $AlCl_3$. The full plot shows all species on a log–log scale to capture the reaction dynamics across all time scales and species concentrations, which span many orders of magnitude. The inset shows the concentrations of the major reactant and products, $AlCl_3$, AlCl, and HCl, on a linear scale.

lower by a factor of ~2. The H and HCl formations might be attributed to reactions including

$$Cl + H_2 \leftrightarrow HCl + H \tag{38}$$

$$AlCl_2 \leftrightarrow AlCl + Cl \tag{39}$$

At times from ~100 nsec to ~100 μsec, the AlCl, H, and HCl concentrations increase with the same slope (on a log–log scale) with which the $AlCl_2$ and Cl concentrations increased at shorter time. At times longer than 100 μsec, the H atom concentration separates from the HCl concentration. This can most likely be attributed to reaction of H atoms with $AlCl_3$. However, rather than continuing to analyze the mechanism based only on the species concentrations, we should also consider reaction

rates and the importance of individual reactions in determining species concentrations, as discussed in the next section.

6 REACTION RATE/FLUX ANALYSIS AND SENSITIVITY ANALYSIS

The next step in analyzing a reaction mechanism, with an eye toward identifying deficiencies and refining the mechanism, is to examine the rates of individual reactions in the mechanism and the dependence of species concentrations on the rates of individual reactions. We will continue with the Al–H–Cl chemistry to illustrate this, first *via* the straightforward reaction rate analysis, followed by the somewhat more involved sensitivity analysis, which identifies which reaction rate parameters are most important in determining particular species concentrations.

In analyzing reaction rates, although we could look at the forward and reverse reaction rates separately, it is often more informative to look at net reaction rates, or reaction fluxes. Since we already have the species concentrations at a series of times, we can simply evaluate equation (34) to obtain the net reaction rates. We could obtain the forward and reverse rates separately by evaluating just one term or the other in equation (34). Fig. 6 shows the net reaction rates for the reactions with the highest net rates, for the same conditions as the concentration profiles shown in Fig. 5.[6] The results in Fig. 6 are consistent with the discussion above that was based on the concentration profiles of Fig. 5. Initially $AlCl_3$ decomposition into $AlCl_2$ and Cl (reaction 1 in Fig. 6, equation (37)) dominates. After ~100 nsec, the rates of $AlCl_2$ decomposition and reaction of Cl atoms with H_2 (reactions 3 and 39 in Fig. 6, equations (38) and (39)) match the rate of $AlCl_3$ decomposition. After a few hundred microseconds, the rate of reaction of $AlCl_3$ with H (reaction 15 in Fig. 6, equation (40)) exceeds the rate of $AlCl_3$ unimolecular decomposition

$$AlCl_3 + H \leftrightarrow AlCl_2 + HCl \tag{40}$$

Likewise, eventually the rate of $AlCl_2$ reaction with H (reaction −27 in Fig. 6, equation (41)) exceeds the rate of $AlCl_2$ unimolecular decomposition

$$AlCl_2 + H \leftrightarrow AlCl + HCl \tag{41}$$

As the system approaches equilibrium, all the net reaction rates approach zero. Overall, it appears that both unimolecular decomposition (equation (37)) and reaction with H atoms (equation (40)) contribute to the decrease in $AlCl_3$ concentration.

[6] A short Matlab function for evaluating the reaction rates is included in the CD that accompanies this text.

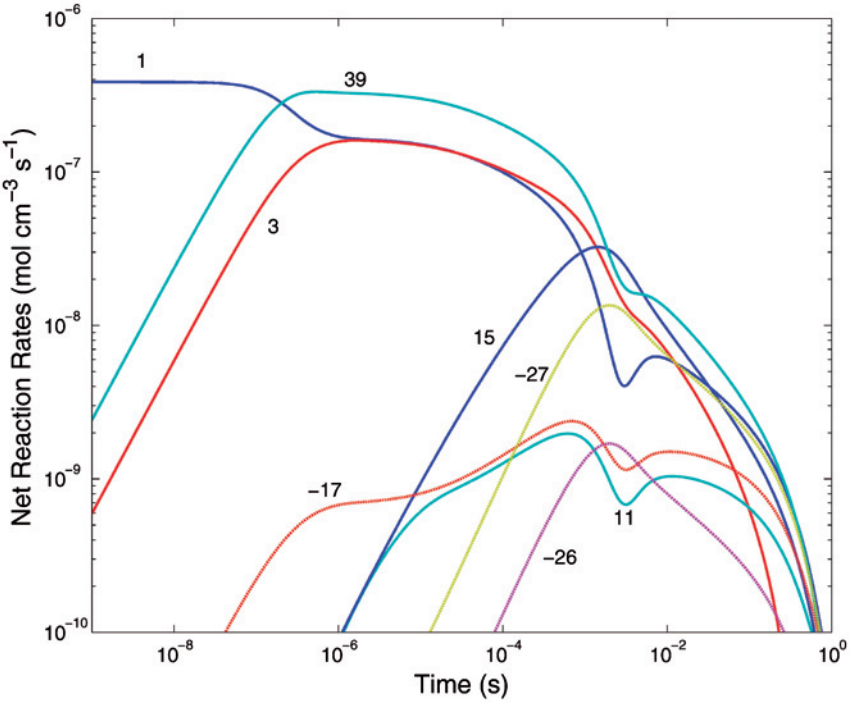

Fig. 6. Net reaction rates for the reactions with the highest net rates, under the same conditions shown in Fig. 5. Curves are labeled with the reaction numbers from Table 10. A negative number indicates that the reaction is proceeding in the reverse direction, relative to the way it is written in Table 10.

The above analyses of species concentrations and net reaction rates clearly indicate which reactions and which chemical species are most important in this reaction mechanism, under the particular conditions considered. However, for purposes of refining a reaction mechanism by eliminating unimportant reactions and species and by improving rate parameter estimates and thermochemical property estimates for the most important reactions and species, it would be helpful to have a quantitative measure of how important each reaction is in determining the concentration of each species. This measure is obtained by sensitivity analysis. In this approach, we define *sensitivity coefficients* as the partial derivative of each of the concentrations with respect to each of the rate parameters. We can write an initial value problem like that given by equation (35) in the general form

$$\frac{\mathrm{d}\mathbf{y}}{\mathrm{d}t} = \mathbf{f}(\mathbf{y};\boldsymbol{\alpha}) \tag{42}$$

where, in our case, $\mathbf{y}$ is a vector containing the species concentrations (the $[X_k]$), $\boldsymbol{\alpha}$ a vector containing the rate parameters, and $\mathbf{f}$ a vector of functions, given by equation (35). The vectors $\mathbf{y}$ and $\mathbf{f}$ will each have K elements (the number of chemical species), while the vector of parameters, $\boldsymbol{\alpha}$, will have $2I$ elements. The number of parameters is twice the number of reversible chemical reactions. For each reaction, there are two parameters, either the forward and reverse rate constants or one rate constant and the equilibrium constant. In a system where the temperature and pressure were not held constant, there would be at least four parameters per reaction, for example, pre-exponential factors and activation energies for the forward and reverse reactions. Pressure dependence, or more complex temperature dependence, of the reaction rates would introduce more parameters. In any case, we will define a matrix of sensitivity coefficients $\mathbf{S}$ that contains the partial derivatives of the solution variables ($\mathbf{y}$, which in this case are the species concentrations) with respect to the parameters ($\boldsymbol{\alpha}$, which in this case are the rate constants). That is, the elements of $\mathbf{S}$ will be defined by

$$S_{ki} \equiv \frac{\partial y_k}{\partial \alpha_i} \tag{43}$$

So, a given element of this matrix describes the dependence of solution variable k on parameter i. By definition, the partial derivative with respect to one parameter is taken with all other parameters held constant, and therefore depends on which other parameters are held constant. This means that sensitivity coefficients with respect to forward rate constants will be different depending on whether the second parameter for each reaction is taken to be the reverse rate constant or the equilibrium constant. Changing the forward rate constant, while keeping the reverse rate constant fixed, changes the equilibrium constant. This is clearly different than changing the forward rate constant, while keeping the equilibrium constant fixed, which changes the reverse rate constant.

With this definition of the sensitivity coefficients, we can write differential equations for the evolution of the sensitivity coefficients by taking a time derivative of equation (43)

$$\frac{\mathrm{d}S_{ki}}{\mathrm{d}t} = \frac{\mathrm{d}}{\mathrm{d}t}\left(\frac{\partial y_k}{\partial \alpha_i}\right) = \frac{\partial}{\partial \alpha_i}\left(\frac{\mathrm{d}y_k}{\mathrm{d}t}\right) = \frac{\partial}{\partial \alpha_i}(f_k(\mathbf{y}, \boldsymbol{\alpha})) \tag{44}$$

where f_k is the kth ordinary differential equation, defined by equation (42). Because f_k depends explicitly on both $\mathbf{y}$ and $\boldsymbol{\alpha}$, and $\mathbf{y}$ also depends (implicitly) on $\boldsymbol{\alpha}$, we cannot simply take the explicit partial derivative of

our equation for f_k with respect to α_i. Instead, we must expand the derivative as

$$\frac{\partial}{\partial \alpha_i}(f_k(\mathbf{y}, \boldsymbol{\alpha})) = \frac{\partial f_k}{\partial \alpha_i} + \sum_{m=1}^{K} \frac{\partial f_k}{\partial y_m} \frac{\partial y_m}{\partial \alpha_i} \tag{45}$$

Recognizing that the last partial derivative on the right side of this equation is, by definition, one of the sensitivity coefficients, we finally arrive at a set of equations for the sensitivity coefficients

$$\frac{\mathrm{d}S_{ki}}{\mathrm{d}t} = \frac{\partial f_k}{\partial \alpha_i} + \sum_{m=1}^{K} \frac{\partial f_k}{\partial y_m} S_{mi} \tag{46}$$

Because the initial species concentrations are independent of the rate constants, the initial conditions for these sensitivity coefficient equations are that all $S_{ki} = 0$ at $t = 0$. Integrating these equations, along with the equations for the species concentrations, provides all the sensitivity coefficients as a function of time. For the case of the rate equations given by equation (35), letting the first I parameters be the forward rate constants and the second I parameters be the reverse rate constants, the function f_k can be written (using new summation subscripts l and m) as

$$f_k = \sum_{l=1}^{I} \nu_{kl}(r_{l,\mathrm{f}} - r_{l,\mathrm{r}}) = \sum_{l=1}^{I} \nu_{kl} \left(\alpha_l \prod_{m=1}^{K} y_m^{\nu'_{ml}} - \alpha_{l+I} \prod_{m=1}^{K} y_m^{\nu''_{ml}} \right) \tag{47}$$

where $r_{i,\mathrm{f}}$ and $r_{i,\mathrm{r}}$ are the forward and reverse reaction rates, respectively. So, we have

$$\begin{aligned} \frac{\partial f_k}{\partial \alpha_i} &= \nu_{ki} \prod_{m=1}^{K} y_m^{\nu'_{mi}} = \nu_{ki} \frac{r_{i,\mathrm{f}}}{k_{i,\mathrm{f}}}, \quad \text{for } 1 \le i \le I \\ \frac{\partial f_k}{\partial \alpha_i} &= -\nu_{k(i-I)} \prod_{m=1}^{K} y_m^{\nu''_{m(i-I)}} = -\nu_{k(i-I)} \frac{r_{i-I,\mathrm{r}}}{k_{i-I,\mathrm{r}}}, \quad \text{for } I+1 \le i \le 2I \end{aligned} \tag{48}$$

and similarly,

$$\frac{\partial f_k}{\partial y_m} = \sum_{l=1}^{I} \nu_{kl} \left(\frac{\nu'_{ml} r_{l,\mathrm{f}} - \nu''_{ml} r_{l,\mathrm{r}}}{y_m} \right) \tag{49}$$

The final set of equations for the sensitivity coefficients is then

$$\frac{\mathrm{d}S_{ki}}{\mathrm{d}t} = v_{ki}\frac{r_{i,\mathrm{f}}}{k_{i,\mathrm{f}}} + \sum_{m=1}^{K}\sum_{l=1}^{I} v_{kl}\left(\frac{v'_{ml}r_{l,\mathrm{f}} - v''_{ml}r_{l,\mathrm{r}}}{y_m}\right)S_{mi}, \quad \text{for } 1 \le i \le I$$

$$\frac{\mathrm{d}S_{ki}}{\mathrm{d}t} = -v_{k(i-I)}\frac{r_{i-I,\mathrm{r}}}{k_{i-I,\mathrm{r}}} + \sum_{m=1}^{K}\sum_{l=1}^{I} v_{kl}\left(\frac{v'_{ml}r_{l,\mathrm{f}} - v''_{ml}r_{l,\mathrm{r}}}{y_m}\right)S_{mi},$$

$$\text{for } I+1 \le i \le 2I \tag{50}$$

Note that if the concentrations and reaction rates have already been computed and stored, then this is a set of *linear* differential equations (with non-constant coefficients) for the sensitivity coefficients. Note also that each sensitivity coefficient depends only on the sensitivity coefficients of the other species to the same parameter, but not on sensitivity coefficients with respect to other parameters. Thus, the sensitivity coefficients with respect to a given parameter (K of them) are coupled and must be computed simultaneously, but it is not necessary to solve for all the sensitivity coefficients ($2 \times I \times K$ of them) simultaneously.

Continuing with the example based on the reaction mechanism of Table 10, the equations for the sensitivity coefficients (equation (50)) were integrated numerically using Matlab.[7] For a mechanism of this size, it was feasible to solve for the species concentrations (15 of them) and all the sensitivity coefficients ($39 \times 15 \times 2 = 1170$ of them) simultaneously. Rather than examining the sensitivity coefficients themselves, it is often more informative to examine *scaled* or *normalized* sensitivity coefficients. These are usually defined as

$$\sigma_{ki} \equiv \frac{\partial \ln y_k}{\partial \ln \alpha_i} = \frac{\alpha_i}{y_k}\frac{\partial y_k}{\partial \alpha_i} = \frac{\alpha_i}{y_k}S_{ki} \tag{51}$$

The sensitivity coefficients defined by equation (43) relate the absolute change in a solution variable (species concentration) to an absolute change in a parameter (rate constant), and thus have units that depend on the units of the rate constant, which in turn depend on the overall reaction order. The scaled sensitivity coefficients defined by equation (51) relate fractional changes in a solution variable to fractional changes in a parameter. Thus, for example, if $\sigma_{ki} = 1$, then a 10% increase in parameter α_i will lead to a ~10% increase in solution variable y_k. Likewise, if $\sigma_{ki} = -1$, then a 10% increase in parameter α_i will lead to a ~10%

[7] A short Matlab function and an example of its use with built-in Matlab ODE solvers to produce the results shown in Fig. 7 are included in the CD that accompanies this text. Such calculations are also easily carried out using the SENKIN code [46] from the CHEMKIN family of codes (http://www.reactiondesign.com) or using elements of the Cantera suite of reacting flow tools (http://www.cantera.org).

decrease in solution variable y_k. These scaled sensitivity coefficients are dimensionless, and therefore can all be plotted on a common scale and compared directly. A full sensitivity analysis generally results in more data than can be looked at in detail. Thus, one must focus on the species of greatest interest, and look at the reactions with the greatest impact on those species. It is often more informative to examine sensitivity coefficients for reaction products, rather than reactants, since during early stages of reaction the reactant concentrations will be very close to the initial concentrations, and all sensitivity coefficients will be small. However, the concentration of a product species that is not initially present will be sensitive to the first reactions that form it, even if it is formed in very small quantities. Thus, for this example we consider the sensitivity of one of the reaction products, AlCl, to all the forward and reverse rate constants. The scaled sensitivity coefficients for AlCl for the same initial conditions of 1% $AlCl_3$ in H_2 at 1300 K and 0.1 bar are shown in Fig. 7, where solid curves labeled with positive numbers represent sensitivities to

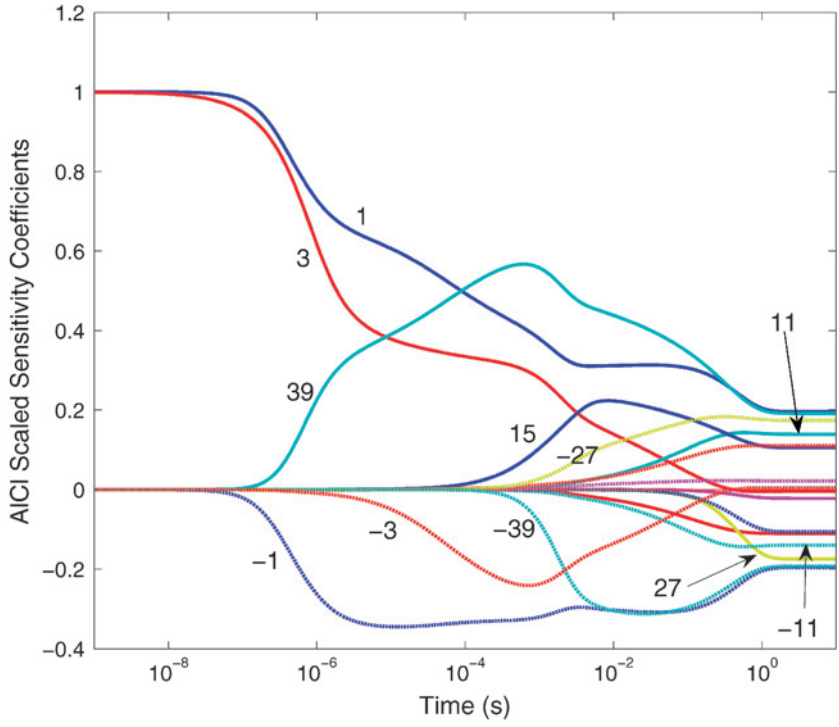

Fig. 7. Scaled sensitivity coefficients for AlCl under the same conditions as in Figs. 5 and 6. Curves are labeled with reaction numbers from Table 10. Solid curves and positive numbers correspond to sensitivities to the forward rate constants, while dotted curves labeled with negative numbers are sensitivities to the reverse rate constants.

the forward rate constants, while broken curves labeled with negative numbers show sensitivities to the reverse rate constants. At long reaction times, where the system is approaching equilibrium, the scaled sensitivity coefficients for each forward and reverse rate constant pair are equal in magnitude and opposite in sign. This is a direct result of our definition of the sensitivity coefficients in terms of changes in one rate constant (forward or reverse) while holding the other constant. Increasing a forward rate constant while holding the reverse rate constant fixed results in an increase in the equilibrium constant. Increasing the reverse rate constant while holding the forward rate constant fixed leads to an equal, but opposite, change in the equilibrium constant for the reaction. From a mechanistic point of view, these sensitivity coefficients tell the same story as the species concentration and reaction rate analyses given above. Initially, the most important reactions in determining the AlCl concentration are $AlCl_3$ decomposition (equation (37), reaction 1 of Table 10) and $AlCl_2$ decomposition (equation (39), reaction 3 of Table 10). These are rather obvious reactions to expect, since together they lead directly to AlCl production from $AlCl_3$. However, at times from 100 n sec to 1 μ sec, AlCl production becomes sensitive to the rate of reaction of Cl atoms with H_2 to generate H atoms (equation (38), reaction 39 of Table 10). It is less obvious, *a priori*, that this reaction should play an important role, since it does not directly involve AlCl or any species from which AlCl is produced. The importance of this reaction arises from the fact that it consumes Cl atoms. It becomes important only after the $AlCl_3$ and $AlCl_2$ decomposition reactions begin to approach equilibrium. Their approach to equilibrium is indicated, in the sensitivity analysis, by the fact that the sensitivities to their forward and reverse rate constants are becoming equal and opposite. As these reactions start to equilibrate, further AlCl formation requires removal of Cl atoms, which are the other product of the $AlCl_3$ and $AlCl_2$ decomposition reactions. At a reaction time near 1 msec, the reaction of Cl with H_2 also begins to approach equilibrium, and the AlCl concentration becomes sensitive to the reaction of $AlCl_3$ with H atoms (equation (40)). Soon after that, the AlCl concentration also becomes sensitive to the reaction of $AlCl_2$ with H atoms (equation (41)). Finally, at longer times yet, reactions involving $AlHCl_2$ become somewhat important.

Taken together, the analyses of species concentrations, reaction rates, and scaled sensitivity coefficients for this particular example and conditions provide a clear and consistent picture of which species and reactions are most important in the overall process of $AlCl_3$ decomposition and reaction with H_2 to produce AlCl and HCl. From the 39 reactions included in Table 10, just 5 seem to be essential. These

are reactions 1, 3, 15, 27, and 39 of Table 10. Thus, if we were to invest effort in refining rate parameters in the reaction mechanism, those would be the reactions for which additional effort would most likely be worthwhile. If we had considered a broader range of reaction conditions, we would probably have found a longer list of important reactions. This brings us to the end of the process illustrated schematically in Fig. 1. At this point, we could proceed to apply the reaction mechanism further to solve the real, physical problem at hand or, to the extent that is necessary and worthwhile, return to earlier stages of the process to make further improvements. Ideally, this would involve comparisons of predictions from this reaction mechanism with real experimental data.

7 SUMMARY AND OUTLOOK

Having reached the end of the process illustrated schematically in Fig. 1, we have also reached the end of the present chapter. Although many details of the individual steps have, by necessity, been omitted, we hope that the overall procedure to be followed is clear and that, in combination with the more detailed treatment of various steps in the process that have been provided in earlier chapters of this text, it provides a clear path to the rational construction of detailed mechanisms of elementary chemical reactions. Detailed chemical kinetic modeling has already demonstrated its potential in a number of applications, including combustion, atmospheric chemistry, hydrocarbon pyrolysis, and a number of vapor-phase materials processing systems. In the earliest and most technologically important of these application areas, reaction mechanisms have evolved over several decades with the support of extensive experimental measurements of species thermochemistry and the kinetics of elementary reactions. In this regard, our predecessors have already traversed much of the steep slope of the learning curve in this field. In recent years, increasingly powerful computational tools for predicting reaction thermochemistry and kinetics, along with the still-growing database of experimental results, have dramatically shortened the time required to develop relatively complete mechanisms of elementary reactions to describe some new overall vapor-phase transformation. This, in turn, makes it increasingly possible to apply detailed chemical kinetic modeling to new problems in propulsion, vapor-phase materials processing, and other applications.

However, the construction and analysis of reaction mechanisms remain far from being a fully automated or automatable process. As seen throughout this chapter, there are many points where educated guessing

and chemical intuition enter the process and, therefore, where the results are highly dependent on the practitioner who produces them. Importantly, the construction of detailed mechanisms of elementary reactions is only a tractable problem in the gas phase, where reactions occur among isolated molecules and, with more difficulty, at gas–solid interfaces. In principle, the same approaches to reaction mechanism development and analysis are applicable in solution, and even in biological systems. However, in solution the parameter spaces are much larger, with reaction rates that depend on solvent composition, and both species thermochemistry (in non-ideal mixtures) and reaction rate parameters are much more difficult to compute. In biological systems, the situation is much more complicated yet, since the environment is often inhomogeneous. Nevertheless, the extension of detailed chemical kinetic modeling to condensed phase and biological systems represents perhaps the most important opportunity to increase the impact of such approaches. Such extensions, along with improved methods of automating the mechanism generation process, improved computational predictions of species thermochemistry and reaction kinetics, and more efficient incorporation of detailed kinetics into multi-dimensional models of physical systems, are important steps to expanding the applicability, reliability, and impact of detailed chemical kinetic modeling.

REFERENCES

[1] R. Atkinson, D.L. Baulch, R.A. Cox, R.F. Hampson Jr., J.A. Kerr, M.J. Rossi, J. Troe, *J. Phys. Chem. Ref. Data*, **26**(6) (1997) 1329–1499.
[2] R. Atkinson, D.L. Baulch, R.A. Cox, R.F. Hampson Jr., J.A. Kerr, M.J. Rossi, J. Troe, *J. Phys. Chem. Ref. Data*, **28**(2) (1999) 191–393.
[3] R. Atkinson, D.L. Baulch, R.A. Cox, R.F. Hampson Jr., J.A. Kerr, M.J. Rossi, J. Troe, *J. Phys. Chem. Ref. Data*, **29**(2) (2000) 167–266.
[4] D.L. Baulch, C.J. Cobos, R.A. Cox, C. Esser, P. Frank, T. Just, J.A. Kerr, M.J. Pilling, J. Troe, R.W. Walker, J. Warnatz, *J. Phys. Chem. Ref. Data*, **21**(3) (1992) 411–711.
[5] D.L. Baulch, C.J. Cobos, R.A. Cox, P. Frank, G. Hayman, T. Just, J.A. Kerr, T. Murrels, M.J. Pilling, J. Troe, R.W. Walker, J. Warnatz, *J. Phys. Chem. Ref. Data*, **23**(6) (1994) 847–1033.
[6] D.L. Baulch, C.J. Cobos, R.A. Cox, P. Frank, G. Hayman, T. Just, J.A. Kerr, T. Murrels, M.J. Pilling, J. Troe, R.W. Walker, J. Warnatz, *J. Phys. Chem. Ref. Data*, **24**(4) (1995) 1609–1630.
[7] L. Catoire, M.T. Swihart, *J. Electrochem. Soc.*, **149**(5) (2002) C261–C267.
[8] M.T. Swihart, L. Catoire, *Combust. Flame*, **121** (2000) 210–222.
[9] M.T. Swihart, L. Catoire, *J. Phys. Chem. A.*, **105** (2001) 264–275.
[10] M.T. Swihart, L. Catoire, B. Legrand, I. Gokalp, C. Paillard, *Combust. Flame*, **132**(1-2) (2003) 91–101.

[11] W. G. Mallard, F. Westley, J. T. Herron, R. F. Hampson, D. H. Frizzell, *NIST Chemical Kinetics Database: NIST Standard Reference Database 17*, version 7.0. National Institute of Standards and Technology, Gaithersburg, MD, 2005.
[12] M.D. Allendorf, C.F. Melius, *J. Phys. Chem. A.*, **109** (2005) 4939–4949.
[13] P. Ho, C.F. Melius, *J. Phys. Chem. A.*, **94** (1990) 5120–5127.
[14] M.T. Swihart, R.W. Carr, *J. Phys. Chem. A*, **101** (1997) 7434–7445.
[15] M.T. Swihart, R.W. Carr, *J. Phys. Chem. A*, **102** (1998) 785–792.
[16] M.T. Swihart, R.W. Carr, *J. Phys. Chem. A*, **102** (1998) 1542–1549.
[17] L.J. Broadbelt, S.M. Stark, M.L. Klein, *Chem. Eng. Sci.*, **49**(28) (1994) 4991–5010.
[18] L.J. Broadbelt, S.M. Stark, M.T. Klein, *Ind. Eng. Chem. Res.*, **33** (1994) 790–799.
[19] L.J. Broadbelt, S.M. Stark, M.T. Klein, *Ind. Eng. Chem. Res.*, **34** (1995) 2566–2573.
[20] L.J. Broadbelt, S.M. Stark, M.T. Klein, *Computers Chem. Engng.*, **20**(2) (1996) 113–129.
[21] R.G. Susnow, A.M. Dean, W.H. Green, P. Peczak, L.J. Broadbelt, *J. Phys. Chem. A*, **101** (1997) 3731–3740.
[22] M.J. De Witt, D.J. Dooling, L.J. Broadbelt, *Ind. Eng. Chem. Res.*, **39** (2000) 2228–2237.
[23] H.-W. Wong, X. Li, M.T. Swihart, L.J. Broadbelt, *J. Phys. Chem. A.*, **108** (2004) 10122–10132.
[24] P. J. Listrom, W. G. Mallard eds., *NIST Chemistry WebBook, NIST Standard Reference Database Number 69*. National Institute of Standards and Technology, Gaithersburg, MD, 2005.
[25] M.W. Chase Jr., *J. Phys. Chem. Ref. Data Monograph*, **9** (1998) 1–1951.
[26] M. W. J. Chase, C. A. Davies, J. J. R. Downey, D. J. Frurip, R. A. McDonald, A. N. Syverud, *J. Phys. Chem. Ref. Data* **14**(Supp. 1) (1985).
[27] M.D. Allendorf, C.F. Melius, B. Cosic, A. Fontijn, *J. Phys. Chem. A.*, **106** (2002) 2629–2640.
[28] S. Petrie, *J. Phys. Chem. A.*, **102** (1998) 7828–7834.
[29] A. Burcat, B. Ruscic, *Ideal Gas Thermochemical Database with updates from Active Thermochemical Tables*, (2005).
[30] H.-W. Wong, J.C. Alva Nieto, M.T. Swihart, L.J. Broadbelt, *J. Phys. Chem. A.*, **108** (2004) 874–897.
[31] H. Rau, *J. Chemical Thermodynamics*, **16**(3) (1984) 287–293.
[32] L. Wang, J. Zhang, *J. Phys. Chem. A*, **108**(46) (2004) 10346–10353.
[33] D.F. Rogowski, P. Marshall, A. Fontijn, *J. Phys. Chem.*, **93** (1989) 1118–1123.
[34] A.G. Slavejkov, A. Fontijn, *Chem. Phys. Lett.*, **165** (1990) 375–378.
[35] J.I. Steinfeld, J.S. Francisco, W.L. Hase, *Chemical Kinetics and Dynamics*, 2nd ed., Prentice Hall, Upper Saddle River, New Jersey, 1999.
[36] D.A. McQuarrie, *Statistical Mechanics*. Harper Collins, New York, 1976.
[37] M.J. Frisch, G.W. Trucks, H.B. Schlegel, G.E. Scuseria, M.A. Robb, J.R. Cheeseman, V.G. Zakrzewski, J.A. Montgomery, R.E. Stratmann, J.C. Burant, S. Dapprich, J.M. Millam, A.D. Daniels, K.N. Kudin, M.C. Strain, O. Farkas, J. Tomasi, V. Barone, M. Cossi, R. Cammi, B. Mennuci, C. Pomelli, C. Adamo, S. Clifford, J. Ochterski, G.A. Petersson, P.Y. Ayala, Q. Cui, K. Morokuma, D.K. Malick, A.D. Rabuck, K. Raghavachari, J.B. Foresman, J. Cioslowski, J.V. Ortiz, B.B. Stefanov, G. Liu, A. Liashenko, P. Piskorz, I. Komaromi, R. Gomperts, R.L. Martin, D.J. Fox, T. Keith, M.A. Al-Laham, C.Y. Peng, A. Nanayakkara, C. Gonzales, M. Challacombe, P.M.W. Gill, B.G. Johnson, W. Chen, M.W. Wong,

J.L. Andres, M. Head-Gordon, E.S. Replogle, J.A. Pople, *Gaussian 98*. Gaussian, Inc., Pittsburgh, PA, 1998.
[38] A. M. Dean, J. W. Bozzelli, in: J. W. C. Gardiner (Ed.), *Gas-Phase Combustion Chemistry*. Springer-Verlag, New York, 2000, pp. 125–341.
[39] R. G. Gilbert, S. C. Smith, M. J. T. Jordan, *UNIMOL program suite (calculation of fall-off curves for unimolecular and recombination reactions)*. Available from the authors: School of Chemistry, Sidney University, NSW 2006, Australia or by e-mail to gilbert_r@summer.chem.su.oz.au, 1993.
[40] S. J. Klippenstein, A. F. Wagner, R. C. Dunbar, D. M. Wardlaw, S. H. Robertson, *Variflex Version 1.00*, 1999.
[41] V. Mokrushin, V. Bedanov, W. Tsang, M.R. Zachariah, V.D. Knyazev, *ChemRate version 1.16,*. National Institute of Standards and Technology, Gaithersburg, MD, 2000.
[42] S. Benson, *Thermochemical Kinetics*. Wiley, New York, 1976.
[43] P. Blowers, R. Masel, *AIChE Journal*, **46**(10) (2000) 2041–2052.
[44] R.J. Kee, F.M. Rupley, E. Meeks, J.A. Miller, *Chemkin-III: A Fortran chemical kinetics package for the analysis of gas-phase chemical and plasma kinetics*. Sandia National Laboratories, Livermore, CA, 1996.
[45] R.J. Kee, F.M. Rupley, J.A. Miller, *The Chemkin Thermodynamic Database*. Sandia National Laboratories, Livermore, CA, 1990.
[46] A.E. Lutz, R.J. Kee, J.A. Miller, *SENKIN: A Fortran program for predicting homogeneous gas phase chemical kinetics with sensitivity analysis*. Sandia National Laboratories, Livermore, CA, 1997.
[47] J. Troe, *Ber. Bunsenges. Phys. Chem.*, **87** (1983) 161–169.
[48] R.G. Gilbert, K. Luther, J. Troe, *Ber. Bunsenges. Phys. Chem.*, **87** (1983) 169–177.

Chapter 6

Optimization of Reaction Models with Solution Mapping

Michael Frenklach, Andrew Packard and Ryan Feeley

1 INTRODUCTION

The use of computer modeling, especially in the area of reaction chemistry, has penetrated deep into many venues of science and technology and the trend is expected to accelerate with time. Chemical reaction models are built for several reasons, such as exploratory modeling with the purpose of identifying possible reaction pathways, analysis of one's own experimental data, testing possible experimental trends, or making predictions for the purpose of design and policy assessment. Many of these applications place an increasing demand on models to be accurate and reliable, i.e., to be *predictive*. What makes a reaction model predictive?

Usually, chemical reaction models are composed from individual reactions steps, ether elementary or global. Each reaction step has a prescribed rate law, which is characterized by a set of parameters. The parameter values are collected from literature, evaluated using theoretical machinery, estimated by empirical rules, or simply guessed. The predictive power of a reaction model is thus determined by two factors, the authenticity of the reaction steps and the correctness of the rate parameters. For the purpose of the present discussion, we assume that the "complete" set of reaction steps (i.e., the *reaction mechanism*) is known and our focus is entirely on the identification of the "correct" parameter values. It is pertinent to mention, though, that the process of reaching conclusions on the authenticity of the reaction mechanism is often based on and is coupled to the parameter identification. The assumption of the "known mechanism" should not be viewed as a simplification of the problem but rather a pedagogical device for presenting the material.

The objective of this chapter is to introduce the reader to determination of "best-fit" parameter values of a chemical kinetics model given a set of experimental measurements and, more generally, to development

Comprehensive Chemical Kinetics, Volume 42, 243–291

ISSN: 0069-8040/doi:10.1016/S0069-8040(07)42006-4

of predictive reaction models. The technical term for the underlying mathematical treatment is *numerical optimization*. The objective of the present discussion is not to cover the mathematical theory or present an exhaustive review of different approaches to the problem but rather to introduce to the chemical kineticist the subject matter and terminology, exposing the specific difficulties and problems associated with optimization of chemical kinetic models, and to provide guidance to a potential user that can lead her or him to practical results.

2 PRELIMINARY MATERIAL AND TERMINOLOGY

2.1 Training data

Assuming that the reaction mechanism is known, we pose the problem of determining a set of parameter values that make the model most closely match some chosen experimental observations. We will refer to these chosen experimental data as *training data*, *training set*, or *training targets*, and the process of fitting the model parameters in this way as *model training*.

How do we select the training data? First of all, the underlying physics of such an experiment must be known to the extent that we can write down the governing equations with certainty. For instance, mixing two streams of gases at the entrance to a high-temperature tubular reactor, with a reaction time on the order of a millisecond, will not provide a good training data point because the mixing aspect of the process is hard to model accurately. Second, we need to know the initial and boundary conditions of the carried-out experiment, since the solution of the model will depend on those numbers. Third, the experimental observation should have high sensitivity to the chemistry in question and not to be masked by less known physical and/or chemical processes. Fourth, the instrumental functions that related the actual properties measured, such as light intensity or transducer voltage, to properties modeled, such as species concentrations or pressure, should be known (although this is a weaker requirement, as the instrumental functions with their own parameters can be included in the overall model of the process). Finally, the accuracy of the experimental target for model training has to be known as well. We will discuss the latter point in further detail below.

Another important consideration in selecting the training targets is the question of what it means "to fit an experiment." Not every experimental "data point" has to be taken as a target of model optimization. The experience shows that creating "summarizing properties" is sufficient

(and actually beneficial) to the analysis. As an example, the GRI-Mech 3.0 included 77 training targets, some representing individual observations and some a group of them, such as an average of several observations or a temperature dependence of a series of measurements [1]. The researcher must identify specific features that are most informative in the context of the analysis, using some preliminary simulations and sensitivity analysis. Such features could be distinctive peaks, their (relative) location, width and height, characteristic times and their temperature dependence, or concentration profiles. When selecting a "profile," one should realize that it can be fitted by selecting just a small set of "key" points, those defining the curve shape [2–4].

2.2 *Objective function*

Having set the model and chosen the training data, the objective is to fit the model predictions to the targets. The simplest and most widely used numerical approach is to formulate a single *objective* function, Φ, usually in the form of the least squares,

$$\Phi = \sum_e w_e[y_e(\boldsymbol{\theta}) - d_e]^2 \tag{1}$$

and to search for its minimum while varying the parameter values. Variables y_e and d_e appearing in equation (1) designate the calculated and experimental values, respectively, of the eth training target (experiment E), and w_e its statistical weight. The values of y are obtained by evaluation of a given model at a given set of *optimization variables*, $\boldsymbol{\theta} = \{\theta_1, \theta_2, \ldots\}$. The latter, in the present discussion, are presumed to be ("unknown") *model parameters*, primarily the rate parameters of the chemical kinetics model, whose "best-fit" values we seek to determine by minimizing the objective function Φ. We will refer to θ's as optimization variables or model parameters interchangeably, pertinent to the context of the discussion. Obviously, any model parameter can become an optimization variable; we will discuss selection of optimization variables later in the text.

The statistical weight represents the degree of confidence we have in the measurement. Rigorously, w_e can be set inversely proportional to the uncertainty of the experimental measurement, e.g., $w_e \sim 1/\sigma_e^2$, with σ_e^2 being the variance of d_e or its estimate. The statistical measure σ_e^2 in this assignment is presumed to characterize the "randomness" of the measured value. However, this does not necessarily expose the true uncertainly of the measurement, as it is often plagued by what is referred as *systematic errors*. Systematic errors might arise from unbalances scales,

an uncalibrated oscilloscope, presence of unaccounted for impurities in the test mixture, and the like. We do not know *a priori* whether we have systematic errors or not, for if we have had such knowledge, the systematic effects would be included in our analysis. In other words, at the outset of the analysis we have to presume the uncertainties of the experimental observations to be purely random, and yet keep our mind open to a possibility of a systematic bias. An example of the latter situation arises when two independent studies report very different values for the same rate constant and each with a relatively narrow range of uncertainty. Often, the numerical uncertainty, σ_e^2, is not known or reported. In light of the above, one is advised to try different sets of w that reflect more closely the researcher's judgment of the quality of the experimental data.

Considering the different nature and magnitude of observed properties, it is often more appropriate to minimize the relative deviations, with the objective function taking the form

$$\Phi = \sum_e w_e \left[\frac{y_e(\boldsymbol{\theta}) - d_e}{d_e} \right]^2 \tag{2}$$

Also, variables y in equation (2) may be set equal to the logarithms of the observed properties; examples of such may include species concentrations and induction times.

The objective function may take the form of the likelihood or posterior distribution functions [5]. It is pertinent to mention that maximization of the likelihood function in case of independent normally distributed errors leads to the sum-of-squares (SOS) of the residuals, such as given by equation (1). Another approach to fitting multiple training targets is to use *multi-objective* optimization, which is concerned with simultaneous optimization of a set of objectives.

Optimization of the objective function on its own, allowing the optimization variables to take any values, is called *unconstrained* optimization. Usually, we have additional information that has to be considered, such as the physical bounds of the reaction rates, limited from above by the collision rate theory and from below by 0, and the uncertainties in the experimental observations. Minimization of equation (1) or (2) simultaneously with additional equalities or inequalities applied to optimization variables is referred to as *constrained* optimization.

2.3 *Optimization methods*

Numerical optimization is perhaps one of the most dazzling issues in all the sciences and engineering. Essentially all modern computational codes,

which provide the researcher with the ability to solve complex problems in areas as diverse as quantum chemistry and computational fluid dynamics, engage in numerical solution of a system of nonlinear equations as part of the algorithm. Many of these algorithms are classified as or rely on numerical optimization techniques. Parameter determination, model discrimination, and similar endeavors invariably entail such approaches.

In spite of the broad use of optimization, from fundamental sciences to practical engineering design, there is no single numerical method that can guarantee a solution. There are a variety of methods available, each one capable of solving a class of problems, and the pursuit of new methods is still an active area of research. The interested reader is referred to textbooks, such as Refs. [6,7], to get a comprehensive view of the methods available and learn the theory behind the different techniques. A brief overview of some of these methods, in the context of parameter estimation in chemical kinetics, is presented in Ref. [8].

In the case of nonlinear models, the kind we consider in the present discussion, the optimization methods can be classified into two major groups of numerical approaches, *gradient* search and *pattern* search. In all approaches, the goal is to find a set of optimization variables $\boldsymbol{\theta}$ that minimize the objective function Φ. The gradient search follows the local slope of the objective function (the gradient of Φ with respect to $\boldsymbol{\theta}$), while the pattern search propagates through comparison of Φ values sampled in a particular pattern. The efficiency and applicability of these search techniques depend on the shape of the objective function. In chemical kinetics, the objective functions usually take the form of long, narrow, gently sloping, crescent-shaped valleys, the type illustrated in Fig. 1. The simple gradient methods (e.g., the steepest descent) tend to oscillate around the locus line of such valleys in a hemstitching pattern [8], resulting in poor convergence. If the search is halted prior to attainment of the global minimum, one would be trapped in misleading conclusions. While variations in the quality of fit along the bottom line of the valley can hardly be discerned, the corresponding changes in parameter estimates may be dramatic. There are numerical methods designed for the valley search [9] and global optimization [6,10–16], which can determine the best-fit values of the optimization variables. We continue the discussion of optimization methods in the next section, focusing on methods of primary interest to the present text.

2.4 Parameter uncertainty

The scope of optimization is usually broader in that one is interested not just in the optimal point, but also in the region of ‘‘uncertainty’’

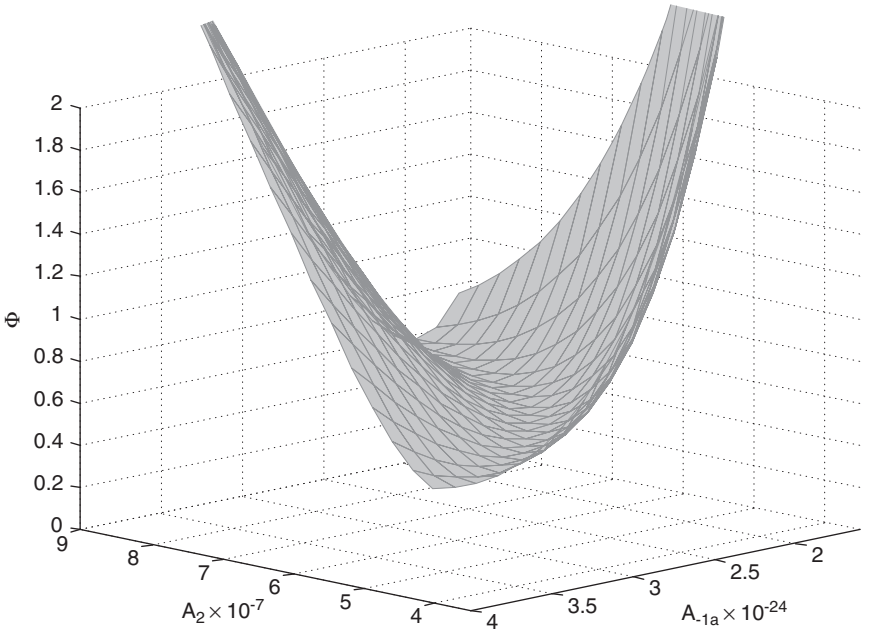

Fig. 1. An example of a two-dimensional valley. Such valley-shaped objective functions are typical for chemical kinetics modeling [8]. This specific example is taken from a study of formaldehyde pyrolysis [3], with A_{-1a} and A_2 being pre-exponential factors of the rate coefficients of reactions $H + HCO + M \rightarrow CH_2O + M$ and $CH_2O + H \rightarrow H_2 + HCO$, respectively.

surrounding this optimization solution. Such a region can be obtained either probabilistically, by finding the *confidence* region [5,8,17–19], or deterministically, by finding the *feasible* region [6]. In the probabilistic approach, given the distribution of errors in d, we ask for a region that contains the values of the optimization variables with a given probability (typically 95%). For a single-variable optimization, we express the results as a 95% confidence interval—the interval of values this variable should have with the probability of 95%. Generally, the model variables are correlated with one another and therefore it is more appropriate to consider the 95% *joint confidence region*. For linear models, such regions take the familiar ellipsoidal shape. For nonlinear models, they can be visualized as cross-sections of the objective function, as illustrated in Fig. 2.

In the deterministic formulation we ask the same question but in a different form: determine the region that model parameter values must belong to in order for the model predictions to remain within specified uncertainty bounds of d. We will formulate the feasible region later in the text. At this time, we want to point out that the feasible region and

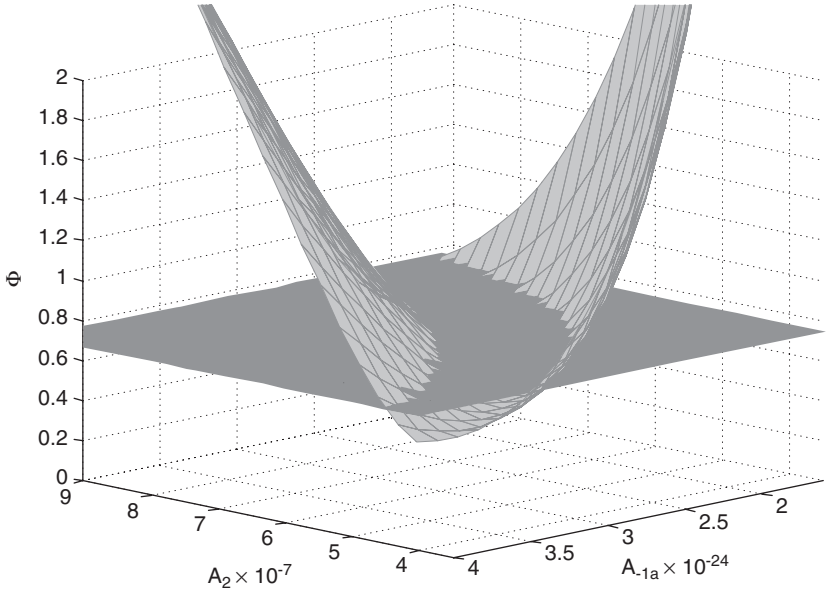

Fig. 2. A cross-section of the objective function shown in Fig. 1, illustrating a typical shape of a confidence region.

the confidence region convey essentially the same information when the uncertainties of all θ are presumed to be distributed uniformly within their respective bounds. The uniform distribution of θ, with each value of θ being equiprobable within a given interval, could be, in fact, an appropriate assumption for chemical kinetics. For instance, Box and Hunter [18] argued this as follows:

> "In considering a parameter like the specific rate [constant] φ which is essentially positive, it is probably most realistic to take $\theta = \ln \varphi$, $-\infty \leq \theta \leq \infty$, as locally uniform a priori. This would mean, for example, that having guessed a value of φ, an experimenter would be about equally prepared to accept a value twice as big as he would to accept a value one-half as big."

Still, 40 years later, only a handful of rate constants are known to a better than a factor of 2; hence, the Box and Hunter argument may apply to many "lesser known" rate constants.

Even for "better known" rate parameters the uniform distribution seems to be an appropriate assumption. For such "important" reactions many years of research resulted in multiple determinations for the same rate constant. It is often the case that the overall span among the different studies may extend over an order of magnitude, while individual determinations report a relatively small uncertainty (say, 10–30%). How does one reconcile this? Obviously, if there is an indication of something being "wrong" with an experiment, it can be excluded from consideration.

Typically, however, there is no apparent reason to prefer one number over another, and it is more appropriate to suspect the presence of systematic yet unknown errors. The most unbiased decision in such a situation is to assume uniform uncertainty within the bounds enclosing all the reported values.

3 PITFALLS OF POOR UNCERTAINTY MANAGEMENT

Model analysis begins with understanding the sources and nature of uncertainties. As mentioned above, the uncertainties (either experimental or assigned to rate constants) are often presumed to be "random," neglecting a possible (and sometimes obvious) systematic bias present, thereby artificially lowering the true uncertainty range. Another typical presumption is that the reaction rate constant estimates are independent from one another. Appearing "innocent" to a newcomer, such an assumption may (and usually does) lead to serious misconceptions. While from the prospective of physical chemistry, differing elementary reaction events indeed occur independently from each other, determination of the parameter values from measurements necessarily incorporates the interdependence due to intrinsic model relationships.

Because of improperly defined or missing uncertainties, undetected inconsistencies, neglected datasets, model oversimplification, and numerical problems it is not unusual for least-squares adjustment to force one or more of the model parameters outside its true uncertainty range without this being apparent to anyone. The error can easily be compounded in the literature if the incorrect parameter value is taken to be "well-determined" and used by others to help determine additional parameters.

The solution of these problems lies in sharing models and data, allowing collaborative processing for validation and estimation with this information. As illustrated below, a lack of such collaborative makes it difficult, if not impossible, to combine "raw," unprocessed information from distinct research groups, and consequently, the implications on distributed efforts to model complex systems are serious.

In chemical kinetics modeling, we have seen artificial controversies arise between research groups solely due to the limited manner in which research is reported and information is shared (e.g., concise, derived conclusions in archival journals). This has led to imprecise and inaccurate extraction of the information truly contained in the community's experimental data records. A typical situation in chemical kinetics goes as follows. In order to improve a complex model's predictive capability, scientist #1 devises an experiment E_1 whose outcome should be dominantly

affected by the (unknown) value of one of the parameters in the model, say θ_1. Once the experiment is performed, modeled, and measurements recorded and analyzed, θ_1 should be determined to a greater precision than previously known. It is acknowledged that values of some other parameters (say θ_2, θ_4, but not θ_3) also play a role in modeling the outcome, but argued that their effect is small relative to the dominant parameter, hence "will be ignored in the analysis." Consequently, any computation involving these other parameters, hence any inferred conclusions, will simply use "literature recommended values." Scientist #1 feels compelled to make these simplifications since otherwise the experiment has "merely" established a complex relationship between several parameters, with no "concrete" (and easy to disseminate) conclusions.

Unfortunately, a completely symmetric train of thought simultaneously plays out in laboratory #2, performing a different experiment whose outcome is dominantly controlled by θ_2. Again, "the minor dependence on θ_1, θ_3 will be ignored in the analysis."

The circularity in the joint, uncoupled analysis is evident. Each party makes a simplifying assumption about precisely the quantity that the other party is studying in detail. For example, scientist #1 will use the literature reported value of θ_2 to update the literature reported value of θ_1, while scientist #2 does the opposite. The analysis is somewhat reminiscent of Gauss–Seidel iteration, but the rate of convergence and the convergence itself to the "correct" model is not guaranteed. Something better should be used.

There can be other problems as well. Scientist #3 has also devised a method to ascertain θ_1, reporting that the minor effects of θ_2 and θ_5 are to be neglected. Unfortunately, after performing the analysis, scientist #3 reports that θ_1 lies in an interval which is contradictory (i.e., has no intersection) with that reported by scientist #1.

How did this happen? Perhaps something was wrong with the experiments. Perhaps something was wrong with the models. Definitely something was wrong with the analysis! Better analysis tools should fix the latter concern and provide guidance to addressing the former two. In actuality, all scientists in the above example are exploring the five-dimensional parameter space—more precisely, establishing constraints within it. Each of their models and experiments constrains which parameters could have produced the data they observe (of course, scientist #1 learns no new information about θ_3 or θ_5). Unfortunately, through a lack of infrastructure to share "raw" data, and inability to publish high-dimensional dense constraints as results, the correctness of the analysis they pursue is compromised. In order to report something concrete, all scientists naively set the less dominant parameters to fixed values and

report the one-dimensional slice (i.e., intervals) of the five-dimensional feasible regions as the result of their efforts. In the case of scientists #1 and #3, although the five-dimensional regions do in fact have points in common (i.e., a nonempty intersection), the one-dimensional slices do not, and a "controversy" has been generated.

A toy linear example can illustrate these effects. Consider three parameters, with prior knowledge $-1 \le \theta_i \le 1$ for each parameter. Suppose that model/data in experiment E_1 determines $0.1 \le \theta_1 + 0.2\theta_2 + 0.2\theta_3 \le 1.4$; similarly experiment E_2 determines $0.1 \le 0.2\theta_1 + \theta_2 + 0.2\theta_3 \le 1.4$, and experiment E_3 determines $0.1 \le -\theta_1 + 0.2\theta_2 + 0.2\theta_3 \le 1.4$. These sets are shown in Fig. 3, with the dark region indicating the common, nonempty intersection. On setting the less dominant parameters to 0 (their literature recommended values), the naive (as above) conclusions are, respectively, $0.1 \le \theta_1 \le 1$, $0.1 \le \theta_2 \le 1$, and $-1 \le \theta_1 \le -0.1$. The sets described by these naive conclusions are coordinate aligned parallelograms, shown in Fig. 4.

None of these logically follow from the model/experiment information, and are easily seen to differ from the correct conclusions illustrated in Fig. 3. Obviously combining the naive conclusions of these three researchers leads to additional incorrect conclusions, and/or inconsistencies, since the parallelograms drawn from the naive conclusions have no common intersection. In practice, this approach could constitute an untrue falsification of an actually unfailing model. In this example, access to all the raw data, coupled with mathematical programming tools—here simply linear programming (LP)—would allow the researchers to jointly ask and answer almost any question concerning the mathematical implications of their experiments and models.

The complexity (apparent or real) in a real scientific endeavor is worse, due to nonlinear, dynamic models, high dimensionality of parameter space, and large numbers of relevant experiments. The high dimensionality impacts the ability that print media can play in propagating the information forward in time. The actual constraints implied by model/experiment pairs will be nonlinear and large, making it difficult (not impossible though) to correctly share raw information. Without a comprehensive infrastructure in place to manage this, it becomes essentially impossible to genuinely track the precise meaning and pedigree of any reported conclusion. Consequently, analysis is done in isolation and forcefully restricted in the manner described above. Hence, the results of excellent scientific work (conceiving experiments whose measurable outcomes will be sensitive to particular groups of parameters, correctly performing the experiment) go unharvested! This leaves the model developer and user community frustrated, and a chemical kinetics model whose predictive capability does not reliably improve with time.

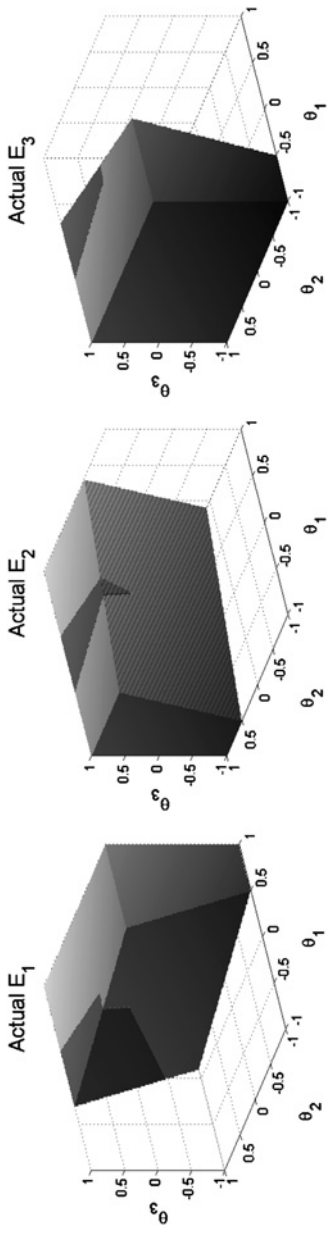

Fig. 3. Actual parameter sets consistent with each experiment's model, measurement, and prior information. Common intersection is the dark region.

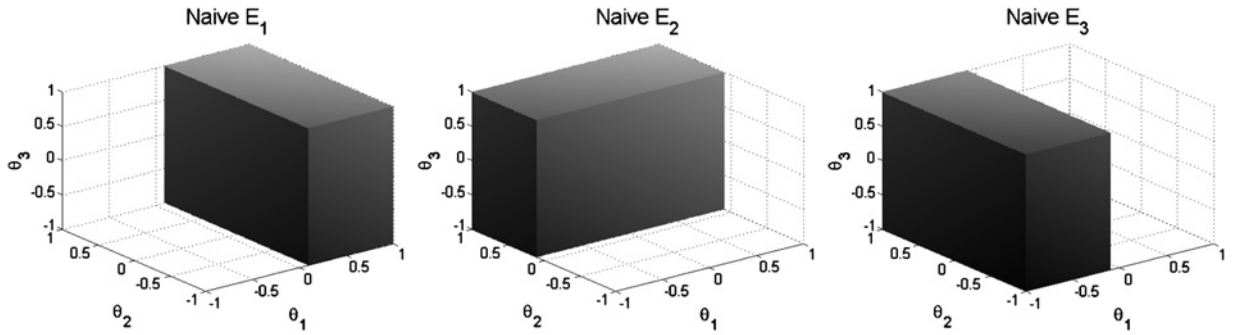

Fig. 4. Parameter sets implied by the naive, in-isolation analysis. These are similar to correct sets, but exclude valid points and include invalid points. Jointly, there is no intersection, generating a controversy among researchers.

4 STATEMENT OF THE PROBLEM

Given a reaction model with parameters with uncertainties, and experimental data with measurement uncertainties, one can consider two identification frameworks, both based on optimization. One framework (parameter estimation) asks *what parameter values give the best fit of the model to the experimental data and how good is this best fit*, generally treating the measurement uncertainties as statistical. An alternative framework (set-based) asks *what parameter values are consistent with the experimental data*, treating the measurement uncertainties as deterministic.

The answer to the first question is a single set of parameter values and an assessment of their validity and uncertainty. If the best-fit set is deemed valid then the parameter values and their uncertainties may be used in subsequent model predictions. If the best-fit set is deemed invalid, then the underlying reaction model and/or the experimental data may be considered invalidated.

The answer to the second question is a set of parameter values as of yet unfalsified by the experimental data. If the unfalsified set is found to be empty, then the underlying reaction model and/or the experimental data may be considered invalidated. The unfalsified set is often hard to describe explicitly, hence additional questions (in the form of constrained optimizations) are typically posed to probe the extent and implications of the unfalsified parameter set. We refer to the approach of applying constrained optimization to query the unfalsified set as "Data Collaboration."

Given that both types of questions may lead to the negative conclusion that current information is invalid, an important property of the optimization methods employed is that they are global. This ensures that minima (for example, associated with best-fit optimizations) are indeed minima and not simply local minima. It also ensures that when no parameter values can be found to be consistent with the experimental data it is indeed true that there are no such parameter values.

The methodology to answering these parameter estimation and set-based questions relies on different mathematical approaches. In principle, the parameter identification of chemical kinetic models can be posed as classical statistical inference [17,19–21]: given a mathematical model and a set of experimental observations for the model responses, determine the best-fit parameter values, usually those that produce the smallest deviations of the model predictions from the measurements. The validity of the model and the identification of outliers are then determined using analysis of variance. The general optimizations are computationally intensive even for well-behaved, well-parameterized algebraic functions. Further complications arise from the highly "ill-structured" character

of the best-fit objective function, with long and narrow valleys and multiple local minima, resulting in an ill-conditioned optimization that lacks a unique solution [8,20]. This is especially relevant in problems with large numbers of parameters, where overparametrization is possible.

Several methods have been suggested to deal directly with the differential equation reaction models and the experimental data [21–23], including the recently developed method of global optimization [15,16]. Yet another class of methods [24] pursues Bayesian statistical inference [5,25].

The approach we call Solution Mapping (SM) decouples the problem, first reducing the differential equation models to algebraic models, and then using global optimization to answer the posed questions. We begin by describing the ideas and practical details of this approach, focusing on the first question—parameter estimation. We then continue with the new developments, the set-based approach of Data Collaboration.

5 PARAMETER ESTIMATION OF DYNAMIC MODELS WITH SOLUTION MAPPING

5.1 Solution mapping approach

In this approach an approximation to the solution of the differential equations is used; hence, the method is referred to as Solution Mapping [8,26]. The approximation is developed through statistical techniques of response surface design, by performing computer experiments with the complete chemical kinetics model and fitting the numerical results obtained to a simple algebraic function, usually a polynomial. The obtained statistical surrogate is then used in the numerical optimization for parameter estimation, replacing thereby the need for solution of the original differential equations.

Consider a dynamic model that describes the time evolution of species concentrations,

$$\frac{\mathrm{d}\mathbf{y}}{\mathrm{d}t} = \mathbf{f}(\mathbf{y}, t, \boldsymbol{\theta}), \quad \mathbf{y}(t = 0) = \mathbf{y}_0 \tag{3}$$

where $\mathbf{y}$ is an array of species concentrations, t the reaction time, $\mathbf{y}_0$ an array of the initial species concentrations, and $\boldsymbol{\theta}$ an array of model parameters, such as reaction rate coefficients and species enthalpies of formation. In chemical kinetics such equations do not have a closed-form solution. A complete solution of the differential equations (3) can be thought of as relationships between the array of *model responses*,

$\boldsymbol{\eta} = \{\eta_1, \eta_2, \ldots\}$, and all the model variables, $\boldsymbol{\theta}$,

$$\boldsymbol{\eta} = \mathbf{g}(\boldsymbol{\theta}, t, \mathbf{y}_0) \tag{4}$$

The responses $\boldsymbol{\eta}$ can be species concentrations at given observation times ($\mathbf{y}$), concentration peaks, peak locations, induction times, flame speeds, etc., i.e., the experimental targets we intend to match. We can refer to functions $\mathbf{g}$ in equation (4) as *response functional relationships*, regardless of whether they are given in an analytical, tabular, or numerical form. In most applications one only needs to know several of these response functional relationships. It is these functions $\mathbf{g}$ that enter into the objective function evaluations by equation (1) or (2).

The essence of the SM technique is approximation of functions $\mathbf{g}$ by simple algebraic expressions $\mathbf{s}$ within a subset H of parameter space $\boldsymbol{\theta}$. The approximating functions for the responses are obtained using the methodology of the response surface technique [17,19,27], by means of a relatively small number of computer simulations, referred as *computer experiments*. They are performed at pre-selected combinations of the parameter values and the entire set of these combinations is called a *design* of computer experiments. The computer experiments are performed using the complete dynamic model (3) and the functions obtained in this manner are referred as *surrogate* models.

Once developed, the surrogate models replace the solution of the original dynamic model whenever evaluation of the latter is required. There is, in principle, no restriction on the mathematical form of the surrogate model. In our work we have used second-order polynomials whose coefficients are determined *via* computer experiments arranged in a special order, called *factorial design*. These designs originate from rigorous analysis of variance, with the objective of minimizing the number of computer experiments to be performed to gain the information required. Factorial designs have found an extensive use in experimental and process development work, and have seen recent application to computer experiments [28,29].

The use of a simple polynomial form as a surrogate model decreases the computational cost of the objective function evaluation by orders of magnitude. Not only does it make the solution of the inverse problem possible for large-scale dynamic models, but it also allows one to use more elaborate numerical methods of optimization, enables a rigorous statistical analysis of confidence regions [30,31], and ties in closely with a more general approach to model analysis, Data Collaboration, discussed later in the text.

We will continue with the discussion of some practical aspects of the SM approach, but first we need to introduce concepts of effect sparsity, active variables, and variable transformation.

5.2 *Effect sparsity and active variables*

In considering optimization of Φ, it is not necessary to include *all* model parameters (e.g., not all rate coefficients). Under conditions of an individual experiment or a set of experiments, the model responses that correspond to the experimental observations do not depend sensitively on all the parameters. In fact, it has been noted by many that usually only a small fraction of the parameters, called *active variables*, show a significant effect on measured responses. This phenomenon has been termed *effect sparsity* [27,32]. We designate in the rest of the chapter active variables by $\mathbf{x}$, to distinguish them from the complete set of the model parameters $\boldsymbol{\theta}$; note that $\mathbf{x}$ is a subset of $\boldsymbol{\theta}$.

The active variables can be readily identified by screening sensitivity analysis when the sensitivities are ranked according to their absolute values. Such examination partitions the model parameters into two groups: the active variables, whose effects on the response(s) are above the experimental noise level, and those below it. In practice, the selection of active variables may depend on considerations other than just the noise-level comparison, such as the certainty with which the parameters are known (i.e., consideration of sensitivity times the range of uncertainty instead of sensitivity alone) or the number of degrees of freedom available for optimization (i.e., the total number of parameters feasible to determine with the given amount of experimental information).

Only active variables need be considered for optimization. Inclusion of parameters with noise-level sensitivity into optimization only worsens the character of the objective function—necessarily increasing the dimensionality of the valley structure. If these parameters are to be the subject of optimization, then conditions have to be found where they become active. One does not have to search for a single set of conditions in which all the parameters of interest are active, which may be impossible to find. Instead, a more practical strategy is to perform experiments where different subsets of parameters are active and combine the results into a joint optimization. The SM methodology provides a convenient basis for implementing such a strategy.

5.3 *Screening sensitivity analysis*

Active variables can be conveniently identified by a screening sensitivity analysis. In a chemical reaction model not all reactions contribute equally

to the chemical history; hence, not all reaction rate parameters contribute equally to the model fit. To identify the numerical effect of a variation in parameter i on computed response j, we use *response sensitivity* [8], expressed either in the differential

$$S_i^j = \frac{\partial \eta_j}{\partial \theta_i} \tag{5}$$

or finite-difference

$$S_i^j = \frac{\Delta \eta_j}{\Delta \theta_i} \tag{6}$$

form. Symbol η, as defined above, designates a general model response, which can be any computed property, not only a species concentration, a transform of a model response, such as $\eta = \log C$, or a functional relationship among model responses, $\eta = C_1/C_2$, where C denotes a species concentration.

Computing sensitivities for all θ for a given response and ranking them by the absolute value produces results illustrated in Fig. 5. In this particular example the main effects are concentrated in just the first few (a dozen or so) parameters, consistent with the effect sparsity, and it is these parameters that can be selected to be active variables for model optimization. Actually, one rather needs to consider a similar ranking but for the parameter *impact* factors, a product of parameter sensitivity and its uncertainty.

One might feel "uneasy" to neglect parameters with small but nonzero sensitivities. However, by including all parameters one faces presently insurmountable numerical difficulties. Making a practical decision of selecting only a small set of parameters—active variables—makes the problem of model optimization manageable. It is analogous, for instance, to agreeing *a priori* that grocery-store scales cannot accurately weigh a dust particle on a heavy book—one has to choose laboratory scales for this purpose.

The evaluation of sensitivities can be accomplished in a number of ways, and there are many different methods and computer codes available (see, e.g., Refs. [8,33] and references cited therein). The simplest among them is the *brute-force* or *one-variable-at-a-time* method: the model response, η_j, is computed by changing the value of a given model parameter, θ_i, while keeping the rest unchanged and then S_i^j is evaluated by equation (6). A newcomer to kinetic modeling is advised to begin with this simple brute-force approach. First, it is easy to use since hardly any additional

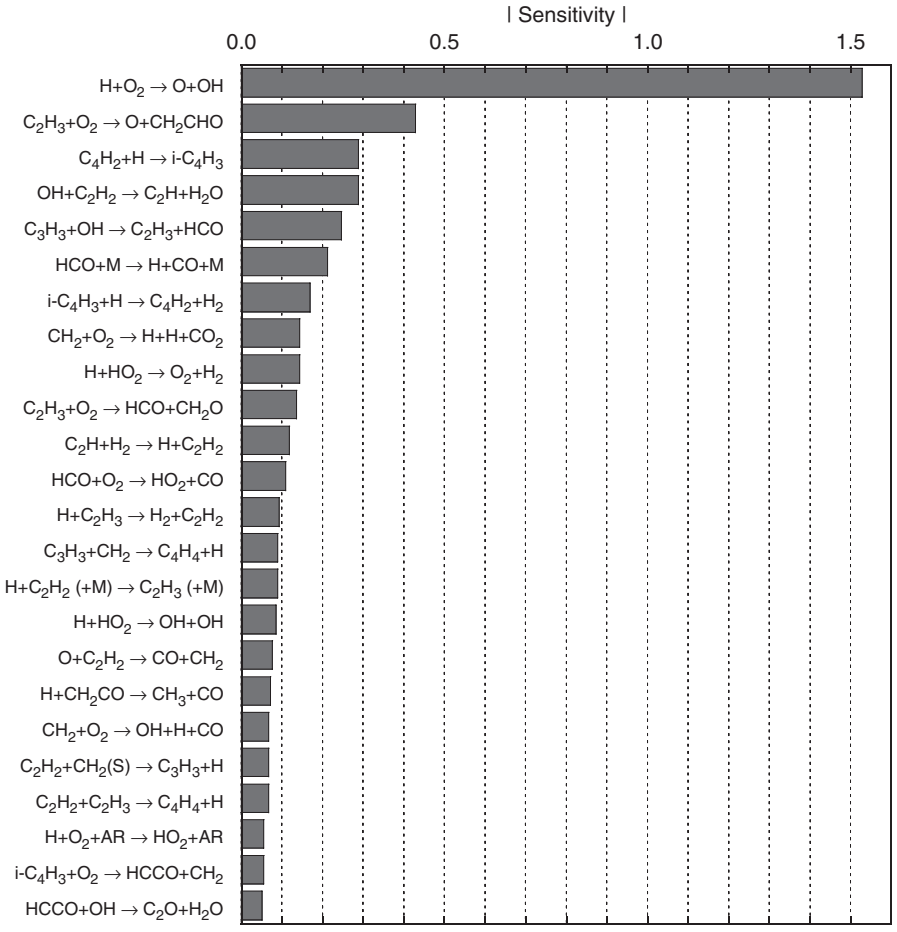

Fig. 5. An illustration of absolute sensitivity ranking: response sensitivities of the decay time of oxygen concentration in shock-tube oxidation of acetylene [4].

programming is required. Second, the interpretation of the computed sensitivities is direct and any conceivable response can be considered. Third, the approximation involved in evaluating expression (6) is harmless, since for the purpose of a screening sensitivity analysis only relative comparison (the ranking) is of interest. And finally, the slighter larger computational costs, as compared to some of the local methods [34], the only ''objection'' to the brute-force method, become insignificant in light of the speed of the modern computers.

A more efficient brute-force approach is to use *screening factorial designs* rather than one-variable-at-a time computations. Using these designs, the response is computed by varying all variables simultaneously

and then all sensitivities are obtained by a linear regression. We will describe such designs at end of the next section.

5.4 *Factorial designs*

Imagine an agricultural study in which the researcher is interested in finding the effects of different soil treatments on the growth of a grain. Let us assume that one experiment takes a year to complete and a limited number of experiments can be performed a year. The knowledge gained after one round of experiments will depend on the way the individual experiments were chosen, i.e., on the experimental design. Some designs may leave the researcher with no information whatsoever, whereas other designs can clearly illuminate the important features. The objective of the response–surface techniques is to provide the most economical designs, the factorial designs [17,19,27]. Choosing such an optimal design, the agricultural researcher can be confident that he obtained the maximum information possible for the constraints and resources given. The effectiveness of the response surface design increases with the increase in the number of variables.

(*i*) *Factorial variables*

Factorial designs are usually specified in terms of *factorial variables*, designated in this section by x and defined as

$$x = \frac{\theta - \theta_0}{(\theta_{\max} - \theta_{\min})/2} \tag{7}$$

where $\theta_{\max}$ and $\theta_{\min}$ are the upper and lower bounds, respectively, of the variation in model parameter θ, and $\theta_0 = (\theta_{\max} + \theta_{\min})/2$ the center of that variation interval. We refer to the half variation interval, $(\theta_{\max} - \theta_{\min})/2$, appearing in the denominator of equation (7) as the *span* of θ. The definition of the factorial variable given by equation (7) assures that $x = 0$ is the central point and $x = +1$ and -1 are the highest and lowest, respectively, points of the chosen interval of variation in x. In other words, in the space of factorial variables, the region of combined parameter variations H is a hypercube with the side equal to 2.

For designs employed in chemical kinetics, one may benefit by using the logarithmic transformation of model rate constants (or pre-exponential factors of the Arrhenius expressions), $\theta = \log k$. This, along with the logarithmic transformation of responses, $\eta = \log C$, helps to get better fits—more accurate surrogate models for the same span in x or a larger span

for the same level of the fitting error. With the transformation $\theta = \log k$, the factorial variable becomes

$$x = \frac{\log(k/k_0)}{\log f} \tag{8}$$

where $f = k_{\max}/k_0 = k_0/k_{\min}$, $k_0 = (k_{\max}k_{\min})^{1/2}$, and $k_{\max}$ and $k_{\min}$ are the upper and lower bounds, respectively, of the variation in the rate constant k. The logarithmic transformation of rate constants is harmonious with Box and Hunter's arguments [18] on uncertainties in k and the assumption of the uniform distribution. Also, the logarithmic transformations of model parameters and model responses normalize sensitivities [8],

$$S \equiv \frac{\partial \eta}{\partial \theta} = \frac{\partial \log C}{\partial \log k} = \frac{k}{C}\frac{\partial C}{\partial k} \approx \frac{\Delta C/C}{\Delta k/k} \tag{9}$$

In this form, the sensitivities can be thought of as ratios of *relative* changes in model responses to *relative* changes in model parameters. This, in turn, allows a meaningful inter-comparison of a set of sensitivities, e.g., for their ranking.

Computer experiments can in principle be handled similarly to physical experiments. One of the key distinguishing features is the fact that computer experiments with deterministic models do not have random errors. Hence, not all the factorial designs can be applied directly to computer experiments—some of them require repeating the same experiments, which is well suited for replicating actual physical experiments (or stochastic models) thereby accounting for random errors but not for deterministic computer simulations.

(*ii*) *Orthogonal designs*

One class of designs directly applicable to computer experiments is *orthogonal* designs [17,27,35]. An example of such a design for three independent factorial variables (x_1, x_2, and x_3) is shown in Table 1. Each row of this table represents a computer experiment—the first column designates its sequential number (1 through 15), the third to fifth columns, labeled "Independent variables," list the factorial variable values held in this experiment, and the last column reports the computed response obtained in this computer run. Several different responses could be obtained in a single computer experiment.

The x_1, x_2, and x_3 columns of Table 1 form the *design matrix*—its every row specifies the values of the model "input" variables (we presume, as described earlier, that only active variables of the model are used as the

TABLE 1
A central composite orthogonal design for three independent variables

Experiment no.	Independent variables			Cross terms			Quadratic terms			Computed response
	x_0	x_1	x_2	x_3	x_1x_2	x_1x_3	x_2x_3	$x_1^2 - \overline{x_1^2}$	$x_2^2 - \overline{x_2^2}$	$x_3^2 - \overline{x_3^2}$	
2^3 design											
1	+1	+1	+1	+1	+1	+1	+1	$1 - \overline{x^2}$	$1 - \overline{x^2}$	$1 - \overline{x^2}$	η_1
2	+1	+1	+1	−1	+1	−1	−1	$1 - \overline{x^2}$	$1 - \overline{x^2}$	$1 - \overline{x^2}$	η_2
3	+1	+1	−1	+1	−1	+1	−1	$1 - \overline{x^2}$	$1 - \overline{x^2}$	$1 - \overline{x^2}$	η_3
4	+1	+1	−1	−1	−1	−1	+1	$1 - \overline{x^2}$	$1 - \overline{x^2}$	$1 - \overline{x^2}$	η_4
5	+1	−1	+1	+1	−1	−1	+1	$1 - \overline{x^2}$	$1 - \overline{x^2}$	$1 - \overline{x^2}$	η_5
6	+1	−1	+1	−1	−1	+1	−1	$1 - \overline{x^2}$	$1 - \overline{x^2}$	$1 - \overline{x^2}$	η_6
7	+1	−1	−1	+1	+1	−1	−1	$1 - \overline{x^2}$	$1 - \overline{x^2}$	$1 - \overline{x^2}$	η_7
8	+1	−1	−1	−1	+1	+1	+1	$1 - \overline{x^2}$	$1 - \overline{x^2}$	$1 - \overline{x^2}$	η_8
Center point											
9	+1	0	0	0	0	0	0	$-\overline{x^2}$	$-\overline{x^2}$	$-\overline{x^2}$	η_9
Star points											
10	+1	$+\alpha$	0	0	0	0	0	$\alpha^2 - \overline{x^2}$	$-\overline{x^2}$	$-\overline{x^2}$	η_{10}
11	+1	$-\alpha$	0	0	0	0	0	$\alpha^2 - \overline{x^2}$	$-\overline{x^2}$	$-\overline{x^2}$	η_{11}
12	+1	0	$+\alpha$	0	0	0	0	$-\overline{x^2}$	$\alpha^2 - \overline{x^2}$	$-\overline{x^2}$	η_{12}
13	+1	0	$-\alpha$	0	0	0	0	$-\overline{x^2}$	$\alpha^2 - \overline{x^2}$	$-\overline{x^2}$	η_{13}
14	+1	0	0	$+\alpha$	0	0	0	$-\overline{x^2}$	$-\overline{x^2}$	$\alpha^2 - \overline{x^2}$	η_{14}
15	+1	0	0	$-\alpha$	0	0	0	$-\overline{x^2}$	$-\overline{x^2}$	$\alpha^2 - \overline{x^2}$	η_{15}

Note: $\alpha^2 = \sqrt{15}\, 2^{(3/2)-1} - 2^{3-1}$; $\overline{x^2} = (8 + 2\alpha^2)/15$.

factorial variables of the computer-experiment design). All the x columns of Table 1 form the associated design matrix

$$\mathbf{X} = \begin{bmatrix}
+1 & +1 & +1 & +1 & +1 & +1 & +1 & 1-\overline{x^2} & 1-\overline{x^2} & 1-\overline{x^2} \\
+1 & +1 & +1 & -1 & +1 & -1 & -1 & 1-\overline{x^2} & 1-\overline{x^2} & 1-\overline{x^2} \\
+1 & +1 & -1 & +1 & -1 & +1 & -1 & 1-\overline{x^2} & 1-\overline{x^2} & 1-\overline{x^2} \\
+1 & +1 & -1 & -1 & -1 & -1 & +1 & 1-\overline{x^2} & 1-\overline{x^2} & 1-\overline{x^2} \\
+1 & -1 & +1 & +1 & -1 & -1 & +1 & 1-\overline{x^2} & 1-\overline{x^2} & 1-\overline{x^2} \\
+1 & -1 & +1 & -1 & -1 & +1 & -1 & 1-\overline{x^2} & 1-\overline{x^2} & 1-\overline{x^2} \\
+1 & -1 & -1 & +1 & +1 & -1 & -1 & 1-\overline{x^2} & 1-\overline{x^2} & 1-\overline{x^2} \\
+1 & -1 & -1 & -1 & +1 & +1 & +1 & 1-\overline{x^2} & 1-\overline{x^2} & 1-\overline{x^2} \\
+1 & 0 & 0 & 0 & 0 & 0 & 0 & -\overline{x^2} & -\overline{x^2} & -\overline{x^2} \\
+1 & +\alpha & 0 & 0 & 0 & 0 & 0 & \alpha^2-\overline{x^2} & -\overline{x^2} & -\overline{x^2} \\
+1 & -\alpha & 0 & 0 & 0 & 0 & 0 & \alpha^2-\overline{x^2} & -\overline{x^2} & -\overline{x^2} \\
+1 & 0 & +\alpha & 0 & 0 & 0 & 0 & -\overline{x^2} & \alpha^2-\overline{x^2} & -\overline{x^2} \\
+1 & 0 & -\alpha & 0 & 0 & 0 & 0 & -\overline{x^2} & \alpha^2-\overline{x^2} & -\overline{x^2} \\
+1 & 0 & 0 & +\alpha & 0 & 0 & 0 & -\overline{x^2} & -\overline{x^2} & \alpha^2-\overline{x^2} \\
+1 & 0 & 0 & -\alpha & 0 & 0 & 0 & -\overline{x^2} & -\overline{x^2} & \alpha^2-\overline{x^2}
\end{bmatrix} \tag{10}$$

and the computed response values form a column vector

$$\mathbf{Y} = \begin{bmatrix} \eta_1 \\ \eta_2 \\ \vdots \\ \eta_{15} \end{bmatrix} \tag{11}$$

The composition of matrix $\mathbf{X}$ is designed to fit the computed responses into the second-order polynomial, the *response surface*,

$$\begin{aligned} \eta \approx s = {} & b_0 + b_1x_1 + b_2x_2 + b_3x_3 + b_{1,2}x_1x_2 + b_{1,3}x_1x_3 \\ & + b_{2,3}x_2x_3 + b_{1,1}x_1^2 + b_{2,2}x_2^2 + b_{3,3}x_3^2 \end{aligned} \tag{12}$$

where b's are the coefficients of the response surface. The numerical values of b's are determined by the least squares [36],

$$\mathbf{B} = (\mathbf{X}'\,\mathbf{X})^{-1}(\mathbf{X}'\,\mathbf{Y}), \tag{13}$$

where $\mathbf{B} = [b_0\ b_1 \cdots]'$ is the column vector of b's of equation (12).

The second column of Table 1 is the so-called fictitious variable, $x_0 \equiv +1$, introduced to obtain the free term of the polynomial expression (12), b_0. The x_0, x_1, x_2, and x_3 columns and the first eight rows of Table 1 constitute a *first-order* orthogonal design, corresponding to the linear model, $\eta \approx b_0 + b_1 x_1 + b_2 x_2 + b_3 x_3$. The first-order design of Table 1 is designated as 2^3, which indicates that three independent factorial variables are varied at two levels ($+1$ and -1). With the additional seven experiments, numbered 9 through 15, the design is second-order. Among the added experiments is one at the center of the design, at all $x = 0$, and others are pairs of so-called "star points," placed at a distance α from the design center on every principal axis. The x_1x_2, x_1x_3, and x_2x_3 columns of Table 1, the binary products of the x_1, x_2, and x_3 columns, are introduced to determine the coefficients of the cross-terms of equation (12) ($b_{1,2}$, $b_{1,3}$, and $b_{2,3}$), and the subsequent three columns to determine the coefficients of the square terms ($b_{1,1}$, $b_{2,2}$, and $b_{3,3}$).

The design given in Table 1 is called orthogonal because the design and associated design matrices are composed of mutually orthogonal columns, i.e., the dot product of every column pair is equal to exactly zero, $\mathbf{x}_i \cdot \mathbf{x}_j = \sum_{k=1, i \neq j}^{15} x_{ik} x_{jk} = 0$. The condition of column orthogonality dictates the makeup of matrix $\mathbf{X}$. This explains the origin of the three $(x_i^2 - \overline{x_i^2})$ columns of Table 1. If, for instance, one were to use just the x_1^2 values for the ninth column of Table 1 with the objective to determine $b_{1,1}$, then the dot product of the x_1^2 and x_0 columns will not be zero. Shifting the x_1^2 values by the x_1^2-column average, equal to

$$\overline{x^2} = \frac{1}{N} \sum_{u=1}^{N} x_u^2 = \frac{2^\kappa + 2\alpha^2}{N} \tag{14}$$

produces a column orthogonal to the x_0 column. The condition of orthogonality determines also the location of the start points,

$$\alpha = \pm \left(\sqrt{N}\, 2^{(\kappa/2)-1} - 2^{\kappa-1} \right)^{1/2} \tag{15}$$

In the above expressions, N is the total number of computer experiments in the design ($N = 15$ in our example) and κ the number of independent variables ($\kappa = 3$ in our example; i.e., $2^3 = 2^\kappa$).

When $\mathbf{X}$ is orthogonal the matrix $\mathbf{X}'\mathbf{X}$ in equation (13) and its inverse, $(\mathbf{X}'\mathbf{X})^{-1}$, are diagonal and possess optimal properties: the determinant of $(\mathbf{X}'\mathbf{X})^{-1}$ is minimal and that of $\mathbf{X}'\mathbf{X}$ (the information matrix) is maximal. The latter properties, in turn, imply the smallest variance obtained for the coefficients b of equation (12), or, in other words, the orthogonal design produces the best possible quadratic fit for a given number

of computer experiments. In addition, the orthogonality of **X** leads to independency in the estimates of coefficients b (i.e., their covariance is zero), and the evaluation of b *via* equation (13) reduces to a simple expression [35]

$$b_i = \frac{\sum_{u=1}^{N} x_{iu}\eta_u}{\sum_{u=1}^{N} x_{iu}^2} \tag{16}$$

Likewise, the variances of coefficients b are obtained by

$$\sigma^2\{b_i\} = \frac{\sigma^2\{s\}}{\sum_{u=1}^{N} x_{iu}^2} \tag{17}$$

where $\sigma^2\{s\}$ is estimated by the residuals

$$\sigma^2\{s\} = \frac{\sum_{u=1}^{N}(\eta_u - s_u)^2}{N - m} \tag{18}$$

and m is the number of coefficients b (i.e., the number of columns of matrix **X**; $m = 10$ in our example). The above implies that performing a computer design, one obtains not only the approximation function itself, equation (12), but also a measure of the fitting error.

The first-order design embedded in Table 1, 2^3, is an example of a *full factorial* design—it employs all combinations of the two level variations of each independent variable, three in this example. The number of experiments of the full factorial designs increases exponentially with the number of independent variables, namely 2^κ. For instance, the first-order full factorial design with 10 variables would require $\sim 10^3$ computer runs and the second-order design would require even more.

From practical considerations, not all combinations of variables need to be considered. A large fraction of them can be eliminated when higher-order interactions can be safely neglected. The designs obtained in this manner are called *fractional factorial* designs. In our example, assuming that the $x_1x_2x_3$ interaction can be neglected (compared to linear, cross, and quadratic terms), the same number of runs, 2^3, can be used to determine (linear) effects of four, not three, variables, by assigning the fourth factorial variable the values of the neglected triple interaction, $x_4 = x_1x_2x_3$. We refer to this design as 2^{4-1}, where the "4" in the power stands for the four independent factorial variables and "-1" indicates that it is a half-fraction of the full 2^4 design (there are two different yet statistically equivalent half-fraction 2^{4-1} designs that when combined form the full 2^4 design). With the increase in the number of factorial variables, there are also quarter ("-2") and higher-fraction ("$-p$") designs. Among all possible same-fraction designs, we usually

look for those with a higher *resolution* (so-called *minimum aberration* designs [17,19,37]), able to provide more independent estimation of different terms. The design resolution is indicated by a roman numeral as a subscript of "2." For instance, the half-fraction design we discussed above is actually the 2^{4-1}_{IV} design. The resolution IV of this design indicates, for example, that the linear term coefficients, the *linear effects*, are estimated independently from the cross-pair and quadratic effects, but are "mixed in" with the third-order effect, $x_1x_2x_3$.

The second-order designs are obtained by augmenting the first-order fractional factorial designs with the center and start points, forming the *central composite* designs, as in the case of the analogous full factorial designs. For further discussion, the reader may consult Refs. [17,19,27] and the literature cited therein, as well as examine specific designs used in optimization of detailed kinetic models [1,26,30,31,38,39]. In creating such composite designs, the total number of the computer experiments comprising the design should be (substantially) larger than the total number of coefficients b to be determined.

(*iii*) *Other designs*

One problem with orthogonal designs is that α increases with the number of factorial variables, moving the start points father away from the main hypercube, for instance, a 2^{8-2} design has $\alpha = 2$ and a 2^{13-4} design has $\alpha = 2.58$. This increases the overall error of the response surface, and sometimes leads to probing conditions that may have no physical meaning or practical value. The alternative is a class of *space-filling* designs that keep all the design points within the hypercube [27,29]. Two approaches are most popular: *D-optimal* designs and *Latin Hypercube* sampling.

The points of a *D-optimal* design are spread within the hypercube so as to minimize the determinant of the $(\mathbf{X}'\mathbf{X})^{-1}$ matrix (the unconstrained minimum leads to the above discussed orthogonal designs with the star points moved outside the hypercube). There are several numerical approaches to developing such designs, and they are available with popular software packages, such as the Statistics Toolbox of Matlab [40] (the reader must be aware, though, that the Matlab Statistics toolbox, up to the current version 5, does not constrain the *D*-optimal designs to having unique rows, and thus results in replicate computer runs).

The *Latin Hypercube* sampling aims at spreading the design points evenly on the basis of various geometric criteria. The reader may find it beneficial to learn about these designs using the function lhsdesign of the Matlab Statistics Toolbox [40].

Other types of experimental designs and various criteria of design optimality are available and new ones are continuously being developed (e.g., [27–29,39,41,42]). The specific choice of a design should consider the ease of development or availability, computational economy of execution, fitting error, and computational benefits of use. For instance, the screening sensitivity analysis for identification of active variables, where the objective is their relative ranking and not high-accuracy prediction, can be accomplished using *saturated* designs [17,27,43], e.g., by using Hadamard matrices (obtained conveniently by the Matlab function hadamard [40]). When the number of factorial variables becomes excessively large, one may consider using *supersaturated* screening designs [35,44].

5.5 *Optimization*

Recall that the developed response surfaces, or surrogate models as we refer to them in the context of model optimization, replace the solutions of the differential equations. Once the surrogate models are developed, *via* the design of computer experiments described in the preceding section, we can turn to optimization. The objective function now takes the form

$$\Phi = \sum_e w_e[s_e(\mathbf{x}_e) - d_e]^2 \tag{19}$$

with two substitutions as compared to equation (1): the model predictions, y_e, are replaced by the corresponding statistical surrogates, s_e, and the set of optimization variables, $\boldsymbol{\theta}$, is replaced by the sets of active variables, $\mathbf{x}_e$, a distinct subset of $\boldsymbol{\theta}$ for every eth response. As the surrogate models take the form of simple algebraic functions, such as second-order polynomials, the optimization can be performed using a variety of numerical methods (e.g., fmincon of Matlab [40]). Several practical examples of chemical kinetics are discussed in a later section.

5.6 *Prior pruning of the reaction model*

The practice of SM with chemical kinetics models showed that not all active variables can be determined by optimization, as the system as a whole is under-constrained. In other words, the objective function is not sufficiently sensitive to some of the optimization variables—those that are in the tail of the screening sensitivity plot. The low sensitivity manifests itself in the appearance of the valley in the objective function, as discussed in the beginning of this chapter, and this geometric feature makes it difficult to determine numerically the global minimum, and the

minimum may be not unique. Even if there exists a unique global minimum at a location of the valley, the difference between its value and that of other points along the locus line of the valley is not substantial by comparison to the experimental uncertainty. In this situation, the mathematical requirement for the global minimum may lose its physical significance. To obtain practical results, additional constraints should be invoked, such as keeping the values of the low-sensitivity variables close to the literature recommendations, or other considerations. In other words, not all active variables have to be optimization variables.

There are practical implications that follow from this observation. First, the assignment of the threshold level for separation of the model parameters into active and inactive variables becomes less critical than might appear at first. There is a definite zone of comfort in making this initially appearing as arbitrary decision: if too many variables are selected to be active at the sensitivity-ranking step, the number of optimization variables can be adjusted at a later stage without any harm done.

If we know that only high-sensitivity model parameters end up playing role in model optimization, then we may (and should) pre-screen the reaction model prior to identification of active variables and construct a smaller, more practical model. This brings us to the discussion of construction and completeness of chemical reaction models. Fifteen years ago, the following prospective was suggested [45]:

> "In principal, the kinetic data base is infinitely large, and the practical reality for this to happen may be not too distant in the future. … This brings to bankruptcy the philosophy of comprehensive kinetic model and leads in a natural way to the following view. All conceivable chemical reactions with the associated rate parameters—available experimentally, calculated theoretically, or simply estimated—constitute a reaction data bank. Given a specific problem, a subset of the data bank should be taken to assemble the reaction mechanism."

There is a current effort to create such a data infrastructure, called Process Informatics Model (PrIMe), with the initial focus on gas-phase chemical reaction kinetics [46]. Starting with the assumption that such a data infrastructure exists, the following strategy is fostered by the framework of SM [47].

The initial reaction model, referred to as the *first-trial* model, is assembled to contain as many reactions as perceived necessary to describe the physical reality of a given response. The consideration at this stage should be given to the completeness of the reaction set, including rather than excluding possible reactions if in doubt, without concern over the reaction set size. The completeness of the first-trial reaction set should be understood as pertained to a single response, not all available or possible ones. In other words, in principle, one constructs a first-trial model for each individual response of the training set.

Not all reactions of the assembled first-trial set contribute significantly to the corresponding response and many can be safely removed without affecting the rest of the analysis. We will refer to this process as *pruning* [48]. A computationally efficient strategy for reaction set pruning was suggested by Frenklach and co-workers [45,47,49,50] (it was then termed *Detailed Reduction*). The strategy consists of considering the contribution a given reaction rate term makes to certain sums of such terms (e.g., those comprising the rates of accumulation of given reaction species). For instance, noncontributing reactions can be identified by comparing the individual reaction rates with the rate of a chosen reference reaction. The reference reaction could be the rate limiting step or the fastest reaction. It was further proposed and demonstrated that the computations used to obtain the required rate data do not have to be performed with the actual full fluid-dynamic/chemical kinetic model—the reduction can be achieved with a much simpler computation using similar but greatly simplified geometry and physical conditions. Additional constraints can be imposed compounding the rate inequality, such as the rate of energy release or species concentration rates, and the degree of reduction, i.e., the accuracy of the obtained reduced model in predicting the given response, can be prescribed *a priori*.

The pruned reaction set can then be subjected to a screening sensitivity analysis, identification of active variables, and development of the surrogate model in thus identified active variables, as described in the previous sections. We perform these procedures—assembly of the first-trial reaction set, pruning, sensitivity analysis, and development of the surrogate model in active variables—for each experimental response of the training set. Having all the surrogate models, we turn to a joint optimization of all the responses, with the optimization variables being a (sub)set of the union of all active variables.

We close this section by noting that reaction set pruning can be attained in other ways. Recent proposals include the use, in addition to the reaction rate inequality constraints [45,47,49–51], inclusion of chemical lifetimes and species sensitivities [52–54] and optimization-based criteria [55–57]. One must weigh in the overall computational efficiency, especially in light of the repeated (and an attractive possibility of on-the-fly) use of pruning. Several examples tested recently with an optimization-based approach [57] resulted in smaller reaction models as compared to the compound-inequality approach [49]. However, the size difference of the pruned reaction sets obtained with the two approaches was rather modest—several species out of several dozens in the initial set—and came at a substantial cost in the computational performance. In the SM approach, having a larger pruned reaction set can easily be ‘‘salvaged’’

in the surrogate-building step without any substantial loss in the computational speed, as discussed below.

5.7 *Strengths and weaknesses of solution mapping*

Here we examine the strengths and weaknesses of the key features of SM, those that have implications to the practice of the technique. We begin with the strengths:

- SM decouples model optimization into two procedures: development of statistical surrogates using direct reaction model simulations and multi-response optimization with the surrogate models. The first benefit of this decoupling is bringing disparate experimental measurements (responses) into the same protocol of model optimization. The experiment specificity (e.g., reactor geometry and diagnostic techniques) and associated time-demanding computations, often compounded with numerical difficulties (such as ODE stiffness), are handled by domain-specific direct simulation codes, whereas the solution of the inverse problem (i.e., optimization) is left to any suitable code because of the simple algebraic form of the surrogate models. In this way, one can solve a multi-dataset, multi-parameter optimization problem without a need for developing new numerical methods and computational software, but "reusing" the available ones, domain-specific simulation codes and optimization solvers.
- When the number of degrees of freedom is positive, i.e., when the experimental responses outnumber the parameters to be determined, SM can facilitate statistically rigorous determination of parameter values and associated confidence regions (see, e.g., Ref. [8] and the literature cited therein). Application of these ideas was demonstrated on thermal decomposition of propane [30,31]. For the small extent of conversion observed under shock-tube conditions, the analysis could be limiting to two active variables. This allowed producing a 95% confidence region and subsequent discrimination among several differing rate constants.
- SM has demonstrated overall computational economy: while the development of the surrogates *via* statistical designs could be computationally intensive, the principal benefits come from the reuse of the surrogates. It is rather typical, especially in the context of developing predictive reaction models, that the researcher is interested not only in a single optimal solution, but also in solution uncertainty, visualization of the objective function and confidence

region, sensitivity of the solution to physical assumptions, and all while trying different statistical weights and different combinations of experimental responses or even different sets of training data. All these features can be obtained with the same set of surrogate models, and it is this reuse that contributes to the numerical efficiency of SM. Further increase in computational economy is possible by noting that SM lends itself naturally to code parallelization, as individual computer experiments comprising the design can be run concurrently, without a need for the cross-talk between processors.

- The decoupling offers an additional benefit of storing the surrogates for their subsequent reuse. Considering the computational speed of optimization with algebraic surrogates, this can enable on-the-fly operation, in support of a collaborative analysis and development of chemical reaction models. Such protocols were indeed developed by the GRI-Mech project team [1] and are planned for PrIMe [46].
- The use of direct numerical simulations for development of surrogate models allows one to consider any observable property or a combination of them as a modeled response. For instance, in addition to species concentrations, typical of most studies, SM can handle with a similar ease also induction times, peak properties (e.g., location, height, width), peak relative positions or their ratios, or peak ratios in different experiments, e.g., testing the effect of a mixture additive. Likewise, any parameter or combination of them can serve as optimization variables. Examples may include, in addition, the typically discussed "rate constants" [30], parameters of rate coefficient expressions (such as activation energies) [2], and species enthalpies of formation [1,4].
- Each step of the SM procedure provides a certain degree of flexibility (a "safety net") in decision making: the researcher does not need to be concerned with an overly large size of the first-trial reaction set, as its "skeletal" size will be determined in the subsequent step of pruning; the pruning does not need to be too stringent either with identifying and removing all noncontributing reactions, since the surrogate model is developed in true active variables, independent of the reaction set size; and the list of active variables can be fine-tuned by selecting a smaller subset of them as optimization variables. In other words, each step of the procedure allows a certain degree of slack that is tightened at the subsequent step. And because each step is computationally efficient, the researcher can experiment with the choices made.

- SM provides means to control the surrogate fitting errors—by changing the size of H. However, this increases the overall computational time, as discussed under the "weaknesses" below.
- SM can be applied to other reaction systems, not just kinetics. Recent examples pertinent to this volume may include optimization of a chemical-activation model of the CO + OH reaction system [58] and geometry optimization in quantum Monte Carlo [59]. It is pertinent to mention that the approach of response–surface optimization is a very general one with numerous applications in many different fields; examples may include electronic circuit design, controlled nuclear fusion, plant ecology, and thermal energy storage [28]. Furthermore, replacing the roles of the $\boldsymbol{\theta}$ and $\mathbf{y}_0$ variables in equation (4) leads to the development of adaptive chemistry schemes for complex reactive flow simulations [48,60–62].

The key weaknesses of SM are the span and dimensionality of the parameter space:

- Recall that the fitting of the surrogate model is done for only a limited region, H, of the parameter space $\boldsymbol{\theta}$, constrained by the range of variation assigned to active variables $\mathbf{x}$. In the case of GRI-Mech, where the years of research led to relatively narrow ranges of uncertainties in key rate parameters, the physical span is small enough so that a single set of the quadratic polynomials over the entire domain of parameter uncertainties, H, was sufficient to get an acceptable level of accuracy of the surrogate functions [1]. What if the span of H is large, exceeding the range over which the quadratic polynomials could be accurate? One solution to this is a *piecewise iteration*—developing multiple sets of surrogate hypercubes. Thus, starting with a (locally accurate) hypercube H_0 and finding that the optimal point is located on an edge of or outside H_0, one builds a new hypercube, H_1, adjacent to or around the H_0 minimum, and so on. This strategy may also be combined with the control of accuracy: starting with a larger and less-accurate H, the size of subsequent H's is reduced as the iteration approaches the (global) minimum. A limited testing of these ideas [30,63] demonstrated convergence of the iterative process, and with a manageable number of iteration steps. A more detailed quantitative study is in progress.
- The response–surface technique outlined above becomes less practical for a number of active variables exceeding ~20. How can one deal with a significantly larger number of parameters? Before

we proceed addressing this question, let us emphasize that the dimensionality of the optimization space, H, and the dimensionality of the surrogate models are not the same. As discussed earlier, each polynomial response function is developed in terms of it own set of active variables. For instance, while the GRI-Mech polynomial surrogate models were each dependent on 10–13 variables, the total dimensionality of H was 102 [1]. In other words, SM has already provisions to handle large dimensionality of H in a practical manner.

The question we posed above concerns the situation when there are a larger number of active variables for a single response (thus defying the effect sparsity). In such a case, one can explore principal component analysis, thereby condensing all the active variables to a small number of principal components, and then to develop surrogate models in terms of these principal components. Again, the experience of using principal component analysis [64,65] and other techniques of model reduction [66,67] in the area of chemical kinetics modeling, along with some limited testing of SM [63], provides grounds for optimism in this case. This is another area of future research.

Currently, one of the most developed, hence most illustrative, examples of practical application of SM is provided by the GRI-Mech project [1]. In its latest release, the GRI-Mech 3.0 dataset is comprised of 53 chemical species and 325 chemical reactions (with a combined set of 102 active variables), and 77 peer-reviewed, well-documented, widely trusted experimental observations obtained in high-quality laboratory measurements, carried out under different physical manifestations and different conditions (such as temperature, pressure, mixture composition, and reactor configuration). The experiments have relatively simple geometry, leading to reliably modeled transport of mass, energy, and momentum. Typical experiments involve flow-tube reactors, stirred reactors, shock tubes, and laminar premixed flames, with outcomes such as ignition delay, flame speed, and various species concentration properties (location of a peak, peak value, relative peaks, etc.).

The project's deliverable was a ''living model'': not the ultimately right one—possibly a utopian goal for the present state of chemical kinetics science—but ''the best current,'' i.e., the best consensus possible with the present state of knowledge and available quantity and quality of data at a given time. This marks a fundamental shift in the general outlook on a (chemical kinetics) model.

The concept of a model and the form it assumes have changed with time: from conceptual statements to simple algebraic relationships to differential equations to numerical algorithms to computer programs and files. The current practice of model development/use is based on the following paradigm: (a) a model is postulated introducing a set of parameters; (b) a ''unique'' set of parameter values are determined from experiment or/and theory, and (ideally) supplied along with a corresponding set of individual uncertainties; and (c) the model is then applied to conditions of interest employing the unique set of parameter values. The natural uncertainties of the underlying experiment and theory must somehow be transferred into the final prediction uncertainty using the uncertainties that were assigned to the model parameters.

Experience shows that this conventional paradigm does not lead to a desirable quality of prediction [26]. As discussed at the beginning of the chapter, each model parameter has associated with it an interval of uncertainty. Taken together, the uncertainties of all parameters form a hypercube in the parameter space. Each point of this hypercube may seem to be consistent with accepted experimental results since each coordinate (parameter) individually belongs to its corresponding interval of uncertainty. However, some parts of the hypercube fit the experimental data base better than others. Typically, the central point of the hypercube, whose coordinates correspond to the individual best-fit values of the individual parameters, is not necessarily the best-fit point for the combined set of parameters. The better-fit parts form a low-dimensional manifold, which is the result of correlations in the experimental data and hence the knowledge of the parameter vector. A methodology that implicitly or explicitly samples preferentially the manifold and not the entire hypercube volume should provide a more realistic estimate of model uncertainty than superposition of individual parameter errors.

The numerical methodology underlying the GRI-Mech project [1] was SM [26]. Recently, we found that the use of a simple polynomial form of the SM statistical surrogates ties in more closely with a general, set-based approach to model analysis, which we discuss next.

6 DATA COLLABORATION

The Data Collaboration methodology puts models, theory, and data on the same footing. It does not change the way experimentation is done, but requires a different approach to analyzing even one's own observations and, as a consequence, places new standards on data reporting. In this approach, measured data, its estimated uncertainty, and a model of the

experimental system are treated as an assertion whose correctness depends on the suitability of the model and the reliability of the measured data. Taken together, the model and the measurement constitute a (low dimensional) constraint in the global unknown parameter space. Specifically, only those parameters that are consistent with the model/measurement pair are possible values of the unknown parameters. By considering only these parameter values, one can harvest a majority of the information content of the data [68], determine realistic bounds on model predictions [69], and test consistency of a dataset [70]. This numerical methodology avoids unnecessary overconstraining of model parameters that plagues many other techniques due to inherent correlations among parameters, and allows one to explore more closely the true feasible region of the parameter space in a computationally efficient manner.

6.1 Data collaboration concepts

(*i*) *Dataset*

The concept of a dataset lays down the foundation for the Data Collaboration methodology. We associate with experiment E a *dataset unit*, which consists of the measured value, d_e, reported uncertainty in the measurements, l_e and u_e, and a mathematical model, M_e. The model M_e is defined as the functional relation between the model active variables, $\mathbf{x}$, and the prediction for d_e, yielding $l_e \leq M_e - d_e \leq u_e$, which ties together data, model, and uncertainty. A *dataset*, D, is a collection of such dataset units $U_e = \{(d_e, u_e, l_e, M_e)\}$. In the present Data Collaboration methodology, the models are the statistical surrogates developed in computer experiments, namely $M_e = s_e(\mathbf{x})$, and so $U_e = \{(d_e, u_e, l_e, s_e)\}$ and $\mathrm{D} = \{U_e\}$.

The creation and organization of a dataset is guided by the system in question, for instance, formation of nitrogen oxides in the combustion of natural gas, concentration levels of ozone in the atmosphere, or transmembrane signaling in bacterial chemotaxis. A single experiment cannot provide complete information on such a system, but rather probes its particular aspect. A collection of such individual "bits" of pertinent information (i.e., dataset units) forms a dataset. The more extensive and diverse the collection, the more complete is the understanding of the system. The unifying principle, the one that determines the "pertinence" of a given experiment to a given dataset, is a presumption that there exists a single chemical kinetics model, common to all dataset units, that is expected to predict d_e when exercised at the conditions of experiment E. In other words, it is presumed that broad consensus exists (at least tentatively) regarding the necessary reaction steps of the system and

hence the mathematical structure of the unifying kinetic model, and that this mathematical model is sufficient, in principle (with the "right" choice of parameter values), to predict all experimental observations included in the dataset.

(*ii*) *Initial hypercube*

We assume that there is prior information on the possible values of the model parameters. This prior information can be expressed as the confinement of possible values of the active variables to an n-dimensional hypercube, $H := \{\mathbf{x} \in \mathbb{R}^n : \alpha_i \leq x_i \leq \beta_i\}$, where α_i and β_i are the lower and upper bounds, respectively, on x_i for $i = 1, 2, \ldots, n$. Each edge of the hypercube H represents the presumed interval of "physically allowed" values of the corresponding model parameter, either the estimated uncertainty or a range containing the differing values.

(*iii*) *Feasible region*

Not every point $\mathbf{x}$ in H predicts all experimental observations of the dataset within their specified uncertainties. The collection of parameter values that are both contained in the hypercube and satisfy $l_e \leq s_e - d_e \leq u_e$ for every dataset unit e in the dataset form the *feasible region*, F. A point $\mathbf{x}$ that is not contained in F has been eliminated from consideration as a possible value for the dataset active variables by either the prior information, through the bounds of H, or by the experimental observations of the dataset, through intervals $(d_e + l_e, d_e + u_e)$. It is in this manner that experimental observations increase our knowledge of kinetic parameters: an experiment may eliminate portions of the hypercube H from consideration, thereby decreasing the uncertainty in the values of the kinetic parameters.

6.2 *Looking at some feasible sets from GRI-Mech dataset*

In this section we further expose features of a feasible set and discuss the implications to the chemical kinetic model analysis. Some low-dimensional slices of feasible parameter sets from the GRI-Mech 3.0 dataset [1] nearly duplicate the scenarios described in the earlier sections of this chapter. We consider an example from Ref. [68]: two active variables, x_{44} and x_{45}, factorial-form pre-exponential factors of reactions $CH + H_2 \rightarrow H + CH_2$ and $CH + H_2O \rightarrow H + CH_2O$, respectively, and two experimental targets, E_{66} and E_{67}, GRI-Mech 3.0 training targets SCH.C12 and SCH.C13, respectively. x_{44} is the highest ranking impact parameter for E_{66} and E_{67}, and x_{45} is the second highest impact parameter for E_{67} and the fourth highest for E_{66}.

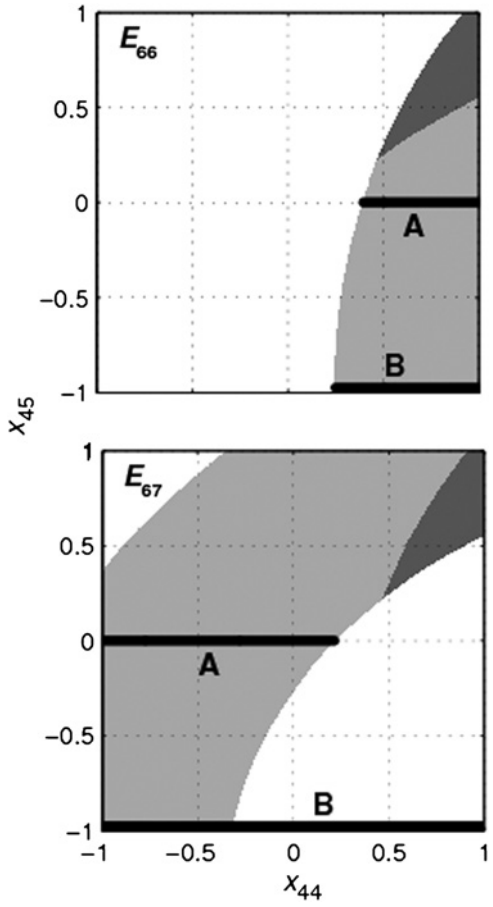

Fig. 6. Feasible sets obtained in analysis of GRI-Mech experimental targets E_{66} (top panel) and E_{67} (bottom panel) individually, with all x's but x_{44} and x_{45} set to 0 [68].

The diagram in Fig. 6 shows the feasible set determined from individual model/experiment pairs, with both x_{44} and x_{45} free (while keeping the remaining 100 x's frozen at zero). Thus, for every pair of the x_{44} and x_{45} values located within the shaded area of the top panel, the modeled prediction for E_{66} lies within the measurement error of the measured value. A similar interpretation applies to the bottom panel, but for E_{67}. We observe that whereas the one-dimensional feasible sets (thick horizontal lines at $x_{45} = 0$) do not overlap, the two-dimensional feasible sets do have a common set of points, within the region shaded in darker gray. In other words, while determination of a single parameter from a single experiment led to an apparent "controversy" (as if the two results disagree with each

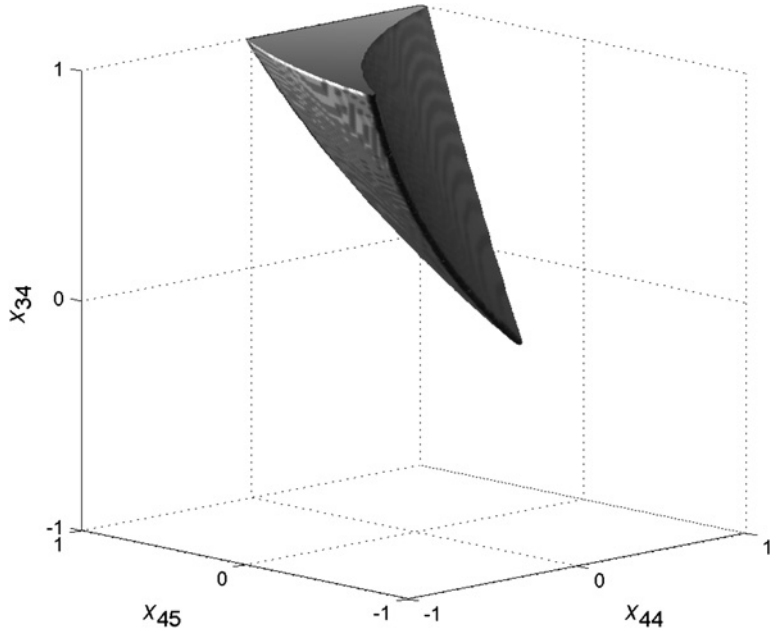

Fig. 7. A feasible set obtained in a joint analysis of GRI-Mech experimental targets E_{66} and E_{67}, with all x's but x_{44}, x_{45}, and x_{34} set to 0 [68].

other), adding just one more active variable into consideration resolves it by finding a "mutually agreeable" set of acceptable values.

Accounting for more active variables expands the feasible set in additional dimensions. For example, expanding the dimensionality of the analysis to include an additional active variable, x_{34}, pre-exponential factor of reaction $OH + CH_3 \rightarrow {}^1CH_2 + H_2O$, reveals more. x_{34} is the second highest impact parameter for E_{66} and the fourth highest for E_{67}. The three-dimensional feasible set is shown in Fig. 7. A cross-section of this feasible set by the plane $x_{34} = 0$ forms the darker shaded area in Fig. 6. With the addition of experiments and active variables, the geometry of the feasible set grows in complexity and is difficult to visualize. This necessitates developing theoretical and numerical methods to accurately account for known constraints (usually implied by data) in nonlinear and hybrid models. This is precisely the capability of the numerical methods described next.

6.3 Optimization techniques primer

The Data Collaboration approach casts problems as constrained optimization over the feasible region, drawn on the entire knowledge

content of a dataset. Presently, it combines SM to generate each s_e and robust control techniques to solve the constrained optimizations. While optimization of general objective functions subject to general constraints is known to be a "hard" problem, we will take advantage of fast new algorithms for polynomial optimization, which use convex relaxations (a "relaxation" is a modification of the original optimization, with a rigorous relation to the original problem, but better computational properties, for example, convexity). In the rest of this section we provide a brief outline of the pertinent concepts; the reader is referred to a more detailed discussion [71] and the literature cited therein.

All the questions posed in the Data Collaboration framework appear as constrained optimization problems [72]. Typically, there are both inequality and equality constraints. If f, g, and h are functions, then a constrained optimization problem is of the form

$$\min_{x\in\mathbb{R}^n} f(x) \quad \text{subject to } g(x) \leq 0, h(x) = 0 \tag{20}$$

The variable x is the optimization variable. The set of values of x which satisfy the two constraints is called the *feasible set*. Replacing f with $-f$ recasts the problem from minimization to maximization. Without loss of generality we restrict the discussion to minimizations.

Ideally, the solution to an optimization problem consists of an optimum value, x_{opt}, for the optimization variable and a proof (often called the *certificate*) of its optimality. Alternatively, one may obtain a suboptimal point, x_{sopt}, that is feasible and achieves an objective value $f(x_{\text{sopt}})$ within some fixed tolerance of the optimum. For general optimization problems such as those in equation (20) this preciseness is rarely obtained, usually requiring a form of optimization called *global optimization*.

Many algorithms can be shown [72] to generate a convergent sequence $\{x_k\}_{k=1}^{\infty}$ whose limit point is a local optimum of (20). A point x^* is a local optimum if it satisfies the constraints and there is an open ball containing x^* such that $f(x)\geq f(x^*)$ for every point x in the open ball satisfying the constraints. Under suitable hypotheses, algorithms such as gradient descent and Newton's method produce such sequences.

Suppose x satisfies all the constraints of (20). Independent of whether x is a local optimum it is clear that $f(x)\geq f(x^*)$. Any upper bound on the value of the constrained minimization is called an *inner bound*. An inner bound effectively says "the minimum is at least this small." Inner bounds are generally easily derived since the value of the objective function at any feasible point is an inner bound. By contrast, an *outer bound* is a lower bound on the value of the constrained minimization. An outer bound effectively says "the minimum can be no smaller than this."

Deriving outer bounds is more challenging than inner bounds and usually must exploit specific problem structure. Many outer bounds are based on the Lagrangian dual of (20).

Branch and bound [73] is a form of global optimization that exploits efficiently computed inner and outer bounds. Typically the feasible set, while not known explicitly, is known to be bounded within a rectangular cube in the optimization variable space. A new constraint that the optimization variable must also lie in this cube is added to the problem. Of course, the extra constraint is superfluous (since the feasible set is known to lie within this cube). Inner and outer bounds are computed on the "modified" problem. If they are within a prescribed tolerance of one another, the algorithm terminates. If the bounds are far apart, the cube is divided into two cubes (the "left" and the "right" children) yielding two minimization problems, the original problem with the left cube constraint and the original problem with the right cube constraint. Inner and outer bounds are generated for each of these two problems. The smallest inner bound is an inner bound on the original problem, and the smallest outer bound is an outer bound on the original problem. Note that if one of the outer bounds is greater than the other inner bound, it is apparent which cube contains the optimal point and one cube can be eliminated from consideration. This process continues recursively generating a binary search tree of cubes. At every stage all cubes whose outer bounds are greater than the smallest inner bound are labeled inactive. If the inner and outer bounds have the property that they converge together as the cube size goes to zero, then eventually (after potentially many cube subdivisions) the composite inner and outer bounds will be close to one another.

Convex programming refers to a minimization problem with a convex objective and a convex constraint set. For example, if f and g are convex functions, then

$$\min_{x\in\mathbb{R}^n} f(x) \quad \text{subject to } g(x) \leq 0 \tag{21}$$

is a convex program. The textbook [7] is a comprehensive treatment of convex programming. Interior point methods [74] play an important role in modern algorithms for these types of problems. Two important instances of convex programs are linear programs and semi-definite programs.

Linear Programming (LP) refers to an optimization problem with a linear objective and many linear constraints. A general form of a linear program is

$$\min_{x\in\mathbb{R}^n} c'x \quad \text{subject to } Ax - b \leq 0 \tag{22}$$

where $A \in \mathbb{R}^{m\times n}$, $b \in \mathbb{R}^m$, and $c \in \mathbb{R}^n$ are given. The notation $Ax-b\leq 0$ is interpreted coordinatewise, representing m linear inequality constraints on x. Practical experience in the 1950s and 1960s using Dantzig's simplex method indicated that "most" linear programs could be solved efficiently (storage requirements and run time growing modestly with problem dimension, n and m) although the worst-case behavior of the simplex algorithm had exponential growth in problem dimension. It was not until 1979 that theoretical results [75] confirmed that all linear programs could be solved efficiently.

A generalization of LP is *semi-definite programming* (SDP). A general form of a semi-definite program is

$$\min_{x\in\mathbb{R}^n} c'x \quad \text{subject to } F_i + \sum_{k=1}^{n} x_k F_k \geq 0 \tag{23}$$

where each F_i is a $m \times m$ given symmetric matrix, and the vector $c \in \mathbb{R}^n$ is given. The inequality constraint requires that the matrix be positive-semi-definite. From a theoretical standpoint, semi-definite programs share many of the properties of linear programs. Using primal-dual methods [7,76] they are solved efficiently, and research continues in algorithms for these problems.

A *mixed integer linear program* (MILP) is a linear program with some of the optimization variables constrained to be integer valued [73]. Integer valued optimization variables often model those decisions which must be drawn from a discrete set. In general, the complexity of MILPs is much greater than linear programs. MILPs can be solved using branch and bound. The outer bounds are obtained by ignoring the integer constraints, and allowing all optimization variables to be real numbers, resulting in a standard linear program.

6.4 *Prediction of model uncertainty*

In what follows, we illustrate the general mathematical strategy of Data Collaboration using as an example our main problem, that of model prediction [69]: given a dataset comprised of N_{D} dataset units (i.e., N_{D} quadratic models s_i with the respective coefficient matrices $\mathbf{M}_i$), obtain a prediction interval for an arbitrary quadratic model s_0. The computational problem we thus focus on is an indefinite quadratic program: for $\mathbf{x} = [x_1, x_2, \ldots, x_n]' \in \mathbb{R}^n$,

$$\text{bound} \begin{bmatrix} 1 \\ \mathbf{x} \end{bmatrix}' \mathbf{M}_0 \begin{bmatrix} 1 \\ \mathbf{x} \end{bmatrix} \quad \text{subject to} \begin{bmatrix} 1 \\ \mathbf{x} \end{bmatrix}' \mathbf{M}_i \begin{bmatrix} 1 \\ \mathbf{x} \end{bmatrix} \in [\alpha_i, \beta_i] \tag{24}$$

for $i = 1, 2, \ldots, N_D$. By "bound" we mean lower bounds on the minimum and upper bounds on the maximum, both of which are referred as outer bounds. Here, all $\mathbf{M}_i$ are symmetric $(1+n) \times (1+n)$ real matrices. There is a family of convex relaxations of this problem, called SOS (sum of squares) relaxations that we employ to compute the outer bounds.

Although the SOS relaxations apply to the original problem in (24), they are more easily described for a modified feasibility problem: given $n \times n$ symmetric matrices $\mathbf{M}_0, \mathbf{M}_1, \ldots, \mathbf{M}_{N_D}$, determine if the relation

$$\bigcap_{i=1}^{N_D} \{\mathbf{x} : \mathbf{x}'\mathbf{M}_i\mathbf{x} \geq 0\} \subset \{\mathbf{x} : \mathbf{x}'\mathbf{M}_0\mathbf{x} \geq 0\} \tag{25}$$

holds. In the first level of SOS relaxations, called the *S*-procedure, the computation to ascertain relation (25) is: if there exist nonnegative real numbers $\{\lambda_i\}_{i=1}^{N_D}$ with

$$\mathbf{M}_0 - \sum_{i=1}^{N_D} \lambda_i \mathbf{M}_i \geq 0 \tag{26}$$

then relation (25) holds. The new feasibility problem requires a search over the $\{\lambda_i\}$ to satisfy (26). While only a sufficient condition is required for (25), the feasible set of $\{\lambda_i\}$ is convex. Determining such λ's (or proving none exist) is an SDP problem, as discussed in the preceding section.

In concluding this section, we note that by posing the question of model prediction in the form of equation (24) the paradigm of a model is shifted from considering model parameters as "unique," pre-determined values with individual, uncorrelated uncertainties to including the actual experimental data, along with the physicochemical theoretical constraints if available, as the integral part of the model, with model parameters playing a role of "internal" variables. In other words, instead of the two-stage approach—i.e., estimation of model parameters from fitting experimental data followed by model predictions using the obtained estimates—we transfer the uncertainties of the "raw" data into model prediction *directly*.

6.5 Consistency of a reaction dataset

The framework of Data Collaboration supports a rigorous numerical approach to dataset consistency, which provides a combined way to look at system uncertainties originating from either rate parameters or experimental observations [70]. The measure of dataset consistency

is defined as

$$C_{\mathrm{D}} = \begin{array}{l} \text{maximum value of } \gamma \\ \text{subject to the constraints :} \end{array} \left\{ \begin{array}{c} -x_j \le -\alpha_j \\ x_j \le \beta_j \\ -s_e(\mathbf{x}_e) + d_e \le -l_e - \gamma_e \\ s_e(\mathbf{x}_e) - d_e \le u_e - \gamma_e \end{array} \right\}$$
$$\text{for } j = 1, 2, \ldots, n$$
$$\text{for each } e \text{ in the dataset} \qquad (27)$$

where α's and β's are the constraints on x's, and l's and u's the lower and upper bounds, respectively, on the experimental uncertainty ranges. The magnitude of C_{D} provides a measure of the relative consistency (or inconsistency) of the dataset, with greater than zero values implying that all the constraints in equation (27) are satisfied and so the dataset is consistent, and with larger values of C_{D} indicating enhanced consistency.

The usefulness of this measure can be illustrated with a simpler, easier to visualize test. We consider pairs of dataset units (U_e, U_f) for e, f (not necessarily distinct) in the index set of the dataset D. For each pair we compute the minimum level of uncertainty, u_{ef}, that leaves the two-element dataset $D_{ef} = \{U_e, U_f\}$ consistent, i.e.,

$$u_{ef} = \text{the minimum value of } u \text{ such that the constraints}$$
$$|s_e(\mathbf{x}_e) - d_e| \le u \text{ and } |s_f(\mathbf{x}_f) - d_f| \le u$$
$$\text{are satisfied by some } \mathbf{x} \text{ in H}$$

The results of such test for the GRI-Mech 3.0 dataset are displayed in Fig. 8. The height of each bar protruding from the (e, f) coordinates of the $u = 0$ plane represents the minimum level of uncertainty for which the two-element dataset $\{U_e, U_f\}$ is consistent. For many pairs this height is negligibly small, indicating that there are $\mathbf{x}$ in H for which $s_e(\mathbf{x}_e)$ is essentially d_e and $s_f(\mathbf{x}_f)$ is essentially d_f. The two "walls" along e, $f = 25$ occur because $|s_{25}(\mathbf{x}_{25}) - d_{25}| \le 0.008$ for every $\mathbf{x}$ in H, so u_{ef} must be at least 0.008 for any pair $\{U_e, U_f\}$ containing U_{25}. Another noteworthy feature in the pairwise graph is the emergence of a few large peaks. One of them is for the $\{U_{57}, U_{58}\}$ pair, showing that an uncertainty level of at least 0.082 (10-fold larger than the one for the "wall") is required for this pair of dataset units to be mutually consistent. The extreme magnitude of these few outstanding peaks signals a possible cause for concern regarding the affected experiments.

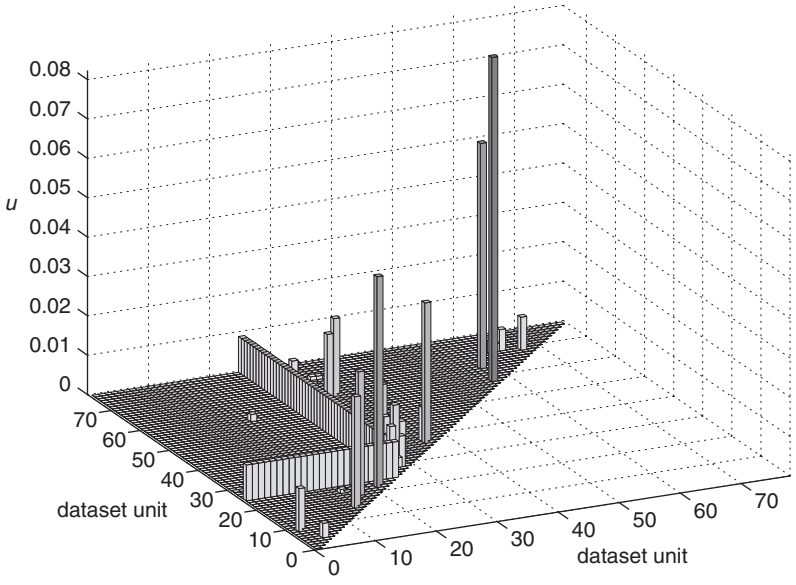

Fig. 8. Pairwise test [70].

The analysis of dataset consistency is assisted by Lagrange multipliers, which gauge sensitivity of the consistency measure to the dataset uncertainties. The example is presented in Fig. 9. The two largest peaks are the sensitivities of the consistency measure with respect to the lower bound l_{57} of the experimental uncertainty of dataset unit 57, and the upper bound u_{58} of the experimental uncertainty of dataset unit 58 (bottom left and right panels of Fig. 9, respectively). These same two dataset units surfaced in the pairwise test. Both facts gave us reason to suspect U_{57} and/or U_{58} as possible outliers. On reexamination of the original experimental data by the researchers involved (see Ref. [70]), errors in data recording were found and the corrections made were exactly in line with what the consistency analysis had indicated was probable.

6.6 Information gain due to data collaboration

We also performed "toy" thought experiments [68] to gauge the information loss by doing "traditional" analysis without the benefit of Data Collaboration at the raw data level. We considered a measure of information gained as a result of the data processing as a relative

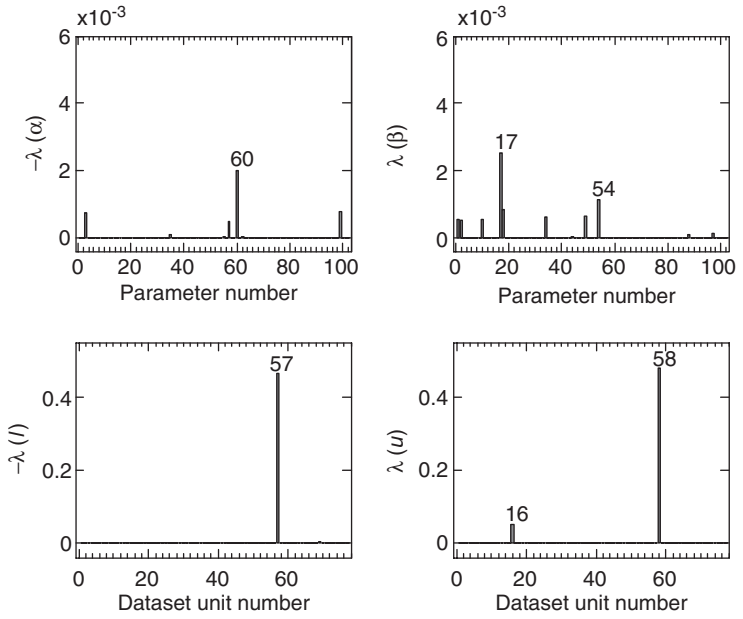

Fig. 9. Lagrange multipliers [70].

decrease in the predicted range R of (an arbitrary) model, s_0,

$$I := 1 - \frac{\Delta R_{\text{posterior}}}{\Delta R_{\text{prior}}} \tag{28}$$

where ΔR is the length of an interval R. Prior to data processing, the variations of $\mathbf{x}$ are confined to the initial hypercube H, and

$$\Delta R_{\text{prior}} = \left[\min_{\mathbf{x}\in \mathrm{H}} s_0(\mathbf{x}) - \max_{\mathbf{x}\in \mathrm{H}} s_0(\mathbf{x})\right] \tag{29}$$

is the range of model prediction on H. $\Delta R_{\text{posterior}}$ denotes the range obtained after considering the dataset constraints, for instance, in the Data Collaboration mode, it becomes

$$\Delta R_{\text{posterior,Data Collaboration}} = \left[\min_{\mathbf{x}\in \mathrm{F}} s_0(\mathbf{x}) - \max_{\mathbf{x}\in \mathrm{F}} s_0(\mathbf{x})\right] \tag{30}$$

where $\mathbf{x}$'s are confined to the feasible region F. Recall that the feasible region F is a subset of H, $\mathrm{F}\subseteq\mathrm{H}$; hence, $\Delta R_{\text{posterior, Data Collaboration}} \leq \Delta R_{\text{prior}}$. If the analysis does not follow the Data Collaboration mode and engages just a subset of the dataset information, we obtain $\Delta R_{\text{posterior, Data Collaboration}} \leq \Delta R_{\text{posterior, without Data Collaboration}} \leq \Delta R_{\text{prior}}$.

We can compare how I changes depending on the mode of data analysis. Specifically, we defined the *information loss*, L, due to not using Data Collaboration as

$$L = \frac{I_{\text{Data Collaboration}} - I_{\text{without Data Collaboration}}}{I_{\text{Data Collaboration}}} \tag{31}$$

and performed 100 runs with a randomly assigned model to predict, s_0, constrained to the GRI-Mech 3.0 dataset [68]. The results, reported in Fig. 10, show ~90% loss—a significant price to pay for the lack of collaboration.

This example illustrates the need (and payoff) for fully collaborative environments in which models and data can be shared, allowing sophisticated global optimization-based tools to reason quantitatively with the community information. Examples of questions that one can address through Data Collaboration by considering set-intersection assertions about the feasible region within the parameter space are:

- Is the feasible region empty? If so, then something is wrong about the dataset, invalidating at least one of the dataset units and/or the underlying reaction model which is common to all the units.
- Which dataset units have the most impact on the overall dataset's (in)consistency? Answering this can signal dataset units that are possibly incorrect, though self-consistent.
- Which model assumptions have the most impact on the dataset's (in)consistency?
- What is the tightest range of predictions about an additional experiment, given that these predictions must be consistent with the dataset?

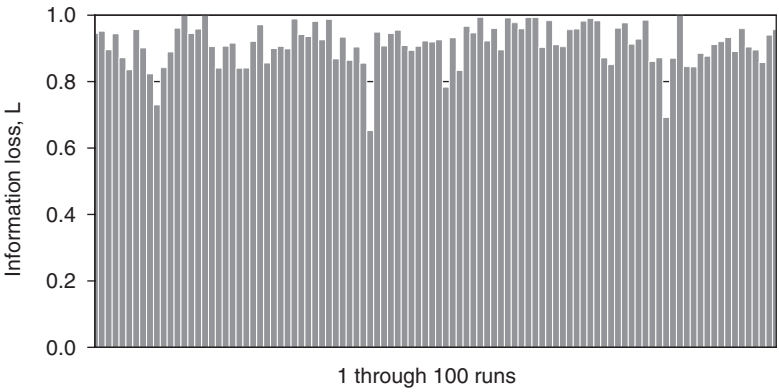

Fig. 10. Information loss without Data Collaboration.

- Which experiment or/and parameter bound is mostly responsible for the given bound on the model prediction? In other words, which experiment/parameter should be improved to tighten the range of model uncertainty?
- What is the utility of a hypothetical experiment to further knowledge regarding the system? In this framework, "what-if" questions can be posed and addressed. For instance, *what if* additional shock-tube experiments are performed at such and such conditions; what is the anticipated contribution that these experiments could make to further knowledge of this system? In other words, what is the likelihood that these new experiments will tighten the range of the model prediction?

Some of these questions can be answered with the methodology available today, and some require further development. To enable Data Collaboration in its full mode one of the upcoming challenges is creation of an infrastructure able to create and curate the dataset by engaging the entire scientific community [46].

7 CONCLUDING REMARKS

Sometimes (or often) one hears skepticism expressed toward "fitting" as compared to a "scientifically pure," "first-principle" approach to developing chemical kinetics models. The implication here is that well-executed experiments together with well-founded theory (such as quantum-chemical computations and reaction rate theories) can supply information that can be used directly, without any need for the "fitting." This could be true if the experimental observations and theoretical analysis had no uncertainties. Unfortunately, the reality is different. Even well-designed experiments have (often unspecified) uncertainties and the highest level (quantum) theory relies on numerical approximations and "internal" parameterization. Moreover, the actual level of uncertainties is hard, if not impossible, to estimate and latent correlation among model variables convolutes further the effect of uncertainties. In light of the above, we must conclude that it is impossible to make a significant progress in the area of building predictive reaction models without resorting to rigorous methods of analysis, of the type presented in this chapter, which do not just propagate the individual errors but incorporate the compound uncertainty into the analysis itself.

ACKNOWLEDGMENTS

The methodology of Solution Mapping was developed while one of us (MF) was working on various projects supported by DOE, NASA, AFOSR, and GRI. The work on Data Collaboration and preparation of this manuscript were supported by NSF, under Grant Nos. CTS-0113985 and CHE-0535542.

REFERENCES

[1] G.P. Smith, D.M. Golden, M. Frenklach, N.W. Moriarty, B. Eiteneer, M. Goldenberg, C.T. Bowman, R. Hanson, S. Song, W.C. Gardiner, Jr., V. Lissianski, Z. Qin, http://www.me.berkeley.edu/gri_mech/.
[2] T. Yuan, C. Wang, C.-L. Yu, M. Frenklach, M. Rabinowitz, *J. Phys. Chem.*, **95** (1991) 1258–1265.
[3] B. Eiteneer, C.-L. Yu, M. Goldenberg, M. Frenklach, *J. Phys. Chem. A*, **102** (1998) 5196–5205.
[4] B. Eiteneer, M. Frenklach, *Int. J. Chem. Kinet.*, **35** (2003) 391–414.
[5] A. Gelman, J.B. Carlin, H.S. Stern, D.B. Rubin, *Bayesian Data Analysis*. Chapman and Hall, Boca Raton, FL, 2004.
[6] T.F. Edgar, D.M. Himmelblau, L.S. Lasdon, *Optimization of Chemical Processes*. McGraw-Hill, New York, 2001.
[7] S. Boyd, L. Vandenberghe, *Convex Optimization*. Cambridge University, Cambridge, UK, 2004.
[8] M. Frenklach, in: W.C. Gardiner, Jr. (Eds.), *Combustion Chemistry*. Springer-Verlag, New York, pp., 1984, p. 423–453
[9] I.M. Gelfand, M.L. Tsetlin, *Dokl. AN SSSR*, **137** (1961) 295–298.
[10] G.E.P. Box, G.A. Coutie, *Proc. IEE*, **103B** (1956) 100–107.
[11] Z. Michalewicz, *Genetic Algorithms+Data Structures = Evolution Programs*. Springer-Verlag, Berlin, 1992.
[12] L. Elliott, D.B. Ingham, A.G. Kyne, N.S. Mera, M. Pourkashanian, C.W. Wilson, *Combust. Sci. Technol.*, **175** (2003) 619–648.
[13] L. Elliott, D.B. Ingham, A.G. Kyne, N.S. Mera, M. Pourkashanian, C.W. Wilson, *Ind. Eng. Chem. Res.*, **42** (2003) 1215–1224.
[14] S.D. Harris, L. Elliott, D.B. Ingham, M. Pourkashanian, C.W. Wilson, *Comput. Methods Appl. Mech. Eng.*, **190** (2000) 1065–1083.
[15] A.B. Singer, P.I. Barton, *J. Global Optim.*, in press.
[16] A.B. Singer, J.W. Taylor, P.I. Barton, W.H. Green, *J. Phys. Chem. A*, **110** (2006) 971–976.
[17] G.E.P. Box, N.R. Draper, *Empirical Model-Building and Response Surfaces*. Wiley, New York, 1987.
[18] G.E.P. Box, W.G. Hunter, *Technometrics*, **7** (1965) 23–42.
[19] G.E.P. Box, W.G. Hunter, J.S. Hunter, *Statistics for Experimenters. An Introduction to Design, Data Analysis, and Model Building*. Wiley, New York, 1978.
[20] L.S. Polak, *Application of Numerical Methods to Chemical and Physical Kinetics*. Nauka, Moscow, Russia, 1969, (in Russian).

[21] H.H. Rosenbrock, C. Story, *Computational Techniques for Chemical Engineers*. Pergamon, New York, 1966.
[22] H.G. Bock, in: K.H. Ebert, P. Deuflhard, W. Jäger (Eds.), *Modelling of Chemical Reaction Systems*. Springer-Verlag, Berlin, 1981, p. 102–125.
[23] J. Milstein, in: K.H. Ebert, P. Deuflhard, W. Jäger (Eds.), *Modelling of Chemical Reaction Systems*. Springer-Verlag, Berlin, 1981, p. 92–101.
[24] W.-W. Pan, M.A. Tatang, G.J. McRae, R.G. Prinn, *J. Geophys. Res.*, **102** (1997) 21915–21924.
[25] R.G. Ghanem, P.D. Spanos, *Stochastic Finite Element: A Spectral Approach*. Springer-Verlag, New York, 1991.
[26] M. Frenklach, H. Wang, M.J. Rabinowitz, *Prog. Energy Combust. Sci.*, **18** (1992) 47–73.
[27] R.H. Myers, D.C. Montgomery, *Response Surface Methodology: Process and Product Optimization Using Designed Experiments*. Wiley, New York, 2002.
[28] J. Sacks, W.J. Welch, T.J. Mitchell, H.P. Wynn, *Stat. Sci.*, **4** (1989) 409–435.
[29] T.J. Santner, B.J. Williams, W.I. Notz, *The Design and Analysis of Computer Experiments*. Springer-Verlag, New York, 2003.
[30] D. Miller, M. Frenklach, *Int. J. Chem. Kinet.*, **15** (1983) 677–696.
[31] M. Frenklach, D.L. Miller, *AIChE J.*, **31** (1985) 498–500.
[32] G.E.P. Box, R.D. Meyer, *J. Res. Nat. Bur. Stand.*, **90** (1985) 494–496.
[33] A. Saltelli, K. Chan, E.M. Scott, *Sensitivity Analysis*. Wiley, Chichester, UK, 2000.
[34] T. Turányi, H. Rabitz, in: A. Saltelli, K. Chan, E.M. Scott (Eds.), *Sensitivity Analysis*. Wiley, Chichester, UK, 2000.
[35] V.V. Nalimov, N.A. Chernova, *Statistical Methods of Design of Extremal Experiments*. Nauka, Moscow, 1965 (in Russian).
[36] N.R. Draper, H. Smith, *Applied Regression Analysis*. Wiley, New York, 1998.
[37] A. Fries, W.G. Hunter, *Technometrics*, **22** (1980) 601–608.
[38] M. Frenklach, *Combust. Flame*, **58** (1984) 69–72.
[39] S.G. Davis, A.B. Mhadeshwar, D.G. Vlachos, H. Wang, *Int. J. Chem. Kinet.*, **36** (2004) 96–106.
[40] http://www.mathworks.com
[41] Y. Zhao, K.-T. Fang, *J. Stat. Plann. Inference*, **98** (2001) 279–285.
[42] J. Sacks, S.B. Schiller, W.J. Welch, *Technometrics*, **31** (1989) 41–47.
[43] R.L. Plackett, J.P. Burman, *Biometrika*, **33** (1946) 305–325.
[44] D.K.J. Lin, *Technometrics*, **37** (1995) 213–225.
[45] M. Frenklach, in: E.S. Oran, J.P. Boris (Eds.), *Numerical Approaches to Combustion Modeling*. American Institute of Aeronautics and Astronautics, Washington, DC, 1991, p. 129–154.
[46] http://primekinetics.org
[47] M. Frenklach, in: A.V. Sapre, F.J. Krambeck (Eds.), *Chemical Reactions in Complex Systems*. Van Nostrand Reinhold, 1991, p. 197–221.
[48] M. Frenklach, *19th International Colloquium on the Dynamics of Explosions and Reactive Systems*, Hakone, Japan, 2003, ISBN4-9901744-1-0.
[49] M. Frenklach, K. Kailasanath, E.S. Oran, in: J.R. Bowen, J.C. Leyer, R.I. Soloukhin (Eds.), *Dynamics of Reactive Systems Part II: Modeling and Heterogeneous Combustion*. American Institute of Aeronautics and Astronautics, Washington, DC, 1986, p. 365–376.
[50] H. Wang, M. Frenklach, *Combust. Flame*, **87** (1992) 365–370.
[51] T. Lu, C.K. Law, *Proc. Combust. Inst.*, **30** (2005) 1333–1341.

[52] T. Løvås, F. Mauss, C. Hasse, N. Peters, *Proc. Combust. Inst.*, **29** (2002) 1403–1410.
[53] T. Løvås, D. Nilsson, F. Mauss, *Proc. Combust. Inst.*, **28** (2000) 1809–1815.
[54] T. Turányi, T. Berces, S. Vajda, *Int. J. Chem. Kinet.*, **21** (1989) 83–99.
[55] L.R. Petzold, W. Zhu, *Am. Inst. Chem. Eng. J.*, **45** (1999) 869–886.
[56] W.H. Green, P.I. Barton, B. Bhattacharjee, D.M. Matheu, D.A. Schwer, J. Song, R. Sumathi, H.H. Carstensen, A.M. Dean, J.M. Grenda, *Ind. Eng. Chem. Res.*, **40** (2001) 5362–5370.
[57] B. Bhattacharjee, D.A. Schwer, P.I. Barton, W.H. Green, *Combust. Flame*, **135** (2003) 191–208.
[58] D.M. Golden, G.P. Smith, A.B. McEwen, C.-L. Yu, B. Eiteneer, M. Frenklach, G.L. Vaghjiani, A.R. Ravishankara, F.P. Tully, *J. Phys. Chem. A*, **102** (1998) 8598–8606.
[59] C.A. Schuetz, M. Frenklach, A.C. Kollias, W.A. Lester, *J. Chem. Phys.*, **119** (2003) 9386–9392.
[60] A.R. Marsden, M. Frenklach, D.D. Reible, *J. Air Pollut. Control Assoc.*, **37** (1987) 370–376.
[61] S.R. Tonse, N.W. Moriarty, N.J. Brown, M. Frenklach, *Isr. J. Chem.*, **39** (1999) 97–106.
[62] M. Frenklach, in: K.J. Bathe (Eds.), *Computational Fluid and Solid Mechanics*. Elsevier, New York, 2001, p. 1177–1179.
[63] M. Frenklach, Unpublished work.
[64] S. Vajda, P. Valko, T. Turányi, *Int. J. Chem. Kinet.*, **17** (1985) 55–81.
[65] N.J. Brown, G. Li, M.L. Koszykowski, *Int. J. Chem. Kinet.*, **29** (1997) 393–414.
[66] S.H. Lam, D.A. Goussis, *Int. J. Chem. Kinet.*, **26** (1994) 461–486.
[67] U. Maas, S.B. Pope, *Combust. Flame*, **88** (1992) 239–264.
[68] M. Frenklach, A. Packard, P. Seiler, R. Feeley, *Int. J. Chem. Kinet.*, **36** (2004) 57–66.
[69] M. Frenklach, A. Packard, P. Seiler, *Proceedings of the American Control Conference*, Anchorage, Alaska, 2002, pp. 4135–4140.
[70] R. Feeley, P. Seiler, A. Packard, M. Frenklach, *J. Phys. Chem. A*, **108** (2004) 9573–9583.
[71] P. Seiler, M. Frenklach, A. Packard, R. Feeley, *Optim. Eng.*, **7** (2006) 459–478.
[72] D. Luenberger, *Linear and Nonlinear Programming*, 2nd ed., Addison Wesley, Reading, MA, 1984.
[73] C. Papadimitriou, K. Steiglitz, *Combinatorial Optimization: Algorithms and Complexity*. Prentice Hall, Englewood Cliffs, NJ, 1982.
[74] Y. Nesterov, A. Nemirovskii, *Interior-Point Polynomial Algorithms in Convex Programming*. SIAM, Philadelphia, PA, 1994.
[75] L. Khachian, *Dokl. Acad. Nauk USSR*, **244** (1979) 1093–1096.
[76] D. Luenberger, *Optimization by Vector Space Methods*. Wiley, New York, 1969.

This page intentionally left blank

Subject Index

This page intentionally left blank